Università degli Studi di Cagliari

PHD DEGREE

IN INNOVATION SCIENCE AND TECHNOLOGIES

Cycle XXXII

TITLE OF THE PHD THESIS

FABRICATION AND CHARACTERISATION OF BIOACTIVE/BIODEGRADABLE MATERIALS FOR TISSUE ENGINEERING

Scientific Disciplinary Sector(s)

ING-IND/22

PhD Student:	Ing. Marina Luginina
Coordinator of the PhD Programme	Prof. Ing. Roberto Orrù
Supervisor	Prof. Ing. Roberto Orrù

Final exam. Academic Year 2018 – 2019

Thesis defence: January-February 2020 Session

To my family and the beloved person who supported me on this journey

Acknowledgments

Throughout my PhD I have had the chance to work with amazing people, to whom I would like to thank and dedicate the following words.

First of all, I would like to express my sincere gratitude for my advisor Prof. Roberto Orrù. During these three years he guided and continuously supported me through my PhD work, encouraged my research and provided insightful comments. I would like to thank him for patience and immense knowledge, as well as for the possibility to practice and collaborate with other projects, and ultimately to grow as a research scientist.

Besides my advisor, I would like to thank Prof. Giacomo Cao, for his encouragements, great discussions and for the hard questions which incented me to widen my research from various perspectives.

Without the precious support of Prof. Orrù and Prof. Cao it would not be possible to conduct this PhD study. It was a great pleasure for me working with them.

I am grateful for the possibility to perform my research activity in the framework of the International PhD in Innovation Sciences and Technologies at the University of Cagliari.

During this three year program I also had chance to collaborate and work at the advanced research centers in France and Germany.

In this regard, I would like to warmly thank Prof. Valeria Cannillo and Dr. Devis Bellucci (Università di Modena e Reggio Emilia, Italy) for the interesting and fruitful collaboration.

I would like also to express my sincere gratitude for my supervisors during my internship at CIRIMAT laboratory (Université de Toulouse, CNRS, France) Dr. Christophe Drouet, Dr. David Grossin and Dr. Fabien Brouillet. This experience

opened new horizons in a field of biomaterial's research for me. To all of them goes my appreciation for their competence and priceless advices.

Furthermore, I would like to express my special gratitude for Dr. Liliana Liverani and Prof. Dr.-Ing. habil. Aldo R. Boccaccini for their valuable guidance and the possibility to conduct the research project at the Institute of Biomaterials (Friedrich–Alexander University Erlangen–Nürnberg, Germany). Their knowledge and professionalism were priceless. This internship has allowed me to gain a broad spectrum of knowledge in the field of hard and soft tissue engineering.

Moreover, I would like to warmly thank my colleagues who have also became my friends, in particular, Francesco, Giovanna, Selena, Barbara, Roberta, Alessandro, Blessing, Gabriele and Fabio. Thank you for always willing to help and support me. I would like to extend my appreciation to the people that I have met during my internships at CIRIMAT and Institute of Biomaterials. Even if it was for a short period of time, I am extremely grateful for their kindness and assistance that make my stay and work in new countries so pleasant.

There are not enough words to describe all my gratitude for my family. Mom, Antonio, Gaia and Gianfranco, most important people in my life, thank you for your love and support during this long journey. Even if you were far, you encouraged and helped me to go even through the toughest moments.

And finally, beyond words, my immense gratitude to Artem. Thank you for always being there for me and for your positive attitude no matter what, for your patience and for your love. You always know how uplift me and how to put a smile upon my face.

Abstract

One of the main concerns in public healthcare in both developed and developing countries which cause handicap, physical disability and patient chronic pain is currently related to musculoskeletal problems and, in particular, to osteoarticular diseases. Since these diseases and induced defects affect millions of people worldwide, treatment of bone tumors, traumatology, osteoporosis and others pathologies, especially for aging populations, gained prime importance.

In the past decades, great effort from scientific/medical society has been addressed to the development of safe reliable synthetic bone graft materials as alternative to allo- and autografts. The use of latter ones is usually associated with transmission complications as well as with immunological rejection and morbidity.

Calcium phosphates, in general, and in particular, hydroxyapatite, nanocrystalline biomimetic apatites and amorphous calcium phosphates, as well as bioactive glasses, recently gained much attention as promising materials for the treatment of non-self-healing bone defects. However, despite undeniable advantages such as biocompatibility, non-toxicity, and good bioactivity, clinical applications of these materials are still limited.

In the present thesis, beyond the state of art, it was attempted to tackle various problems related to the development and essential systematic characterization of innovative materials for hard and soft tissue engineering.

In the first part of the study, bioactivity of novel low alkaline glass using simulated body fluid (SBF) was assessed. Specifically, the effects produced by devitrification phenomena which take place during the consolidation of amorphous glass powder on the biological behavior of the resulting material was considered.

The second part of the study was dedicated to the evaluation of biological compatibility of different calcium phosphate/bioactive glass composites. To this

purpose, different composites obtained by combining of hydroxyapatite with a low alkaline bioactive glass were first sintered into bulk discs via innovative spark plasma sintering technique and then exposed to the cell tests using murine long bone osteocyte-like immortalized cell line. The results were compared with the findings deriving from the SBF tests performed previously.

The third part of the thesis was focused of the development of novel functionally graded materials in the calcium phosphate/bioactive glass system.

In the fourth part of the thesis, the synthesis, sintering and physico-chemical characterization of highly carbonated magnesium-doped amorphous calcium phosphates, a novel family of bone substitute materials, was reported and discussed.

Fifth part of this thesis deals with the fabrication and characterization of fibrous polymer/bioactive glass composite scaffolds for soft tissue engineering. Recently, it has been shown that bioactive glasses are able not only directly bond with the bone, but they also possess angiogenesis potential (bioactive glass ion dissolution products can induce new blood vessels regeneration). The latter property is crucial for the treatment of soft tissue wounds. The extension of bioactive glass application to areas such as peripheral nerve repair, healing of burn injures and chronic wound healing attracted much attention lately. In the present study, fibrous scaffolds from different biodegradable polymers coupled with bioactive glasses were fabricated using electrospinning technique. Biological performances in a presence of bone murine stromal cells as well as mechanical properties of prepared scaffold were investigated.

Keywords: *bone repair, calcium phosphates, bioactive glasses, spark plasma sintering, bioactivity, amorphous calcium phosphates, electrospinning.*

Table of contents

List of figures

Chapter 2.

Chapter 3.

Chapter 4.

Chapter 5.

Chapter 6.

Chapter 7.

Chapter 8.

Chapter 9.

List of tables

Chapter 2.

Chapter 3.

Chapter 5.

Chapter 6.

Chapter 7.

Chapter 8.

Chapter 9.

List of abbreviations

Amorphous Calcium Phosphate (ACP)

α; β-Tricalcium phosphate (α; β-TCP)

Bioactive glass (BG)

Biomimetic nanocrystalline apatite (BNA)

Bone tissue engineering (BTE)

Calcium-deficient hydroxyapatite (CDHA)

CaO-rich bioactive glass (CaMix)

Capacitor discharge sintering (CDS)

Carbonated hydroxyapatite (HCA)

Constant-rate of heating (CRH)

Critical-sized defects (CSD)

Extracellular matrix (ECM)

Hot Isostatic Pressing (HIP)

Hot Pressing (HP)

Hydroxyapatite (HA)

Nuclear magnetic resonance (NMR)

Octacalcium phosphate (OCP)

Phosphate buffered solution (PBS)

Poly(ε-caprolactone) (PCL)

Poly(glycerol-sebacate) (PGS)

Pressureless sintering (PSL)

Scanning electron microscopy (SEM)

Select laser sintering (SLS)

Simulated body fluid (SBF)

Spark plasma sintering (SPS)

Tissue engineering (TE)

Two-step sintering (TSS)

Ultraviolet (UV)

Ultra-high molecular weight polyethylene (UHMWPE)

X-ray diffraction (XRD)

Chapter 1. Introduction

1.1 Aim and Objectives

During this PhD program I had chance to work and contribute to different research projects. Beyond the state of art, the general aim of this thesis is to provide new insights related to the development and systematic characterization of biomaterials for tissue engineering, their fundamental properties along with possible applications. The present thesis is divided into independent chapters according to the arguments studied. The specific problematics and research objectives of each considered subject are reported in chapter's introduction part.

1.2 Thesis structure

The layout of thesis is described as follows:

Chapter 1 introduces the general aim and structure of the thesis.

Chapter 2 provides an overview about bone nature, in particular, bone functions, structure, composition and mechanical properties. It concludes with a description of the bone remodeling process and gives a brief overview about bone capacity to self-regenerate. Better understanding of bone biology is essential for the development of novel biomaterials that can closer mimic the native tissue at the site of restoration.

Chapter 3 represents a current state of art in the field of bone tissue repair. It begins by illustrating the existing clinical need of materials for bone tissue repair and regeneration; then naturally-derived bone substitutes are discussed. Furthermore, the necessity of the development of synthetic biomaterials and their ideal properties are discussed. Subsequently, a brief classification of biomaterials, depending on the host tissue response, is given. The variety of currently investigated and applied biomaterials is discussed as well. Specific focus is given to bioceramics, in particular to hydroxyapatite, biomimetic apatites, amorphous calcium phosphates and bioactive

glasses. An overview on how it is possible to evaluate by means of *in vitro* test the bioactivity of bioceramics is also given.

In **Chapter 4** first a general overview on sintering techniques which can be applied to process biomaterials into final bulk products is provided. Additionally, fabrication of functionally graded materials, promising candidates for hard tissue repair, is also discussed.

The following chapters specifically deal with the results of the different research projects carried out during this PhD program.

Chapter 5 is dedicated to the assessment of crystallization effect on *in vitro* bioactivity of novel CaO-rich bioglass-derived glass-ceramic.

In **Chapter 6**, the results obtained during a cell biological study involving a novel CaO-rich bioactive glass and hydroxyapatite/CaO-rich bioactive glass composites are described and discussed.

Chapter 7 is dedicated to the development of advanced functionally graded materials in the calcium phosphate/bioactive glass system. Some preliminary results are reported.

Chapter 8 is based on the achievements from the experimental work obtained during my internship at CIRIMAT laboratory (France). In particular, the synthesis routes which allow to produce highly carbonated/magnesium doped amorphous calcium phosphates are described and discussed.

In **Chapter 9**, the results relative to the research project carried out at the Institute of Biomaterials (Germany) are presented. Fabrication of polymer/bioactive glass composite electrospun scaffolds along with cell biological test and assessment of mechanical properties is reported.

And finally, the concluding **Chapter 10** gives a general overview on the main results, achieved in the framework of my PhD research program.

Chapter 2. Human bone tissue

Human bone is a complex biological tissue where minerals are integrated into soft matrices. It represents one of the types of mineralized or calcified tissues. Within human body, mineralized tissues can be also found in forms of enamel, dentin and cementum. They possess unique hierarchical structure and chemical composition [1]. However, the differences occur on a level of crystal size and shape, in percentage of minerals and proteins, as well as in allocation of trace mineral ions [2].

2.1 Functions and structure of human bones

The human skeleton system, consisting of 206 bones and connective tissues called ligaments, tendons, and cartilage, is generally aimed to internal structural support (Fig. 2.1) [3,4]. Moreover, it displays other important functions [5,6]:

- *Mechanical:* bones possess specific mechanical properties which allow human body to withstand the effect of gravity and mechanical stresses; additionally, skeleton system facilitates mobility by serving as points of attachment for muscles;
- *Protective:* it fences vital organs and soft tissues;
- *Hematopoietic:* bone provides a milieu for hematopoiesis (bone marrow situated in cancellous bone produces red and white blood cells for oxygenation of other tissues);
- *Metabolic:* bones are responsible for the maintaining of mineral homeostasis. More precisely, bone mineral act as storage for inorganic minerals such as calcium, phosphorus and magnesium which are crucial for normal body functioning. These mineral ions, being released into the bloodstream, support physiological processes and help to avoid muscles and nerves disorders [7,8].

Based on the anatomy, structure and functions, different classifications of bones are available.

Anatomical classification

Axial skeleton consisting of about 80 bones, including the cranium, facial bones, rib cage, vertebral column, and others, mainly performs protective functions, as well as allows supporting of the central weight, and maintaining the posture.

Appendicular skeleton, in turn, ensures balance and stability, and also provides locomotion and manipulation function. Appendicular bones are located symmetrically within human body, and mainly consist of the long bones.

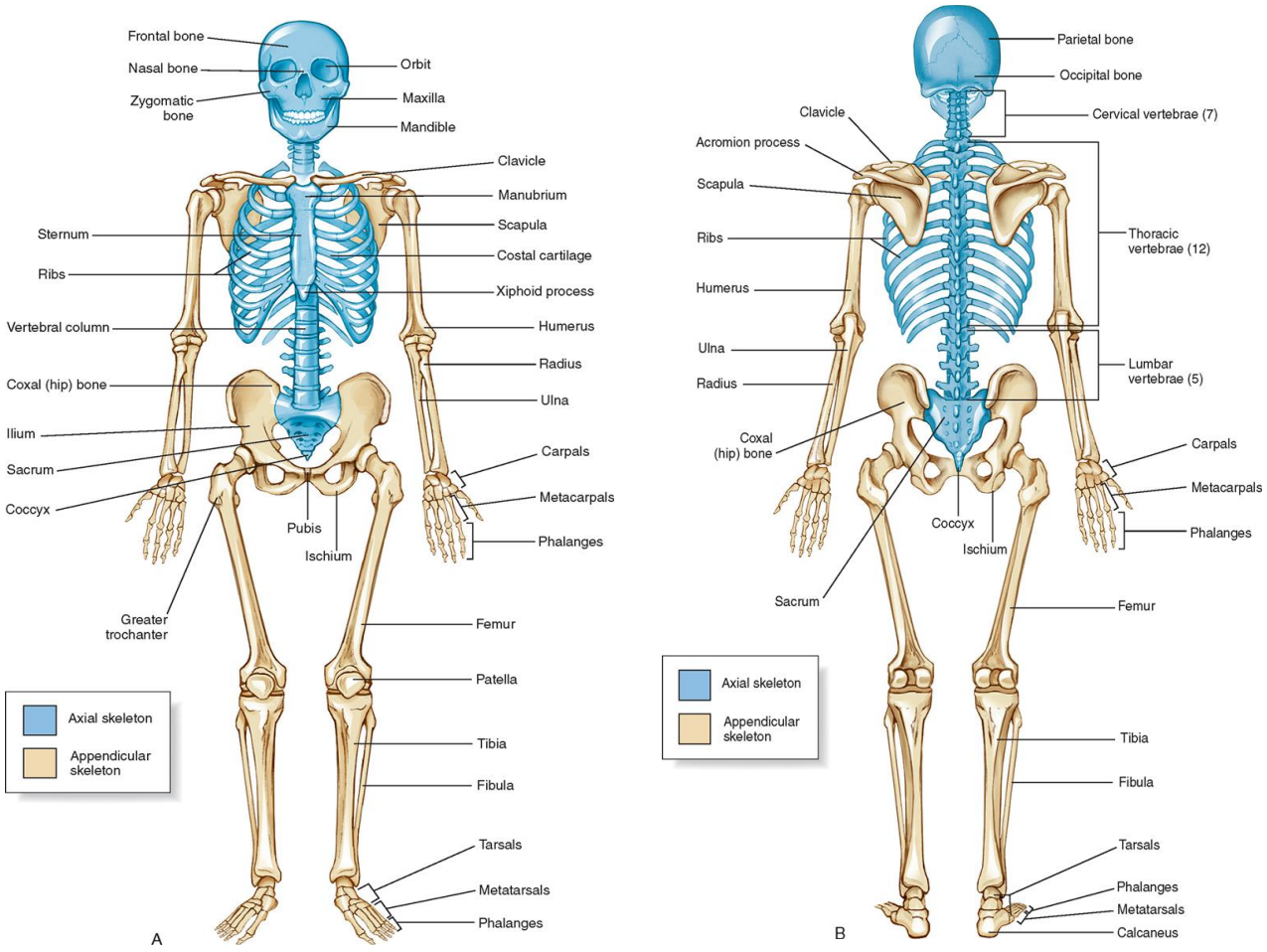

Figure 2.1: Human Skeletal System (axial and appendicular bones) [4].

According to the morphological features, i.e. shapes, the following types of bones can be distinguished:

- *Long bones*: clavicle, humerus, radius, femur, tibia, fibula et al.
  This kind of bones provides strength, structure and mobility. They have shaft (diaphysis) and two ends (epiphysis). Bone marrow which produces blood cells is located inside long bones.
- *Short bones*: carpus, patella, tarsus.
  Their primary function is to ensure stability and some movement.
- *Flat bones*: hip, parietal, frontal, nasal bone et al.
  The main function of flat bones is a protection of internal organs such as brain, heart, and pelvic organs.
- *Irregular bones*: ethimoid, palatine, maxilla, vertebrae et al.
  This kind of bones possesses a fairly complex shape, which helps to protect inner organs and nerves.
- *Sesamoid bones*: patella, pisiform.
  This type of bones can be defined as subtype of short bones embedded within a tendon of the hands, knees and feet.

Structural classification

From the microscopic viewpoint, human bones are classified into two different types: *woven* and *lamellar* bones (Fig. 2.2) [6]. Woven bone, which is considered as primary and immature, is a major bone type during the development of fetus, however, it also occurs during the bone remodelling process in adults. Woven bone is characterized by haphazard collagen fibres arrangements and possesses low mechanical resistance. In turn, lamellar bone is characterized by regular parallel alignment of collagen fibres (lamellae). This is a typical mature form of adult bones with relatively strong mechanical properties [9].

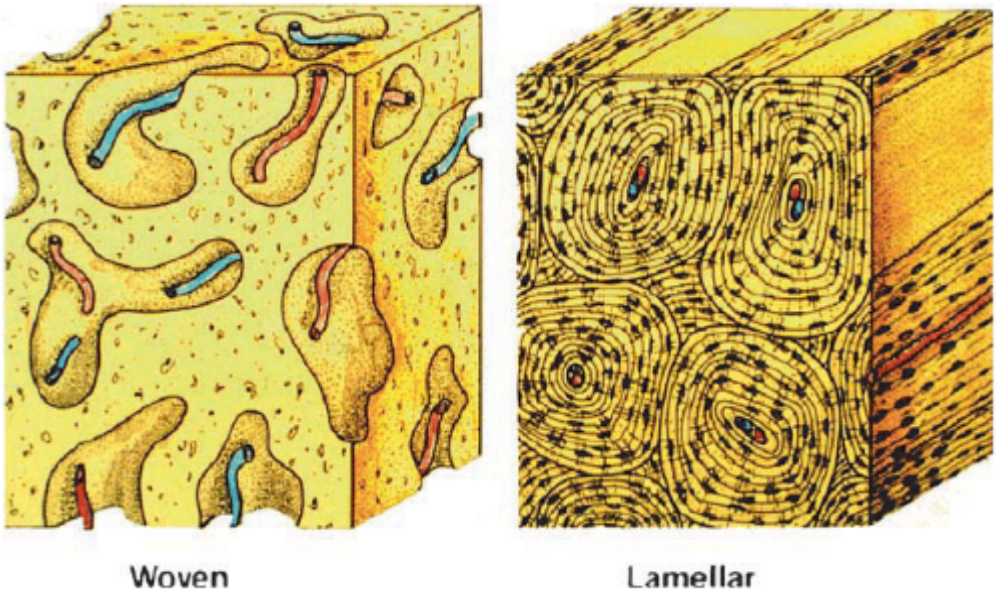

Figure 2.2: Schematic image of woven (immature) and lamellar (mature) bones. Woven bone shows a disorganized lamellar structure due to the interlacing arrangement of collagen fibers [10].

According to the macroscopic classification, bones can be divided into *trabecular* (also known as *spongy* or *cancellous*) and *cortical* (*compact* or *cortex*) types [10,11]. Although, the elemental composition is identical for those two types [12], they differ with respect to microarchitecture and porosity, and, consequently, mechanical properties are also diverse (Table 2.1).

Bone type	Tensile strength (MPa)	Young's Modulus (GPa)	Compressive strength (MPa)	Fracture toughness	Porosity	Density, g/cm^3
Cortical bone	50-151	3-30	130-180	2-12	<30%	1.7-2.0
Cancellous bone	10-20	0.02-0.5	2-12	0.1-0.8	50-90%	0.15-1

Table 2.1: Mechanical properties of human cortical and cancellous bone [13–17].

Cortical bone

Cortical bone contributes for approximately 80% to the human skeleton weight. It consists of closely packed multiple columns, also known as osteons or Haversian systems (Fig. 2.3). Osteon is built of concentric layers (lamellae) that surround haversian canals which contain bone's vascular supplies. Periosteum (fibrous layer) and endosteum are external and internal layers of cortical bone, respectively. Osteons are connected via Volkmann's or perforating canals.

Cancellous bone

Due to its high porosity, cancellous bone is less dense and stiff than cortical bone and its specific surface area is larger. It fills the interior and ends of long bones, as well as the interior of vertebrae. Trabeculae are primary atomical and functional units of cancellous bone that form a network (Fig. 2.3). Trabeculae network is covered by thin layer of endosteum (connective tissue) and creates a room for blood vessels and marrow.

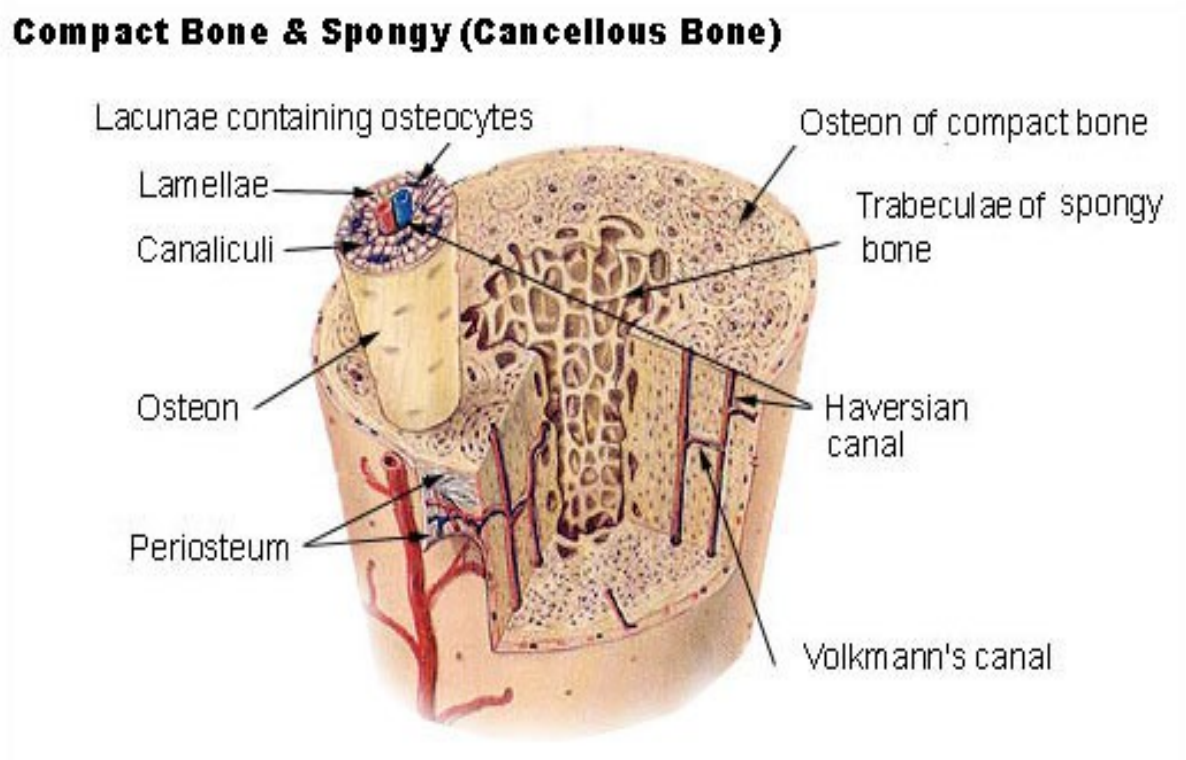

Figure 2.3: Schematic structure of compact and cancellous bone (cross-section) [18].

2.2 Bone composition

General composition of bones can be defined by the subsequent parts [6,10,12,19]:

i) cells (osteoblast, bone lining cells, ostecytes, osteoclasts) (Fig. 2.4);

ii) extracellular matrix (consisting of organic and inorganic parts).

2.2.1 Bone cells

Bone is a dynamic complex system which is exposed to growth, modelling and remodelling during life through the coordinated activities of osteoblasts, osteocytes, osteoclasts, and bone lining cells [20,21]. Bone growth, modelling and remodeling processes are discussed in more detail in Paragraph 2.3.

Each type of bone cells plays a specific role, for instance *osteoblasts* (4-6% of all bone cells), being located mainly on bone surface, are responsible for bone formation [22].

Bone lining cells are thought to be involved in a joining process between bone resorption and formation [23]. The presence of bone lining cells was detected on the bone surface, covering area where neither resorption nor bone formation occur [24].

Osteocytes, the most numerous family of cells (up to 95%), are involved in bone development [25,26]. In particular, at the final part of newly bone formation, a subset of osteoblasts turns into octeocytes and integrates into the internal part of bone matrix.

Osteoclasts, in turn, operate as mediators responsible for the dissolution and adsorption of bone tissue. Osteoporosis and other bone disorders could be launched by anomalous growth in osteoclast formation and activity, causing disproportion between resorption and formation. This process leads to decreasing of bone density and favours bone fractures [27]. However, it was found that octeoclasts produce cytokines, a broad class of proteins which is crucial in cell signalling [28]. Cell signalling is a complex process which governs cells activity and ensures the correct

response to the environmental changes taking place during the development, tissue repair and normal mineral homeostasis.

Osteoblasts, bone lining cells and osteocytes, also known as osteoprogenotor cells, originate from mesenchymal stem cells (MSCs), whereas osteoclasts derive from hemopoietic stem cells (Table 2.2).

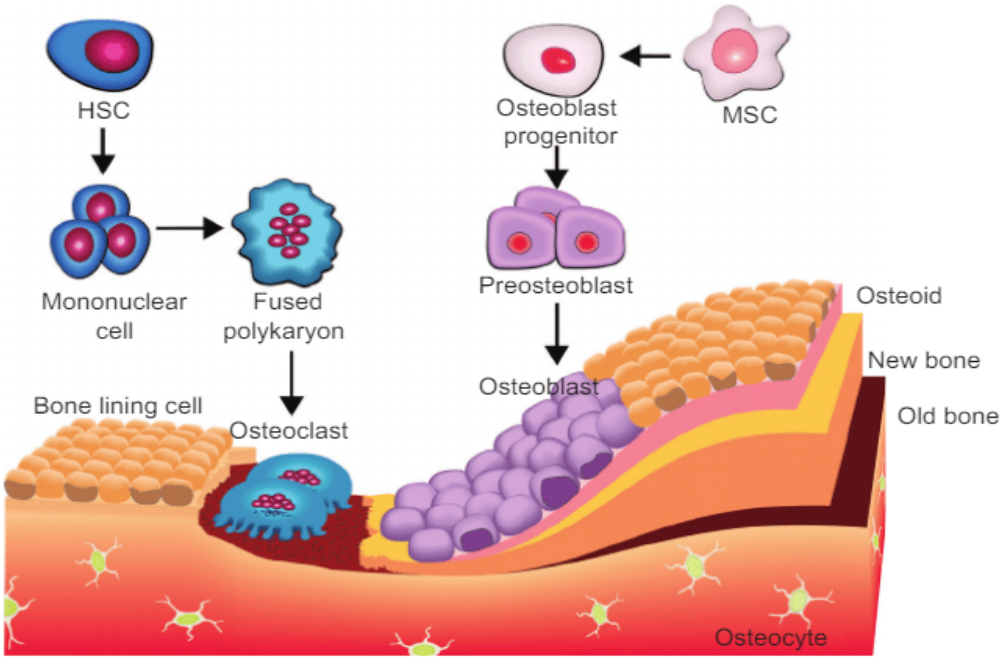

Figure 2.4: Schematic representation of the evolution of osteoblasts and osteoclasts in bone formation [29].

Cell type	Location	Origin	Morphology
Osteoblast	bone surface	mesenchymal stem cells	cuboidal cells
Bone lining cells	bone surface	mesenchymal stem cells	thin cells
Ostecytes	inner part of the bone	mesenchymal stem cells	star-shaped cells
Osteoclasts	bone surface	hemopoietic stem cells	giant, multi-nucleated cells

Table 2.2: Summary on bone cells types, sites and morphology [10,29–31].

2.2.2 Extracellular bone matrix

Bone is a heterogeneous composite material composed of 50 to 70% of inorganic substances (bone mineral or apatite), 20 to 40% of organic matrix, 5 to 10% of water and approximately 3% of lipids [6,32]. The organic component is the main responsible for bone resistance to tensile stress whereas the inorganic portion for the one to compression.

2.2.2.1 Organic matrix

Organic extracellular matrix serves as a scaffold upon which inorganic bone mineral deposits. In general, organic matrix provides elasticity and structural flexibility to bone, which otherwise would be unduly rigid.

Organic bone matrix is mainly composed by collagenous proteins, primarily type I collagens (85-90%) and non-collagenous proteins including osteocalcin, osteonectin, osteopontin, fibronectin and bone sialoprotein II, bone morphogenetic proteins (BMPs), and growth factors [33–36]. Extracellular matrix proteins and their functions are reported in Table 2.3.

Type I collagen, representing the most abundant protein in bone tissue, is involved in the process of inorganic bone apatite mineralization [37–39]. It was also found that type I collagen, without the presence of any other agents, can intrinsically initiate and manage the *in vitro* growth of apatite minerals (inorganic part of extracellular matrix) [40].

In turn, osteocalcin generated by the osteoblast cells represents the most abundant non-collagenous protein in extracellular bone matrix, and its role is to inhibit bone formation [41,42]. Osteopontin, another non-collagenous protein, plays an essential part in regulation of osteoclast activity, and it directs the inhibition or nucleation of bone apatite [43,44].

Additionally, small leucine-rich proteoglycans including decorin, biglycan, lumican, osteoaderin, and seric proteins affect bone cell activity and help to regulate matrix mineralisation.

Protein (Chromosome Location)	Function
Collagen-related proteins	
type I (17q21.23, 7q22.1)	Most abundant bone matrix protein
type X (6q21)	Found in hypertrophic cartilage
type III (2q31)	Trace amounts in bone; may regulate collagen fibril diameter
type V (9q34.2-34.3; 2q24.3-31; 19q13.2)	Trace amounts in bone; may regulate collagen fibril diameter
Serum proteins in bone matrix	
albumin (4q11-13)	Decreases apatite crystal growth
α2-HS glycoprotein (3q27)	Bovine analog is fetuin
Glycoaminoglycan-containing proteins and leucine-rich repeat proteins	
aggrecan (15q26.1)	Matrix organization, retention of calcium/phosphorus
versican (5q14.3)	Defines space destined to become bone
decorin (12q21.3)	Regulates collagen fibril diameter; binds TGF-β
biglycan (Xq28)	Binds collagen; binds TGF-β; genetic determinant of peak bone mass
hyaluronan (multigene complex)	May work with versican to define space destined to become bone
Glycoproteins	
alkaline phosphatase (1p36.1-p34)	Hydrolyzes mineral deposition inhibitors
osteonectin (5q31.3-32)	Regulates collagen fibril diameter
SIBLING proteins	
osteopontin (4q21)	Regulates osteoclasts; inhibits mineralization and remodeling
bone sialoprotein (4q21)	Initiates mineralization
MEPE (4q21.1)	Regulator of phosphate metabolism
RGD-containing glycoproteins	
thrombospondins (15q15, 6q27, 1q21, 5q13, 19p13.1)	Cell attachment
fibronectin (2q34)	Binds to cells
vitronectin (17q11)	Cell attachment
fibrillin 1 and 2 (15q21.1, 5q23-31)	Regulates elastic fiber formation
γ-Carboxy glutamic acid–containing proteins	
matrix Gla protein (12p13.1-p12.3)	Inhibits mineralization
osteocalcin (1q25-q31)	Regulates osteoclasts; inhibits mineralization
protein S (3p11.2)	Liver product, may be made by osteoblasts

Table 2. 3: Extracellular matrix proteins (adapted from [6]).

2.2.2.2 Bone mineral

The inorganic part, also known as bone mineral or biological apatite, represents the main forming component of the bone.

Bone mineral, firstly exposed to structural identification by XRD in 1926, was recognized as calcium phosphate similar to geological hydroxyapatite [45]. However, following studies on chemical composition and crystal structure of geological, synthetic and biological apatites revealed significant differences between them. From the structural viewpoint, bone mineral crystals, unlike synthetic and geological apatites, exhibit extremely small particle size. First studies, based on the measurements of X-ray diffraction peaks broadening, revealed that bone crystal sizes vary from 31Å to 290Å. In the fifties, more detailed studies carried out by using electron microscopy and diffraction [46] showed that bone crystals possess plate form approximately 500Å long, 250Å wide, and 100Å thick. For a long period of time, the main issue to overcome in order to precisely evaluate the bone crystal shape and size was the necessity to remove the entire organic matrix without altering the bone crystals. This step is essential to provide accurate measurements by high resolution transmition electron microscopy (HRTEM) and electron diffraction. Subsequently, it was established and confirmed by atomic force microscopy, that bone apatite crystals are thin crystals in nanometer range, which display a plate-like habit, i.e. 1-4 nm thick, 8-15 nm wide, and 20-35nm long [47,48].

From the compositional viewpoint, it was soon evidenced that stoichiometric hydroxyapatite (HA), previously used as a model for biological apatite, does not correspond to the bone mineral composition. Indeed, anionic/cationic substitutions and the existence of different types of ion vacancies within the structure of bone apatite were detected. Bone mineral was found to be calcium-deficient and hydroxyl-deficient carbonated apatite [49,50]. Regarding the presence of (OH^-) hydroxyl groups, typical for stoichiometric hydroxyapatite, different analysis techniques, comprising solid state Nuclear Magnetic Resonance (NMR) [51] and Raman

spectroscopy [52], revealed a very small percentage of hydroxyl groups. In contrast, a significant amount of carbonate ions (CO_3^{2-}) [53,54] was detected. According to various studies, such content can vary in a range between 3 to 9 wt.% [49,55,56]. Further detailed investigations evidenced that carbonate ions can occupy two anionic sites in the apatite structure: OH^- sites (type A carbonated apatite) and PO_4^{3-} sites (type B carbonated apatite) [57,58]. The presence of A-type or B-type depends on the origin of mineralized tissue. For instance, bone mineral is mainly composed of B-type whereas enamel corresponds to both A and B carbonate substitute types. Another feature that was observed within the structure of biological apatites is that PO_4^{3-} sites can be also occupied by hydrogen phosphate ions (HPO_4^{2-}) [49].

However, it is worth mentioning that, due to numerous difficulties including the interactions between crystals and surrounding environments, as well as instability of newly formed crystals and their phase transformations, it is hard to describe a single chemical composition and structure for nanosized bone mineral crystal. Therefore, only general formulations can be provided. In this light, huge efforts were dedicated not only to study biological apatites but also to evaluate the properties of biomimetic synthetic apatites. The final aim was to extrapolate the obtained results to better understand the chemical composition of biological apatites.

For instance, the phenomena of internal hydrolysis (eq. 1) between PO_4^{3-} ions and water was firstly observed for the synthetic apatites and further confirmed for the biological ones [59,60].

$$PO_4^{3-} + H_2O \rightarrow HPO_4^{2-} + OH^- \text{ (eq. 1)}$$

In addition, besides the carbonate (CO_3^{2-}), which is the main substituent ionic group in bone mineral [61], other trace elements like Mg^{2+}, Na^+, Cl^-, F^-, K^+, Sr^{2+} have also been detected [19,62] in various amounts. Typical compositions of the mineral part of calcified tissues in the human body are summarized in Table 2.4.

Composition (wt%)	Enamel	Dentine	Cementum	Bone	HA
Calcium (Ca)	36.5	35.1	~35	34.8	39.6
Phosphorus (P)	17.7	16.9	~16	15.2	18.5
Ca/P (molar ratio)	1.63	1.61	~1.65	<1.67	1.67
Sodium (Na)	0.5	0.6	-	0.9	–
Magnesium (Mg)	0.44	1.23	0.5–0.9	0.72	–
Potassium (K)	0.08	0.05	-	0.03	–
Carbonate (CO_3^{2-})	3.5	5.6	-	7.4	–
Fluoride	0.01	0.06	Up to 0.9	0.03	–
Chloride	0.30	0.01	-	0.13	–
Pyrophosphate ($P_2O_7^{4-}$)	0.022	0.10	-	0.07	–
Total inorganic	97	70	60	65	100
Total organic	1.5	20	25	25	–
Water	1.5	10	15	10	–

Table 2.4: Inorganic phases composition of adult human calcified tissues (adapted from [62]).

The most representative chemical formula of the bone mineral, suggesting a relatively homogeneous composition and taking into account different substitutions within the structure of biological apatite, was proposed by Legros based on the generalization of different cortical bone analyses [49]:

$$Ca_{8.3}(PO_4)_{4.3}(CO_3, HPO_4)_{1.7}(CO_3,OH)_{0.3}$$

Although the use of carbonated apatite as a model for biological mineralized tissues of vertebrates is currently accepted, the issue of the bone mineral crystal surface remains highly debated.

Some particularities on the surface of bone mineral crystals were firstly highlighted in the early fifties during ionic exchange experiments [63]. Further investigations showed the presence of a significant amount of water, and an increased concentration of Ca and Mg ions on the bone crystal surface [63–65]. It is worth to mention that about 66% of all Mg in the human body is located on this surface hydrated layer. Therefore, Mg ions can be easily involved into the ion exchange processes, enter in

extracellular fluids and be rapidly delivered to the various organs, tissues and nerves [66,67].

In turn, different spectroscopic studies revealed the presence of specific lines which cannot be attributed to crystalline apatite [68–70]. FTIR analysis clearly evidenced the appearance of specific "non-apatitic" environments in ν_4PO_4 and ν_2CO_3 domains. A significant content of labile HPO_4^{2-} groups situated on the surface of apatite crystals was detected by NMR [71]. Further ion exchange experiments proved that these "non-apatitic" environments are located in the same domain as a surface hydrated layer [72,73]. NMR analysis performed on the synthetic biomimetic apatites suggested that the nature of this mineral disordered hydrated surface layer can be related to octacalcium phosphate phase (OCP) [74]. Recently, a study based on advanced solid-state nuclear magnetic resonance (ssNMR) carried out on the freshly extracted bone 'kept in its native hydration state' confirmed a model where apatite nanocrystals are covered by a highly hydrophilic disordered mineral layer that consists of Ca^{2+}, HPO_4^{2-}, CO_3^{2-} ions, and water (Fig. 2.5) [75]. Authors identified this layer as amorphous calcium phosphate (ACP)-related phase rather than OCP related phase [74]. Additionally, the core/shell model was confirmed for apatite particles in dentine [76–78].

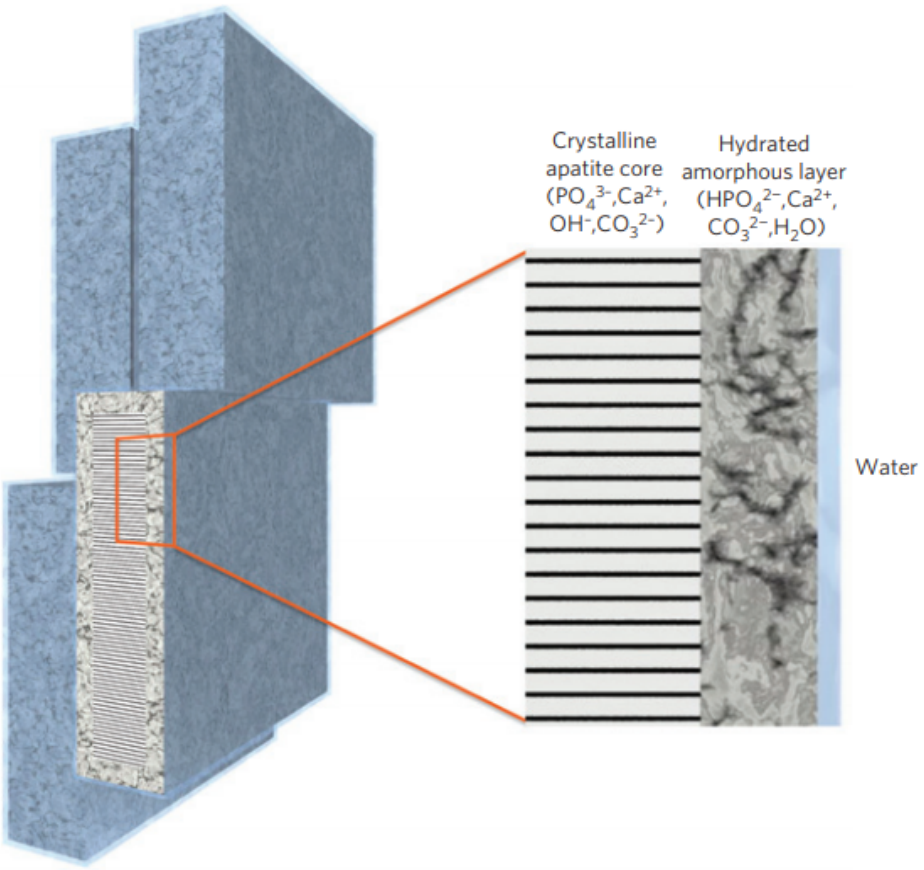

Figure 2.5: Schematic representation of the stacking of apatite platelets. The platelets are composed of a crystalline apatitic core and an amorphous layer composed of (PO_4^{3-}, Ca^{2+}, OH^-, CO_3^{2-}) and (HPO_4^{2-}, Ca^{2+}, CO_3^{2-}, H_2O), respectively. Water molecules that form a structuring network with the hydrated ACP-like layer induce the orientation of the HA platelets [75].

2.3 Remodeling and bone capacity to regenerate

As mentioned previously, bone is a dynamic tissue that adapts its structure over a lifetime. It is initially formed during development through either an intramembranous or endochondral ossification process [79]. Once formed, the bone grows and changes its shape by modeling. The latter one is the process through which bone changes its shape as a response to physiologic or mechanical stimuli. During this process, bone resorption and formation are two uncoupled pathways, happening on distinct surfaces [6]. In normal conditions, bone remodeling occurs due to the coupled activity of

osteoclasts, which break down bone, and osteoblasts, that form a new bone matrix [80,81]. Resorption followed by the tissue formation take place in the same anatomical site, to maintain bone mass (Fig. 2.6). Remodeling is a complex coordinated process which is regulated by hormones, large number of growth-factors and cytokines [82,83]. It allows to guarantee bone tissue turnover in adult skeleton while preserving bone strength and integrity. It also plays an important role in maintaining the normal mineral homeostasis [84]. Bone renewing is an essential process in order to repair microdamages caused by daily physical load. Interestingly, during the human life time, the total mass of bone substance in the skeletal system is synthesized and resorbed, in normal conditions, every five to six years [85].

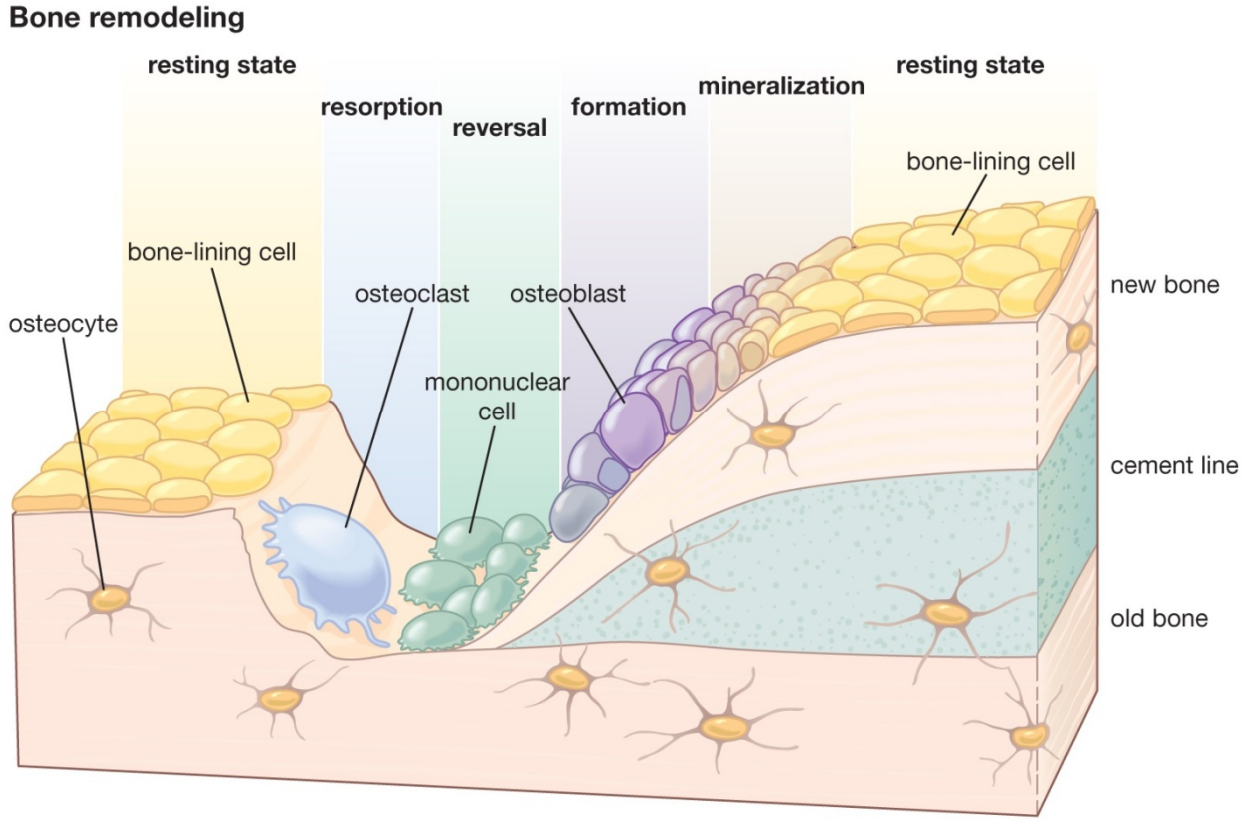

Figure 2.6: Schematic diagram representing the process of bone remodeling [86].

The remodeling cycle consists of five sequential phases, namely, activation, resorption, reversal, formation, and mineralization. The activation phase starts by initiating a remodeling signal triggered by osteocytes. In the resorption step,

osteoblasts respond to signals generated by osteocytes, or direct endocrine activation signals, by recruiting osteoclast precursors to the remodeling site. The subsequent reversal phase is characterized by disappearance of almost all osteoclasts. The formation stage is characterized by the complete replacement of osteoclastic cells with osteoblastic ones. The mineralization step includes the terminal differentiation of the osteoblasts. The resting bone surface environment is maintained until the next wave of remodeling is initiated.

Since bone is a highly active metabolic tissue, it possesses the capacity to regenerate even in case of severe fractures (Fig. 2.7) [87].

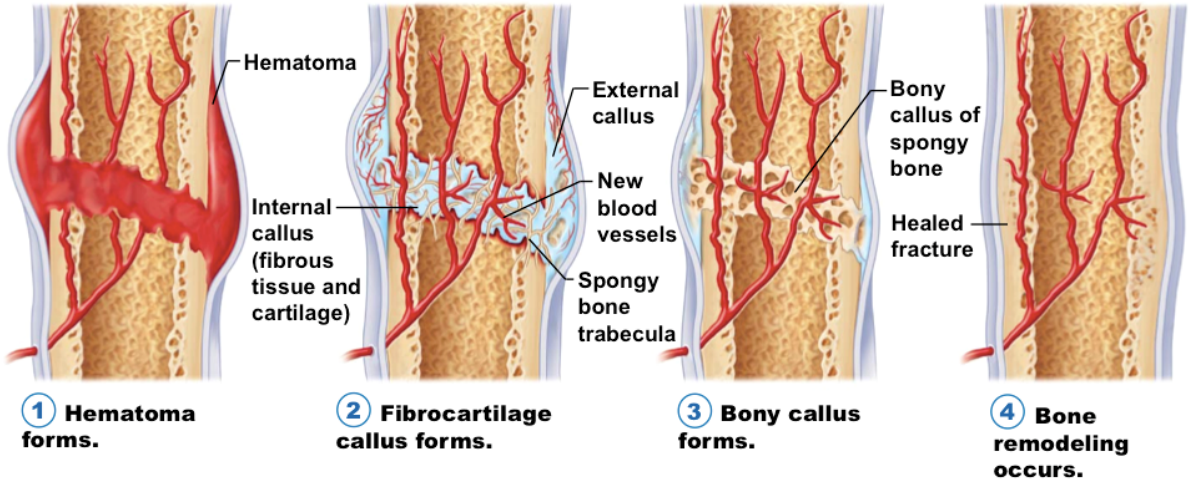

Figure 2.7: Schematic process of bone self-healing [88].

Generally, bone defects can heal spontaneously without fibrous scar formation, at least under suitable physiological conditions. In particular, the fracture bone undergoes four stages of healing:

- Formation of a hematoma (blood-filled swelling);
- Formation of a fibrocartilage callus;
- Bony callus replaces fibrocartilage callus;
- Bone remodeling occurs as response to mechanical stresses.

Each of these steps is characterized by a specific set of cellular and molecular events.

However, when the bone loss exceeds a critical size, self-repair is hindered, which means that cells cannot migrate from one bone side to the other. In the literature, this kind of defects is known as critical-sized defects (CSD). Due to the specific factors that affect healing process, there is no consensus regarding the exact dimension of the CSD [89]. In general, “critical-sized bone defects are technically defined as those that will not heal spontaneously during the patient’s lifetime” [90]. They should cause the damage in both cancellous and cortical bone and be stable [91]. Currently, the animal model that describes critical bone defects is considered as the most suitable for studying bone healing mechanisms [92].

Among the causes of large bone defects, the most common ones are fractures, infection, inflammatory arthritis, osteoporosis, osteonecrosis, metabolic bone disease, tumors, and musculoskeletal disorders such as rheumatoid arthritis [93,94]. Additionally, the risk of fractures increases with age due to the reduced release of specific agents and hormones involved in bone regeneration process. Indeed, osteoblasts become gradually less effective in repairing of microfactures, which, in general, leads to the decrease of bone density.

It should be noted that, the process of bone formation, healing and remodeling has to be considered in the due attention when addressing the challenge of designing biomaterials for bone regeneration.

Chapter 3. State of Art in Bone Repair

3.1 Clinical need of materials for bone repair

Every year more than two million of people undergo different bone grafting procedure, including knee and hip replacement, spinal fusion, reconstructive, maxillofacial and others operations [95,96]. Indeed, bone one of the most transplanted tissues all over the world, the second only after blood [97]. Bone grafts made from different biomaterials are utilised in order to fill voids and to provide solid support on which cells can anchor and build new bone.

Currently there are different accepted definitions of biomaterials (materials used for grafting). The first one was given by the American National Institute of Health in 1984 and described biomaterial as ‘‘any substance or combination of substances, other than drugs, synthetic or natural in origin, which can be used for any period of time, which augments or replaces partially or totally any tissue, organ or function of the body, in order to maintain or improve the quality of life of the individual’’. Additionally, on the Consensus Conference of the European Society for Biomaterials (1986) it was stated that biomaterial is “a nonviable material used in a medical device, intended to interact with biological systems”. In this regard, another important term that needs to be specified is “tissue engineering” (TE). According to the currently accepted definition, TE is “an interdisciplinary field that applies the principles of engineering and life sciences toward the development of biological substitutes that restore, maintain, or improve tissue function or a whole organ” [98].

Generally, the ideal bone tissue substitute for critical-sized bone defects has to provide an environment that mimics bone’s natural healing process. More accurately, it should possess both osteogenesis and angiogenesis properties, be sufficiently

resistant from the mechanical viewpoint and provide integration with host tissues, as well as facilitate load transfer under weight-bearing conditions.

Traditionally, due to their biological origin, the applied materials for the treatment of large bone defect are the following:

- autologous bone (from the same patient),
- allogeneic bone (from another patient),
- xenogeneic bone substitutes (from an animal or coral).

Autologous (or Autogenous) grafts

Nowadays, the procedure involving the use of autologous bone, is accepted as a 'gold-standard' in bone grafting [99,100]. In this case, bone tissue is transplanted from one site to another within the same individual [101].

The advantage of autogenous bone lies in the possession of all essential elements for successful bone repair. For instance, autogenous bone is osteoconductive and osteoinductive, as well as it houses growth factors and osteogenic cells with no associated immune-related risks. During the healing process, autologous bone is gradually replaced by the newly forming bone. However, there are various issues and risks associated with the use of autologous bone, namely: high percentage of donor site morbidity [102,103]; difficulties related to the shaping of the bone graft, limited quantity of the material, infections, and neurovascular injury [104]. Additionally, in case of pediatric and elderly patients, autogenous bone availability is significantly limited.

Allogeneic bone

Allogeneic bone can either be derived from cadavers or living donors. It represents alternative approach to the autologous bone. In order to avoid host-versus-graft immune response, allografts have to be processed, prior implantation, to remove all living cellular components. This procedure alters the biological properties of allograft. In particular, the final bone graft contains the osteoconductive mineral basis

for bone healing, but lacks the osteogenic properties of autologous bone. The main drawbacks associated with the use of allogeneic bone are the inherent risk of infection transmission and induced unfavourable host immune response, which leads to the rejection and additional operations [105,106].

Xenogenic bone

Xenogeneic bone, another heterologous grafting material, is derived from animal species other than humams. For instance, coral (natural source of hydroxyapatite), cattle, horses, and pigs. Generally, this type of materials is relatively inert and slowly resorbable in physiological conditions. Skeleton of corals that consists of calcium carbonate ($CaCO_3$) are used to obtain natural hydroxyapatite (HA). Bovine bone is also utilized in bone grafting. Similarly to allogeneic bone, bovine bone has to undergo a specific treatment, namely, deproteinization, meaning that all organic components should be chemically removed.

Despite its high biocompatibility, main disadvantages of this type of materials include brittleness and difficulty to handling [107]. The availability of xenogeneic formulations is also limited and, similarly to their allogeneic counterparts, the use of xenografts is associated with risks of infection transmission.

3.2 Properties required to design materials for bone tissue repair

An alternative approach, developed in order to overcome limitations of autologous, allogeneic and xenogeneic bones, consists of using synthetic materials with tuneable properties to restore areas of bone loss. The ability to control the chemical composition and structure of such material is crucial in order to obtain a correct biological interaction between the artificial graft and host living tissue. It is worth to mention also that, depending on the application, specific characteristics of biomaterials are required. Ideally, the synthetic biomaterial should as possible mimic the tissue at the site of restoration. However, since this is a difficult task to achieve, the following characteristics are generally required:

Biocompatibility

This property implies no toxicity, no inflammatory reaction, no hemolysis, and no coagulation reaction, meaning that a material can be safely used in the human body. Definition of biocompatibility was provided by various authors depending on the context [108,109]. In general terms, "Biocompatibility is defined as the ability of a biomaterial to perform its desired function with respect to a medical therapy, without eliciting any undesirable or systemic effects in the recipient or beneficiary of that therapy, but generating the most appropriate beneficial cellular or tissue response in that specific situation, and optimizing the clinically relevant performance of the therapy" [110].

Osteoinductivity

Osteoinductivity can be defined as the ability of a material to trigger osteogenesis (the process of new bone formation) [111,112]. It "means that primitive, undifferentiated and pluripotent cells are somehow stimulated to develop into the bone-forming cell lineage" [113].

Osteoconductivity

An osteoconductive material should allow cell attachment, proliferation, multiplication, migration, in order to form extracellular matrix on its surface and into its pores [113].

Mechanical properties

The material for bone graft should possess suitable mechanical properties to match those of natural bone at the site of implantation, i.e. bending, compressive and tensile strengths as well as fatigue resistance, to sustain loads applied during bone growth and remodelling [114,115].

Biodegradability

The material resorption rate should match the one of bone regeneration growth [115].

Porosity and pore size

There is no consensus on the optimal porosity and pore size. Porosity and interconnectivity between the pores are important for the distribution of nutrients, especially in a microenvironment that lacks neovascularisation. Additionally, the size of the pores determines the types of molecules that can navigate through or that can be entrapped for subsequent release [115–118].

Surface properties

In order to provide effective cell attachment, differentiation and proliferation, a suitable surface chemistry and topological features are required [119–121].

Processing

The fabrication process of a final graft should not affect the original material properties and subsequent clinical use. Additionally, grafts should be readily produced into irregular shapes that match the defects in the bone of individual patients [122].

Commercialisation

Materials for bone grafting should be fabricated at an acceptable cost for commercialization [122].

3.3 Classification of biomaterials depending on a type of host tissue response

As mentioned above, when a synthetic material is placed within the human body, tissue reacts towards it. This specific reaction depends on the characteristics of the implant material. According to these types of the reactions, the following classification of biomaterials can be defined (Table 3.1, adapted from [123]). It worth to mention that, the classification reported below is very simplified and does not strictly provide the real biomaterial behaviour.

Graft/tissue interaction	Tissue reaction	Materials examples
Biotoxic	Atrophy, pathological change or rejection of living tissue near the material as a result of chemical, galvanic or other processes	Alloys containing cadmium, vanadium, and other toxic elements, carbon steels, carbides, methylmethacrylate
Bioinert	Coexistence with the material without noticeable change, separation from material by a layer of fibrous tissue	Tantalum, titanium, alumina and zirconia ceramics
Bioactive	Formation of direct biochemical bonds with the surface of the implanted material, new bone free growth	Bone autografts, hydro-xyapatite and tricacium phosphate, bioglasses
Bioresorbable	Gradual dissolution of the material by the biosystems of the organism, replacement without toxicity and rejection	Porous tricalcium phosphate, calcium phosphate salts, some bioglasses, polyurethan

Table 3.1: Biomaterials classification according to the surrounding tissue reaction.

Indeed, as pointed out very recently when considering the typically called bioinert ceramics the term “bioinert” should be used carefully, since any material placed within living body provokes a response [124]. However, for sake of simplicity, such classification will be still considered hereto after in the present study.

3.4 Biomaterials for bone tissue repair

In general, materials that can be used for bone grafting can be classified into the four main groups: metals, polymers (natural and synthetic), ceramics (as well as glasses) and composites. Metals, polymers and ceramics possess different properties that, in turn, determine their applications. However, on their own, these materials are able to mimic biological tissues only to a certain extent, especially in case of bones. The use of composites, which combine the properties of two or more biomaterials, represents a promising approach to overcome the current limitations of single-phase materials.

3.4.1 Metals

Traditionally, metals are used in order to replace load-bearing bones [125], for instance, in case of total hip joint replacement. Other important applications of metallic biomaterials are in the field of dentistry and orthodontics. Metals and alloys which are currently applied for implant manufacturing include Fe, Cr, Co, Ni, Ti, Ta, Mo and W. They possess a combination of favourable mechanical properties, such as tensile strength, fracture toughness and fatigue strength, which are required for load-bearing or strain applications. In addition, they are relatively non-cytotoxic, at least in limited quantities. However, one of the main drawbacks of the metallic biomaterials is the fact that metal cannot mechanically replicate bone due to the dramatically different Young's moduli (Table 3.2, adapted from [100]). Therefore, after implantation, surrounding bone tends to undergo undesirable change in the mechanics (stress shielding) and, as a long term outcome, bone gradually become weaker and prone to fracture. Another crucial issue related to the use of metals for grafts is corrosion caused by the chemical reaction with the physiological environments (enzymes and acids). As a result, loss of the structural integrity of the implant, accompanied by the release of toxic elements in high amount, can occur in some cases [126,127].

Material	**Young's modulus (GPa)**	**Ultimate tensile strength (MPa)**
Cortical bone	7-25	50-150
Cancellous bone	0.1-1	<1
Stainless steel 316L	200	207-1160
CoCrMo alloy	230	430-1028
Ti-6Al-4V	105	780-1050

Table 3.2: Comparative mechanical properties of bone and metals used for biomedical purposes (adapted from [100]).

3.4.2 Natural and synthetic polymers

Natural and synthetic polymers typically exhibit excellent biocompatibility and customizable properties, i.e. their chemistry and biodegradation rate can be tailored according to the application [125,128]. Therefore, they are widely applied in field of tissue engineering and regenerative medicine.

Collagen, heparin, chitosan, gelatine, hyaluronan, alginate, and cellulose represent biopolymers that can be derived from natural sources in abundant amount. Natural polymers mimic components which are present in extracellular matrices, while synthetic ones are relatively versatile, for instance Poly(Epsilon-Caprolactone) (PCL), Poly-vinyl chloride (PVC), Poly(Lactic-co-Glycolic acid) (PLGA) and others. The particular advantage of polymers is that they can promote cell attachment, proliferation, and differentiation through the use of bio-functional molecules [129,130]. However, the application of polymers, especially natural ones, is limited nowadays because of their poor stability during processing (instability at high temperatures), propensity to swell when in contact with organic fluids, and, mostly, due to the strength limitations.

3.4.3 Bioceramics

Bioceramics represent a broad class of advanced materials to be employed in bone grafting and dentistry. According to the definition given by Hench “bioceramics are those ceramics used for the repair and reconstruction of diseased or damaged parts of the musculoskeletal system” [13].

Bioceramics constitute a subset of biomaterials that can display either amorphous or crystalline structure. This class of the materials includes bioactive glasses, such as Bioglass®, glass-ceramics, and Calcium Phosphates (CaP) based ceramics [56,131,132].

Within the human body, bioceramics can be applied in different forms, i.e. as solid pieces (parts of joint prosthesis or in the reconstruction of middle ear ossicles), or as

powders and granules, to be used for bone filling. Other forms of bioceramics currently applied in the field of tissue engineering include coatings and porous scaffolds. The broad range of bioceramic's clinical applications is shown in Figure 3.1 [133].

It is worth mentioning that, according to the general classification (Table 3.1), bioceramics can also be divided into the following subtypes, based on the associated *in vivo* reaction:

(i) Bioinert: ceramics that have a modest interaction with the body (e.g., alumina, and zirconia);
(ii) Bioactive: ceramics that bond directly with bones, without having fibrillar connective tissue between them (e. g. hydroxyapatite, bioactive glasses);
(iii) Resorbable: ceramics that degrade gradually over time allowing bone in-growth and eventual replacement of the artificial material with the natural tissue (Tricalcium phosphate (TCP)-based ceramics).

Bioinert ceramics, such as Al_2O_3 and ZrO_2 have a high chemical stability *in vivo* as well as high mechanical strength; they induce a minimal adverse response in the surrounding physiological environment [134–136].

As indicated above, HA and glass-based ceramics belong to the class of *bioactive ceramics* that differ from bioinert one through the ability to bond directly with the living tissue [137]. According to the definition of bioactivity: "A bioactive material is one that elicits a specific biological response at the interface of the material which results in the formation of a bond between the tissues and the material" [138]. The concept of "bioactivity" will be discussed in more detail in Paragraph 3.5.

On the other hand, *bioresorbable ceramics* completely dissolve over time and are intended to be replaced by the natural host tissue [73, 74]. In this regard it is worth to mention that, the ceramic dissolution rate should match the kinetic of the newly bone formation, as well as ceramic graft should exhibit appropriate mechanical properties

during the healing process. On the other hand, generally, bone formation is slower, with respect to ceramic resorption, so that particular attention should be paid when designing bioresorbable ceramics.

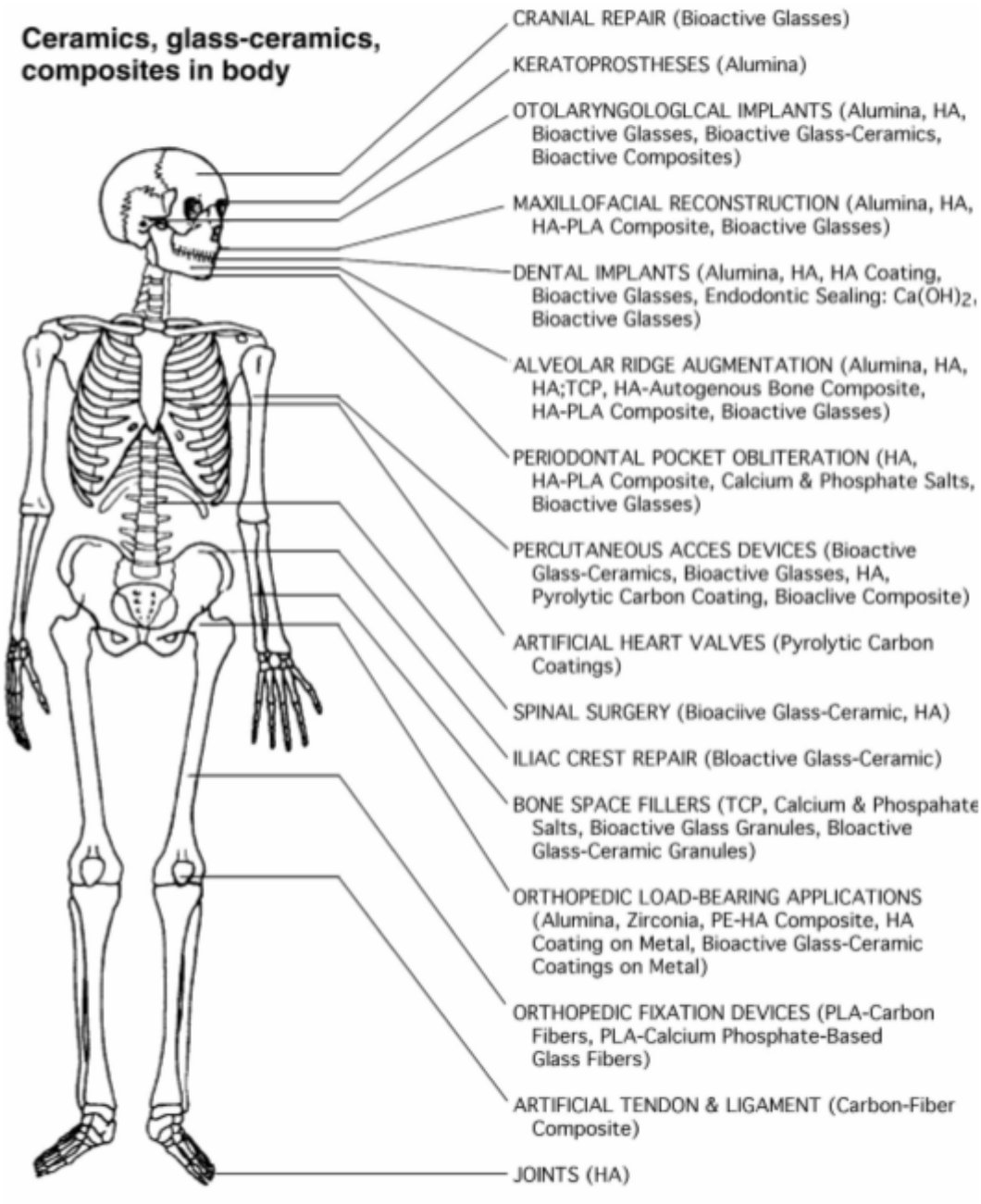

Figure 3.1: Clinical use of bioceramics and composites [133].

3.4.3.1 Calcium Phosphate-based Ceramics (CaP)

Among bone substitute materials, calcium phosphate (CaP)-based ceramics have drawn great interest due to the similarity with the mineral component of human bone [139]. Indeed, they have been extensively applied for hard tissue repair and regeneration, both in orthopedics and dentistry, due to their good biocompatibility, osseointegration and osteoconduction for the last 40 years [140].

There are numerous compounds in the CaP-based system (Table 3.3 adapted from [139]); the most commonly investigated ones are the following: HA, β-tricalcium phosphate (β-TCP) and biphasic calcium phosphate (BCP) [134,139,141].

Compound	Abbreviation	Chemical formula	Ca/P ratio
Monocalcium phosphate monohydred	MCPM	$Ca(H_2PO_4)\cdot H_20$	0.5
Dicalcium phosphate dihydred	DCPD	$CaHPO_4\cdot 2H_20$	1.0
Octacalcium phosphate	OCP	$Ca_8H_2(PO_4)_6.5H_2O$	1.33
α-Tricalcium phosphate	α-TCP	α-$Ca_3(PO_4)_2$	1.5
β-Tricalcium phosphate	β-TCP	β-$Ca_3(PO_4)_2$	1.5
Amorphous Calcium Phosphate	ACP	$Ca_9(PO_4)_6$	1.2-2.2
Hydroxyapatite	HA	$Ca_{10}(PO_4)_6(OH)_2$	1.67
Fluorapatite	FA	$Ca_5(PO_4)_3F$	1.67

Table 3.3: Selected CaP-compounds with corresponding chemical formula, abbreviations and ratio Ca/P (adapted from[139]).

3.4.3.1.1 Hydroxyapatite (HA)

HA is a complex phosphate of calcium with a Ca/P ratio equal to 1.67 and chemical formula $Ca_5(PO_4)_3OH$ or, more often, $Ca_{10}(PO_4)_6(OH)_2$, to indicate that the crystal cell unit consists of two molecules. Among the family of CaP-based compounds, HA represents the most investigated one. Morphological features, physicochemical and

biological properties of HA have been extensively explored for biomedical applications [142–146].

Structurally and compositionally, HA shares similarities to inorganic component of bone tissue; therefore, for a long period of time, HA was exploited as a model compound to mimic the biomineralization process [147,148].

The main advantages of HA-based ceramics comprise [149]:

- excellent biocompatibility;

- bioactivity (indeed, HA supports nucleating sites for the precipitation of apatite crystals in culture medium [150]);

- non-inflammatory behavior, non-immunogenicity;

- high osteoconductive, osteoinductive properties.

In order to describe the interaction between HA-based ceramic and bone tissue, the model schematically shown in Figure 3.2 was suggested [151]. The mechanism consists of the following 8 subsequent steps:

1-2) solubilization of the hydroxyapatite surface; 3) achievement of the equilibrium condition between physiological fluids and the modified surface of hydroxyapatite; 4) adsorption of proteins and organic material; 5-6) cell adhesion and proliferation; 7) beginning of new bone formation; 8) new bone formed.

Despite undeniable advantages offered by HA-based ceramics, there are also different drawbacks currently limiting their applications, such as resorption rate *in vivo* and mechanical properties.

Indeed, from the thermodynamical point of view, HA is the most stable CaP compound under the physiological conditions (body temperature, pH and body fluids composition) [152].

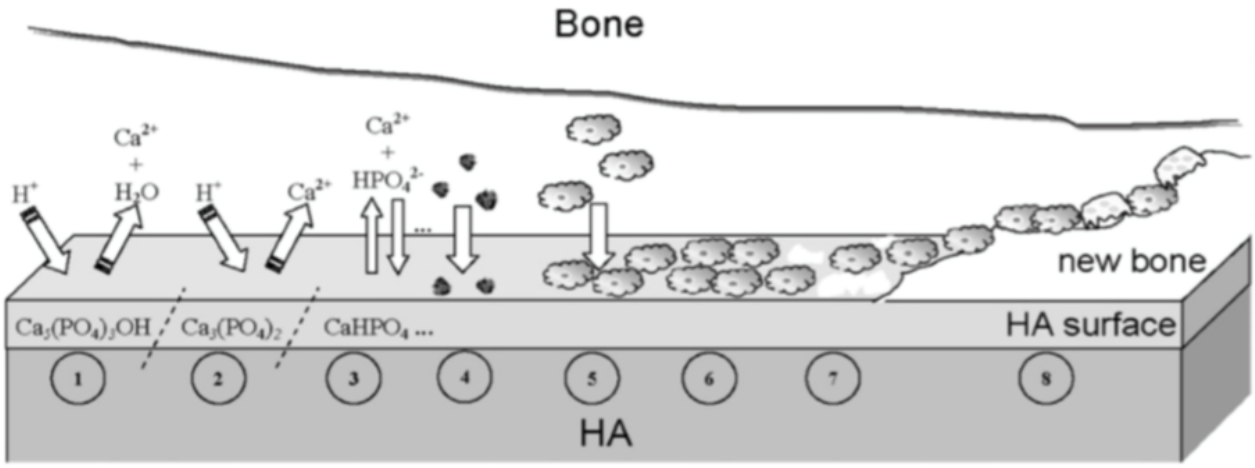

Figure 3.2: Schematic representation of the phenomena that occur on the surface of HA after implantation [151].

Thus, HA resorbs slowly and undergoes little conversion to a bone-like material after implantation. The native dissolution rate of crystalline HA *in vivo*, approximately 10 wt.% per year, is significantly lower than the growth rate of newly formed bone tissue [153]. Therefore, the application of crystalline HA-based bioceramics is hindered in bone grafting, where an adequate degradability level is required.

Another major limitation of HA-based ceramics concerns their mechanical properties. Depending on the porosity, density, sinterability, and crystal size, mechanical properties of HA may vary significantly [154]. In general, HA-based ceramics are brittle with a poor fatigue resistance, so that they are not generally suitable for load-bearing applications [155].

However, despite such limitations, HA is used in a number of different applications, namely, in craniomaxillofacial reconstruction, spinal surgery, as well as coating in orthopedic (e.g., hip joint prosthesis) and dental implants [155–158]. Due to the similarity to biological apatite, HA is also employed in diverse non-medical applications including chromatography of nucleic acids, proteins, and other biological compounds and for drug delivery purposes [140]. Additionally, HA is added to some brands of toothpaste [159].

Since pure HA cannot be found in biological systems, different techniques have been developed so far in order to synthesize it. In general, they can be divided into solid-state reactions and wet methods [160], including precipitation, hydrolysis, and hydrothermal synthesis [161]. It should be stressed that physicochemical properties and morphology of HA significantly depend on the origin/preparation method.

3.4.3.1.2 Biomimetic nanocrystalline apatites (BNAs)

As discussed in Chapter 2 (Paragraph 2.2.2.2), the main inorganic part of animal and human normal bone tissue can be reliably represented as an ion-substituted nanocrystalline apatite [162]. The better understanding of the structure and composition of biological apatites allowed recently to synthesize their biomimetic analogous, which are also referred in the literature as calcium-deficient hydroxyapatites (CDHAs). For instance, it is known that biological apatites appear to be poorly crystalline compounds; their chemical composition depart from the stoichiometric crystalline phase, namely hydroxyapatite (HA, $Ca_{10}(PO_4)_6(OH)_2$), by calcium and hydroxide ions deficiency [163]. In this light, BNAs attracted much attention so far, since they can closer approach the natural biological apatite. Indeed, the deficiency in the amount of Ca, the imperfections, and vacancies, are taken into account in the BNA structure [164]. Disorders and vacancies, in turn, determine the fact that BNAs are more soluble, and possess higher resorption rate *in vivo* [165]. Moreover, the vacancies present in nanocrystalline apatites can be occupied by divalent anions, such as hydrogen phosphate (HPO_4^{2-}) or carbonate (CO_3^{2-}). Magnesium or strontium can also substitute calcium ions in BNAs.

Regarding the preparation of synthetic biomimetic apatites, several routes have been proposed, such as, precipitation by double decomposition, hydrolysis, sol-gel, and hydrothermal methods. It is worth to mention that, the method selected to prepare BNA determines the amount and kind of substitutions [166].

In case of precipitation by double-decomposition, the temperature and pH are strictly related to the degree of crystallinity and calcium deficiency in the obtained apatite. An effect produced in these materials by their maturation or aging in solution was also observed. Specifically, freshly-precipitated poorly crystallized, non-stoichiometric apatites exhibit a tendency to evolve in solution toward stoichiometry and greater crystallinity [72,167]. The systematic studies of the physico-chemical properties and the impact of synthesis and post-synthesis parameters on BNA formation are available in the literature [163,166,168,169].

BNA is considered as a very promising material for artificial bone substitutes [170]; for instance, it can be used to prepare cements, coatings and composites biomaterials [166].

3.4.3.1.3 Amorphous Calcium Phosphates (ACPs)

ACPs represent a special class of CaP and can be found in various biological systems, especially in primitive organisms [171]. ACP possesses short range order in the form of roughly spherical $Ca_9(PO_4)_6$ units, with an average diameter of 0.95 nm, known in the literature as “Posner’s clusters” (Fig. 3.3) [172].

It is worth to mention that, ACP is an intermediate phase formed during the preparation by precipitation of the several CaPs reported in a Table 3.3, and it is currently considered as a precursor phase of bone mineral in vertebrates. Indeed, several authors have recently provided evidence that ACP appear as a transitory phase during the mineralization of calcified tissue. More precisely, ACP was detected in newly formed (outer) murine tooth enamel, newly formed fin bones of zebrafish and in the early intramembranous mineralisation of murine calvaria tissue [173–175]. However, due to the various crucial aspects related to the accurate sample preparation and/or analysis without altering of initial material state, even nowadays the issue of the occurrence of an ACP phase in such newly mineralised tissues of vertebrates remains highly debated.

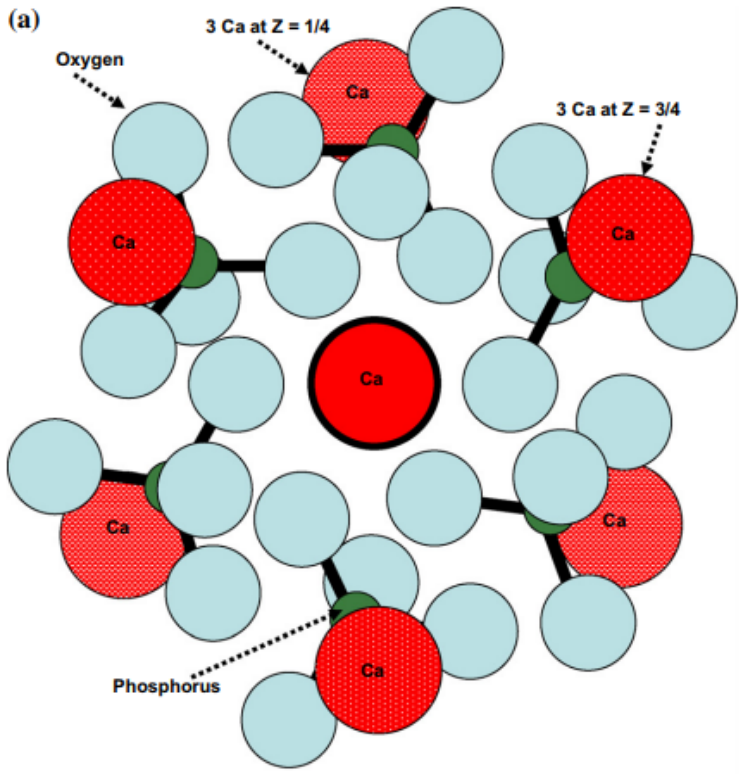

Figure 3.3: Structure of ACP. Representation of Posner's cluster with a S_6 symmetry. Three calcium ions are superimposed (red), forming a column on the C_3 axis of the figure located at z = 0, 1/2 and 1. Two other groups of three calcium ions are at the periphery of the cluster at z = 3/4 and z = 1/4 positions. Phosphorus atoms (green) of phosphate groups are at z = 1/2 position, with two of the oxygen atoms (blue) of the phosphate tetrahedrons. The global chemical composition corresponds to $Ca_9(PO_4)_6$ [176].

The various methods adopted so far to prepare and stabilize the ACP phase were summarized in a comprehensive review by Combes and co-workers [176]. For instance, ACPs can be synthesized at low-temperature by wet precipitation technique [177] or using high energy processing method. The latter one, a dry route, appears to be less common, since it does not allow to obtain large amounts of pure ACP. On the other hand, the wet technique based on the double decomposition of calcium and phosphate salts in aqueous or water–alcohol solutions are more widely applied. However, the chemical composition of ACPs prepared by precipitation strongly depends on the pH, temperature and concentration of solutions [164]. Indeed, due to

instability of ACP and its reactivity in solution, it could easily convert into nanocrystalline apatite (analogous to bone mineral, see 3.4.3.1.2). This feature is particularly interesting for the preparation of novel biomaterials which can better mimic the composition of a bone mineral. Among the current applications of ACPs, there are injectable cements for orthopaedic applications, dental fillers and coatings on metal prosthesis [176].

3.4.3.2 Bioactive Glass and Glass Ceramics

Glasses are non-crystalline amorphous solids without long-range order that are commonly composed of silica-based materials with other constituents. Those ones which are used in biomedical properties ("bioglasses") differ from soda-lime glass (commonly used in windows or bottles) compositionally; in particular, less silica and higher amounts of calcium and phosphorus are present in bioglasses. The original bioactive glass, also known as Bioglass® 45S5, was developed in 1969 by Professor Larry Hench.

Herein a short historical overview on "how bioglass was invented?" [178]:

… Bioglass is important to biomaterials as one of the first completely synthetic materials that seamlessly bonds to bone. It was developed by Professor Larry Hench and colleagues. In 1967 Hench was Assistant Professor at the University of Florida. At that time his work focused on glass materials and their interaction with nuclear radiation. In August of that year, he shared a bus ride to an Army Materials Conference in Sagamore, New York with a US Army Colonel who had just returned from Vietnam where he was in charge of supplies to 15 MASH units. This colonel was not particularly interested in the radiation resistance of glass. Rather, he challenged Hench with the following: hundreds of limbs a week in Vietnam were being amputated because the body was found to reject the metals and polymer materials used to repair the body. "If you can make a material that will resist gamma rays why not make a material the body won't resist?"

Hench returned from the conference and wrote a proposal to the US Army Medical R and D Command. In October 1969 the project was funded to test the hypothesis that silicate-based glasses and glass-ceramics containing critical amounts of Ca and P ions would not be rejected by bone. In November 1969 Hench made small rectangles of what he called 45S5 glass (44.5 weight % SiO_2), and Ted Greenlee, Assistant Professor of Orthopaedic Surgery at the University of Florida, implanted them in rat femurs at the VA Hospital in Gainesville. Six weeks later Greenlee called: "Larry, what are those samples you gave me? They will not come out of the bone. I have pulled on them, I have pushed on them, I have cracked the bone and they are still bonded in place." Bioglass was born, and with the first composition studied! Later studies by Hench using surface analysis equipment showed that the surface of the bioglass, in biological fluids, transformed from a silicate rich composition to a phosphate rich structure, possibly hydroxyapatite …

The concept proposed by Professor Larry Hench completely revolutionized the field of biomaterials. Indeed, the general trend in bone repair shifted from the development of non-toxic inert biomaterials to the obtainment of materials that once implanted, directly bond with host tissues and, most importantly, stimulate body's own regenerative capabilities. The mechanism for bone bonding between bioglass and host tissue was further attributed to the formation of hydroxycarbonate apatite (HCA) layer on the surface of the glass, following the initial glass dissolution. HCA is close compositionally to bone mineral and is thought to interact with collagen fibrils to integrate (bond) with the host tissue [179]. Paragraph 3.5 describes in details the bioactivity mechanism and HCA formation.

Other valuable features of bioactive glasses include their ability to enhance revascularization, osteoblast adhesion, enzyme activity, and differentiation of mesenchymal stem cells [179].

The original glass invented by Prof. Hench, that further was trademarked as 45S5, had the following composition (wt.%): 45% silica (SiO_2), 24.5% calcium oxide

(CaO), 24.5% sodium oxide (Na_2O), and 6% phosphorous pentoxide (P_2O_5) in weight percentage [180].

It is worth to mention that, depending on the chemical composition of bioactive glass, its biological behavior (in particular, the ability to bond with bone) can vary significantly. In this regard, Figure 3.4 shows Na_2O-CaO-P_2O_5-SiO_2 glass composition (constant 6 wt% of P_2O_5) dependence for hard and soft-tissue bonding.

Region I is the bioactive-bone bonding zone, and glasses with composition inside it are able to bond with the bone.

Region II (e.g. composition of those silica glasses have applications including window, bottle or slides of microscope) behaves almost as inert materials and forms fibrous morphology at the implant-tissue interface.

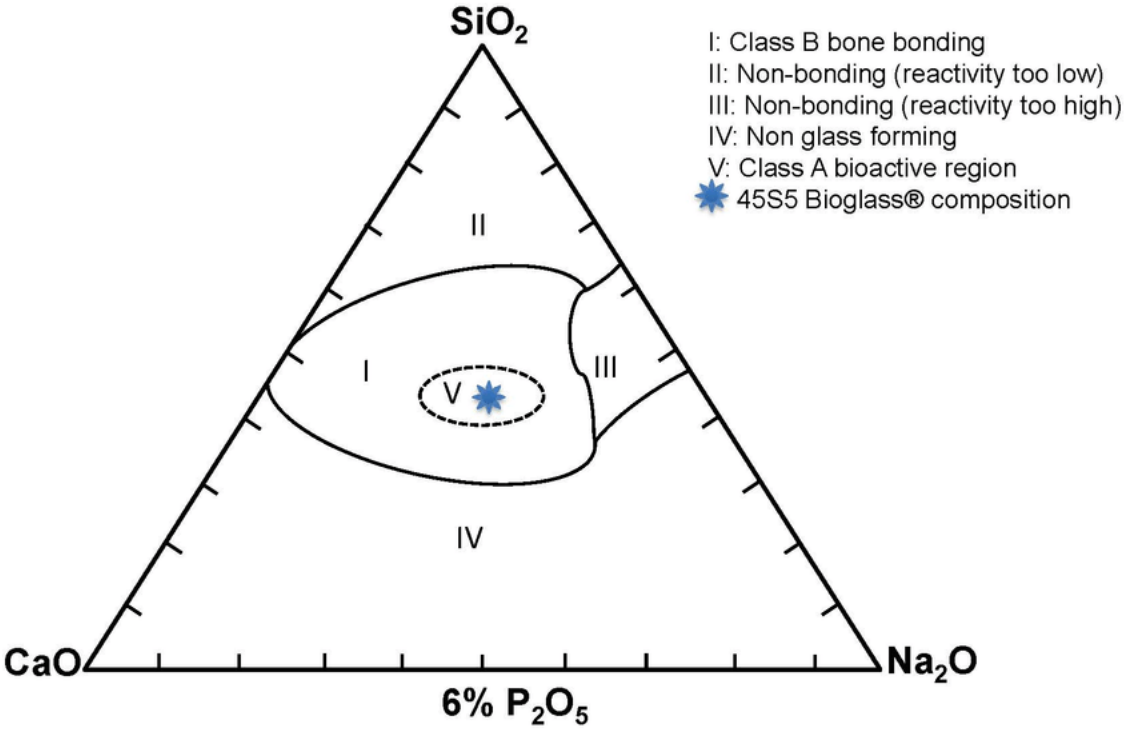

Figure 3.4: Compositional diagram for bone-bonding [181].

The compositional boundary between bonding to bone and non-bonding was found to be in the range of 60 wt% silica [182].

Region III compositions correspond to resorbable glasses, which disappears within a day once implanted.

Region IV is not practical technically and not tested in vivo.

Region V and * represents a bioactive region and 45S5 composition, respectively.

Afterwards, in order to improve the characteristics of original Bioglass®, systems with various compositions were proposed and investigated [179,183]; some of them are reported in Table 3.4.

Composition (wt%)	45S5	13-93	58S	70S30C	77S	13-93B1
SiO_2	45	53	58.2	71.4	80	34.4
K_2O	0	12	0	0	0	11.7
Na_2O	24.5	6	0	0	0	5.8
MgO	0	5	0	0	0	4.9
P_2O_5	6	4	9.2	0	4	3.8
B_2O_3	0	0	0	0	0	19.9
CaO	24.5	20	32.6	28.6	16	19.5

Table 3.4: Composition of different bioactive glasses [183].

The SiO_2-Na_2O-CaO-P_2O_5 system and, particularly, its ancestor (45S5 Bioglass®), is still used as a template to develop new silica-based formulations [184]. Recently, also borate [185,186] and phosphate formulations have been investigated [187,188]. However, according to review of Jones [179] even after a 40-year span of research on bioactive glasses, no other composition has been found to be more bioactive than 45S5 Bioglass®.

As far as the glass production techniques is concerned, various methods have been developed so far, such as the conventional melt quenching (for the first time introduced by Prof. Hench) [180] and the sol–gel [189–191].

It has been established that *in vivo* Bioglass® degrades more rapidly, and favors more rapid bone regeneration, unlike the synthetic hydroxyapatite [186]. Indeed, bioglass dissolution products (cations such as Na^+, K^+, Ca^{2+}, etc.) stimulate osteoprogenitor cells at the genetic level. After 1 week, there was 17 times more bone in defects filled with Bioglass, and twice as much bone after 24 weeks, compared to defects filled with HA [192].

Since 1985, several devices made from 45S5 Bioglass® have been used in clinical applications [180], for instance:

- "Bioglass® Ossicular Reconstruction Prosthesis" (tradename MEP®).
  It represents a device used to treat conductive hearing loss by replacing the bones of the middle ear.
- "Endosseous Ridge Maintainence Implant" (tradename ERMI®).
  This device was designed to support labial and lingual plates in natural tooth roots and to provide a more stable ridge for denture construction following tooth extraction.
- PerioGlas®.
  The initial indication for this product was to restore bone loss resulting from periodontal disease in infrabony defects. In 1996, PerioGlas® was approved to be used in tooth extraction sites and for alveolar ridge augmentation.

More recently, Bioglass® has been also employed for the treatment of dentinal hypersensitivity. It is used as an active repair agent in toothpaste, under the name NovaMin (GlaxoSmithKline, UK). Clinical studies show that the dentifrice can mineralize tiny holes in dentine, reducing tooth sensitivity (Fig. 3.5) [193].

Bioglass® is also used in different orthopedics, cranial-facial and dental-maxillofacial clinical applications [194].

Despite evident advantages demonstrated by bioactive glasses, in general they all suffer from several common drawbacks. First of all, due to the limited mechanical

strength, particularly low fracture toughness, bioactive glasses are suitable only for low-load bearing application areas in the human body.

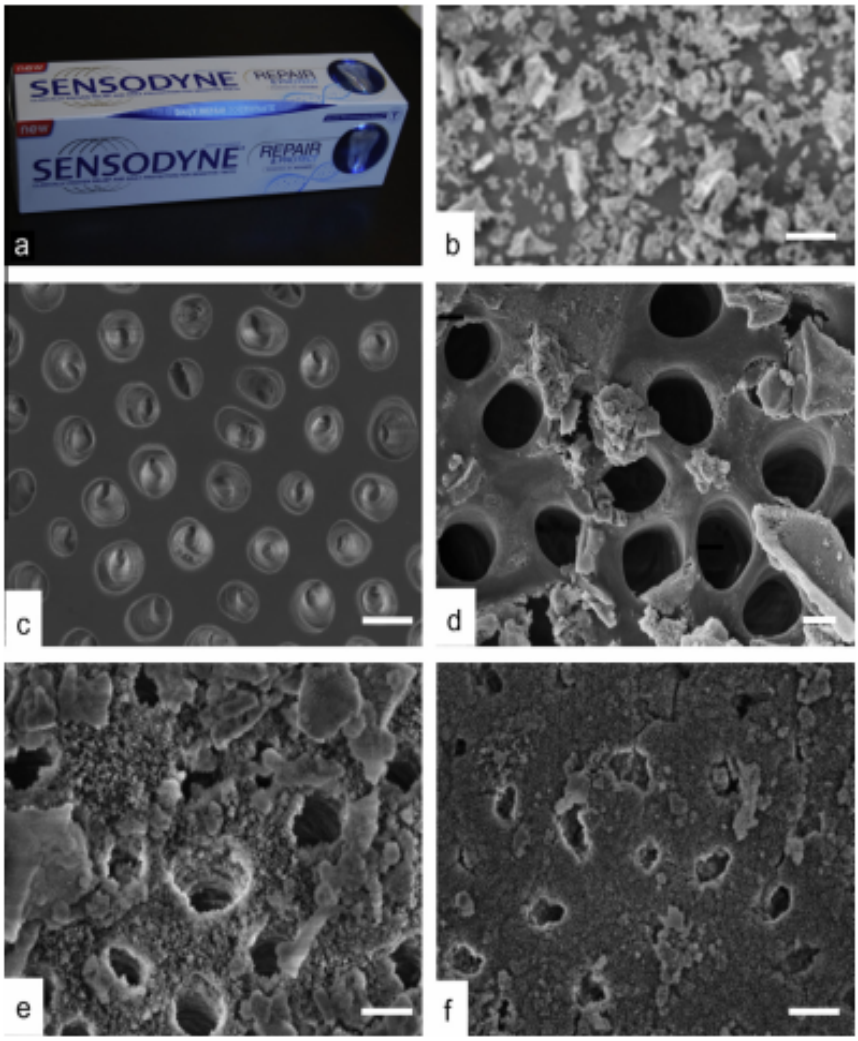

Figure 3.5: (a) Photograph of Sensodyne® Repair and Protect toothpaste, which contains NovaMin®; (b) SEM image of NovaMin® particles. (c-f) SEM micrograph of human dentine: (c) untreated, (d) immediately after application of Novamin® in artificial saliva (AS); (e) 24 h after application of NovaMin® in AS; (f) 5 days after application [179].

Another challenging issue is related to the processing of bioactive glasses, since alterations in glass amorphous structure arise during the sintering into bulk bodies or 3D porous scaffolds.

Indeed, the temperature and pressure levels, which typically need to be applied to densify BG powder, induce transitions from its original amorphous nature and modifications in its composition. Structural and compositional transformations in the 45S5 bioglass which occur, depending on the temperature, are reported in Figure 3.6.

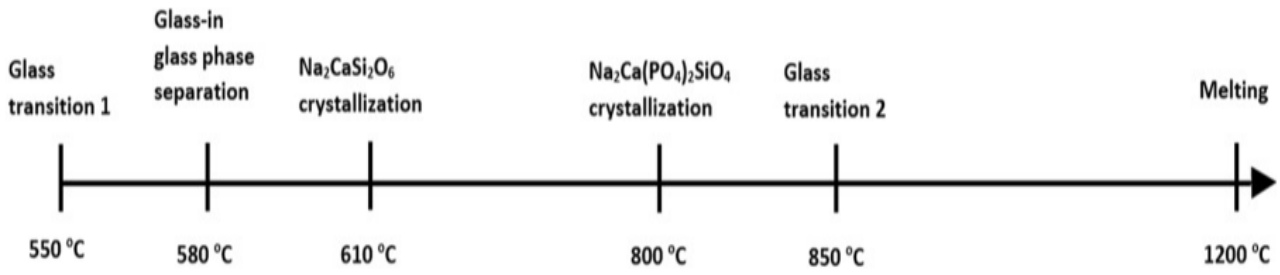

Figure 3.6: Summary of 45S5 structural transformation [195].

The devitrification process (crystallization) of 45S5 starts at approximately 610°C. The formation of different crystalline phases occurs correspondingly. As a result, crystallisation was reported to produce the deterioration in bioglass bioactivity performance, in particular, the reduction of the HCA precipitation rate was observed [196]. However, the effect of crystallization on the bioactivity is still controversial, since it was found that certain crystallization degree might be beneficial in terms of bioactivity [197,198]. In general, the limited sintering ability of glass leads to bulk materials with low densification level; thus weaker and less interconnected structures, accompanied by the formation of micro-cracks and poor mechanical strength, are obtained [199].

Recently, based on the understanding how the glass composition can be tailored to delay crystallization, new formulations have been proposed (a more detailed description can be found in Chapter 5).

As mentioned previously, the sintering step is fundamental to accurately control the structural and compositional changes of the powders during consolidation. In the Chapter 4, sintering phenomena and techniques will be discussed in details.

3.5 In vitro bioactivity of bioceramics

According to their definition, bioactive ceramics are the ceramics that possess “the ability to bond with host bone tissue” [13]. The concept of bioactivity attracted much attention since Hench introduced it at the beginning of 70’s, by the describing of the bonding process between 45S5 and host bone. The core concept of bioactivity lays in partial dissolution of the glass and the corresponding release of ions, followed by an increase of local concentrations of calcium and phosphate ions and the final precipitation of biological apatite (also known as carbonated hydroxyapatite layer) on the surface of ceramics *in vivo.* The sequence of reaction events involved during the bond formation between bone and a bioactive glass, initially proposed by Hench and subsequently modified by Gerhardt and Boccaccini [200], is reported in the Figure 3.7.

In order to avoid high costs of *in vivo* tests, the following *in vitro* assays were proposed:

1. A first approach, to estimate the HCA-formation ability of bioceramics soaked in an acellular simulated body fluid (SBF) [201].
2. A second one, to study *in vitro* bone cell response on bioceramics [202,203].

Regarding the first *in vitro* method, at least when considering bioactive glasses or apatite-wollastonite ceramics, in 1991 Kokubo stated that “the essential requirement for an artificial material to bond to living bone is the formation of bone-like apatite on its surface when implanted in the living body, and that this *in vivo* apatite formation can be reproduced in a simulated body fluid” [204].

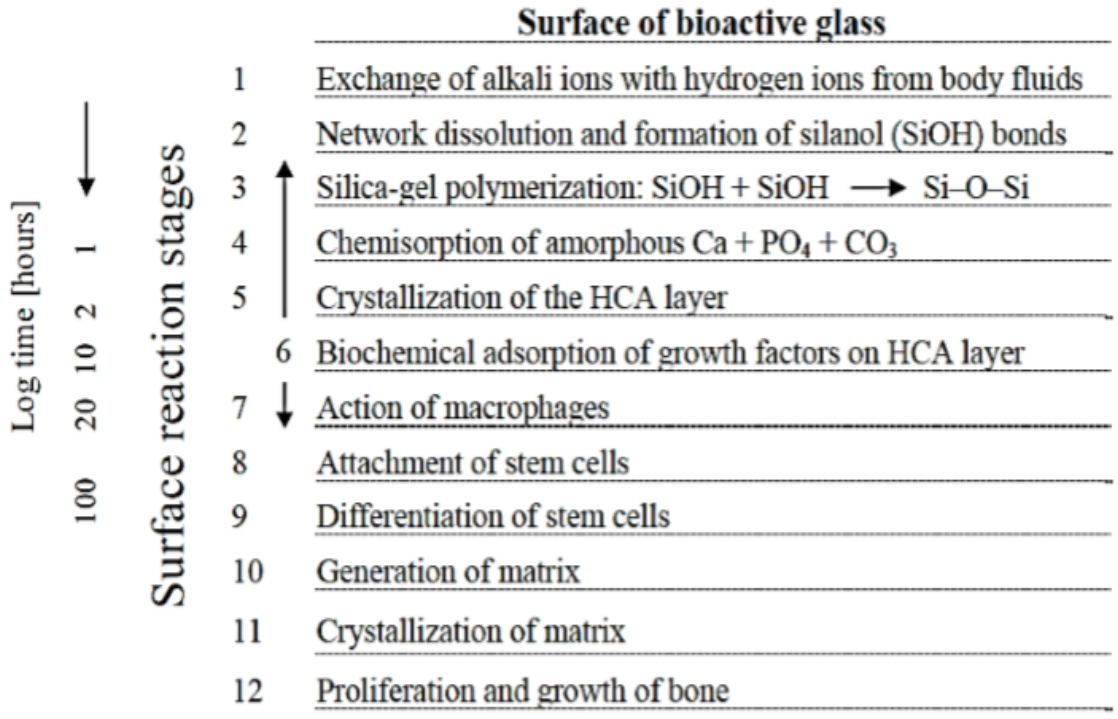

Figure 3.7: Sequence of reactions on the surface of a bioactive implant [205].

The key idea proposed by Kokubo comprises the use of an acellular SBF solution with an ionic concentration close to human blood plasma (Table 3.5). Since Kokubo protocol was proposed, the *in vitro* apatite formation on the surface of a material, when immersed in SBF, has been considered a useful method for assessing the potential *in vivo* bioactivity of new glasses or glass-ceramics.

	Na^+	K^+	Mg^{2+}	Ca^+	Cl^-	HCO_3^-	HPO_4^{2-}	SO_4^{2-}
Human blood plasma	142.0	5.0	1.5	2.5	103.0	27.0	1.0	0.5
SBF	142.0	5.0	1.5	2.5	148.8	4.2	1.0	0

Table 3.5: Ion concentration (*mM*) of human blood plasma and SBF solution [71].

However, Bohner and colleagues recently pointed that there is not enough scientific data to support Kokubo's statement [150]. Indeed, the reliability of this method

depends on the category of bioceramics tested and results of SBF assay need to be interpreted very carefully.

In case of silicate-based bioceramics, excellent apatite forming abilities in SBF have been observed. Correspondingly, excellent *in vivo* bioactivity was observed, which indicates that SBF testing is an efficient method to evaluate *in vitro* bioactivity. However, in case of phosphate-based bioceramics (HA for instance), and sulfate-based materials ($CaSO_4$), behavior *in vitro* and *in vivo* differs significantly. Indeed, while these materials exhibit good bone formation abilities during *in vivo* test, SBF experiments did not the reveal same good formation of HCA layer. As a result, test in SBF alone cannot be considered sufficient to predict the bioactivity.

A most likely explanation of this discrepancy can be related to the fact that "the biochemistry of *in vivo* bone formation of these bioceramics is significantly different" [206]. Briefly, the mechanism of the bonding with host bone of silicate-based bioceramics lies in the formation of bone-like apatite layers after the initial glass dissolution and ions release. On the other hand, the apatite-formation ability of phosphate-based ceramics depends on their crystallinity, porosity and material properties. For instance, it was found that fully sintered HA bulk ceramics are difficult to induce bone-apatite formation.

The second *in vitro* method implies using of cells. In particular, these biological tests are aimed to study the material ability to support bone cell attachment, proliferation and differentiation. However, on their own, also cell based experiments cannot be completely reliable. For instance, highly resorbable ceramics such as $CaSiO_3$ are destructive to the *in vitro* growth of human osteoblasts, due to their high dissolution rate followed by an abrupt local change of pH environment [207]. On the other hand, it has been recently shown that $CaSiO_3$ ceramics possess excellent *in vivo* bone-formation ability [208].

In this regard, the combination of SBF and cell experiments may represent compromising solution to evaluate the *in vitro* bioactivity of ceramics. Implementation and optimization of these two methods is then important to provide a first bioactivity assessment of novel biocecamics or composites, prior to their *in vivo* implantation.

Chapter 4. Materials processing

This chapter provides a general overview about materials processing routes, and, in particular, it focuses on the sintering method adopted in the present PhD thesis.

4.1 Sintering techniques

Biomaterials processing is an important step that involves mechanical and/or thermal treatments of the source material to obtain the final designed product. The selection of the processing technique to be adopted predominantly depends on the required application and type of biomaterial.

Among the different processing techniques, sintering is a process consisting in compacting and forming initial powder of certain material by heat and/or pressure application. It allows bonding particles together into a coherent, predominantly solid structure via mass transport phenomena, that occur largely at the atomic level [209]. The possible action of a mechanical load promotes powder consolidation. Briefly, when solids are heated to high temperatures, constituent ions or atoms are driven to move to compensate the surface energy differences among their convex and concave surfaces. Bottlenecks are formed and grow among powders at the initial stage (Fig. 4.1). As a result, strong chemical bonds are formed among powders, and loosely compacted green bodies are hardened to compact materials.

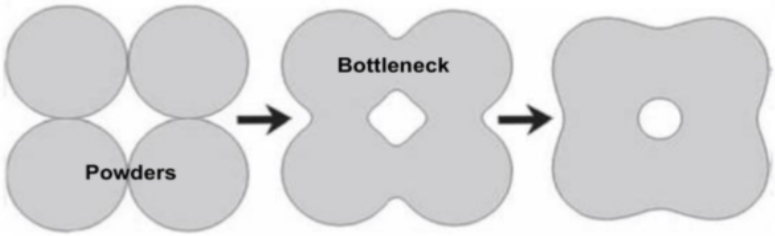

Figure 4.1: Schematic representation of the sintering mechanism: a) particles free flowing, b) neck formations and c) voids shrinkage [210].

The general mechanism of sintering can be divided in three main stages [211]:

- Initial stage of sintering ("powder rearrangement");

During this step, densification level of initial powder increases modestly up to about 10 *vol%*. For instance, if the initial green density of the powder compact was 60%, after this step it could reach at most about 70% of the theoretical density (TD). This initial step is relatively quick (seconds or minutes) and occurs right after exposing the powder to high temperature, due to the large surface area and the high driving force for sintering under such conditions.

- Intermediate stage of sintering;

This stage results in an additional increasing of powder consolidation up to about 25 vol%, resulting in powder compact density of about 93-95% of TD value. The sample shrinkage enhances due to the different diffusion mechanism such as neck growth; formation of pore interconnected cylindrical channels, etc. In some cases, during the intermediate step of sintering the shrinkage doesn't occur via described phenomena. For instance, shrinkage is characterized by low level, if matter is transported from the particle surface, and proceeds through either gas, solid or along interface, as surface diffusion.

- Final stage;

This final sintering step starts when the powder compact reaches about 93-95 *vol%* of its TD. In an ideal case, this stage results in the elimination of all residual porosity. However, the elimination of residual porosity can be achieved if all pores are mainly located nearby the grain boundaries. In fact, the defective character of the grain interfaces allow easier path for diffusion that, eventually, promotes densification.

The graph given in Fig. 4.2 summarizes how the relative density of the compact increases in each stage as a function of sintering time. As said before, the initial stage is relatively fast and leads to low density increase, while the intermediate and final

stages take longer time to reach high consolidation levels, possibly near to the theoretical value.

It worth to mention that, for further characterization/application of bioceramic powders, obtained after the synthesis, it is necessary to produce bulk specimens. In this regard, the sintering represents effective technique that uses thermal energy to form chemical bonds between bioceramic particles, resulting in strong, coherent, solid structures. Sintering has been successfully adopted to consolidate various bioceramics and bioactive glasses [212,213].

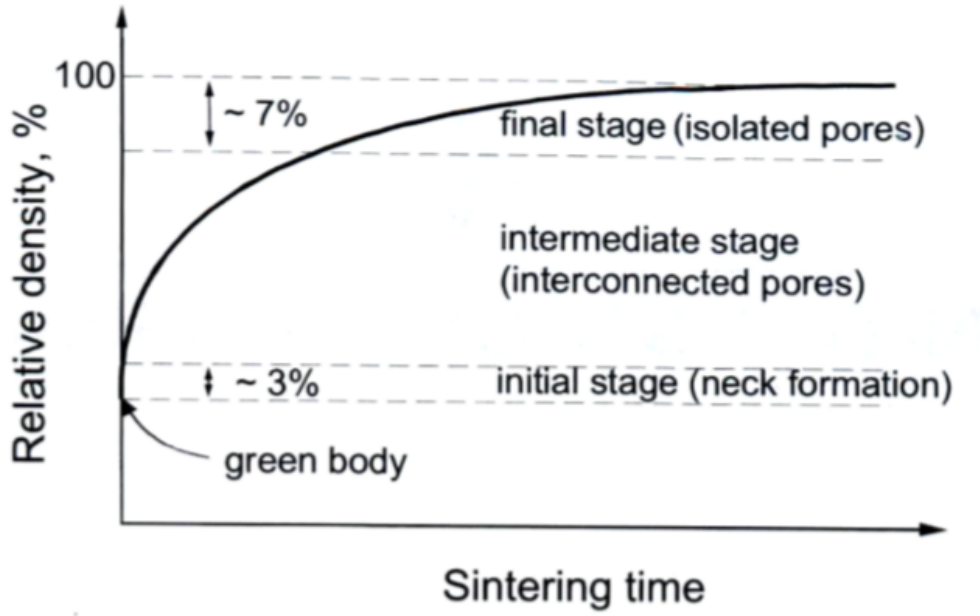

Figure 4.2: Influence of the sintering time on the relative density of powder compacts [214].

It should be noted that, the bioceramics densification behavior depends, in general, on the following factors: the applied temperature (thermal profile), particle size, specimen dimensions, heating rate, phase transformations, liquid phase formation and porosity [210,215,216].

In turn, mechanical and biological properties of post-sintered specimens mainly depend on the final microstructure, which is also strictly affected by the selected sintering technique.

The most frequently adopted conventional and innovative sintering methods will be described in the following sections.

Pressureless Sintering (PLS)

This processing route represents the simplest sintering approach based on heating the powder compact without application of an external pressure.

Three different heating schedules can be performed with pressureless sintering: constant-rate heating (CRH), rate-controlled sintering (RCS), and two-step sintering (TSS). During TSS, the sample is first heated to T_1, then cooled to T_2 and held at the latter temperature until densification is completed. The microstructure and grain size of the ceramics may vary depending on the material and schedule used [217].

Generally, in order to reach high densification levels by PLS, it is necessary to operate at high temperatures and long processing times. However, the resulting samples usually display residual porosity.

Pressure-Assisted Sintering

Differently from PLS, these techniques involve the application of a pressure during powder heating. Pressure or hydrostatic stress influences particle sliding, as well as pore shrinkage and densification rate. Shear induces particle rearrangement by sliding, collapsing large pores, while disrupting particle surface films [218]. Since pressure increases the driving force for densification, the temperature needed for sintering can be reduced to a level as low as half of the melting point of the ceramic. Additionally, shape forming and densification can be accomplished in a single step.

There are two main pressure-assisted sintering methods known as hot pressing (HP) and hot isostatic pressing (HIP).

In conventional HP approach, the pressure is applied uniaxially at high temperatures during powder heating. In traditional HP, external heating elements are used as an energy source (Fig. 4.3).

It should be stressed that it is difficult to obtain complex shape samples by hot pressing. Moreover, HP is slow (processing times on the order of hours) and high energy consuming process, since heating rates which can be typically achieved are relatively low.

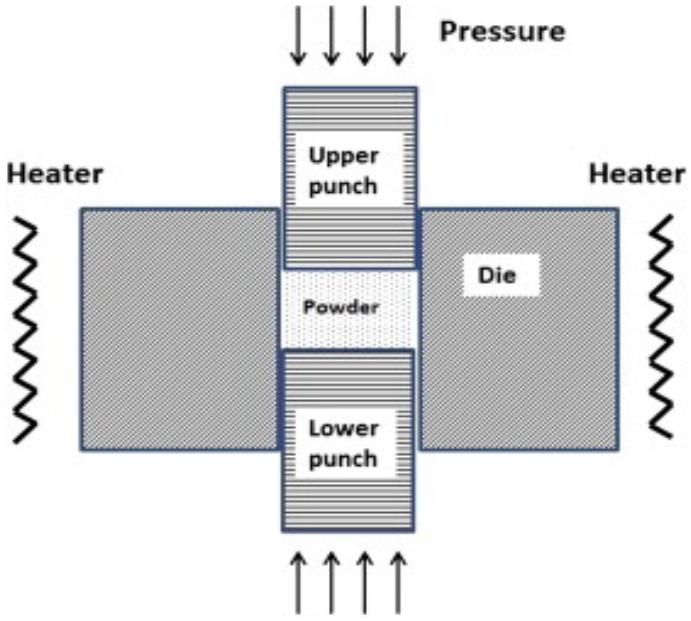

Figure 4.3: Schematic representation of Hot Pressing technique [219].

Hot isostatic pressing (HIP) involves the simultaneous application of an isostatic pressure and elevated temperature to a workpiece [220,221] (Fig. 4.4). The main features of this method are:

- powders are consolidated to higher densities at low temperatures;
- highly complex shapes with homogeneous density can be obtained;
- brittle materials, such as ceramics, can be processed, because of the more uniform heating.

However, the related equipment and tooling are relatively complex and the process overall is more expensive than the sequential approach of compaction followed by conventional sintering [222].

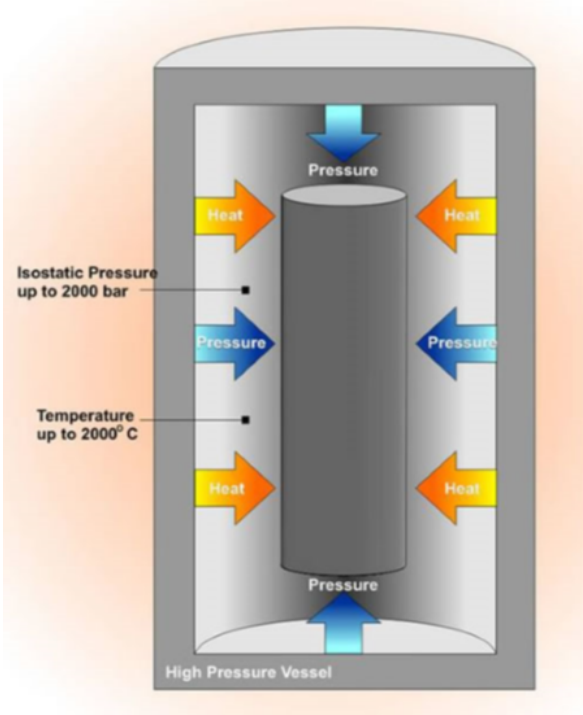

Figure 4.4: Schematic representation of the Hot Isostatic Pressing process [223].

Spark Plasma Sintering

The previously described conventional sintering techniques leave a room for their improvements, particularly because of the use of external energy sources, which make powders heating relatively slow and energy consuming. Furthermore, the microstructure of the resulting products is typically quite coarse, since grain growth is promoted by either an increase in the sintering temperature or the processing time. To overcome such drawbacks, some innovative, more efficient, sintering methods were proposed in the last decades.

These include the Selective Laser Sintering (SLS), the Capacitor Discharge Sintering (CDS) and the Spark Plasma Sintering (SPS). The last technique, which is widely

exploited in the present thesis for the fabrication of various bioceramics, will be described in details further.

SPS, also known as plasma-activated sintering, pulse electric current sintering, and pulse discharge pressure sintering [224,225], is an advanced technique that uses pressure-driven powder consolidation in which a pulsed high DC direct electric current passes through a sample placed inside a graphite conductive mould (Fig. 4.5) [226]. This technique represents a more energy-saving technology due to its short processing times (on the order of minutes) and few steps.

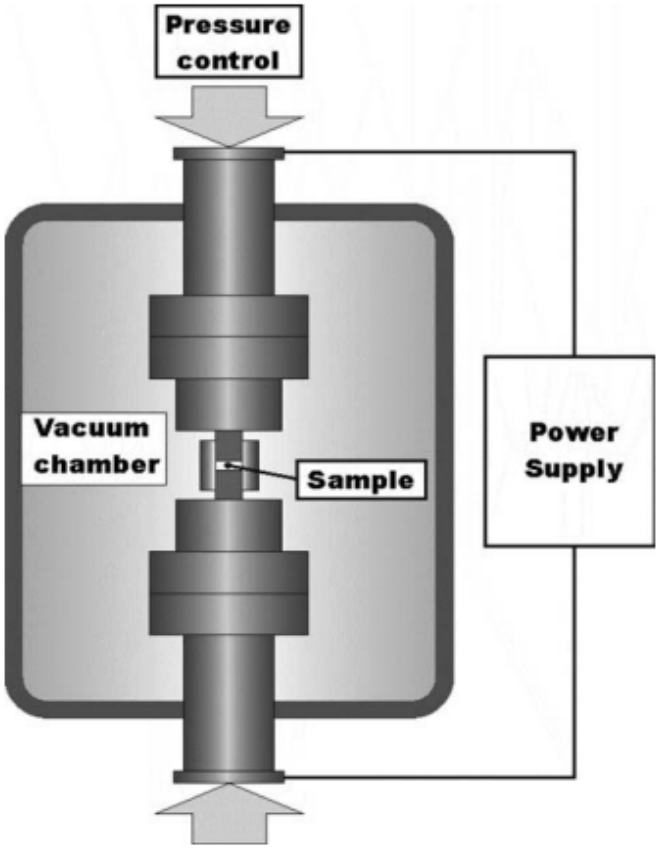

Figure 4.5: Schematic representation of the SPS process [227].

During this process, powders are placed inside a die (typically made of graphite) and exposed to a pulsed DC current, which flows through the die and the sample (if the latter is conducting). Heating of the powders occurs mainly by means of Joule effect generation, while a pressure is applied on the powder. The presence of other effects

(electromigration, sparks formation, etc.) also postulated to promote powder consolidation by SPS [225].

In any case, the simultaneous application of low-voltage/high current power along with a mechanical axial load generally leads to high densification levels at lower temperatures and, above all, shorter times with respect to conventional PLS and HP methods. Moreover, SPS can significantly limit the unwanted reactions in highly reactive systems, therefore the formation of undesirable product phases can be avoided or hindered.

During SPS runs, the most important operating parameters such as temperature, current, and voltage between the machine electrodes, mechanical load and vertical sample displacement, can be monitored and recorded in real time. In particular, the displacement output provides a real-time indication of the evolution of the powders densification. However, the thermal expansion of sample, electrodes, graphite blocks, spacers and plungers is also responsible for the measured value [228].

As summarized in a comprehensive review by Munir and coworkers [227], the use of SPS for the powder consolidation allows to obtain cleaner grain boundaries in sintered materials, a remarkable increase in superplasticity of ceramics, higher permittivity in ferroelectrics, improved magnetic and thermoelectric properties, bonding quality, as well as reduced impurity segregation at the grain boundaries.

Indeed, SPS technology has been successfully applied to produce various advanced material both monolithic and composite ones [225]. More recently, the latter technique has been exploited also for the fabrication of Functional Graded Materials (FGMs) discussed in Paragraph 4.2 [229,230].

In the present thesis, SPS is extensively applied to obtain monolithic and composite bioceramics based on calcium phosphates and bioactive glasses.

4.2 Functionally Graded Materials (FGMs)

FGMs represent a special class of composite materials and can be defined as "inhomogeneous materials, consisting of two (or more) different materials, engineered to have a continuously varying spatial composition profile" [231].

The idea of FGMs was firstly proposed in the 1984 in Japan to potentially solve the issues related to the design and production of heat-resistant materials for the aerospace applications. Indeed, it is known that when a space shuttle enters to and from the atmosphere, it undergoes harsh external conditions, to which the traditional homogeneous single-phase materials are unable to withstand. To meet this demand, FGMs represent an intriguing concept, since by the gradual variation in composition and structure over the volume, it is possible to create multi-phase composite materials with advanced properties.

Conceptionally, two different types of FGMs have been proposed so far. The first type possesses a continuous structure, as shown in Fig. 4.6 (a); differently, the second type, illustrated in Fig. 4.6 (b) corresponds to a stepwise structure. The second type of FGMs, represents a multilayered structure with the presence of interfaces between discrete layers.

Additionally, FGMs can be also divided according to the type of gradient, i.e. compositional, microstructural and porosity gradient FGMs, etc.

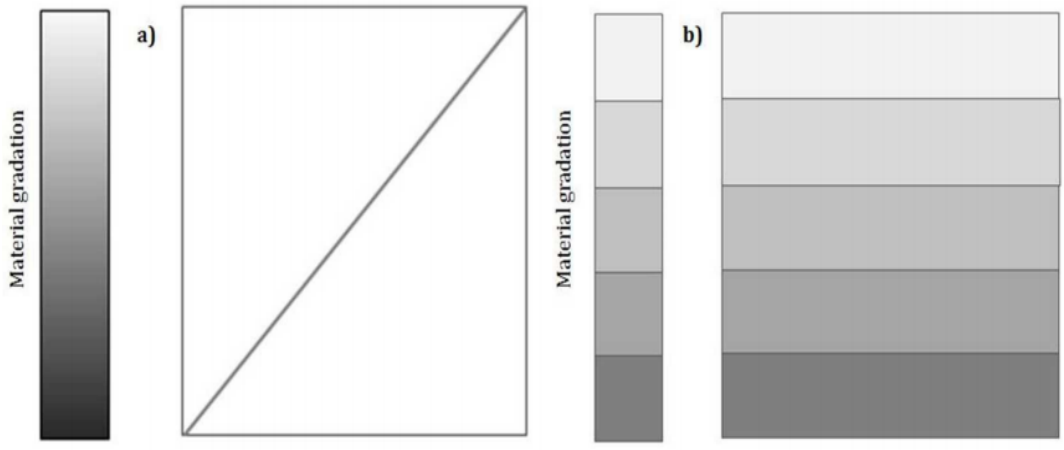

Figure 4.6: Schematic diagram of concept of gradation in FGMs [231].

Processing

The fabrication process is one of the most crucial aspect to deal with in FGM research [232,233]. Among the processing technique adopted so far to obtain synthetic FGMs, two main types can be distinguished:

1. Densification/sintering methods based on powder metallurgy techniques.
2. Coating methods: electro-deposition, plasma spray, laser cladding, vapor/chemical deposition *et al.*

As far as the first approach is considered, it should be noted that, Spark Plasma Sintering technique [225], which was discussed more in details in Chapter 4 (Paragraph 4.1), represents an advanced method compared to other densification routes, since it permits to produce high quality materials in relatively short periods of time, due to the combined simultaneous application of electrical energy and high pressures.

Materials which can be used to produce FGMs can vary from metals (and their alloys), to ceramics and plastics. The current areas of applications of FGMs include aerospace, automobile, biomedical, defence, electrical/electronic, energy, marine, opto-electronics, and thermoelectronics [234].

FGMs in the human body

It is worth to mention that FGMs are widespread in nature since functional gradation is one of the characteristic features of living tissues. Moreover, in a human body the majority of tissues and organs are made up of naturally occurring functionally graded materials. Skin and mineralized tissues like bones and teeth are among them.

For instance, long bones change from a dense, stiff external structure (the cortical bone) to a porous internal core (the cancellous bone). In this case, functional gradation is essential biological adaptation to perform the required functions.

Moreover, the surface of human teeth is made up of hard enamel, while the inner core appears in a form of soft dentine. The transition from the enamel to dentine is

provided by intermediate FGM layers, where the composition gradually changes from one material to another. Therefore, the production of implants which mimic the structure and composition of natural human tissues, i.e. using a biologically inspired approach, represents one of the current challenges in biomaterials research.

Biomedical application of FGMs

It is known, that an ideal biomaterial has to fulfill several needs, such as biocompatibility, corrosion resistance, thermal conductivity, suitable mechanical characteristics, and many other properties (See Chapter 3, Paragraph 3.2) [235]. Natural biomaterials (for example, allografts) have the structure of Functionally Graded Materials (FGMs) which allow them to satisfy these requirements. However, synthetic biomaterials with single composition and uniform structure can barely fulfill all these requirements simultaneously. Composites and, preferably, FGMs may represent a possible solution. In this regard, the latter class of materials have been extensively investigated in last decades for biomedical applications, such as in dental restorations and orthopaedic implants [236–238].

In case of dental implants, it is worth to mention that specific biomechanical features are required; namely, implant should first provide an improved integration with the host living tissue (i.e. the cortical and cancellous bones) for better matching the mechanical properties; on the other hand, the region connected to crown should also be more stable and enduring against daily loads. Therefore, ideal dental implants should adapt to the different loading regions to provide stable support in the entire restoration.

Different attempts to produce compositional FGMs which can meet these requirements have been proposed so far. FGMs based on Ti/HA, titanium/cobalt (Ti/Co), Ti/ZrO_2, titanium/ silica (Ti/SiO_2), and TiN/HA composition, as well as hydroxyapatite/collagen (HA/Col) mixtures, have been studied [239,240]. HA in these cases is used to improve bone/implant osseointegration. However, the crucial

issue related to the clinical use of titanium implants coated with HA is related to the fact that HA can be possibly biologically absorb with time, evoking defects and debonding in the coated layer.

Regarding the use of FGMs in orthopaedic implants, different advanced compositions have been proposed and studied so far, including some which involve the use of ultra-high molecular weight polyethylene (UHMWPE) fibers [241] for total hip, shoulder and knee joint replacements. UHMWPE is utilized because of superior mechanical properties and biocompatibility. On the other hand, the fabrication of FGM systems based on the combination of metal oxides and stainless steel has been also considered [230,242,243]. Specifically, in these studies, zirconia partially stabilized with 3 mol% yttria (3Y-PSZ) or Al_2O_3 were combined with stainless steel, mainly 316L or 410L [229]. Additionally, other advanced compositions which are currently under investigation were reviewed by Sola and co-workers [238].

Moreover, porous gradient functional materials also appear to be attractive as materials for hard tissue engineering, since they can mimic more closely the structure at the site of implantation. For example, permanent skeletal replacement implants made of titanium with graded porosity were proposed to improve structural compatibility and minimize the stress shielding [244]. Furthermore, it was found that titanium with gradient porosity can favor implant osseo-integration properties [245]. In addition, graded porous hydroxyapatite (HA) is suitable to mimic the bimodal structure of the human bone (cortical and cancellous), which helps to promote the new tissue growth, and also satisfy the desired mechanical properties [246,247].

The results obtained in the various research topics considered in the framework of this PhD will be described and discussed in detail in the following Chapters.

Chapter 5. Novel CaO-rich bioglass-derived glass-ceramic: crystallization and effect on the *in vitro* bioactivity

5.1 Introduction

As previously mentioned in Paragraph 3.4.3, due to their ability to elicit favorable host response during interaction with biological tissues, bioactive glasses have become one of the most important and investigated classes of materials for biomedical application [179,205].

Several *in vivo* studies demonstrated that bioglass stimulates bone growth away from the bone-implant interface and, in particular, bonds to bone more rapidly than other bioactive ceramics. In spite of this, calcium phosphates, such as tricalcium phosphate and hydroxyapatite, are currently still more widely used in clinical practice. This is mostly due to the fact that standard bioactive glasses display some critical aspects.

For instance, a crucial issue concerning the use of original 45S5 Bioglass® is related to its high tendency to crystallize: in fact, this system starts to devitrify approximately at 600^{o}C and a crystallization peak is shown between 650°C and 690°C [197,213,248,249]. This aspect represents the primary limitation of such bioactive glass. Crystallization, which occurs during the sintering step, significantly alters mechanical and biological properties of 45S5 Bioglass® and hinders the densification process itself. Thus, when the corresponding powders are exposed to the thermal levels required by pressureless sintering to obtain bulk materials, fully crystallized ceramics or glass-ceramic composites are produced [195,213]. In contrast, highly porous samples characterized by poor mechanical properties can be obtained when operating below the crystallization temperature.

Although the lack of mechanical strength in amorphous 45S5 is improved after crystallization takes place, this feature could also lead to negative consequences [179,196,213]. Specifically, a precocious crystallization can retard the sintering

process [250,251]. In addition, it has been reported that the newly formed crystalline phases are scarcely bioactive or, at least, less bioactive than the “parent” amorphous phase. Nonetheless, *in vitro* tests recently carried out with acellular SBF solution and involving 45S5-based dense samples produced by Spark Plasma Sintering (SPS) evidenced that the enhanced apatite formation was promoted in crystallized samples as compared to the mainly amorphous material [198,252]. In any case, partial crystallization can lead to implant instability [253], since the residual glassy areas are degraded preferentially by physiological fluids, as reported when investigating a glass-ceramic material called Ceravital®, which failed due to long-term instability, although it results bonded to bone [179].

For these reasons, in the last years, several investigations have been performed to understand how the glass composition can be modified to properly control or prevent crystallization during thermal treatments. It should be noted that, the crystallization of bioglass depends on the composition, i. e. relative amounts of oxide constituents. New formulations with relatively higher CaO/Na_2O ratio with respect to 45S5 Bioglass® were recently considered [254,255]. The introduction of suitable amounts of K_2O in these CaO rich bioglass materials was also examined [256]. A novel CaO-rich low alkaline bioglass was recently developed to be used whenever a thermal treatment is necessary, by virtue of its high bioactivity combined to a low tendency to crystallize [249,256]. The composition of this bioglass, so-called CaMix, is presented in Table 5.1.

Bioglass type	CaO	SiO_2	Na_2O	K_2O	P_2O_5
Bioglass®45S5 [13]	26.9	46.1	24.4	-	2.6
CaMix [256]	45.6	47.2	2.3	2.3	2.6

Table 5.1: Composition (oxide mol%) of Bioglass® 45S5 and CaMix bioglass powders.

It was found that the amorphous nature of CaMix bioglass is preserved when the starting powders are processed at 800°C for 3h by pressureless sintering.

In recent years, CaMix has been also successfully employed to obtain hydroxyapatite-based composites, produced either by means of pressureless [257] or Spark Plasma Sintering [258]. Although the results obtained so far are quite promising for the possible use of the CaMix-based glass-ceramic system in biomedicine, additional investigations are still needed to gain further insights on the behavior of this novel class of materials when exposed to biological environments.

5.2 Aim

In this regard, it is particularly useful to provide for the first time a quantitative analysis of the amounts of apatite produced on the CaMix bioglass surface during in-vitro experiments in SBF, when using glass-ceramic samples with different compositional and structural properties.

To this aim, in this part of thesis, three groups of fully dense specimens with different composition, crystallization degree and crystallites size were produced by SPS from lab-made CaMix powders. The obtained sintered samples were subsequently immersed in SBF for various time periods in the range 0–14 days and the corresponding temporal changes of their mass, composition and microstructure were monitored. The concomitant modifications in the SBF solution (pH and the concentration of the more significant species) were also determined and discussed.

5.3 Experimental

5.3.1 Materials and Methods

Bioglass

Powder of CaMix Bioglass was produced and provided by the Department of Engineering “Enzo Ferrari”, Università degli studi di Modena e Reggio Emilia

(Italy). The bioglass was obtained by a classical melt-quenching route reported elsewhere [256], with the following composition: 47.3% SiO_2, 45.6% CaO, 2.3% Na_2O, 2.3% K_2O, and 2.6 P_2O_5 (mol. %). Briefly, the commercial raw powder reagents – all reagent grade – (SiO_2, Na_2CO_3, $CaCO_3$, K_2CO_3, $Ca_3(PO_4)_2$ by Carlo Erba Reagenti, Rodano Milano, Italy) were mixed in a laboratory shaker for 2 h and then melted at 1450ºC for 1 h. The molten CaMix was then quenched in water to obtain a frit which was dried at 110ºC for 12 hours. The resulting glass powder showed an average particles size value of about 20μm, as revealed by laser light scattering analysis (CILAS 1180, France).

Consolidation

Dense cylindrical disks with 14.7 mm diameter and 3mm thickness were prepared by Spark Plasma Sintering (SPS 515S model, Fuji Electronic Industrial Co., Ltd., Kanagawa, Japan) (Fig. 5.1) starting from CaMix powder. SPS runs were conducted under vacuum conditions (20Pa) and temperature controlled mode using a K-type thermocouple (Omega Engineering Inc., USA) inserted inside a small hole drilled at the centre of the external surface of a cylindrical graphite die containing the CaMix powders to be consolidated.

The die and the plungers shown in Figure 5.2 (a) and (b), respectively, were both made of AT101 graphite (Atal s.r.l., Italy). The powder to be sintered (1.40 g) was placed inside a cylindrical die with outside diameter of 30 mm, inside diameter of 15 mm, and 30 mm high. In order to facilitate release of the bulk samples after sintering, the green compact was covered with a 0.13 mm thick graphite foil (cf. Figure 5.2 (c)) (Alfa Aesar Karlsruhe, Germany). Additionally, a graphite felt (3 mm thick, Atal s.r.l., Italy) was used to isolate the die and limit thermal losses (cf. Figure 5.2 (d)).

The most important SPS parameters, i.e. temperature, current, voltage between the machine electrodes, applied load, vertical sample displacement and displacement-rate, were monitored and recorded during each experiment. The final consolidation

level was evaluated by measuring the density of the samples obtained after the sintering process by Archimedes method, using distilled water.

During each SPS experiment, the temperature was increased from the room value to a maximum level (T_D) according the following steps order:

1. From the room temperature up to (T_D -100^{o}C) with the rate of 50^{o}C/min.
2. From (T_D -100^{o}C) to T_D with the rate of 10^{o}C/min.

Then, the T_D value was maintained for a prescribed duration (t_D). Cooling process was also controlled; the rate of cooling was 50^{o}C/min.

Figure 5.1: Spark Plasma Sintering Equipment (model 515S) used in this work.

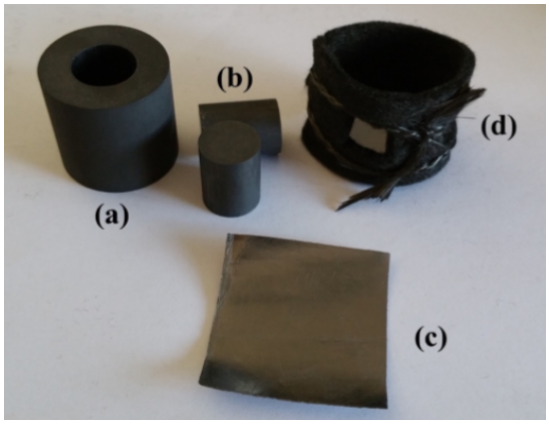

Figure 5.2: (a) graphite die, (b) plungers, (c) foil and (d) felt used during the SPS experiments

For *in-vitro* tests in SBF, three series of sintered samples have been prepared under different T_D and t_D conditions (Table 5.2) in order to induce the generation of different crystallization levels, phases and crystallite size in the sintered products. All experiments were conducted under a mechanical pressure of 16MPa. Before SBF tests, the sintered disks were first accurately sanded using abrasive paper, to remove any residual graphite contamination, and then finely polished. The thickness of polished samples was approximately 2.6 mm.

Sample ID	T_D(°C)	t_D(min)
S1	730	2
S2	850	2
S3	1000	20

Table 5.2: Designation of CaMix bioglass samples and related SPS conditions (P=16MPa).

5.3.2 In-vitro tests

The a-cellular SBF solution for *in-vitro* tests was prepared according to the Kokubo protocol [204]. Specifically, NaCl (8.035g), $NaHCO_3$ (0.355g), KCl (0.225g), $K_2HPO_4 \cdot 3H_2O$ (0.231g), $MgCl_2 \cdot 6H_2O$ (0.311g), 1M HCl (39ml), $CaCl_2$ (0.292g), Na_2SO_4 (0.072g) and $(CH_2OH)_3CNH_2$ (6.118g) were added one by one to distilled water at 37°C to obtain 1000 mL of solution. The pH of the solution was adjusted at 7.4 using 1M HCl.

Each sample was immersed for different time intervals (6h, 1, 3, 7 and 14 days) in about 46 mL of solution (Vs), that was determined according to the Kokubo procedure without refreshing, i.e.

$$V_s \text{ (mL)} = S_a \text{ (mm}^2\text{)}/10 \quad (eq.\ 5.1)$$

where S_a, approximately 460 mm^2 in the present work, is the apparent surface area of the sample. For the sake of reproducibility, each SBF test was repeated at least three times.

After the prescribed storage period, glass samples were rinsed with distilled water, dried and weighted using an analytical balance (KERN mod. ABS 120-4, Balingen, Germany).

Structural characterization of the surface of glass-ceramic samples before and after their immersion in SBF was carried out by X-ray diffraction analysis (Philips PW 1830, Netherlands) using a Ni filtered Cu Kα radiation (λ =1.5405Å) (Fig. 5.3).

The relative content of the different phases and the corresponding average crystallite size were determined taking advantage of a Rietveld analytical procedure [259,260].

In addition, the compositional and microstructural changes of the samples' surface were also examined by high resolution scanning electron microscopy (HRSEM) (mod. S4000, Hitachi, Tokyo, Japan) equipped with a UltraDry Energy-dispersive X-ray (EDS) Detector (Thermo Fisher Scientific, Waltham, MA, USA) (Fig. 5.4).

Figure 5.3: X-Ray Diffractometer (model Philips PW 1830).

Figure 5.4: High –resolution Scanning Electron microscope (model Hitachi S4000).

The most significant compositional changes induced in the SBF solution by the interaction with the three classes of glass-ceramics were also examined. To this regard, it should be noted that the solution was not refreshed during the test, to emphasize, with respect to the initial condition, the changes produced in the SBF by the contact of the various samples with the fluid. In particular, Ca, P, and Si concentrations as well as pH were measured at the prescribed immersion time ends. The content of the species above was determined by Inductively Coupled Plasma Optical Emission Spectroscopy (ICP-OES CCD Simultaneous, Vista – MPX Varian, Mulgrave, Australia).

5.4 Results

5.4.1 Powder consolidation

The sintering parameters adopted in this study (Table 5.2) have been selected based on the results obtained in a previous investigation, aimed to identify the optimal SPS conditions for achieving the full densification of CaMix powders while preserving their original amorphous nature [249]. It resulted that completely dense and still amorphous materials can be obtained under the milder conditions of T_D=730°C, t_D=2min and P=16MPa. Therefore, such parameters have been chosen for the fabrication of the first class of specimens, indicated as S1 in Table 5.2, for SBF tests. Moreover, to investigate the possible effects of crystallization from the parent glass on the material bioactivity, the processing time and/or sintering temperature were increased to produce the two additional series of CaMix-derived glass-ceramics, listed as S2 and S3 in Table 5.2.

5.4.2 In-vitro experiments

5.4.2.1 XRD analysis

The CaMix samples were examined in detail by XRD analysis to evidence the compositional and structural changes taking place on their surface during SBF experiments. The estimation of the relative amount of the different phases present, as well as the corresponding crystallite size, was performed according to the Rietveld procedure.

The experimental patterns (red rhombohedral) and the corresponding best-fit (dark line) for the S1 samples are reported in Fig. 5.5. The first pattern, named “original powders”, corresponds to an amorphous CaMix glass powder. This phase has been computed using a pseudo-crystalline structure factor ($Ca_{1.5}Na_{2.64}Si_9O_3$, crystallite size: 20Å, microstrain: 0.03) according to the LeBail approach [259–261]. In the pattern of bulk materials obtained when the initial powders were consolidated by SPS

at 730°C for 2 min (indicated in Fig. 5.5 as t=0d), the amorphous component is completely preserved. The subsequent pattern, named t=6h, is referred to the sample soaked in SBF for 6h. With respect to the previous pattern, a tangible difference can be observed only when focusing on the background at lower (23°) and middle (45°) 2θ angle. This effect can be also visualized in the sample stored in the solution for 1 day. After 3 days, the peaks of the nanoapatite phase (around 9 wt.%) can be clearly detected in the corresponding pattern (t=3d). Specific data, concerning microstructure features and phases abundance are summarized in Table 5.3.

Sample	Phases	Crystallite sizes (Å)	Wt. %
Original powders	Amorphous CaMix	-	100
t = 0d	Amorphous CaMix	-	100
t = 6h	Amorphous CaMix/apatite	-	>95/trace
t = 1d	Amorphous CaMix/apatite	-	>95/trace
t = 3d	Amorphous CaMix/apatite	/435	91/9
t = 7d	Amorphous CaMix/apatite	/421	74/26
t = 14d	Amorphous CaMix/apatite	/421	73/27

Table 5.3: Phases and quantitive phase analysis results relatively to S1 samples immersed for different time intervals in the SBF.

Nanocrystallites of around 44 nm have been estimated for the apatite phase. Therefore, it could be assumed that a thin layer of apatite is growing on the amorphous matrix of glass, presumably covered by a silica gel layer.

Nanocrystalline CaMix, together with the apatite and amorphous glass phases, has been also detected when the sample was aged for 3 days. However, its quantity was below 6 wt.% in all the patterns, so it is not considered. In the samples immersed for 7 and 14 days, the amount of nanoapatite increases up to 27 wt.%. In addition, the formed apatite presents a texture with a preferred orientation situated on the reflection

002 (25.84°). A similar outcome was obtained in a previous study focused on the conventional 45S5 Bioglass® [198]. Thus, it is possible to state that the apatite crystallites formed onto amorphous glass nucleated or grew with (002) orientation.

The experimental patterns and the best-fitted profiles of the S2 group of CaMix samples are reported in Fig. 5.6. As evinced in the pattern corresponding to t=0d, the more severe sintering conditions adopted in this case (T_D=850°C) lead to drastic changes in the microstructure of the CaMix-derived product. Crystalline peaks of both $CaSiO_3$ polymorphous are detected (α-pseudowollastonite and β-wollastonite phases) accompanied by an amorphous component ascribable to the glass (46, 28 and 21 wt.%, respectively - see Table 5.4).

In addition, the Rietveld analysis provided similar crystallite sizes for α- and β-$CaSiO_3$, i.e. about 95 and 90 nm, respectively (Table 5.4). Interestingly, traces of Kilchoanite ($Ca_3Si_2O_7$) and Combeite ($Ca_{1.5}Na_{2.64}O_9Si_3$), 2 and 3 wt.%, respectively, have been also found in the SPS sample. This feature is visualized in detail in Fig. 5.7, where the deconvolution profiles of the pattern at t=0d are shown. No significant changes can be detected by XRD for the S2 system immersed in SBF for 6h, whereas, after 1 day, the samples undergo a partial amorphization with a decrease of the α and β-$CaSiO_3$ phases. However, the presence of apatite (3 wt.%) can be detected after 3 days in the related pattern. Correspondingly, the amorphous component was found to increase up to 76 wt.%, with lower amounts of α- and β-$CaSiO_3$ phases. Other silicates were not detected under these conditions. In the sample soaked for 7 days, the content of nanoapatite further increases up to 20 wt.%, while the amorphous component remained the dominant phase. No significant changes could be revealed by XRD when the storage period was extended to 14 days. In particular, a slightly larger amount of apatite (21wt. %) was formed under such conditions.

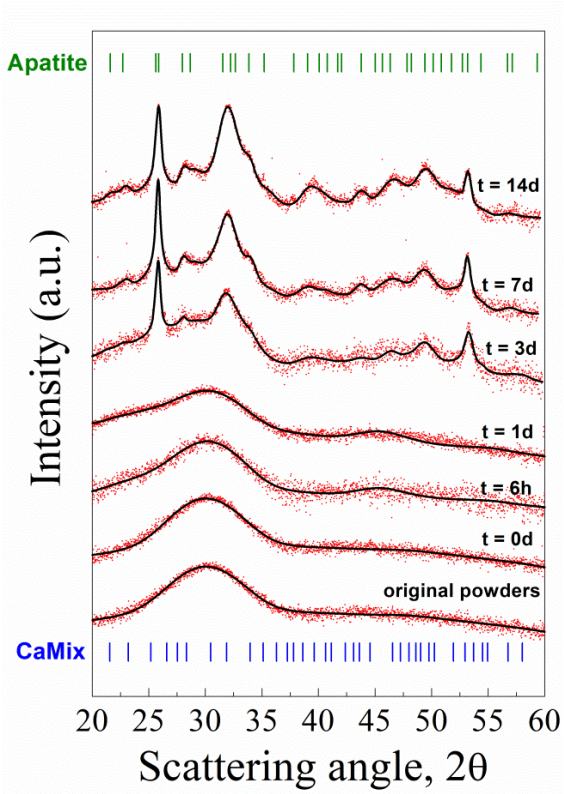

Figure 5.5: XRD patterns and related Rietveld refinements of S1 samples as function of the storage time in the SBF solution.

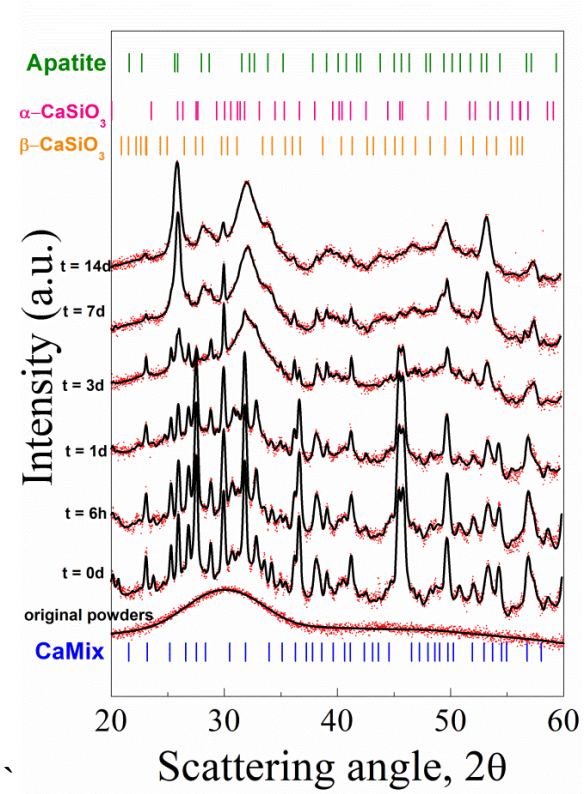

Figure 5.6: XRD patterns and related Rietveld refinements of S2 samples as a function of the storage time in the SBF solution.

Data relative to the original bioglass powders are also shown for the sake of comparison. Label CaMix refers to the $Ca_{1.5}Na_{2.64}Si_9O_3$ phase.

Sample	Phases	Crystallite sizes (Å)	Wt. %
Original powders	Amorphous CaMix	-	100
t = 0d	Amorphous CaMix/α-$CaSiO_3$/β-$CaSiO_3$/ Kilchoanite/Combeite	/950/900/	21/46/28/2/3
t = 6h	Amorphous CaMix/α-$CaSiO_3$/β-$CaSiO_3$/ Kilchoanite/Combeite	/950/900/	20/45/30/3/2
t = 1d	Amorphous CaMix/α-$CaSiO_3$/β-$CaSiO_3$/ Kilchoanite/Combeite	/970/950/	43/31/22/4/0
t = 3d	Amorphous CaMix/α-$CaSiO_3$/β-CaSiO3/ apatite	/1000/920/180	76/7/14/3
t = 7d	Amorphous CaMix/α-$CaSiO_3$/β-$CaSiO_3$/ apatite	/1290/1010/233	64/5/10/20
t = 14d	Amorphous CaMix/α-$CaSiO_3$/β-$CaSiO_3$/ apatite	/1300/1040/274	65/5/8/21

Table 5.4: Phases and quantitive phase analysis results relatively to S2 samples immersed for different time intervals in the SBF.

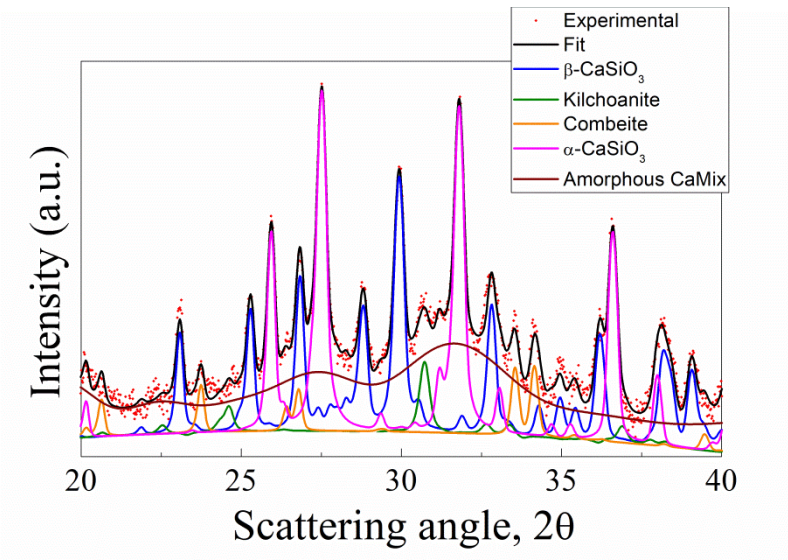

Figure 5.7: Deconvolution of the XRD pattern relative to the S2 product before being immersed in the SBF solution.

Regarding the behavior of the S3 group of the glass-ceramic specimens resulting when the sintering temperature and the dwell time were increased to 1000°C and 20

min, respectively (pattern t=0d in Fig. 5.8), the XRD analysis evidenced that, under such heat treatment conditions, the amorphous glass crystallizes to form β-$CaSiO_3$ (main one) and Kilchoanite ($Ca_3Si_2O_7$) phases, whereas no traces of the other polymorphous, α-$CaSiO_3$, could be found.

The Rietveld analysis evidenced an increased size of β-$CaSiO_3$ crystallites (about 110nm), as compared to that one obtained for the S2 class of glass-ceramic products. When the material was exposed to the SBF solution for 6h, the only relevant change is represented by the relative increase of the kilchoanite phase (see Table 5.5). A rather similar situation was encountered after 1-day contact.

On the other hand, appreciable changes are observed in the XRD pattern after 3 days, when the occurrence of an amorphization process can be readily deduced. As the storage time is prolonged to 7 days, the amorphous component increases significantly (from to 18–56 wt.%), although a relevant amount of crystalline $CaSiO_3$ (34wt.%) is still present on the sample surface. More important, the presence (5 wt.%) of the apatite phase is clearly identified for the first time when considering the S3 system. Finally, when the contact time was extended to 14 days, the amount of apatite on the sample surface rises to 10 wt.%.

To better compare the bioactivity of the three classes of CaMix-based sintered materials, the temporal profiles of the relative content of apatite produced during the *in-vitro* test, as determined by the Rietveld method, are plotted in Fig. 5.9. From these data, it appears that the amount of apatite on the samples surface follows the hierarchical order at each time point: S1 > S2 > S3. In addition, when considering the S1 and S2 systems, the presence of apatite can be unequivocally detected and quantitatively evaluated for immersion times equal to 3 days.

In contrast, when the S3 counterpart is examined, the incipient formation of apatite is observed only after 7 days contact with the SBF solution.

Sample	Phases	Crystallite sizes (Å)	Wt. %
Original powders	Amorphous CaMix	-	100
t = 0d	Amorphous CaMix/β-$CaSiO_3$/ Kilchoanite	/1103/984	12/85/4
t = 6h	Amorphous CaMix/β-$CaSiO_3$/ Kilchoanite	/1100/926	12/72/16
t = 1d	Amorphous CaMix/β-$CaSiO_3$/ Kilchoanite	/1119/925	12/70/18
t = 3d	Amorphous CaMix/α-$CaSiO_3$/β-$CaSiO_3$	/1135/923	18/64/18
t = 7d	Amorphous CaMix/β-$CaSiO_3$/ Kilchoanite/ apatite	/850/923/450	56/34/5/5
t = 14d	Amorphous CaMix/β-$CaSiO_3$/ Kilchoanite/ apatite	/846/922/450	54/29/7/10

Table 5.5: Phases and quantitive phase analysis results relatively to S3 samples immersed for different time intervals in the SBF.

4.4.2.2 SEM/EDS

Compositional and structural modifications promoted on the surface of the three classes of CaMix samples by the contact with the SBF solution were also examined by SEM/EDS. The obtained results are reported in Fig. 5.10. Several fractures, particularly on S1 samples, are observable on the samples' surface after 6h (Fig. 5.10b) and 1 day (Fig. 5.10c) immersion in SBF, whereas other degradation and apparently minor effects are correspondingly observed on S3 specimens. An intermediate behavior is shown by S2 products. Such cracks are due to the drying of the micro-porous hydrated silica film, which covers the samples surface – in particular if the starting sample was amorphous – after the extraction of the sample from the SBF; the degradation of the silica film is further enhanced by the SEM vacuum [256,262].

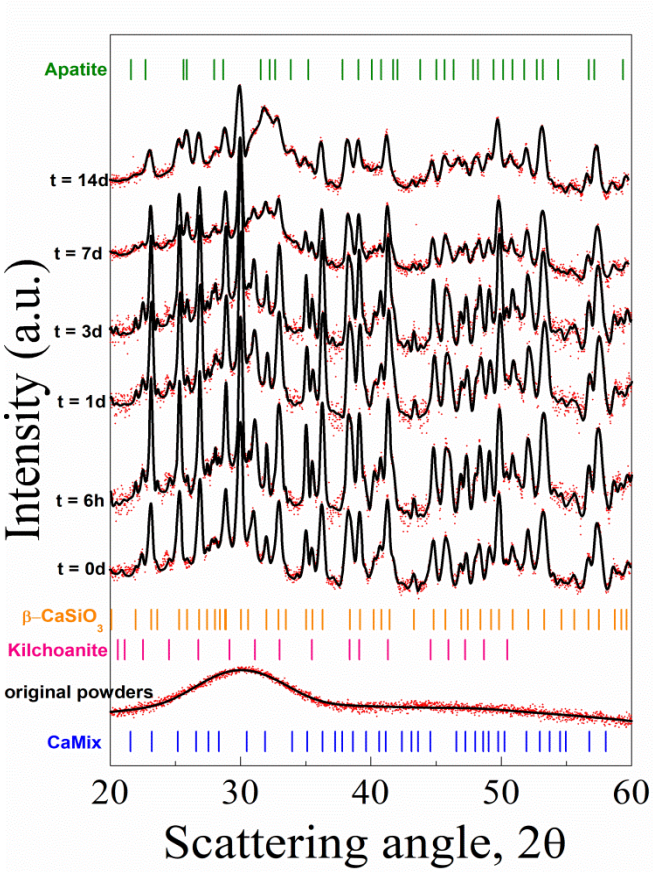

Figure 5.8: XRD patterns and related Rietveld refinements of S3 samples as function of the storage time in the SBF solution.

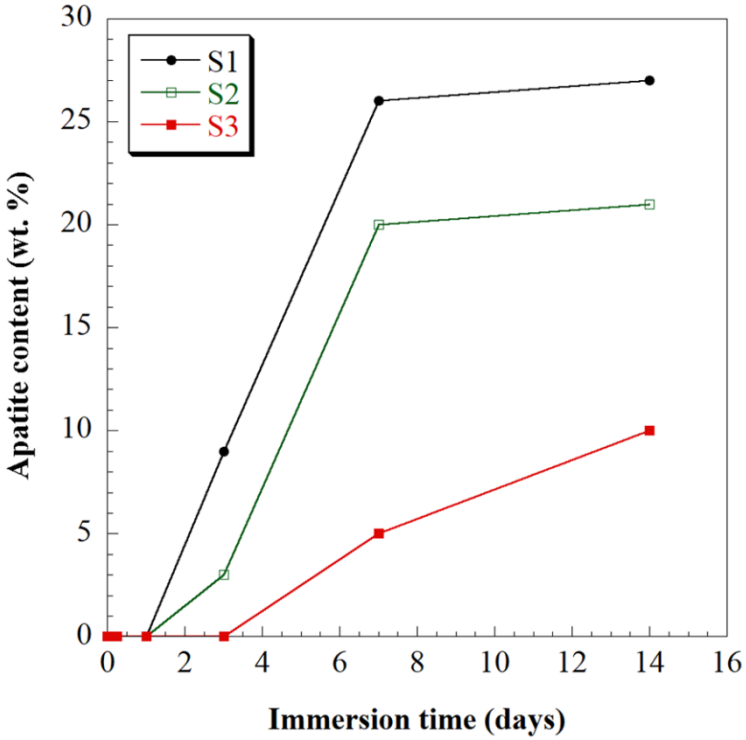

Figure 5.9: Time evolution of the apatite content on the surface of the three series of CaMix samples during in-vitro test, as determined by the Rietveld analysis.

SEM observation does not evidence the presence after 6h of new phases on the surface of the three types of samples. This holds also true when examining the materials exposed for t=1d to the solution (Fig. 5.10c).

However, the EDS analysis evidenced significant and sudden changes in the composition of the surface of S1 and S2 groups of specimens during such storage period (Fig. 5.11). Specifically, the decrease of the relative content of Si and O, particularly when considering S1 sample, is accompanied by a rapid increase of Ca and P, due to the deposition of calcium phosphate precipitates on the top of the silica gel film. In contrast, only modest variations are observed when S3 products were immersed. Fig. 5.11 also shows that the Ca/P atomic ratio drops to lower values during the first 6h immersion for all the systems. However, this ratio becomes less than 2 for S1 and S2 in 1 d, whereas it takes quite longer time intervals (t=7d) to reach the same achievement when considering the S3 system.

The SEM micrographs shown in Fig. 5.10d evidenced that after 3d storage, the surface of the S1 sample is almost fully covered by a layer of a new phase, i.e. globular shaped agglomerates with the typical morphology of the apatite which forms in vitro in SBF. Such phase is also clearly formed, although at a lower level, also when examining the micrograph of the S2 sample. On the other hand, this feature can be observed on S3 products only when the soaking time was prolonged to 7 days (Fig. 5.10e).

Independently from the CaMix system, the new phase produced on the materials surface exhibits a lamellar structure, as seen in the detailed micrographs shown in Fig. 5.12 for the cases of S1 and S3 samples contacted with the SBF solution for 7 days. The corresponding EDS spectra, also reported in Fig. 5.12, are consistent with the presence at this stage of the phases identified by XRD analysis. As the storage time was further increased, Fig. 5.11 shows that, when considering S1 and S2, the relative amounts of Ca and P achieved a maximum value and then slightly decreased, whereas an opposite trend was correspondingly found for O. Differently, Ca and P

slightly increase while O content displays only modest changes when S3 samples were taken into account. Nonetheless, very close values in the Ca/P atomic ratio, i.e. about 1.8 (Ca/P ~ 1.67 for the stoichiometric hydroxyapatite [263]), were finally reached for the three classes of glass-ceramic products.

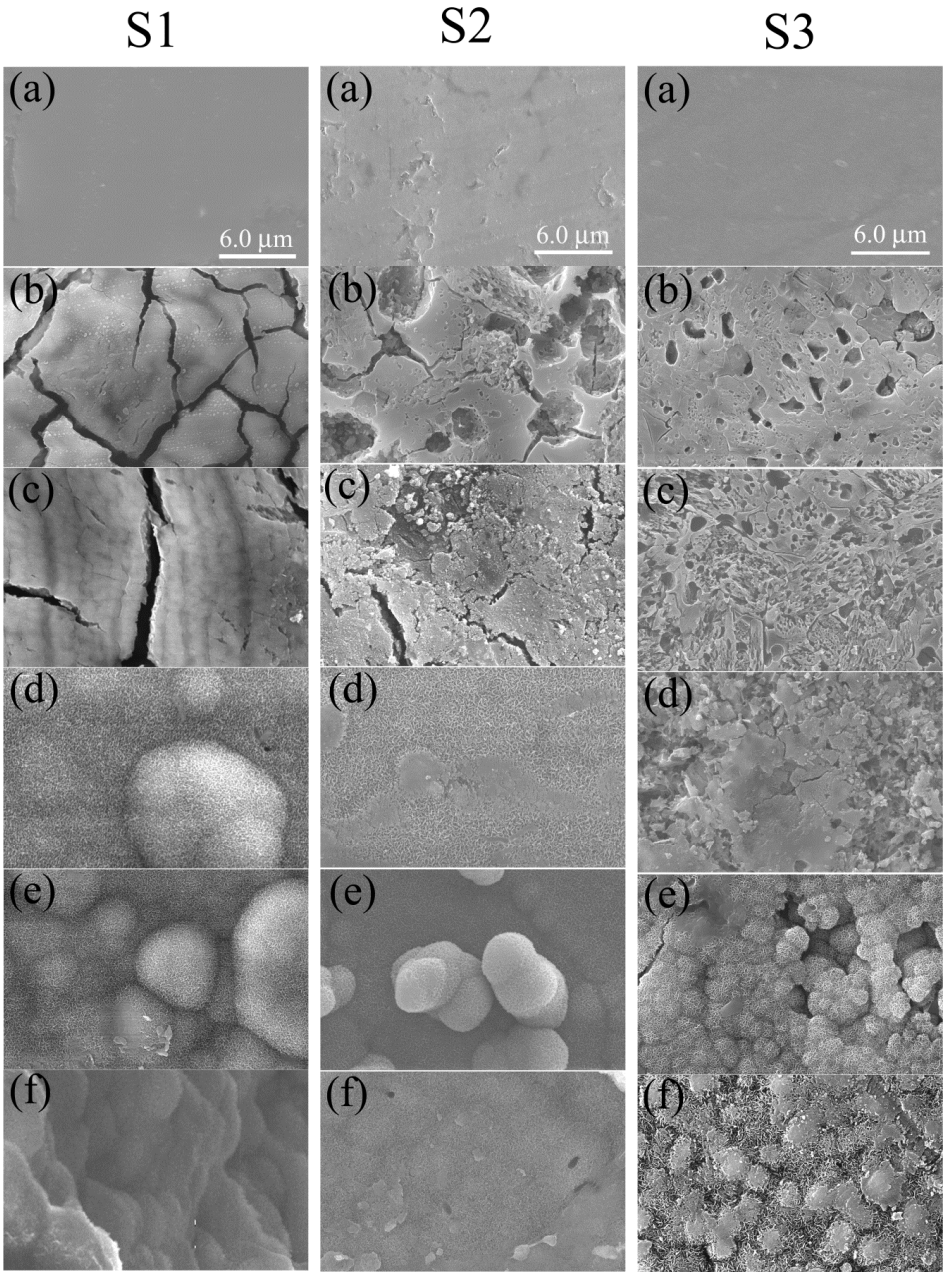

Figure 5.10: SEM micrographs of the three series of CaMix specimens at different storage times in the SBF solution: (a) 0h, (b) 6h, (c) 1 d, (d) 3 d, (e) 7 d and (f) 14 d.

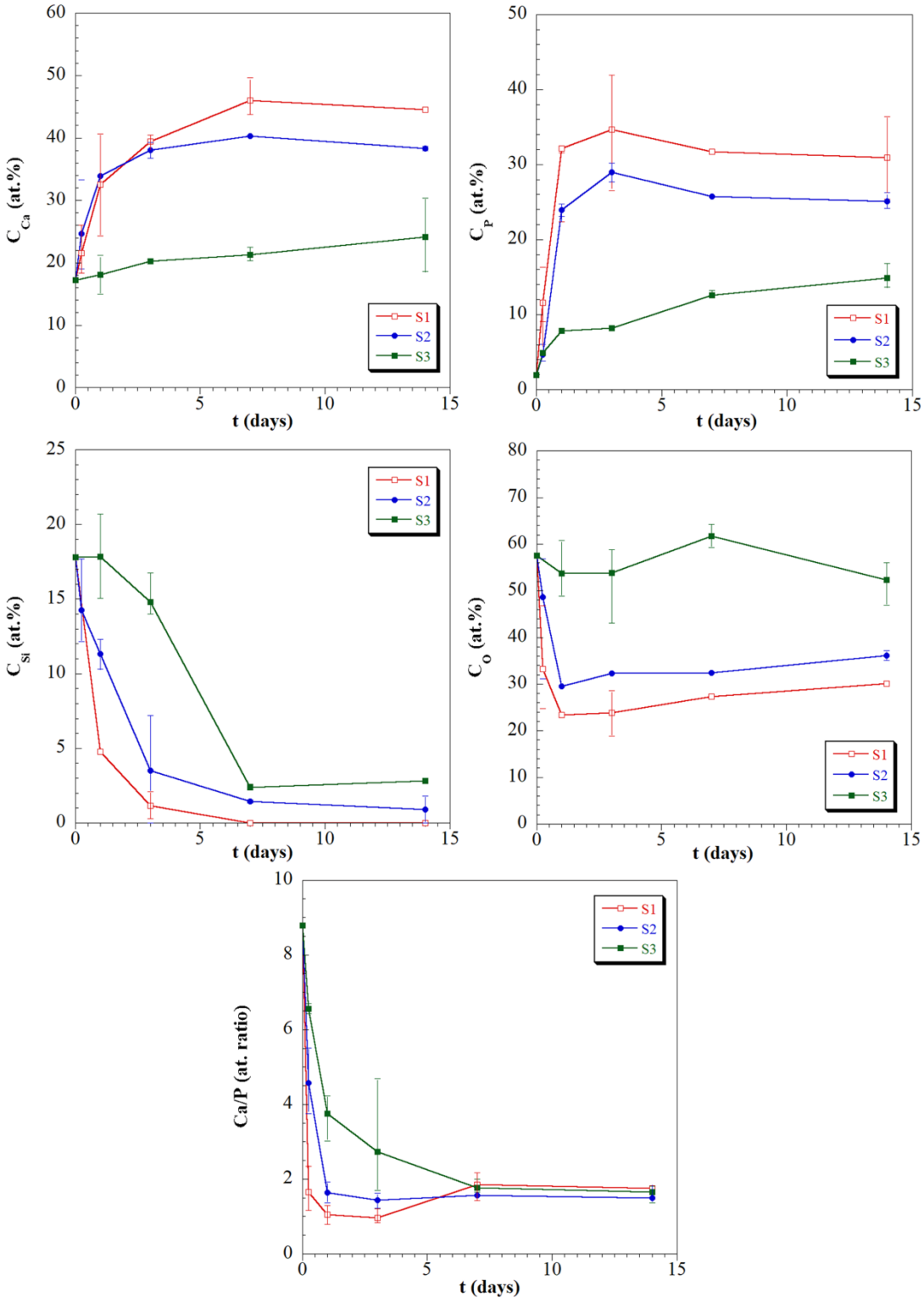

Figure 5.11: Compositional changes (EDS analysis) on the surface of the three series of CaMix products during their storage in the SBF solution.

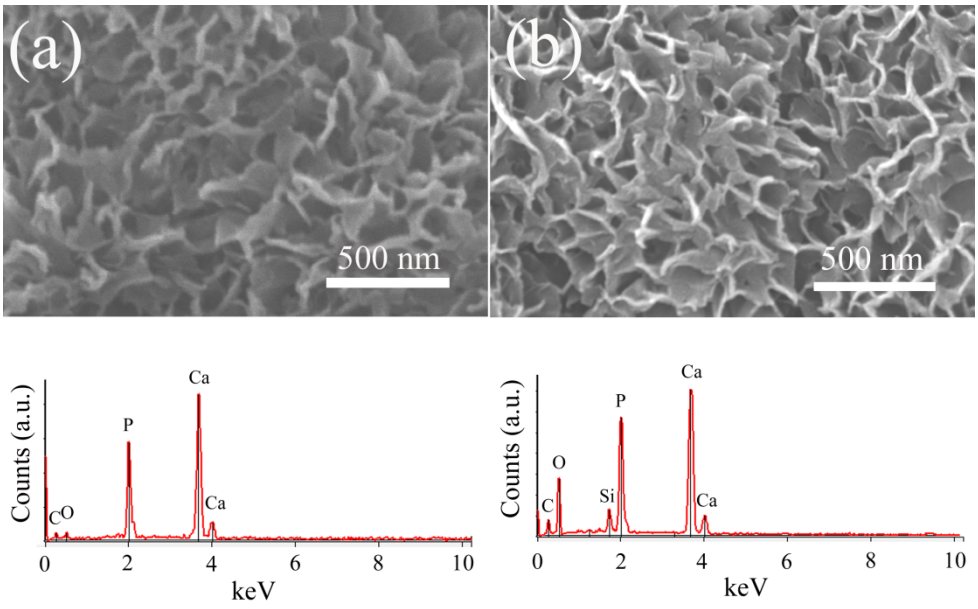

Figure 5.12: High magnification micrographs and related EDS spectra of (a) S1 and (b) S3 samples after 7 days immersion in the SBF solution.

5.4.2.3 Sample mass changes

The behavior of the three types of samples in term of weight variation, as a consequence of their contact with the SBF solution, is compared in Fig. 5.13. During the first day immersion, S1 and S2 reduce significantly (and similarly) their mass; on the contrary, the mass of S3 decreases only slightly. As the test proceeds, also S1 and S2 behave differently. Indeed, while a further mass loss was observed for S2, although with a progressively lower rate, S1 specimens displayed a certain weight gain during the immersion period from 1d to 3d. As the soaking time was further prolonged, sample weight remained approximately unchanged for the latter system, whereas the mass of S2 reached a minimum value for t=7d and then increases. As for the S3 class of samples, a progressive and slow weight loss takes place for the entire storage period investigated. Based on the obtained results, it is possible to state that S1 dissolution prevailed up to 1d with respect to the corresponding weight gain caused by the apatite formation on the materials surface. However, the opposite situation occurs when the contact time is augmented to 3d. A similar qualitative

behavior is also manifested by the S2 system, but in this case mass gain overcomes dissolution effects only after 7 d. Finally, the latter phenomena are always predominant in S3 specimens, as they lose their weight in a monotonic manner for the complete test duration.

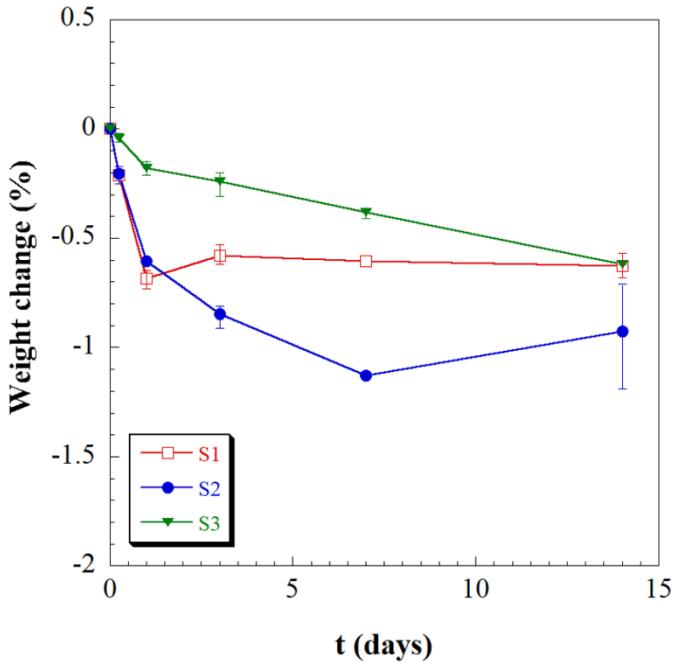

Figure 5.13: Weight changes of the three series of CaMix samples as a function of storage time in the SBF solution.

5.4.2.4 Compositional changes in SBF

Fig. 5.14 provides the immersion time dependence of pH and the concentration of certain relevant species in the SBF solution during the in-vitro test. As far as pH is concerned, a very similar behaviour is observed when comparing S1 and S2 systems. In particular, a very rapid pH increase from the initial value to about 7.8 is observed during the first day storage. As the test proceeds, this parameter still increases, albeit at a much lower rate, to approach a value of about 8 after 14 days contact. On the other hand, markedly minor changes are ascertained in the solution during the interaction with S3 samples, as proved by the relatively small increase in pH reached at the end of the test, i.e. 7.75 at most. Similar outcomes are found when the species

concentration plots for the three systems are compared. Indeed, Si and Ca release from samples to the solution occurred relatively faster for S1 and S2 systems with respect to S3. In particular, during the first day immersion Si released was relatively higher for the S1 system, as compared to S2, whereas comparable values are obtained during the progress of the test. Moreover, the P content in the solution decreased rapidly and very similarly as soon as the S1 and S2 groups of specimens were soaked in SBF. In contrast, when the solution was in contact with the S3 system, the most marked depletion of this species is observed to take place during the immersion period from 3 to 7 days.

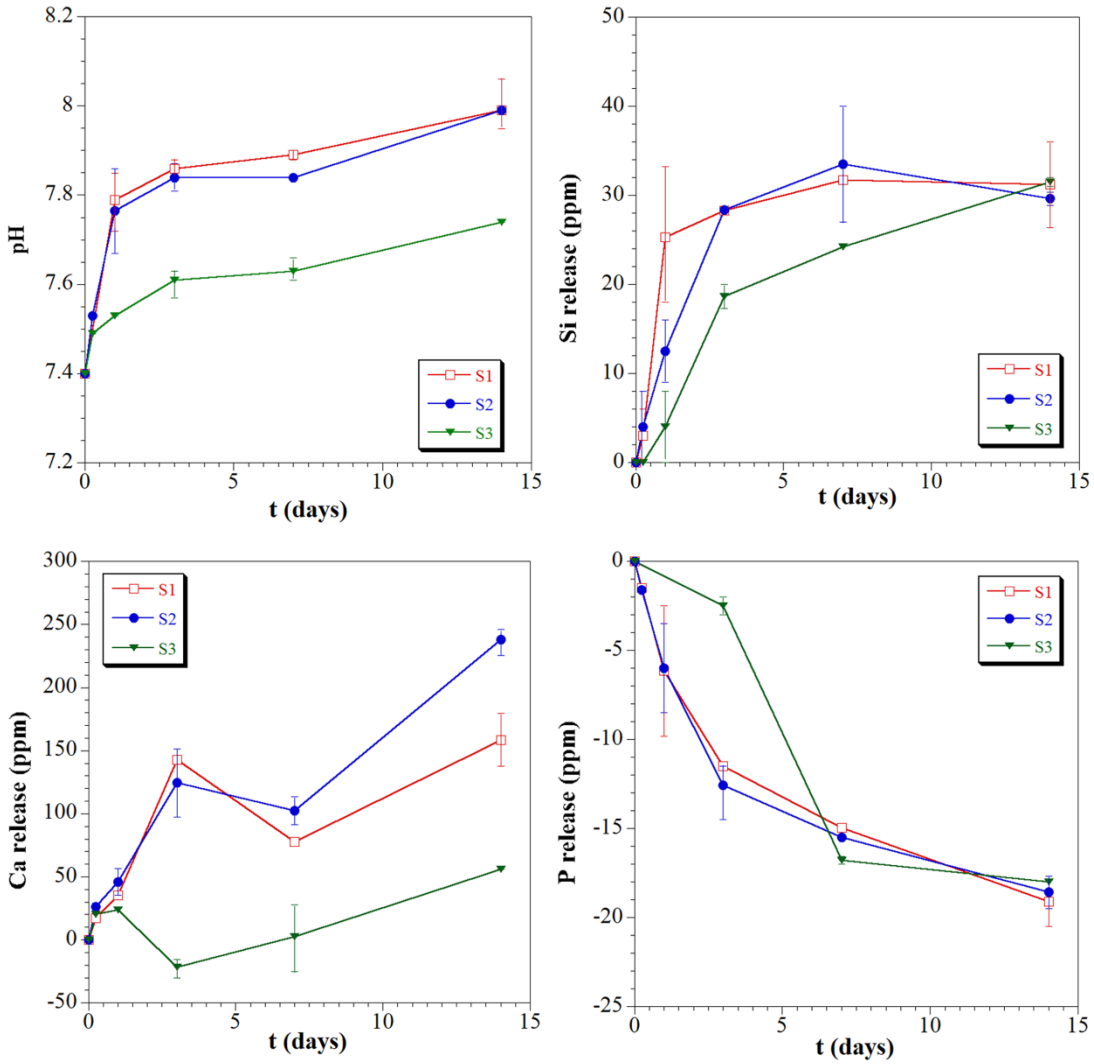

Figure 5.14: Time evolution in pH, Si, Ca and P species content in the SBF solution where the three series of CaMix samples were stored.

5.5 Discussion

The present part of PhD represents a follow-up of a recent study where a similar approach was considered to investigate the behavior of three groups of glass-ceramics, produced under different SPS conditions from standard 45S5 Bioglass® powders, when soaked in SBF [198]. The most important finding was that crystallized 45S5 samples, consisting of $Ca_{1.5}Na_{2.64}Si_9O_3$ with 20 nm sized crystallites were able to generate a larger amount of apatite, as compared to mainly amorphous materials obtained at relatively lower T_D values, i.e. 600°C and 550°C, respectively. Furthermore, the use of ceramic products resulting when the temperature was further increased (700°C) and the dwell time prolonged (from 2 to 20 min) determined the formation of the highest apatite content, when the SBF experiment was extended at relatively long immersion time intervals (7–14 days). The latter feature was ascribed to the beneficial presence of the rhenanite phase formed under more severe SPS conditions.

Based on the outcomes described in the previous section, it is possible to state that a quite different situation is encountered when the SBF test was conducted on the three series of CaMix-derived samples produced as reported in Table 5.2. Such groups of samples are all completely dense, while they differ from the structural and compositional points of view, as evidenced by the Rietveld analysis used to simulate the related XRD patterns. In particular, as reported in Tables 5.3-5.5 (t=0d), specimens S1 obtained when the initial powders were sintered for 2 min at 730°C resulted completely amorphous. In contrast, the about 80wt. % crystallized S2 products, with α-$CaSiO_3$ as a dominant phase, was obtained when the dwell temperature was raised to 850°C. Finally, as the T_D and t_D were both increased to 1000°C and 20 min, the S3 class of glass-ceramics, mostly constituted by β-$CaSiO_3$, with no α-$CaSiO_3$ and containing a residual 12 wt.% amorphous phase, was generated. The presence of such crystalline phases, which are not expected to be detrimental for the *in vitro* apatite-forming ability [264,265], is consistent with the

results obtained in previous investigations [249,257]. The more severe sintering conditions correspondingly adopted were also accompanied by a moderate crystallites growth, i.e. from 90 to 95 (S2) to 110 nm (S3). Minor amounts (2–4wt.%) of other silicate phases, namely Kilchoanite and Combeite, were also formed in the latter two systems.

With regard to the *in vitro* test results, it is generally seen that the formation of the apatite phase is always preceded by the amorphization of the material. This fact could be likely ascribable to partial nucleation and growth of apatite (micro- and nanocrystallites), together with the formation of an underlying silica gel film. In fact, as reported in the literature [262,266], the apatite precipitates formed on bioactive glasses in SBF are very defective and microcrystalline, therefore their XRD spectra are characterized by relatively weak and broad peaks. The latter ones become more intense with increasing soaking times in the solution, due to a more complete conversion of the samples surface into apatite. Moreover, the additional presence, detected after short immersion times, of a broad signal at lower diffraction angles (typically at 2θ values between 20° and 25°) than those correlated to the halo of the as-prepared glass was already explained in previous works [267,268]. Specifically, such signal can be ascribed to the development of a silica gel film on the glass surface, i.e. a Si-rich layer with a lower content of alkaline and alkaline earth ions as compared to the original glass, whose formation is reported among the initial steps which lead to the apatite precipitation on the glass surface [13]. The presence of signals ascribable to micro and nanoapatite (i.e. a broad band at about 2θ ~ 32°, where the most intense peak of apatite usually appears, an additional peak in the 25°-27° 2θ range and a broad signal in the 45°-55° 2θ interval [268]) can be clearly detected (around 9 wt.%) in the corresponding pattern at t=3d.

More important, a relevant discrepancy is evidenced between the three systems when examining the amount and the rate of formation of the apatite phase produced on

their surface. In particular, both these aspects follow the subsequent decreasing order S1>S2>>S3.

Such a different biological behavior has to be necessarily associated to the initial structural and compositional characteristics of these three classes of glass-ceramics, as discussed in what follows. The full amorphous character of S1 products makes them prone to display a high dissolution rate since during the first stage immersion, as proved by the related weight loss as well as the corresponding increase in pH, Ca and Si contents. In addition, the slight weight gain recorded in the storage range from 1 to 3 days could be readily explained by the fact that, during such time interval, sample dissolution is more than compensated by the formation of the apatite layer on its surface. Indeed, as mentioned above, the rate of formation and the amount of apatite generated are both higher for the S1 system with respect to the other two contenders.

The relevant crystallization (up to 80wt.%) induced in the CaMix material when the sintering temperature was raised from 730°C (S1) to 850°C (S2) is observed to provide some, albeit not dramatic, depressing effects in term of apatite production. In particular, the maximum content of apatite, as revealed by Rietveld analysis (Tables 5.3 and 5.4), decreased from 27 to 21 wt.% after 14 d storage. Such differences, also evidenced for shorter immersion time intervals, are also likely responsible for the weight loss behavior observed in S2 samples up to 7 days, since at this stage the amount of apatite produced for this system is apparently not sufficient to compensate dissolution effects. On the other hand, the opposite situation is established for relatively longer soaking times (Fig. 5.13).

More relevant discrepancies, with respect to the previous systems, are observed when the test was conducted using the S3 group of samples. Indeed, the dominant presence of β-$CaSiO_3$ in the resulting sintered material is found to determine, as compared to S1and S2 systems, not only a marked reduction in the amount of the apatite produced on the sample surface but also a delay in the generation of such phase (Fig. 5.9). This fact can be readily associated to the markedly slower dissolution rate (Fig. 5.13), the

minor pH increase and moderate change in the concentration of the species present in the SBF (Fig. 5.14) correspondingly manifested during the test involving S3 specimens. Of particular importance is the very slow and modest P depletion from the SBF (Fig. 5.14), which represents the main source of this element for the formation of apatite.

All these outcomes clearly indicate the rather modest interaction occurring among the last group of samples and the fluid. Therefore, although different studies in the literature have reported that both α- and β-$CaSiO_3$ exhibit good bioactivity and biocompatibility [269–271], the results obtained in the present investigation clearly indicate that the presence of such phases, particularly the β-configuration, could reduce, even strongly, the capability of the original glass to produce the apatite layer during SBF tests.

In conclusion, some final considerations should be made regarding the use of the SBF protocol in this work, as well as the utilization of fully dense samples, instead of porous scaffolds, for such tests. Regarding the first issue, it was evidenced in the literature that the use of SBF for bioactivity testing might lead to some controversial results [150]. Therefore, the latter approach did not allow to unequivocally predict the *in vivo* behavior of the material. Despite these criticisms, the SBF testing is still broadly utilized by scientists, in particular, as for the present work, to compare the apatite forming ability of different samples when dipped in the same solution.

As far as the use of dense samples is concerned, it should be mentioned that, although bioglasses are commonly utilized as porous scaffolds, some applications of pore-free structures are also reported in the literature, for instance for the repair of orbital floors [179]. In any case, the fabrication of fully dense bioglass-derived products should not be necessarily addressed to their direct application, while it is considered more suitable for the primary purpose of the present study, i.e. to better compare their ability to form apatite when immersed in SBF. Therefore, the obtained results provide useful preliminarily indications of the material behavior, that could be subsequently

validated when considering porous bodies. In the latter regard, it is worth to mention that, although the primary use of the SPS technology is certainly the fabrication of dense materials, porous structures could be also produced through this technique by properly controlling the operating conditions (applied pressure/sintering temperature, initial powder, porogens addition, etc.) [272–274].

5.6 Concluding remarks

There is no unequivocal answer relative to the effects produced by devitrification phenomena which take place during the consolidation of amorphous powder on the biological behavior of the resulting material. Indeed, although this event is often reported to negatively affect the latter property, more recent studies highlighted that this aspect depends also on the crystallization degree achieved, the specific crystalline phases formed as well as the size of their crystallites. In turn, these features are specifically related to the sintering technique adopted. Therefore, the validation of novel glass compositions for biomedical applications has to be duly accompanied by an accurate experimental activity aimed to optimize their bioactivity characteristics.

To this purpose, in this part of PhD work, the biological response during *in vitro* tests in SBF of three groups of dense samples, produced by SPS from a recently developed glass with high CaO content, was investigated in detail. Although all the examined specimens display apatite-forming ability when stored in SBF, noticeable discrepancies in their behaviour were clearly observed when the formation process dynamic and the new phase content are compared quantitatively. Specifically, the mildest sintering conditions adopted (730°C, 2min) corresponded to a completely dense and amorphous material, which exhibited superior capability to generate in shorter times (less than 3 days) amounts of the apatite phase up to 27 wt.% during in-vitro tests in SBF. Such attitude was only moderately reduced when considering the 79 wt.% crystallized specimens, obtained by SPS at 850°C and mainly consisting of about 95nm sized α-$CaSiO_3$ crystallites, with smaller amounts of β-$CaSiO_3$ and other

minor phases. On the other hand, the apatite formation process significantly slowed down, when the SBF solution was interfaced with the third group of glass-ceramic samples produced at 1000°C and 20 min and mainly consisting of β-$CaSiO_3$. Thus, the presence of the latter phase in CaMix derived products seems to play the major role, rather than the relatively modest increase of the crystallization degree (from 79 to 88 wt.%), to determine the observed reduction in the generation of the apatite layer. This feature is readily associated to the correspondingly lower weight loss, pH increase and ions released, to indicate a scarce interaction of these materials with the physiological fluid.

Remarks

This part of PhD was mainly conducted in the Department of Mechanical, Chemical Engineering and Materials Science at the University of Cagliari in collaboration with Dipartimento di Ingegneria "ENZO Ferrari", Università degli Studi di Modena e Reggio Emilia (Italy). As a PhD student involved in this project, I was working with my colleague Dr. Selena Montinaro (PostDoc, University of Cagliari) on the preparation and characterization of bulk bioactive glass samples. Rietveld analysis was conducted by Dr. Sebastiano Garroni (PhD, University of Sassari). The research activity was mainly guided by Prof. Roberto Orrù.

The results of this investigation were published in Journal of the European Ceramic Society Volume 39, Issue 4, April 2019, Pages 1603-1612.

Article title: *Spark plasma sintered CaO-rich bioglass-derived glass-ceramics with different crystallinity ratios: A detailed investigation of their behaviour during biological tests in SBF.*

doi.org/10.1016/j.jeurceramsoc.2018.12.003

Chapter 6. Study of cell biocompatibility of CaO-rich bioactive glass and bioceramic composites

6.1 Introduction

As discussed in Chapter 3 (Paragraph 3.4.3), bioceramics represent a broad class of materials that is employed in bone grafting and dentistry. Among them, calcium phosphate-based materials, and in particular hydroxyapatite (HA), are commonly used, in place of autografts and allografts, due to their biocompatibility and osteoconductivity [141,210]. Several investigations also demonstrated the osteoinductive character of HA, as the latter one is able to promote new bone formation [275,276]. HA is commonly used as bone grafts – in form of granules, powders, porous or dense bodies – and as coatings for metal implants with the aim to increase the biomimetic response of the prosthesis [157]. Nonetheless, this material is thermodynamically stable at body temperature and physiological pH, so that its reactivity *in vivo* is typically low and HA resorption occurs very slowly [277,278]. This fact represents the major clinical drawback, since bone grafts should degrade at the same rate as the new tissue forms, thereby resulting in the complete substitution by functional bone tissue. Another crucial aspect is associated to the realization of bulk HA products, which typically involves pressureless or classical pressure-assisted sintering methods to consolidate the starting powders, so that high temperature conditions are required (between 1150°C and 1350°C [279]). Consequently, possible HA decomposition [280] and, correspondingly, negative effects on the biological and mechanical performance of the final materials could arise.

The production of HA-based composites with bioactive glasses as second phase is an intriguing alternative to go beyond these limitations [280,281]. In fact bioactive glasses, and in particular the 45S5 Bioglass® [13] – bond to bone more rapidly than HA. It is known that 45S5is osteoinductive, seems to induce neovascularization and it exerts an antibacterial effect on a range of oral bacteria [282,283]. For these reasons,

the fabrication of HA/bioactive glass composites could lead to innovative systems with tunable bioactivity, tailored to specific clinical applications [281]. In fact, by modifying the volume fractions of the constituents, it is possible to control the biological performance of the final system. At the same time, bioactive glasses can be used to incorporate important ions from a biological point of view (i.e. strontium, magnesium, silicon, etc. [284]) within the HA lattice, in order to closely mimic the composition of the biological apatite, i.e. the mineral phase of bone.

As for the case of dense HA, also HA/bioglass composites are usually fabricated by means of pressureless or conventional hot-pressing sintering techniques. Unfortunately, such methods require high temperatures (up to 1200°C–1300°C, depending both on the HA to glass ratio and the glass composition [280]), which exceed the crystallization point of the glass. For example, as described in a Chapter 3 (Paragraph 3.4.3.2, see Fig. 3.5), 45S5 Bioglass® starts to crystallize at about 600°C and it has a crystallization temperature between 650°C and 690°C, depending on the heating rate and particle size [197,213,249]. Such high temperature treatments not only induce the devetrification of the bioglass in the composite, with possible negative effects on the resulting bioactivity [179], but may also cause HA decomposition and reactions between the ceramic and the glassy phase. For these reasons, the production of more suitable HA/bioglass composites requires:

(1) novel bioactive glass compositions with high bioactivity and lower tendency to crystallize than 45S5;

(2) the exploitation of more efficient densification techniques to obtain fully dense ceramic products under milder sintering conditions, as an alternative to classical sintering.

In this context, a novel CaO-rich, K_2O-containing bioglass (CaMix) with the composition described in details in Chapter 5 (See a Table 5.1) was specifically designed to be employed whenever a thermal treatment is required, thanks to its

lower tendency to crystallize, higher devetrification temperature of about 880°C [256] and higher sinterability than 45S5 [285,286]. The feasibility of CaMix/HA-based composites with different ratio of constituents has been recently investigated [257]. Unfortunately, even though it was possible to fabricate such composites by means of pressureless sintering, the samples with lower bioglass amounts were characterized by some residual porosity after the heat treatment, which negatively affected their mechanical properties.

On the other hand, HA/CaMix composites with lower porosity, higher compactness and hardness, than the counterparts obtained by conventional sintering techniques were successfully produced by means of Spark Plasma Sintering (SPS) [287]. As described more in details in a Paragraph 4.1 SPS represents an efficient and powerful consolidation method with respect to conventional ones, in terms of both temperature and processing time [225].

Most important, the bioactivity of the HA/CaMix composite samples produced by SPS has been successfully tested *in vitro* using a SBF solution; in particular, it was demonstrated that the relative amount of hydroxycarbonate apatite (HCA) which formed on the samples' surface during the immersion in SBF increased when the amount of CaMix is augmented [287].

6.2 Aim

In this light, the scope of the present part of PhD is to investigate the *in vitro* biocompatibility towards cells of different HA/CaMix composites as well as to study the possible influence of the relative amount of CaMix on cells viability and proliferation.

For this purpose, the biocompatibility of a set of pure HA, pure CaMix and HA/CaMix composites with different HA/CaMix proportions (i.e. from 20 wt.% to 70 wt.% HA) produced by SPS will be tested with murine long bone osteocytes (MLO-Y4) by means of a multi-parametric approach. Tetrazolium salt XTT and

Neutral Red (NR) uptake assays will be used to investigate cell viability, while Bromodeoxyuridine (BrdU) assay will be employed to evaluate the effects of the produced materials on cell proliferation. Possible cytotoxic effects of the samples' extracts will be also considered. The findings arising from the SBF tests previously cunducted on HA/CaMix composite samples prepared by SPS [287] will be compared with the results of the present biological investigation.

6.3 Experimental

6.3.1 Materials and Methods

6.3.1.1 Glass and Composites preparation

The CaMix glass (composition: 47.3 mol% SiO_2, 45.6 mol% CaO, 2.3 mol% K_2O, 2.3 mol% Na_2O, and 2.6 mol% P_2O_5) was prepared by a melt-quenching route [256,288,289] at the Department of Engineering "Enzo Ferrari", Università degli studi di Modena e Reggio Emilia (Italy). Briefly, the commercial raw powder reagents – all reagent grade – (SiO_2, Na_2CO_3, $CaCO_3$, K_2CO_3, $Ca_3(PO_4)_2$ by Carlo Erba Reagenti, Rodano Milano, Italy) were mixed in a laboratory shaker for 2 h and then melted at 1450°C for 1 h. The molten CaMix was then quenched in water to obtain a frit which was dried at 110°C for 12 hours. Subsequently, the frit was ground for 40 min in dry conditions to produce a powder (grain size< 67µm).

Proper amounts of commercial HA powders (CAPTAL® Hydroxylapatite, Plasma Biotal Ltd, UK) were mixed for 6 hours with CaMix powders in order to prepare the following set of composites [287]:

- 80 wt.% CaMix and 20 wt.% HA powders ("80BG_20HA");
- 50 wt.% CaMix and 50 wt.% HA powders ("50BG_50HA");
- 30 wt.% CaMix and 70 wt.% HA powders ("30BG_70HA").

6.3.1.2 Spark Plasma Sintering of glass, HA and composite powders

The SPS 515S apparatus (described in the previous Chapter, Paragraph 5.3.1) was used for the consolidation of CaMix, 80BG_20HA, 50BG_50HA, 30BG_70HA, and HA powders. The amount of powders used for the obtainment of the various dense specimens is reported in Table 6.1 along with the adopted SPS conditions. It should be noted that the latter ones have been defined based on the systematic investigation conducted in previous works on the effect of the SPS parameters on powder densification [228,249,287].

System	Powder amount (g)	Dwell temperature, T_D (^oC)	Dwell time, t_D	Mechanical pressure, P (MPa)
CaMix	1.4	730	2 min	16
80BG_20HA	1.49	800	3s	30
50BG_50HA	1.53	1000	3s	30
30BG_70HA	1.56	1150	3s	30
HA	1.6	1200	5 min	30

Table 6.1: Experimental conditions adopted to produce bulk CaMix, HA, HA/CaMix composites by SPS.

Five series of sintered disks with 14.7 mm diameter and about 3 mm thickness were correspondingly obtained. For each composition 10 samples were prepared.

The relative density (ρ) of each polished specimen was measured by Archimedes method using distilled water. Weighting of the specimen was carried out taking advantage of a Ohaus Explorer Pro (Ohaus Corporation, NJ, USA) analytical balance (± 0.0005 g precision). The theoretical densities of the composite systems, i.e., 2.915 (80BG_20HA), 3.015 (50BG_50HA) and 3.074 g/cm^3 (30BG_70HA), were determined using a rule of mixture *(Eq. 6.1)* [290] and by considering the values of 3.16 and 2.86 g/cm^3 for HA and CaMix, respectively [287].

$$\frac{1}{\rho_c} = \frac{w_{HA}}{\rho_{HA}} + \frac{w_{BG}}{\rho_{BG}} \quad (eq.6.1)$$

where ρ_c, ρ_{HA}, ρ_{BG}, represent the density of the composite, HA and CaMix, respectively; w_{HA}, w_{BG} the weight fraction of HA and CaMix respectively, in the composite.

In this regard, it should be noted that the amount of powder used for the preparation of about 3 mm thick nearly fully dense products was varied as reported in Table 6.1, according to the relative content of the two constituents in each series of bioceramics taken into account.

6.3.2 Biocompatibility tests

In this work, MLO-Y4 (murine long bone osteocyte-like immortalized cell line) cells were selected to investigate the ability of the prepared samples (CaMix, HA, 80BG_20HA, 50BG_50HA and 30BG_70HA) to support cell growth.

The cytotoxicity of the materials was evaluated both through indirect contact, with the aim to test the possible negative effects of the materials' eluates, and direct contact, where the cells are seeded on to the sample and subsequently incubated under proper conditions.

Cell survival, viability and proliferation were studied by means of Neutral Red (NR) uptake, tetrazolium salt XTT (2,3bis(2-methoxy-4-nitro-5-sulfophenyl)-5-[(phenylamino) carbonyl]-2H-tetrazoliumhydroxide) and Bromodeoxyuridine (BrdU) assays.

6.3.2.1 Cell culturing and preparation of materials' extracts

MLO-Y4 cells were cultured, as indicated by the supplier, in Dulbecco's modified Eagle's medium (DMEM) (Invitrogen, Karlsruhe, Germany), supplemented with 10% fetal bovine serum (Invitrogen), sodium pyruvate 1 mM (Invitrogen), D-Glutamine 2mM and 100 µg/ml penstreptomycin (Invitrogen). The cells were seeded

in 6 well plates with the materials for the direct contact tests and the NR assay (see next paragraphs) was performed. The plates were incubated at 37±1∘C in 5%±1% CO_2 humidified air (90%± 5% humidity) and subcultured every about 72 h to maintain the cell populations at less than 70% confluent.

The materials' eluates for the indirect contact test were obtained by treating them in centrifuge tubes (6 cm^2/ml area) containing DMEM. DMEM only and DMEM with 0.45% of phenol solution were used as negative (CTRL-) and positive (CTRL+) controls, respectively. The vials were maintained at 37ºC for 5 days and every eluate was filtered by means of a 0.22 µm filter, according to ISO 10993–5 [291] and ISO 10993–12 [292] standard procedures. pH measurements were periodically carried on to control the physiological conditions of the culture medium.

6.3.2.2 NR test

The NR cytotoxicity (Neutral Red solution N6264 Sigma, Germany) assay is a widely used procedure to investigate cell survival/viability. It is based on the ability of healthy viable cells to incorporate and bind neutral red, a supravital dye. MLOY4 cells were cultured in direct contact with the materials for 24 h and 72 h at 37∘C±1∘C, 90%±5% humidity, and 5.0%±1% CO_2/air. After the removal of the samples and the culture medium, 250 µL of NR solution (Neutral Red solution N6264 Sigma, Germany) were added to all wells including the CTRL+ and the CTRL- and left to incubate for 3h. Subsequently, the NR solution was removed, the cells were rinsed with 250 µL D-PBS and 100 µL NR Desorb (ETOH/acetic acid) solution, which is used to extract the NR from the cells, was added to all wells. After incubation (20 min), the amount of dye which has been incorporated by the cells was measured employing a spectrophotometer (Multiscan RC by Thermolab system, Finland) at 540 nm. CTRL+ and the CTRL- were used as references.

6.3.2.3 Morphological evaluations

The cells morphology after 24 h and 72 h direct/indirect contact with the materials was observed using optical microscopy (Nikon TMF, Japan).

6.3.2.4 XTT test

The XTT test was used to evaluate the cell viability after exposure to the samples' eluates. Such colorimetric assay is widely used to study the mechanisms of cell activation and damage via cellular metabolic activity. XTT protocol evaluates the cell viability based on the activity of mitochondrial enzymes in metabolic active cells that reduce the yellow tetrazolium salt XTT to a water-soluble orange coloured product, whose amount is proportional to the number of living cells. Such newly synthesized orange formazan dye can be quantified by measuring absorbance at wavelength of 490 nm [293,294]. Cells were grown in 96 well culture plates and incubated with the materials' eluates for 24 h and 72h. Subsequently, the incubation XTT labeling solution (Cell Proliferation KitII (XTT) Roche diagnostics, USA) was added (final concentration 0.3 mg/ml) and left to incubate for 4h. The amount of the orange formazan dye generated from XTT was then measured by spectrophotometry (Multiscan RC by Thermolab system, Finland), using CTRL+ and the CTRL- as references.

6.3.2.5 Bromodeoxyuridine (BrdU) test

BrdU cell proliferation test is a commonly used assay to quantify the incorporation of 5-bromo-2-deoxyuridine in replicating DNA of proliferating cells, with the aim to evaluate cell proliferation. Cells were grown in 96 well culture plates and exposed to the materials' extracts for 24h. Subsequently, 50µl/well of BrdU labeling solution (Cell Proliferation ELISA, BrdU, Roche) was added and left to incubate. The incubation time (90 min) is long enough as BrdU is incorporated in place of thymidine into the newly synthesized DNA of the cycling cells. Subsequently the

labeling culture medium was removed and FixDenat solution (Cell Proliferation ELISA, BrdU, Roche) was added, with the aim to fix cells and denature DNA in one step. Such solution was then removed and the samples were further incubated with an antibody conjugated to peroxidase (anti-BrdU-POD), which is able to bind to the BrdU incorporated into the newly synthesized cellular DNA; in this way, it is possible to detect the immune complexes through the subsequent substrate reaction. The amount of the reaction product can be quantified by measuring absorbance at wavelength of 370 nm by means of a spectrophotometer (Multiscan RC by Thermolab system, Finland). The signal intensity is correlated to the amount of the newly synthesized DNA, and, therefore, to the number of proliferating cells.

6.3.2.6 Statistical analyses

One-way variance analysis (ANOVA) was used to statistically treat the obtained results, which are expressed as the mean ± standard deviation; t-test analysis by a two populations comparison was employed to establish differences among groups. Statistical significance was considered at a probability $p < 0.05$.

6.4 Results and Discussion

Prior considering the results obtained in the present study, some findings related to the evaluation of different properties of HA/CaMix composites obtained in previous works should be discussed [228,249,287]. In particular, the microstructure and mechanical behavior of the five series of sintered products, obtained under the SPS conditions summarized in Table 6.1, as well as phase composition and *in vitro* bioactivity in SBF. The main outcomes can be summarized as follows:

1. The obtained bioglass, HA and composite samples are characterized by higher compactness and density with respect to the counterparts obtained with classical sintering methods. In particular, it was possible to produce for the first time by SPS a

set of HA/CaMix composites with high HA content (≥ 50wt.%) with a density close to the theoretical value.

2. Thanks to both aspects, the low tendency to crystallize of CaMix and the milder sintering conditions required by SPS, it was possible to reduce the crystallization of the glassy phase in the samples, with positive effects on their bioactivity. The XRD spectra acquired on the samples are compared in Fig. 6.1. It is seen that the bioglass specimens maintained their original amorphous character after sintering. This holds also partially true when considering the composite system richer in the bioglass constituent. Indeed, the initial occurrence of the glass crystallization during SPS was evidenced by the presence of minor amounts of α-$CaSiO_3$, as detected by the XRD analysis. Moreover, the content of $CaSiO_3$ in both the α- and β-configurations was found to increase as the holding temperature was progressively augmented to achieve the nearly full densification in the other two HA-richer composites systems. Finally, the glass-free HA product is only composed of apatite, with no evidence of secondary phases.

3. The samples' bioactivity in SBF improved when the amount of CaMix in the sample is augmented.

4. Finally, the biocompatibility of CaMix and of HA/CaMix composites with different HA to glass ratio, produced by conventional sintering, has been successfully tested with respect to murine osteocytes and/or fibroblasts [257,295].

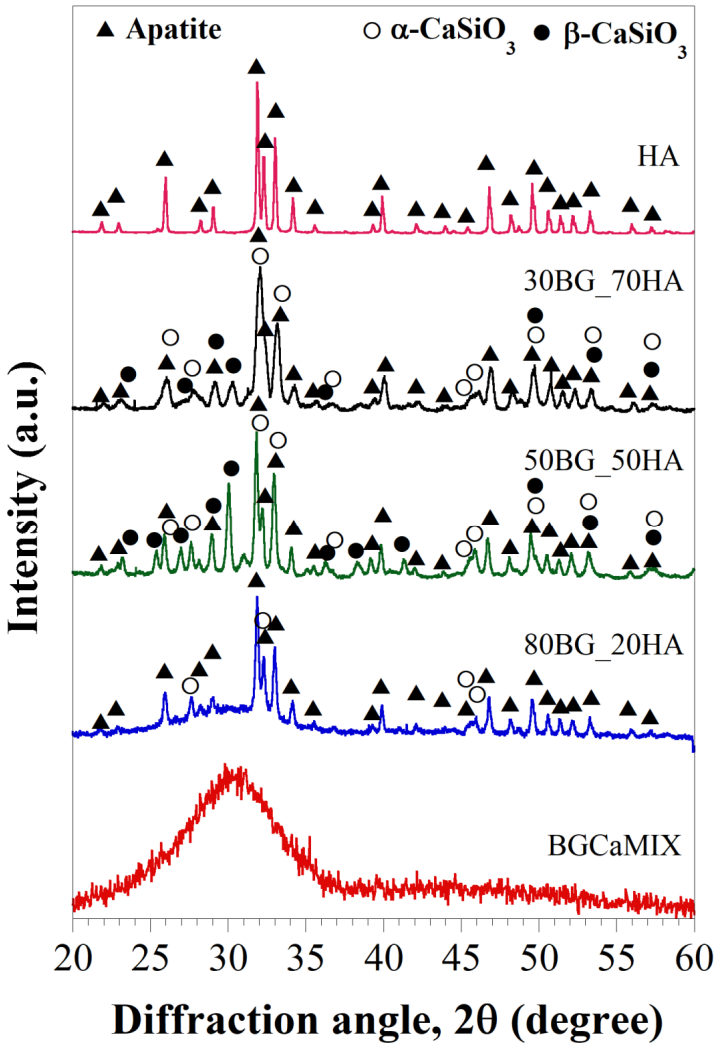

Figure 6.1: XRD patterns of bulk BG, HA, and BG-HA composite samples produced by SPS. A detailed description of the XRD analysis performed on the samples discussed in the present work has been previously reported in [228,249,257].

As outlined in Chapter 3 (Paragraph 3.5), the SBF assay aims to qualitatively evaluate the bone bonding ability of a material (typically bioactive glass, bioceramics or bioactive coatings) by examining the ability of apatite to form on its surface once in contact with SBF, which is a solution with ions concentration similar to that of human blood plasma [204]. In this light, the study performed by Bellucci et al. [287] on pure HA and various HA/CaMix sintered composite samples immersed in SBF revealed that the HCA precipitation, which should reflect the samples bioactivity and their bone bonding ability, increased when the CaMix content in the

sample was increased. Indeed, Figure 6.2 shows the surface of the HA and the 80BG_20HA samples (images observed by Scanning Electron Microscopy) after soaking in SBF for 3 days [287]. It can be clearly observed that the relative content of the apatite precipitates is much higher in the sample with the higher content of CaMix bioglass.

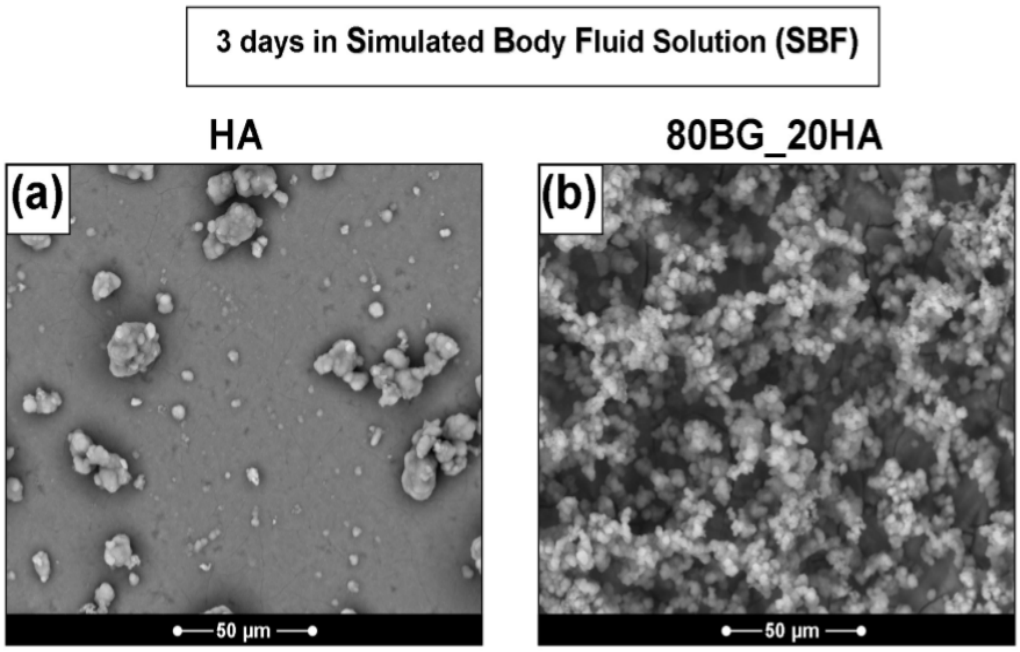

Figure 6.2: Scanning Electron Microscope images of the HA and the 80BG_20HA surfaces after immersion in SBF for 3 days. A detailed description of the SBF tests performed on the samples discussed in the present work has been previously reported in [228,249,287].

In this regard, the present work aims not only to test the biocompatibility towards cells of bioceramics samples obtained by SPS, but also to further demonstrate that SBF assays should be considered as a preliminary screening test. Indeed, the latter one is not able to mimic in a reliable way the complexity of a real physiological environment, which contains cells, proteins, specific trace elements, etc. [150]. Cytotoxicity tests, based on *in vitro* cell culture assays, are therefore crucial to confirm the findings from the bioactivity evaluation with SBF, which has been reported in the literature to lead both to false negative and false positive results [296–

298]. In this context, probably the most striking case is that represented by β-Tricalcium Phosphate: despite its high bone-bonding ability *in vivo*, this ceramic does not always induce the formation of apatite in SBF [150]. Moreover, *in vitro* cell culture assays provide an estimate of cell viability, differentiation, proliferation and they can be employed to determine if a material has potential to be cytotoxic (i.e. through the so-called direct contact tests) or to release agents or degradation products that may be cytotoxic (the so-called indirect contact tests). In this work, the biological performance of HA, CaMix and HA/CaMix composites produced by SPS was studied by means of both direct and indirect contact approaches. Since the materials here proposed have been developed to be used in bone repair and regeneration, the samples were tested with respect to MLO-Y4, which is an osteocite-like immortalized cell line isolated from murine long bones [299,300].

Figure 6.3 shows the results of the viability test with NR uptake, a colorimetric assay which is commonly used to investigate the toxic effects of chemicals and biomaterials on a variety of cell lines from different origin [301,302].

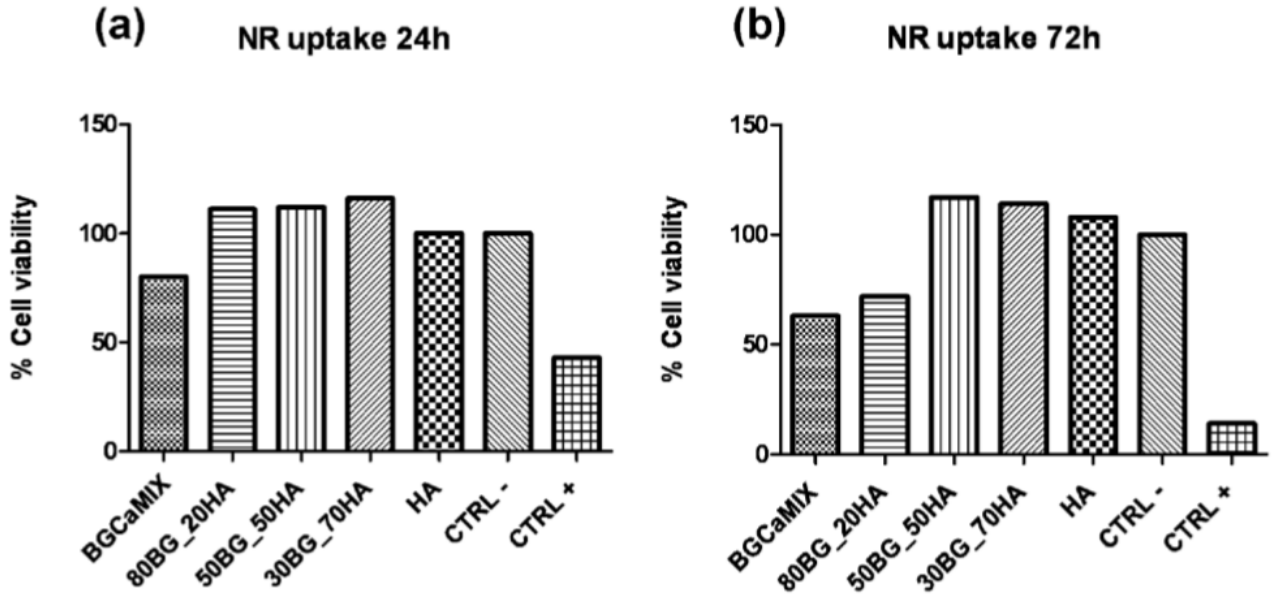

Figure 6.3: NR uptake after 24h (a) and 72h (b) in the different samples.

It shows that healthy cells are able to incorporate the supravital dye neutral red, which is accumulated within their lysosomes. Therefore, a potential loss of integrity and function of the cell (for example, alterations of the cell or the lysosomal membrane), due to exposure to cytotoxic xenobiotics, is expected to result in a decreased uptake and binding of NR [303].

In this way, it is possible to distinguish between injured (or dead) and viable cells. The NR uptake test has been adopted as a recommended assay for qualitative evaluation of biomaterials' safety by several agencies for testing and normalization [304]. The NR uptake and the cell cultures have been here evaluated after 24h (Fig. 6.3(a)) and 72 h (Fig. 6.3(b)) of exposure to the materials. It should be noted that, based on the results of the SBF tests performed on these materials [287] and Fig. 6.2, an enhanced biological performance of the samples with higher CaMix content, which lead higher formation of hydroxyapatite on their surface, could be expected.

On the contrary, the results obtained in this work indicated that, after 24h (Fig. 6.3(a)), the exposure to CaMix induces a slightly lower cell viability, although the decreasing in the lysosomal activity is not so significant to be considered a cytotoxic effect. Such effect is more pronounced after 72h (Fig. 6.3(b)), where the samples with higher CaMix content (i.e. CaMix itself and 80BG_20HA) correspond to a lower cell viability. However, also in this case, the produced materials remained not cytotoxic. This fact was detectable only by considering the results from the NR uptake assay (see the next paragraphs), which is a direct contact test, and it could be ascribed to the high release of ions and particulate from the glassy phase.

It is known that bioactive glasses have a typically higher reactivity than apatite. On the other hand, it is also reported in the literature that the presence of particles and crystals in the culture medium may affect the accuracy of the absorbance readings employed to detect the dye neutral red [305,306]. Therefore, it is crucial to integrate such test with the results from additional cytotoxicity assays, in particular based on an indirect approach. In such an indirect test it is typically evaluated if a solution,

which contains the extractable compounds of a given material, has potential to cause changes cells' morphology and/or lysis. The NR uptake after 24 h and 72 h of direct contact to 50BG_50HA, 30BG_70HA and HA was analogous or even higher than CTRL- (Fig. 6.3), therefore also these materials did not show a cytotoxic response.

A morphological evaluation of MLO-Y4 cells after 24h indirect contact with the samples is reported in Fig. 6.4. Despite the CaMix content is different in these samples, no relevant effects were here observable in the cells' behaviour. In fact, MLO-Y4 grew very well in all the materials' extracts and showed a morphology similar to that of the cells in the CTRL-: no significant cell morphology changes were observed, including lysed or rounded cells.

Fig. 6.5 (a, b) shows the results of the viability test performed by means of XTT colorimetric assay [294,307]. After 24h and 72h of culture in the samples' eluates, the mitochondrial activity of the cells is higher than CTRL- for all the materials, including the samples with higher CaMix content, thus indicating that MLO-Y4 grew and proliferated normally. However, also in this case, the pronounced *in vitro* bioactivity in SBF of CaMix and 80BG_20HA ([287] and Fig. 6.2) did not result in an enhanced biological performance with respect to pure HA.

Finally, Bromodeoxyuridine test (BrdU) was used to evaluate the proliferation of MLO-Y4 cells cultured in extracts from the developed materials. BrdU is incorporated into the newly synthesized DNA in place of thymidine, therefore it acts as a marker of the cycling cells, which can be detected by immunohistochemistry [308]. According to the results reported in Fig. 6.5(c), the produced materials did not affect negatively the cells. Specifically, it is possible to observe that CaMix, 80BG_20HA and 50BG_50HA samples preferably stimulate the cell proliferation. While this fact has been previously observed and discussed in several works (see, for example, [284,309]) when dealing with the "gold" standard 45S5 in powder or bulk form, analogous investigations carried out using sintered bioglasses and, in particular, bioglass-based composites sintered by SPS are lacking in the literature. Based on

these findings, SPS seems to be a promising tool to produce sintered bioglasses and bioglass-based composites, without negatively affecting the biocompatibility of the powder undergoing consolidation.

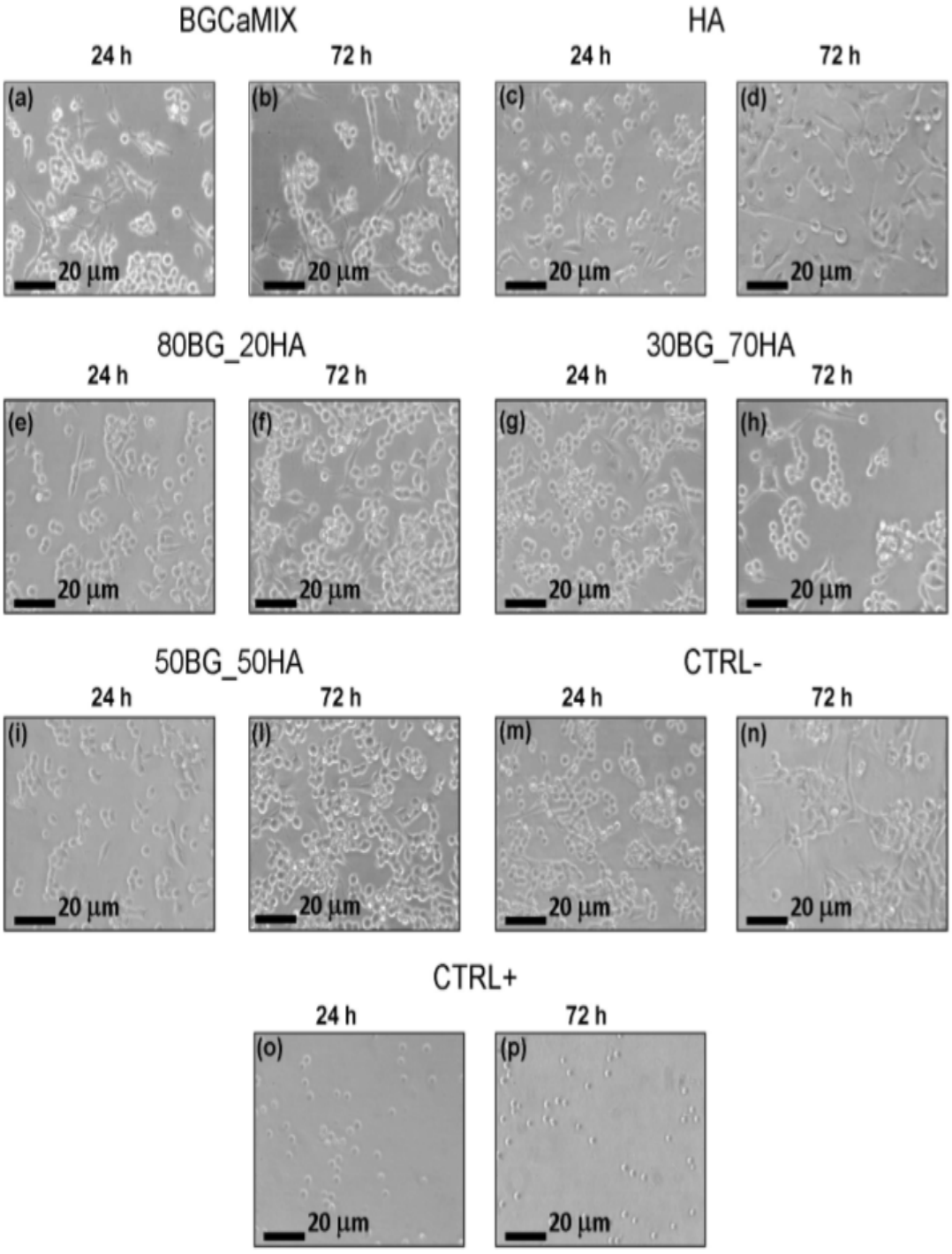

Figure 6.4: Morphological evaluation of MLO-Y4 cells after 24h indirect contact with the samples using optical microscopy (Nikon TMF, Japan).

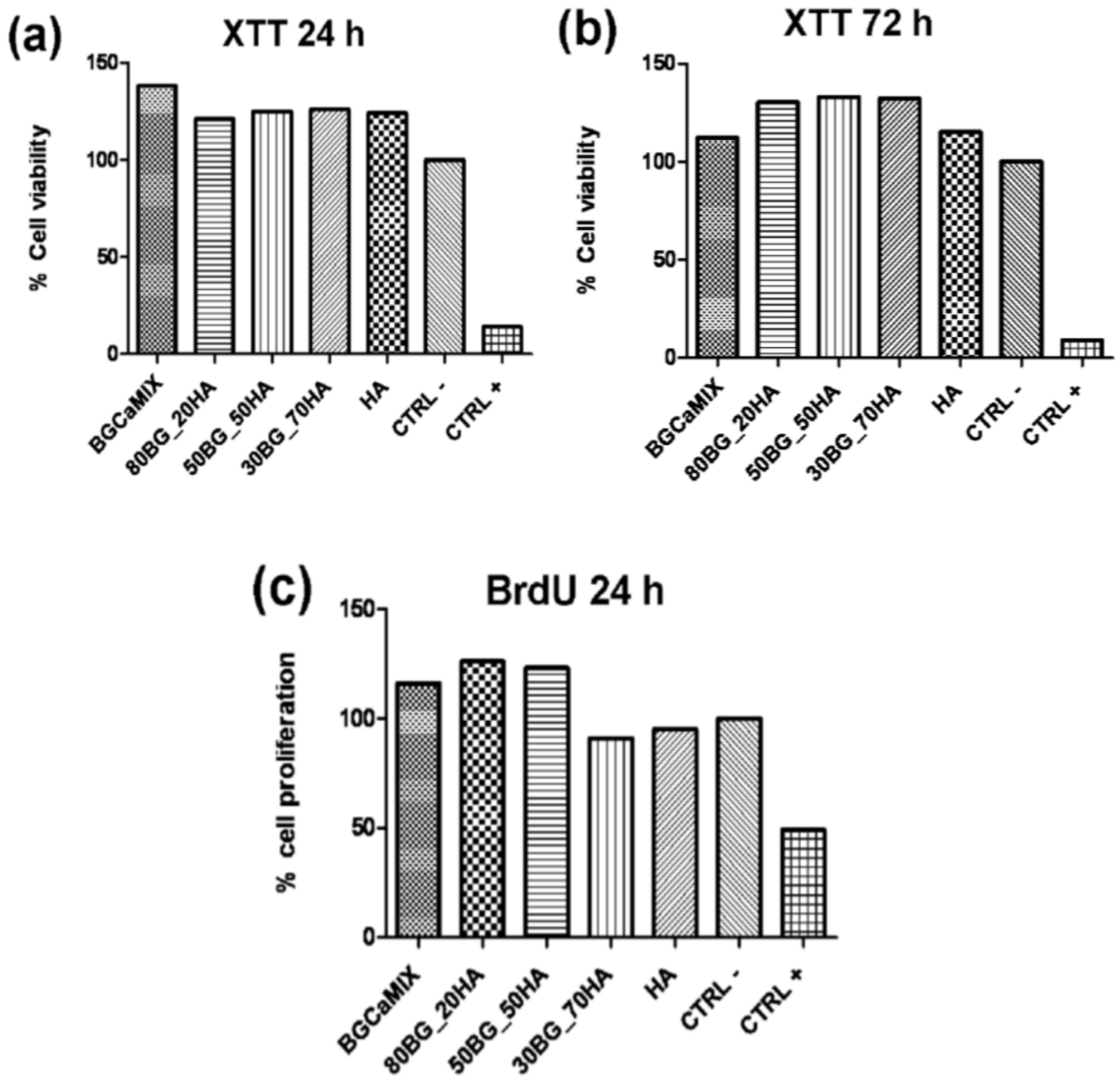

Figure 6.5: XTT test of MLO-Y4 cells cultured in eluate from the samples after 24h (a) and 72h (b); BrdU test after 24h (c).

6.5 Conclusions

Some recent investigations were addressed to the fabrication by SPS of bulk bioglasses, HA and HA/bioglass composites. In this context, a novel lab made CaO-rich, K_2O containing glass, named CaMix was also considered. It should be recalled

that CaMix was specifically designed to be employed whenever a thermal treatment is required, thanks to its lower tendency to crystallize with respect to the widely used 45S5 . According to SBF tests, the *in vitro* bioactivity of the samples, which should, in principle, reflect the bone bonding ability of the material, is progressively improved with the increasing amount of CaMix in the sample itself. In this work, for the first time, the biocompatibility of a set of pure HA, pure CaMix and HA/CaMix composites produced by SPS was evaluated with respect to murine long bone osteocytes by means of both direct (NR uptake) and indirect test (XTT and BrdU). It should be noted that, although previous works [257,295] confirmed the biocompatibility of both CaMix and HA/CaMix composites produced by conventional sintering, analogous investigations involving bioglasses and bioglass-based composites sintered by SPS are lacking in the literature.

Despite none of the samples here considered was cytotoxic, the findings of the biological evaluation did not confirm the outcomes arising from the SBF assay. In particular, the results of direct tests did not show an enhanced “biological performance” in the samples with increasing glass content. This fact may be ascribed to the high release of ions and particulate from the glass phase, which could affect the cell viability. Nonetheless, it should be noted that it is also reported in the literature that the presence of particulate in the culture medium may affect the accuracy of the absorbance readings employed in the colorimetric assay. In general it is found that, the samples with a higher glass content (CaMix, 80BG_20HA and 50BG_50HA) slightly stimulate the cell proliferation. It is possible to conclude that SPS is a convenient technique for the preparation of sintered bioglasses and bioglass-based composites, under less severe conditions, so that the suitable biological properties of initial powders are highly preserved.

Moreover, the present work demonstrates once more that the results of the SBF assays should be interpreted with great care, making sure that the results arising from direct contact tests are integrated with those deriving from the indirect ones.

Remarks

This part of PhD was carried out thanks to the collaboration between Dipartimento di Ingegneria "ENZO Ferrari", Università degli Studi di Modena e Reggio Emilia (Italy) and Università di Cagliari (Department of Mechanical, Chemical Engineering and Materials Science). As a PhD student, I was involved in this project primarily for the preparation of bioactive glass, hydroxyapatite and composite samples, and the related characterization by XRD. Biological tests were conducted at Università degli Studi di Modena e Reggio Emilia. This study was mainly guided by Prof. Valeria Cannillo, Dr. Devis Bellucci and Prof. Roberto Orrù.

Results of this investigation were published in the Biomedical Glasses journal (2018); 4:21-31.

Article title: *Bioglass and bioceramics composites processed by Spark Plasma Sintering (SPS): biological evaluation Versus SBF test*

doi.org/10.1515/bglass-2018-0003

Chapter 7. Advanced Functionally Graded Materials in Calcium Phosphate/Bioactive glass system

7.1 Introduction

A significant challenge in orthopaedic and dentistry clinical practice is currently addressed to long-term stability of implants usually made from metals and their alloys. Indeed, in this context, mismatch of mechanical properties, i.e. Young's modulus, between host tissue and implant can cause a stress shielding; additionally, the release of metallic ions, which can occur due to the implant corrosion in contact with the physiological fluids, may give rise to inflammatory reaction in the body. In order to improve implant surface properties coatings with more biocompatible/bioactive materials such as hydroxyapatite on the metal substrates were proposed so far [310,311]. However, still nowadays coating failure due to the poor adhesion with substrate remains unsolved issue. In this regard, functionally graded materials (FGMs) may represent an intriguing alternative.

According to a definition of Udupa and co-workers (see Chapter 4, Paragraph 4.2), functionally graded materials (FGMs) are "inhomogeneous materials, consisting of two (or more) different materials, engineered to have a continuously varying spatial composition profile" [231].

The concept of FGMs is relatively new, firstly proposed in the middle of 80s to solve the challenges related to the design and production of heat-resistant materials for the aerospace industry. Further, the interest in FGMs was extended to automobile, defence, electrical/electronic, energy and biomedical fields.

The idea behind the possible explotation of functional gradient in biomaterials (either compositional and/or porosity gradient) is that properties of such materials can be tailored in accordance with the specific needs at the site of implantation.

Indeed, implants made of FGM can adapt to the different regions of hosting tissues, therefore creating an improved overall integration and stability in the entire restoration.

As stated in Chapter 4 (Paragraph 4.2), there are two main types FGMs: the first one characterized by a continuous gradient; while the second one with a stepwise structure. Generally, when considering stepwise FGMs, it is intended to obtain two different single-phase materials on the opposite sides of the sample (for example, HA and bioactive glass), while the material in between usually consist of composites based on the two constituents and functional change through space occurs in a discontinuous way.

For example, it is possible to couple a more stable osteoconductive material, on one side of a device, and a more bioactive and bioresorbable one on the other side, thus avoiding any abrupt interface that can negatively affect the system's reliability.

Among the different calcium phosphates studied for bone substitutes, hydroxyapatite (HA), a highly crystalline form of synthetic calcium phosphate $Ca_{10}(PO_4)_6(OH)_2$ (see the Chapter 3, Paragraph 3.4.3.1.1), is known to posseses osteoconductive properties, and also to promote new bone formation *in vivo* [276,312]. However, bioactive properties of HA are limited, meaning that it shows scarce stimulation of osteogenic differentiation and comparably low surface reactivity, i.e. once implanted HA is thermodynamically stable at physiological pH and body temperature.

On the other hand, bioactive glasses (BG), for instance, 45S5 Bioglass® (see the Chapter 3, Paragraph 3.4.3.2), display osteostimulative functions. Therefore, through the formation of a carbonate-substituted hydroxyapatite-like (HCA) layer on their surfaces, both *in vitro* and *in vivo,* this material can provide faster and stronger bonding to bone and surrounding tissues rather that HA [179,188]. Furthermore, according to various studies, certain bioactive glasses were found to stimulate

angiogenic and osteogenic differentiation of stem cells by releasing some bioactive ions [313,314].

However, it is also well recognized that bioglasses suffer from poor mechanical properties, and it is a matter of fact that properties of initially amorphous bioactive glasses can be altered because of the crystallization which can occur during the processing into a final product (i.e. bulk or 3D scaffold).

Moreover, it also should be stressed that the 45S5, especially when used *in vitro* ("static") experimental conditions, can cause a strong local pH-increase because of significant release of sodium in physiological fluids. This alkaline media might be harmful to cells [315,316], in particular, osteoclasts function was found to decrease [317].

In order to overcome the mentioned above limitations of 45S5, a novel CaO-rich, K_2O-containing bioglass (CaMix), with the composition described in details in the Chapter 4 (See a Table 4.1), can represent a promising alternative. Thanks to its low tendency to crystallize, it is possible to obtain fully dense amorphous bulk samples at higher temperature in contrast to 45S5 Bioglass®.

It is known that the fabrication process is one of the most crucial fields in FGM research. Therefore, an appropriate technique which can allow to fabricate samples without altering their initial properties is required. Spark Plasma Sintering was found to be effective for the consolidation of HA [228], CaMix bioglass powders [249] (See Chapter 4) and their composites (See Chapter 5) [287] and permitted to obtain the samples with lower porosity, higher compactness and hardness in comparison to the counterparts produced by conventional sintering techniques. Due to the relatively milder conditions generally required, with respect to conventional consolidation methods to achieve high density levels, several beneficial effects, such as avoiding or limiting decomposition and crystallization phenomena, as well as retaining grain growth, are associated with the use of SPS.

As mentioned above, the use of composites materials in stepwise FGMs, allows to smoothly vary their composition along a given direction of the sample. In this regard, it should be mentioned that the composites made from calcium phosphates and bioactive glasses have been extensively investigated so far, specifically for the bone tissue engineering. As pointed in a comprehensive review by Bellucci and coworkers [280], there are two main motivations for the fabrication and application of CaP/BG composites:

- The first one is related to the biological behavior: in particular, by combining two materials, it is possible to tailor the dissolution and the resorption rate of the final product in order to achieve improved biological properties.
- The second justification concerns the mechanical properties: the addition of BGs to CaPs as a sintering aid make the obtainment of improved mechanical properties, compared to either BGs or CaPs sintered alone possible.

Indeed, according to another extensive review by Karadjian et al. [281], which summarizes the results obtained so far when investigating both *in vitro* and *in vivo* biological properties of different calcium phosphate bioactive glass composites, it can be concluded that, in general, the BG-addition has positive effects on cell adhesion, viability, and proliferation, as compared to pure CaP materials. As far as *in vivo* behavior is concerned, the presence of BG is found to support integration of the material into bone and enhances bone formation.

7.2 Aim

In this light, taking advantage of findings resulting from previous studies where HA, CaMix and HA/CaMix composites were investigated [228,249,287], the main aim of this part of PhD is to fabricate crack-free samples based on advanced stepwise functionally graded HA/CaMix system, where the bioactive glass content varies according to the axial direction.

7.3 Experimental

7.3.1 Materials

Commercial HA powders (CAPTAL® Hydroxylapatite, Plasma Biotal Ltd, UK) with average particle size of 45.7 μm were utilized.

Powder of CaMix bioactive glass was produced and provided by the Department of Engineering "Enzo Ferrari", Università degli studi di Modena e Reggio Emilia (Italy). Glass was obtained by a classical melt-quenching route reported elsewhere [256], with the following composition: 47.3% SiO_2, 45.6% CaO, 2.3% Na_2O, 2.3% K_2O, and 2.6 P_2O_5 (mol. %). The resulting bioactive glass powder showed an average particles size value of about 20μm, as revealed by laser light scattering analysis (CILAS 1180, France).

7.3.2 Preparation of FGMs

FGMs with two different compositional profiles were studied; for the sake of brevity they were assigned as FGM-S1 and FGM-S2 (Table 7.1). HA and CaMix powders relative to each intermediate composite layer were mixed for 1 hours in specified amounts according to Table 7.1.

Layer	**FGM-S1**	**FGM-S2**
(1)	100 wt.% HA	70 wt.%HA-30 wt.% CaMix
(2)	70 wt.%HA-30 wt.% CaMix	50 wt.%HA-50 wt.% CaMix
(3)	50 wt.%HA-50 wt.% CaMix	20 wt.%HA-80 wt.% CaMix
(4)	20 wt.%HA-80 wt.% CaMix	10 wt.%HA-90 wt.% CaMix
(5)	100 wt.% CaMix	100 wt.% CaMix

Table 7.1: FGM-S1 and FGM-S2 layers compositions.

A schematic representation of the FGM-S1 and FGM-S2 to be prepared is reported in Fig. 7.1. Both FGMs were prepared by loading, layer by layer of 5 different mixtures with prescribed composition (Table 7.1).

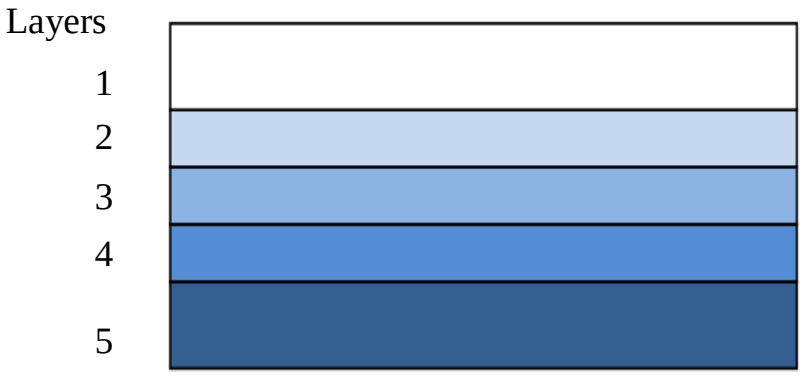

Figure 7.1: Schematic representation of FGM systems based on the combination of HA and CaMix.

The amount of powders utilized for the obtainment of the various dense specimens is reported in Table 7.2 It should be noted that the latter ones have been defined based on the systematic investigation conducted in previous works on the effect of the SPS parameters on powder densification [228,249,287]. It should be noted that the amounts indicated in Table 7.2 correspond to fully dense layers of the following prescribed thickness: layer (1) and (5) of approximately 1.5 mm; layers (2)-(4) of about 1 mm. The larger thickness of the layers located on the opposite sample ends is because an accurate grinding/polishing is required with consequent reduction of the high of the disks, before the characterization

7.3.3 Spark Plasma Sintering

The SPS 515S apparatus (described in previous Chapters) was used for the consolidation of both FGM-S1 and FGM-S2 samples.

The configuration of the die which was designed to sinter FGM samples in this work is reported in a Fig. 7.2. The aim of changing the cross section of the die along the axial direction, in principle, is to correspondingly modify the current density and to generate a temperature gradient.

Layer	FGM-S1 Powder amount (g)	FGM-S1 Powder amount (g)
(1)	0.7	0.7
(2)	0.5	0.5
(3)	0.5	0.5
(4)	0.5	0.5
(5)	0.8	0.8

Table 7.2: Amount of powders used to prepare each layer of FGM-S1 and FGM-S2.

This is necessary to satisfy the following needs:

- Sufficiently high temperatures for layer 1 (located on the top in Fig. 7.2) to guarantee that powder mixtures rich in HA will be highly consolidated.
- Not too high thermal levels for level 5 (bottom part in Fig. 7.2), to avoid or limit devetrification phenomenon from glass phase.

This aspect will be discussed in detail in the following sections.

The die was fabricated from AT101 graphite (Atal s.r.l., Italy). A protective graphite foil (0.13 mm thick, Alfa Aesar, Karlsruhe, Germany) between the compact and inner walls of die/plungers was used to facilitate sample release after SPS. During the process, the die was covered by the graphite felt (3 mm thick, Atal s.r.l., Italy) for the thermal insulation purpose.

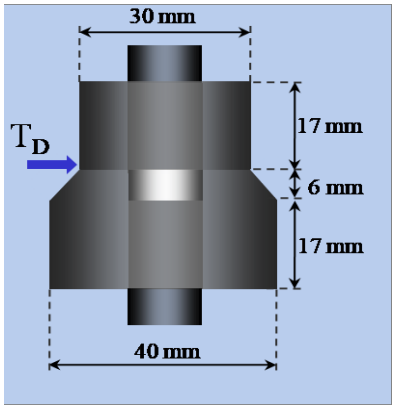

Figure 7.2: Design of the die used to sinter FGM specimens in this work.

SPS experiments were carried out under temperature controlled mode using a thermocouple (Omega Engineering Inc., USA), placed inside in the upper part of the graphite die (see T_D Fig. 7.2). A digital pyrometer (CHINO, mod. IR-AHS2, Japan) focused on the lateral surface of the graphite die was used to monitor the temperature in bottom part of the die.

7.3.4 Characterization of powders and sintered samples

Structural characterization of the initial powders and the opposite surfaces of sintered FGM samples was carried out by X-ray diffraction analysis (Philips PW 1830, Netherlands) using a Ni filtered Cu Kα radiation (λ =1.5405Å).

7.4 Results and discussion

7.4.1 Sample's densification

It is known that, in order to convert hydroxyapatite powder into fully dense bulk specimen temperature conditions generally between 1150ºC and 1350ºC [279] are required. On the other hand, the densification of bioactive glasses typically implies much lower temperature values. For instance, it was reported that, to obtain fully dense, still amorphous, bulk samples from CaMix the temperature of 880ºC [256] is needed. Therefore, it is not possible, when processing FGMs to obtain fully dense hydroxyapatite layer on the one side and keep the amorphous state of bioactive glass layer on the other side of the sample if using the conventional die setup where the temperature is distributed uniformly. In order to generate a suitable temperature gradient along a chosen direction, during SPS a modified die configuration is indeed required. In this context, Jajarmi and co-workers [229] reported the successful densification of FGM samples based on 3mol% Y_2O_3-partially stabilized ZrO_2 (3Y-PSZ) and 316L stainless steel (3Y-PSZ/316L) using a specifically engineered die where the upper cross-section diameter was 28 mm, while the bottom part was 30

mm diameter. A similar approach was also utilized in the present study, to provide a temperature gradient across the axial direction (Fig. 7.2).

A systematic investigation to identify the optimal dwell temperature, pressure and holding time conditions which allow to obtain crack-free FGM-S1 samples, where the pure hydroxyapatite layer is placed on one side of the sample while CaMix bioactive glass layer is placed on a opposite site, was first conducted. The identified optimal parameters are reported in Table 7.3. It is seen that slightly lower temperature (950^{o}C) was required when operating at 50MPa instead of 16MPa.

Temperature, ^{o}C	Pressure, MPa	Dwell time, min
950	50	2
1000	16	2

Table 7.3: Optimal SPS parameters which allowed to obtain crack-free FGM-S1 samples.

However, despite the different temperatures, pressures and dwell periods tested, it was not possible to preserve the initial amorphous nature of the bioactive glass layer. Indeed, the XRD analysis carried out on the surface of the BG layer revealed the occurrence of glass devetrification (Fig. 7.3a).

In both cases, the crystallization of initially amorphous BG powder produced α- and β-$CaSiO_3$.

A different behavior was observed, when considering the FGM-S2 system processed under conditions listed in Table 7.4, amorphous BG was preserved on the bottom side of the sample. The initial occurrence of glass devetrification on the top side of the specimen was evidenced by XRD analysis (Fig. 7.4a). Indeed, the presence of β-$CaSiO_3$ was detected in all 70wt.%HA-30wt.%BG prepared by SPS at 800^{o}C under different processing conditions.

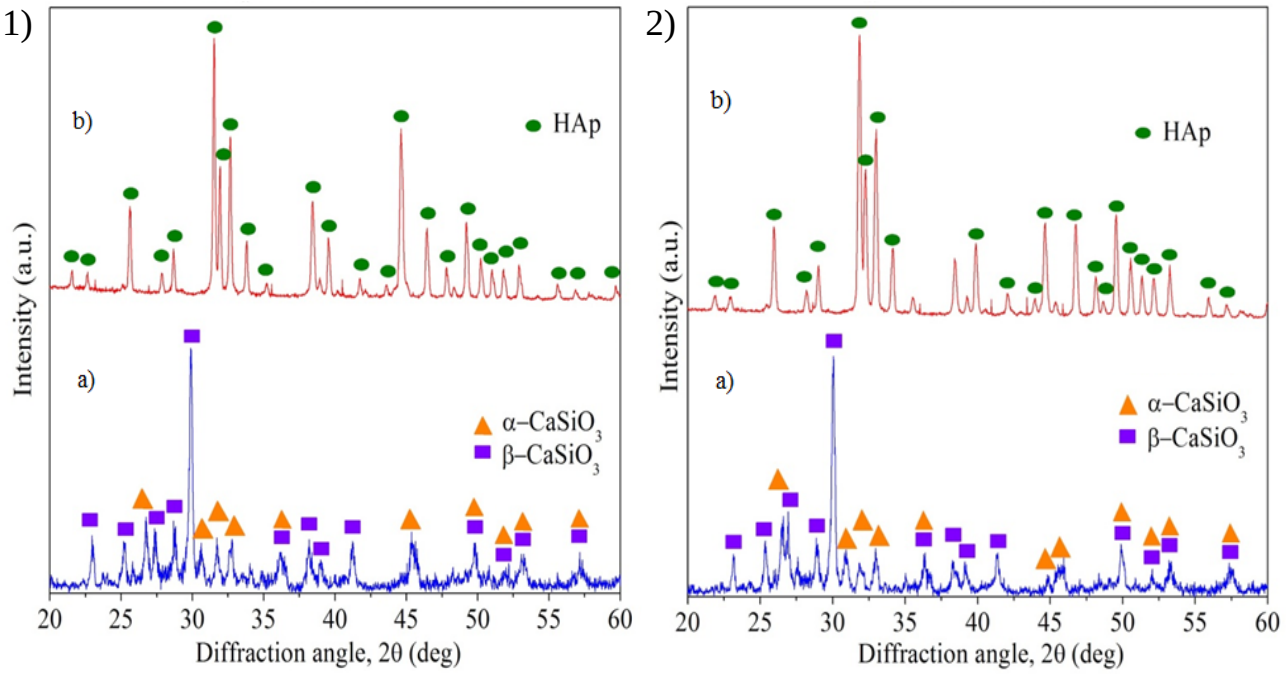

Figure 7.3: XRD patterns of (a) pure BG and (b) pure HA sides of the FGM-S1 samples corresponding to the SPS condition applied: (1) 950°C, 50MPa, 2 min; (2) 1000°C, 16MPa, 2 min.

Nonetheless, these results seem to be promising for the future development of HA-BG based FGMs.

Temperature, °C	Pressure, MPa	Dwell time, min
800	16; 30; 50	2

Table 7.4: Optimal SPS parameters which allowed to obtain crack-free FGM-S2 samples.

Some representative images of FGMs samples obtained in this work for the two systems taken into account are shown in Fig. 7.5.

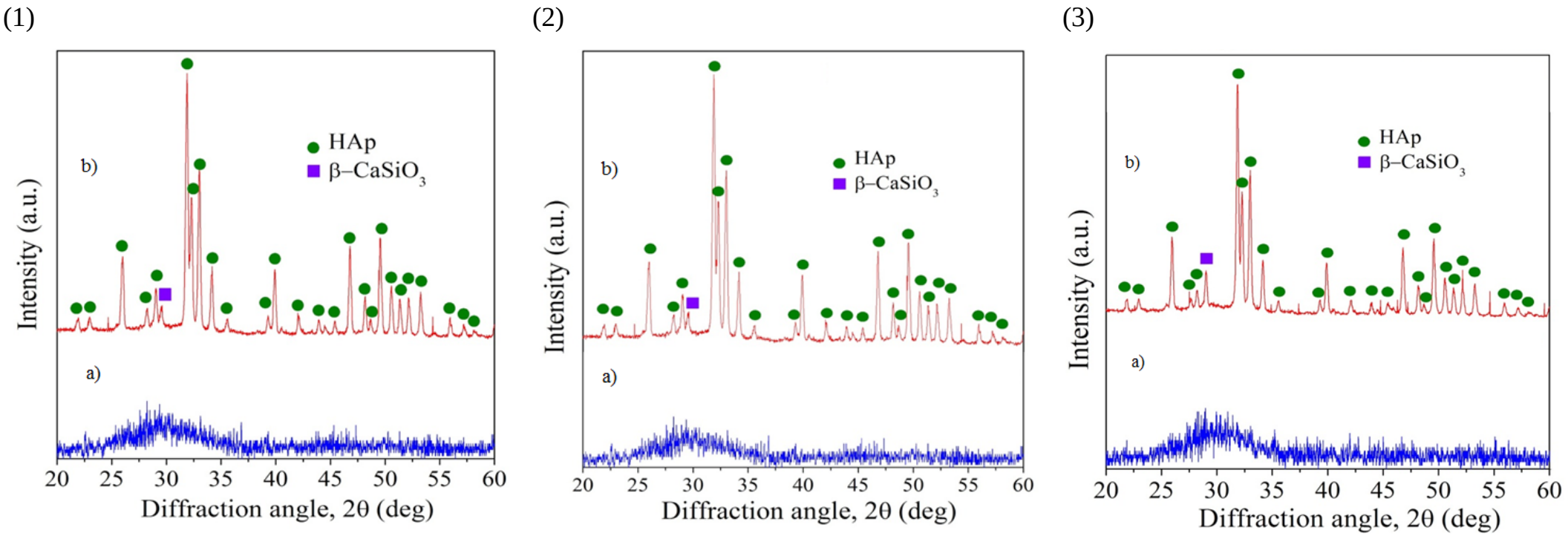

Figure 7.4: XRD patterns of (a) pure BG and (b) 70wt.%HA/30wt.%BG sides of the FGM-S2 samples corresponding to the following SPS conditions: (1) 800°C, 16MPa, 2 min; (2) 800°C, 30MPa, 2 min; (3) 800°C, 50MPa, 2 min.

The produced samples are currently under characterization from mechanical and biological points of view (sample diameter 14.7±0.1 mm, thickness 6.0±0.2 mm).

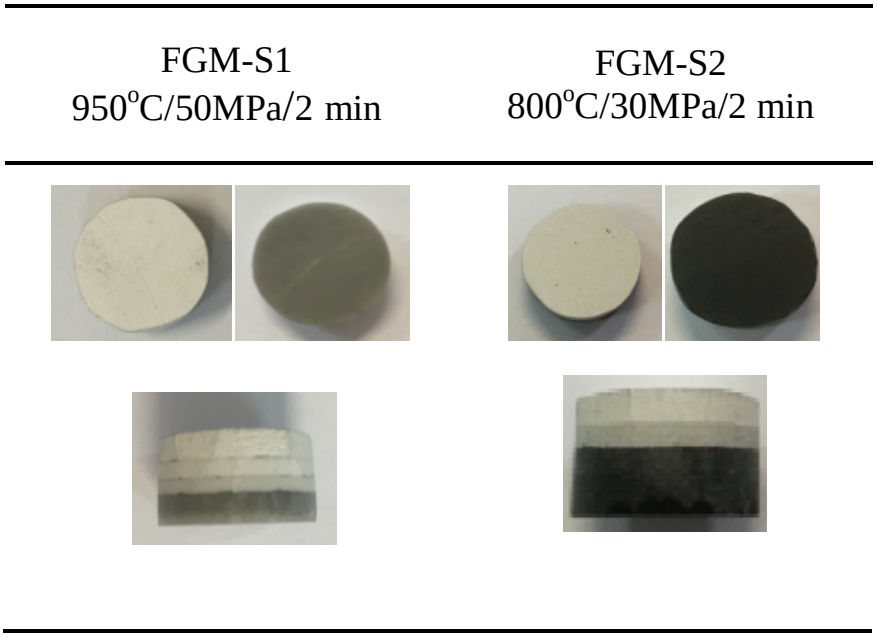

Figure 7.5: Photos of the FGM-S1 and FGM-S2 samples obtained in this work.

Remarks

This part of PhD was carried out thanks to the collaboration between Dipartimento di Ingegneria "ENZO Ferrari", Università degli Studi di Modena e Reggio Emilia (Italy) and Università di Cagliari (Department of Mechanical, Chemical Engineering and Materials Science). As a PhD student, my activity was mainly focused on the preparation of FGM samples and their characterization by XRD analysis. Unfortunately, by the moment this PhD program was concluded, the mechanical and biological characterization of FGM-S1 and FGM-S2 samples was still in progress. This study was mainly guided by Prof. Roberto Orrù, Prof. Giacomo Cao and Prof. Valeria Cannillo.

Chapter 8. Development of novel bioresorbable ceramics from Carbonated/Magnesium doped Amorphous Calcium Phosphates

8.1 Introduction

In the past decades, the development of synthetic calcium-phosphate-based bioceramics as alternative approach for allograft and autograft tissue replacement has been a major subject of research [210,318,319]. As already pointed in previous Chapters, hydroxyapatite (HA), ($Ca_{10}(PO_4)_6(OH)_2$), due to its good biocompatibility and structural similarity to the mineral part of calcified tissues, is one of the most commonly used bioactive ceramics as of today [141]. However, it is thermodynamically stable under physiological conditions and thus exhibits a low resorption rate *in vivo*. Additionally, due to limited surface reactivity, HA bioactivity is hindered after implantation [277,278]. Such differences with respect to bone mineral, also called biological apatite, are ascribed to the fact that the latter consists of nanocrystalline, non-stoichiometric polysubstituted apatite[162]. Besides carbonate (CO_3^{2-}), which is the main substituting ionic group in biological apatite (5-9 wt.%) [54–56], other ions such as HPO_4^{2}, Mg^{2+}, Sr^{2+}, Na^{+} and F^{-} are also encountered [62,320]. According to Legros et al. [49], the composition of bone mineral is characterized by significant vacancy contents in Ca and OH sites, and it can be described (omitting trace elements) by the general formula $Ca_{8.3}(PO_4)_{4.3}(CO_3,HPO_4)_{1.7}(CO_3,OH)_{0.3}$. A recent report, when a fresh bone specimen was analyzed by NMR and vibrational spectroscopies, evidenced in particular a high amount of HPO_4^{2-} ions besides carbonates [321]. In apatites, whether biological or synthetic, hydroxide (OH^-) and phosphate (PO_4^{3-} or HPO_4^{2-}) ionic groups can indeed be replaced by carbonate ions, leading respectively to A and B-type carbonated apatites. Additionally, AB mixed-type apatites are also often reported [322]. One important feature of nanocrystalline apatites, whether in bone or dentine or their

synthetic biomimetic analogs, is the presence of a hydrated non-apatitic ionic layer covering the surface of the nanocrystals, and conferring very reactive properties [73,75]. In bone, this layer is used for maintaining ion homeostasis in body fluids. Thus, in synthetic analogs, these characteristics can be tailored and exploited to modulate the reactivity/bioactivity of the nanocrystals, in view of a variety of biomedical applications, like bone regeneration but also nanomedicine [323,324]. This may also imply ionic substitutions, to modulate the bioactivity of the nanocrystals, which may be achieved either for impacting the stability/ degree of crystallinity/ thermodynamic properties of the apatitic phase [323], or for tuning biological properties, or for both. For example, doping with Mg^{2+} ions can activate osteoblast cells, and Mg-doped apatites also exhibit a less pronounced crystallinity (lower maturation state) than Mg-free ones, thus leading to a higher reactivity. Like magnesium, carbonate ions are also growth inhibitors for the apatite structure, having also an impact on apatite nanocrystals reactivity/solubility [325].

These substitutions and subsequent structural disorder provide thus a way to prepare biomaterials with a higher solubility, as compared to stoichiometric hydroxyapatite, which may be particularly appealing to rapidly confer constitutive building blocks of mineral in view of activated bone regrowth.

In fact, in bones, not only apatite nanocrystals but also transient metastable calcium phosphate (CaP) precursors are considered to be naturally present and actively serve as a basis for bone neoformation. Although the mechanisms of bone mineralization have not yet been fully clarified, it was suggested that the formation of new bone may involve amorphous calcium phosphate (ACP) reactive precursors [326–328]. The latter are not crystallized but possess short-range order in the form of small organized units with average size of about 0.9 nm, known as Posner's clusters of chemical formula $Ca_9(PO_4)_6.nH_2O$ [172]. Despite the relevance of ACP in the field of bone regeneration, these amorphous compounds have not yet found the development they deserve – except as ingredient in bone cement formulation [329,330]. This can

probably be linked to the difficulty to process ACP to make granules or 3D pieces, while avoiding their crystallization into apatite. Two main techniques have been proposed so far to obtain synthetic ACP, i.e. a wet route, in aqueous medium [177,331], and a dry method, carried out at high temperatures [332]. The consolidation of ACP represents a difficult goal to achieve, due to the thermal instability of this amorphous precursor. Therefore, relatively mild conditions are required to consolidate it, while preserving its metastable character. Solving of this issue could then provide a new family of CaP compounds with even greater reactivity and bioresorbability (resorbability *in vivo* being directly related to solubility [319]).

Along these lines, the use of Spark Plasma Sintering (SPS) at very low temperature (150°C) was reported to be effective for the consolidation of biomimetic nanocrystalline apatite powders [163,333,334], thus opening the way to so-called "cold sintering" approaches. It should be noted that, these initial experiments were performed on non-carbonated apatites. More recently, the possibility to adjoin natural polymers, such as cellulose fibers, to obtain reinforced biomimetic apatite/polymer composites, has also been demonstrated [335]. Very recently, the exploration of low temperature SPS has been extended to the obtainment of carbonated apatites [336].

Despite SPS has been used extensively for the fabrication of a variety of advanced materials, very few reports have been focused on cold sintering. On the other hand, sintering at very low temperature (<300°C) is of relevant importance, especially for consolidating biomimetic apatites, to preserve their nanocrystalline, hydrated and thermodynamically metastable features [334].

8.2 Aim

In this light, the goal of this study was to investigate the ability of SPS to consolidate at low temperature amorphous CaP compounds, with the general aim of producing ACP-based highly reactive and resorbable biomaterials, as a novel family of bone substitutes. It should be noted that all previous attempts to stabilize ACP after

sintering, including by SPS at low temperature [336], have failed since the crystallization into apatite was systematically observed. This may be related to several factors such as inadapted synthesis protocols or too low carbonate contents, thus they cannot fully play their crystallization inhibition role.

In the present work, alternative synthesis routes to prepare very highly carbonated ACP powder precursors, eventually also containing magnesium ions, were investigated. This approach was utilized for stabilizing/retaining the powder amorphous character even after SPS consolidation. Indeed, carbonate and magnesium ions are two crystallization inhibitors for the apatitic structure [325], but their effect on low temperature sintering had not been investigated so far. Thus, for the first time, the possibility to obtain still-amorphous calcium phosphates, after the SPS treatment, was studied. As a main scope it is intended to prepare highly resorbable CaP ceramics for fast release of bioactive building blocks relevant to bone tissue regeneration. The most important physicochemical characteristics of the obtained samples are also investigated, by taking advantage of complementary techniques.

8.3 Experimental

8.3.1 Materials and methods

8.3.1.1 Synthesis of amorphous powders

The synthesis of five types of ACP-based powders was carried out by double decomposition method [166,337], with and without carbonate and eventually magnesium ions.

The starting materials used to this aim are listed in Table 8.1, along with the selected relative amounts.

Two different solutions, indicated as A and B, respectively, were prepared individually by dissolving the precursors in deionized water. The pH of both

solutions was adjusted to ~10 (experimental value of 9.9). To this purpose, either ammonium hydroxide (NH_4OH 20%, Fisher Chemical) (method 1) or potassium hydroxide solution (KOH, Fisher Chemical) (method 2) were utilized. As explained in the Result and Discussion section, the Mg30-cACP powders were prepared according to both methods. In this regard, di-ammonium hydrogen phosphate $(NH_4)_2HPO_4$ was also replaced in the initial solution B by di-potassium phosphate (K_2HPO_4), in the same proportion. To reach pH 9.9, KOH solutions with pH = 13 or 15 were added to solutions A and B, respectively. Solution B containing HPO_4^{2-} ions exhibited buffer properties, so that a stronger initial alkaline solution was required to increase its pH. The rest of the synthesis procedure was the same for both methods. In each case, solution A was added to solution B at room temperature (~22°C). The resulting mixture was stirred for few minutes and then immediately filtered on a Buchner funnel, washed with alkalinized deionized water (pH 9.9) and, finally, freeze-dried. Pure ACP powder was prepared, as a reference, using the method described by Heughebaert [177].

Name of the sample/ Method	Composition			
	Solution A		Solution B	
	$Ca(NO_3)_2{\cdot}4H_2O$, wt.%	$Mg(NO_3)_2{\cdot}6H_2O$, wt.%	$(NH_4)_2HPO_4$, wt.%	$NaHCO_3$, wt.%
ACP [177](1)	100	0	100	0
cACP (1)	100	0	50	50
Mg5-cACP (1)	95	5	50	50
Mg15-cACP (1)	85	15	50	50
Mg30-cACP (1,2)	70	30	50	50

Table 8.1: Starting composition used to synthesize amorphous calcium phosphates.

8.3.2 Spark Plasma Sintering (SPS)

SPS experiments for the consolidation of amorphous precursors were carried out by means of a 2080 Sumitomo Coal Mining equipment under argon atmosphere. This equipment provides uniaxial pressing and simultaneous heating via DC pulsed

current (maximum 8000 A and 10 V). During the experiments, current was limited to 4000 A, and the sequencing of pulses was 12:2 (12 pulses of 3.3 ms followed by two time intervals without current). Powder samples (0.35 g) were placed in a graphite die with internal diameter equal to 8 mm covered with Papyex® graphite foil, to facilitate sample release after SPS.

Sintering runs were performed following temperature and pressure programmed sequences shown in Fig. 8.1, similar to those used in previous studies aimed to the consolidation of biomimetic apatites and derived composites [334,335].

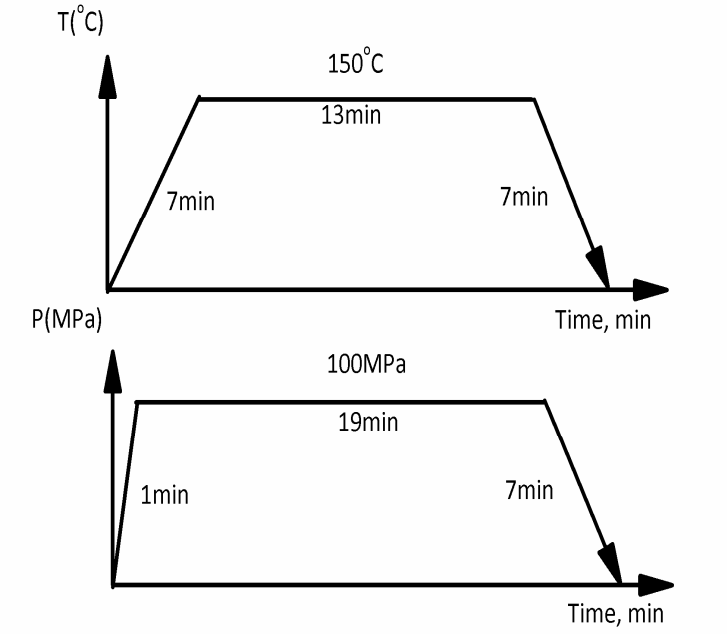

Figure 8.1: SPS conditions (temperature and pressure programs) adopted for the consolidation of ACP-based powders.

8.3.3 Physicochemical Characterization

Initial powders and sintered samples obtained after SPS were first characterized by X-ray diffraction, using a BRUKER D8 Advanced diffractometer with a CuKα radiation. XRD spectra were recorded in the range 10-90°, with a step size 0.02 and dwell time 1s. In addition, vibrational spectrometry analysis was conducted on a Nicolet 5700 Fourier transform infrared (FTIR) spectrometer. Spectra were recorded

in transmission mode in the 400–4000 cm^{-1} range with 64 scans and 4 cm^{-1} resolution, the KBr pellet method was used. The obtained FTIR spectra were analyzed using the OMNIC software (Thermo Fisher Scientific).

8.4 Results and discussion

8.4.1 Powder synthesis and characterisation

The first systems considered in this study were synthesized using ammonium hydroxide solution as alkalinization medium. The XRD patterns of the corresponding powders are shown in Fig. 8.2. Standard ACP is shown on Fig. 8.2a. All the other CaP-compounds were precipitated in presence of carbonate ions, hence the denomination cACP, and with increasing magnesium concentrations (Fig. 8.2b-e). For magnesium contents in the starting powder mixture system equal or less than 15 wt.% (Fig. 8.2b-d) our results indicated that no defined peaks could be detected in the XRD patterns. This finding indicates the full amorphous character of these carbonated or non-carbonated "ACP" samples. On the other hand, the XRD pattern of Mg30-cACP powder (Fig. 8.2e) showed, in addition to the broad halo with maximum 2θ value at around 30°, several other prominent peaks, which are attributed to the presence of a secondary crystalline phase $NH_4MgPO_4.6H_2O$, Struvite (ICDD-PDF 01-077-2303).

The formation of undesired struvite beyond a limit Mg content may be related to the use of ammonium hydroxide in the synthesis protocol, thus providing the necessary NH_4^+ ions. Therefore, this biphasic Mg30-cACP sample was not further considered for the rest of the study.

FTIR analyses were also carried out for complementary characterization, and the related spectra are presented in Fig. 8.3. All the spectra reveal broad bands, which are similar to those reported in previous works related to ACP obtained by precipitation in an alkaline medium [336,338]. The broad band between 3700 and

2800 cm^{-1} and the one at ~1640 cm^{-1} can be attributed to the presence of water (respectively O-H stretching and H-O-H bending modes) associated to Posner clusters [339].

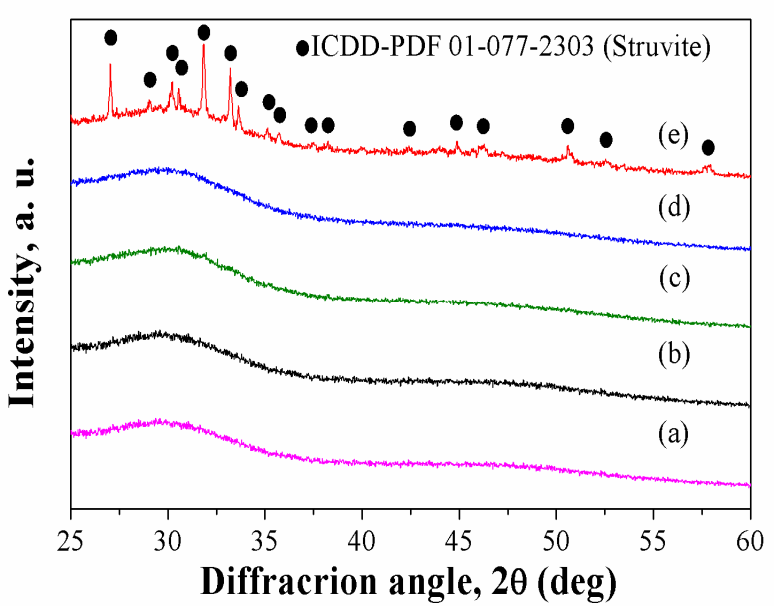

Figure 8.2: Diffraction patterns of powders synthesized when using the ammonium hydroxide solution: (a) ACP; (b) cACP; (c) Mg5-cACP; (d) Mg15-cACP; (e) Mg30-cACP.

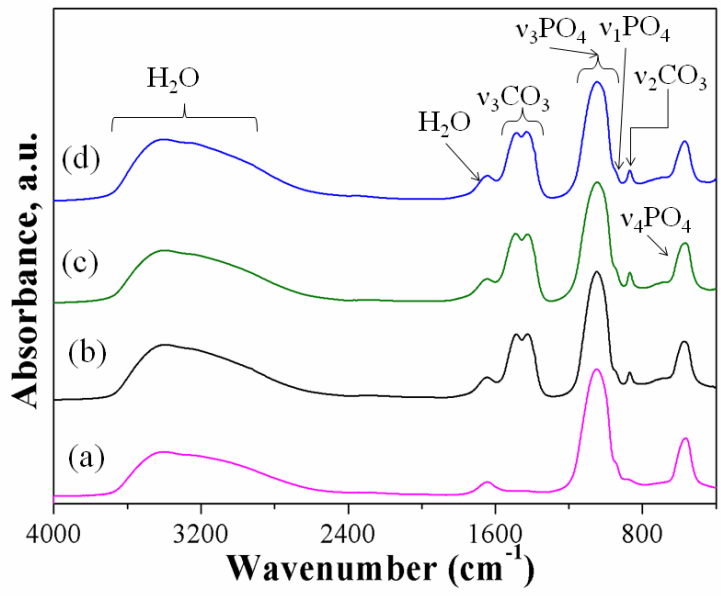

Figure 8.3: FTIR spectra of the synthesized powders: (a) ACP; (b) cACP; (c) Mg5-cACP; (d) Mg15-cACP.

The amorphous character of the samples leads to poorly defined phosphate vibration bands, especially associated to the $\nu_3(PO_4)$ and $\nu_4(PO_4)$ modes, as opposed to the observations with other CaP compounds like apatites [340], and also to a position of the $\nu_1(PO_4)$ band close to 959 cm^{-1} (instead of ~ 961-962 cm^{-1} for apatites) [341]. For carbonated compounds, additional bands, assignable to the CO_3^{2-} ionic group, are also detected (Fig. 8.3). In particular, typical regions of the spectra, where signals of carbonate ions can be observed, are 850-900 cm^{-1} and 1350-1550 cm^{-1}, related to the $\nu_2(CO_3)$ and $\nu_3(CO_3)$ vibration modes, respectively. Details of these regions are given in Fig. 8.4(I), for the case of cACP synthesized powder. For comparative purposes, the characteristic features of A and B-type carbonate environments in carbonated apatite, which correspond to carbonate ions replacing some hydroxyl and phosphate groups in the apatite structure, have also been pointed out in this figure. The wavenumbers corresponding to CO_3^{2-} ionic groups in nanocrystalline apatites are summarized in Table 8.2. In addition, the estimated position of IR bands corresponding to surface carbonates (i.e. CO_3^{2-} ions located on the hydrated layer on apatite nanocrystals) [342,343], also known as "labile" has also been indicated in Fig. 8.4 and Table 8.2.

Vibrational band	A-type substitution	B-type substitution	Labile CO_3^{2-}	References
ν_2	882 cm^{-1}	872 cm^{-1}	866 cm^{-1}	[58,344]
ν_3	1465 cm^{-1} 1542 cm^{-1}	1412 cm^{-1} 1462 cm^{-1}	1417 cm^{-1} 1480 cm^{-1}	[342]

Table 8.2: Characteristic wavenumbers of ν_2 and ν_3 vibration modes of CO_3^{2-}.

Such labile carbonates are indeed characteristic of metastable chemical environments that may be found in hydrated amorphous domains, not embedded into the crystallographic apatitic structure. It is interesting to note that, in the case of this cACP amorphous precursor, carbonate species seem to mostly correspond to such labile CO_3 (see Fig. 8.4), to confirm their similarity to the labile surface carbonates

found in the amorphous hydrated layer on nanocrystalline apatites. The same behavior was also observed in the cases of Mg5 and Mg15-cACP initial powders.

The overall content of CO_3^{2-} ions was estimated for all samples by exploiting the FTIR features in a quantitative way, according to Grunenwald et al.'s updated methodology [343] (Table 8.3). In particular, the ratio $r_{c/p}$ between the integrated intensity of $\nu_3(CO_3)$ (1550-1350 cm^{-1} domain) and $\nu_4(PO_4)$ band (1230-912 cm^{-1}) was measured and compared to the calibration curve. For the carbonated ACP (cACP), the total amount of CO_3 was found to be around 17 wt.%, while it reached a value of 18.3 wt.% for Mg15-cACP. To the best of our knowledge, such highly carbonated amorphous calcium phosphate powders have been synthesized in the present work for the first time.

By comparison, it should be noted that amorphous powders with carbonate content reaching around 3.1 wt.% was reported by Ortali et al., and such level was found insufficient to allow the preservation of the amorphous character after SPS consolidation [336]. The obtained improvement of the carbonation level can be explained on the basis of the several modifications in the synthesis procedure employed in the present work as compared to literature reports: unheated synthesis (room temperature ~22°C), high alkaline pH, raised close to 10, high starting C/P ratio ~1.6 (as opposed to a maximum of 0.5 in ref. [336]), low starting Ca/P ratio, close to 1.1, and the absence of precipitate maturation.

These conditions thus favor the carbonation process by providing not only fewer cations and more carbonate ions per unit volume, but also by ensuring of a more stable chemical environment for limiting CO_2 release (high pH, absence of maturation).

In order to avoid the precipitation of Struvite during the synthesis of Mg30-cACP, the preparation of the latter system was attempted by substituting NH_4OH with KOH, as described in the Materials and Methods section. FTIR spectra of the synthesized

powder and the corresponding sample consolidated by SPS are given in Fig. 8.5a and 8.5b, respectively.

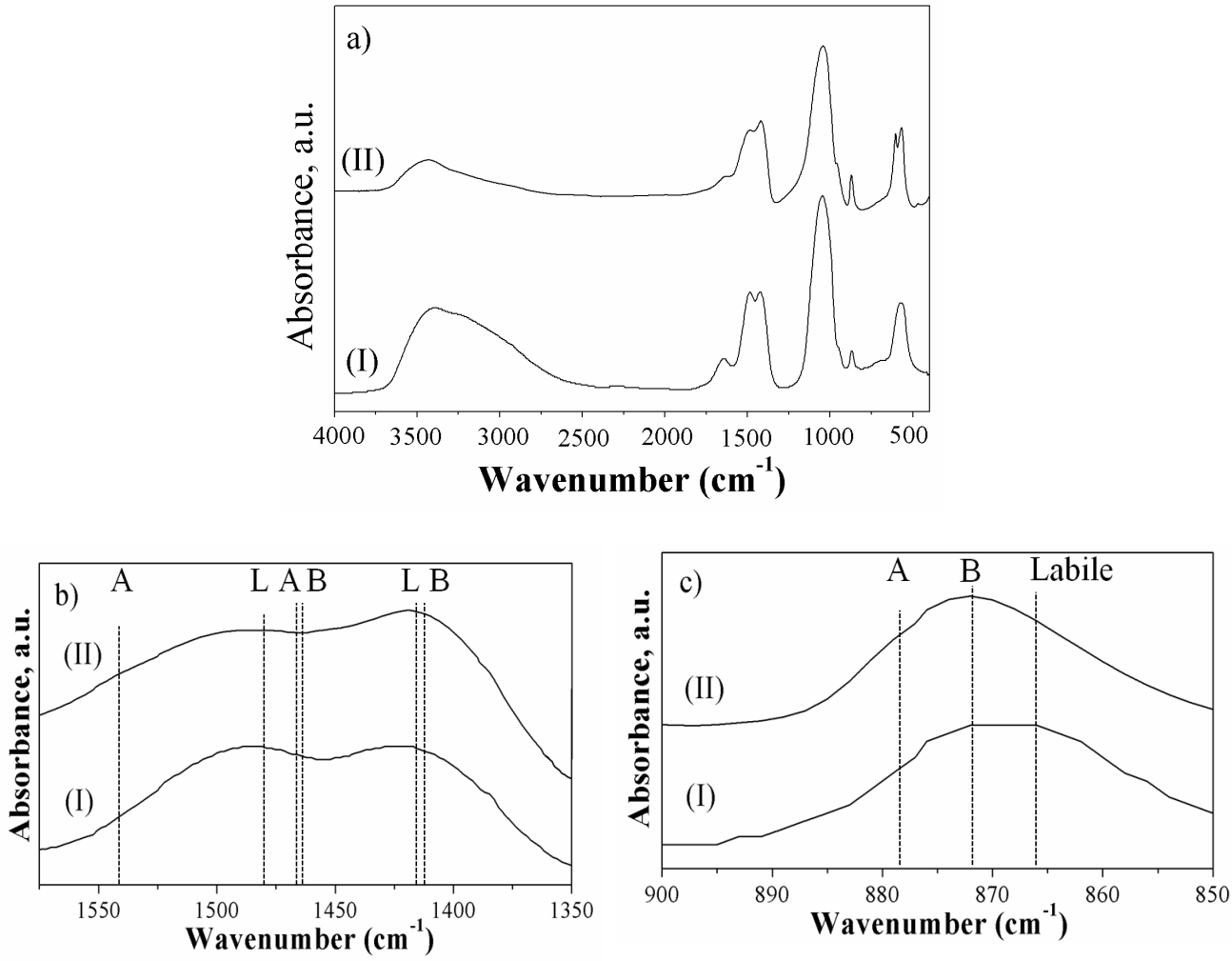

Figure 8.4: FTIR spectra of the cACP powders: 4a(I) initial powder; 4a(II) sample after SPS; 4b zoom on the $\nu_3\,CO_3^{2-}$ band; 4c zoom on the $\nu_2\,CO_3^{2-}$ band.

The carbonation level of raw Mg30-cACP powder was found to be around 13.8 wt.%, while its amorphous character was confirmed by XRD analysis (Fig. 8.6a).

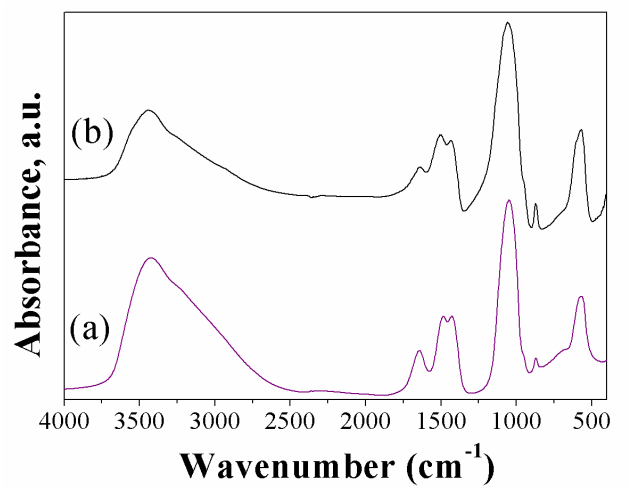

Figure 8.5: FTIR spectra of Mg30-cACP synthesized with KOH solution: (a) initial powder; (b) after SPS.

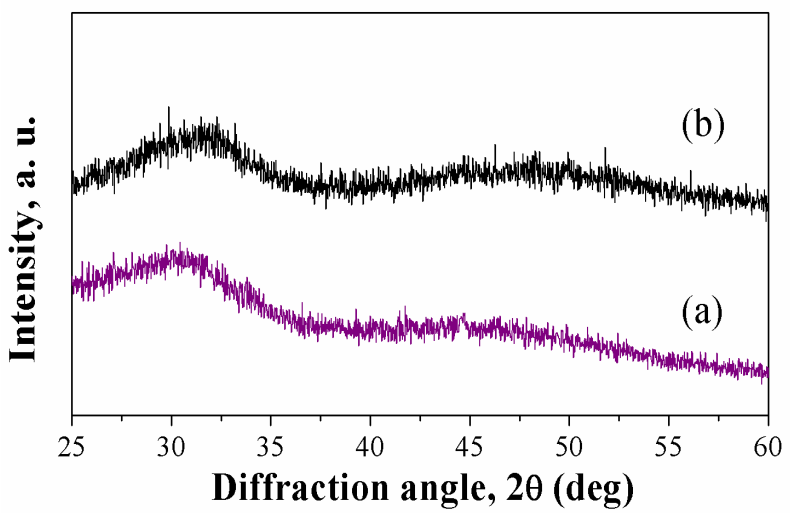

Figure 8.6: XRD patterns of Mg30-cACP synthesized with KOH solution: (a) initial powder; (b) after SPS.

The above data clearly confirm that we were able to prepare single-phase, highly carbonated ACP powders, with or without co-incorporation of Mg^{2+} ions.

The next step therefore consisted of checking their consolidation at low temperature by SPS, and the characterization of the obtained bioceramic pellets. This is the object of the following section.

8.4.2 Characterisation of Spark Plasma Sintered bioceramics

SPS consolidation was then carried out on each of the carbonated/magnesium ACP compositions prepared (see Fig. 8.1). The XRD pattern of the ceramic obtained from pure ACP (Figure 8.7a) revealed, as anticipated, that crystallization into an apatite phase (ICDD-PDF 00-009-0432) occurred during SPS. Attempts to avoid this crystallization were then made by investigating the effect of the carbonation and magnesium contents of the amorphous precursor powder. The apatite formation was also noticed for the cases of cACP exempt of magnesium (Fig. 8.7b) as well as for low amounts of Mg, namely for samples Mg5-cACP (Fig. 8.7c) and Mg15-cACP (Fig. 8.7d). However, it may be noted that samples with high Mg content display patterns with relatively low resolution of their peaks to evidence their low crystallinity character (similarly to bone mineral [345]), in contrast to pure ACP. This tendency toward lower apatite crystallinity is progressively more obvious as the Mg content increases (Fig. 8.7).

Therefore, it can be stated that, in these conditions, carbonate and magnesium ions limit, but do not block the progression of apatite crystallization during SPS. This conclusion agrees with previous results reported in the literature [325,346]; however such findings thus indicate that these starting CO_3/Mg compositions were not sufficient to stabilize amorphous CaP after SPS.

FTIR spectra also revealed the occurrence of the transformation of amorphous powders into low-crystallinity apatite after SPS treatment for these samples (Fig. 8.4a-II). Carbonate ions can then enter the apatite lattice, leading to the formation either A or B-types of substitution. In particular, based on the FTIR spectral analysis, partial transformation mostly into B-type apatite can be noted after SPS of these samples, when examing 1462 cm^{-1} (Fig. 8.4b-II) and 872 cm^{-1} (Fig. 8.4c-II) domains.

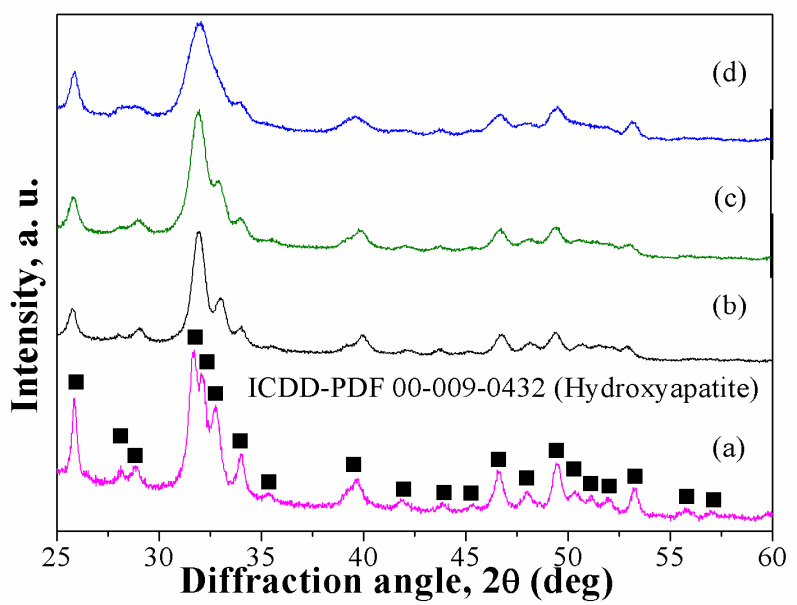

Figure 8.7: Diffraction patterns of the SPS samples obtained from the amorphous powders in presence of ammonium hydroxide solution: (a) ACP; (b) cACP; (c) Mg5-cACP; (d) Mg15-cACP.

FTIR spectra relative to the specimens consolidated by SPS also evidenced a decrease in the carbonation level (Table 8.3), albeit samples still remained highly carbonated. This diminution can be linked to the partial decomposition of carbonate ions, followed by expulsion of CO_2 gas, during SPS.

Name of the sample	CO_3 wt.% Initial powders	CO_3 wt.% Samples after SPS
ACP	0	0
cACP	17.0	14.0
Mg5-cACP	15.9	11.3
Mg15-cACP	18.3	14.1

Table 8.3: Chemical composition of the powders before and after SPS.

In order to stabilize ACP even after SPS, larger levels of Mg were then tested. SPS treatment at 150°C was again found to be effective in the consolidation of the sample Mg30-cACP synthesized using the KOH solution. As main difference, in this case,

the initial amorphous character of calcium phosphate powder could be successfully maintained even after SPS, as confirmed by XRD analysis (Fig. 8.6b). To the best of our knowledge, this outcome is obtained for the first time in the literature, thus opening the way for identifying new families of bioceramic/composite materials with high metastability/surface reactivity/resorption abilities The preservation of this amorphous state even after SPS is thought to be related to the strong inhibiting effect of Mg^{2+} ions which, in combination with that of carbonates prevent apatite crystallization. The carbonation level on this sample after SPS was found to be kept around 9 wt.%.

8.5 Conclusions

Carbonated and magnesium co-doped amorphous calcium phosphate powders with different compositions were first synthesized in present work using modified precipitation method. The resulting powders then were consolidated at low temperature by Spark Plasma Sintering (150^{o}C) in view of cold sintering. The content of carbonate ions in initial powders and sintered samples was evaluated. In particular, maximum carbonate content of about 18.3 wt.%. was achieved for Mg15-cACP initial powder. Cold-sintering at 150^{o}C by SPS was found to be effective to consolidate all types of powders. The influence of the introduction of carbonate and magnesium ions in ACP on the consolidation process was also investigated. After SPS, both undoped ACP, carbonated ACP (cACP) and 5/15 wt.% Mg-doped cACP transformed into low crystallinity apatites. However, high carbonation (mostly B-type) was preserved even after SPS; it is expected that they could lead to high resorption rates *in vivo* and concomitant fast release of bioactive ions. Indeed, an increased amount of carbonate ions in the apatite lattice alters its thermodynamic and biological characteristics, carbonated apatite being more soluble than HA [347]. Thus, the highly carbonated low crystalline apatite-based ceramics obtained in this work will likely to exhibit enhanced biological behavior in terms of reactivity and resorbability. However, the main finding of the present work is the identification of

suitable experimental conditions allowing, for the first time, to retain the amorphous nature of ACP compounds system even after SPS. We show that suitable mild SPS conditions associated to adequate Mg and CO_3^{2-} substitutions in ACP are needed to obtain this original result. These findings open the way to the development of consolidated ACP-based bioceramics with high (bio)reactivity.

Remarks

This part of PhD was carried out thanks to the collaboration between CIRIMAT (University of Toulouse, France) and University of Cagliari. During my internship at the research group of "Phosphate, Pharmacotechnics, Biomaterials" I worked on the synthesis, characterization and sintering of ACP samples. Study was guided by Dr. Christophe Drouet, Dr. Davis Grossin, Dr. Fabien Brouillet and Prof. Roberto Orrù.

Article submitted to Journal of Materials Chemistry B:

First successful stabilization of consolidated Amorphous Calcium Phosphate (ACP) by cold sintering: toward highly-resorbable bioceramics.

Chapter 9. Electrospun PCL/PGS composite fibers incorporating bioactive glass particles for soft tissue engineering applications

9.1 Introduction

The fabrication of synthetic, degradable scaffolds able to mimic native features of extracellular matrix (ECM) represents a significant challenge for soft and hard tissue engineering (TE) [348]. Among the different scaffold fabrication techniques, electrospinning (ES) has emerged as a promising approach for different biomedical applications, since it provides a simple and versatile tool to produce interconnected porous nano- and microfibrous structures from various synthetic and natural polymers [349,350]. Briefly, the principle of ES is based on the application of a high intensity electrical potential between two electrodes of opposite polarity, a metallic needle containing the polymeric solution and a grounded target. ES process is strongly affected by different factors, which can be generally grouped in three main categories, i.e. solution features (e.g. concentration, viscosity, rheological properties, etc.), process parameters (e.g. electrical field, flow rate, distance between the tip of the syringe and the type of collector), and, external environmental conditions (e.g. relative humidity and temperature). The effects of these factors on ES have been already extensively investigated in the literature [349,351,352].

Poly(glycerol-sebacate) (PGS), a biocompatible and biodegradable soft elastomer firstly introduced by Wang and co-workers [353], has recently attracted much attention since its properties appeared to be particularly interesting for regenerative medicine [354]. Indeed, PGS was studied for a broad range of applications including cardiovascular patches [355–358], heart valves [359], cartilage [360,361] and nerve [362,363] tissue engineering, retina [364,365] and tympanic membrane healing [366,367]. Synthesis of PGS consists of a two steps procedure: first, PGS pre-polymer (PGS_p) is synthesized from pre-polycondensation of glycerol and sebacic

acid, then the cross-linked polymer can be obtained by an additional vacuum heat treatment of the PGSp precursor. The PGS mechanical properties and degradation kinetics, which are relevant features for tissue engineering applications, can be tailored during the synthesis process by altering the molar ratio of glycerol and sebacic acid constituents, curing time and temperature. For example, Chen and co-workers studied the effect of the curing temperature on the mechanical properties of PGS patches for the myocardial tissue healing [355]. It is also worth to mention that, electrospinning of neat PGS represents a challenging task due to the low solution viscosity caused by the low molecular weight of the polymer [353,354]. To increase the solution viscosity, PGS can be blended with other biodegradable polymers, synthetic or natural [368,369].

In this context, poly(ε-caprolactone) (PCL) is a semi-crystalline biocompatible, non-toxic, degradable, suitable to be processed by ES, polymer, which has been already approved by the US Food and Drug Administration (FDA) for certain biomedical applications [370,371]. Generally, PCL is used in the field of hard TE, where longer healing periods are required [372,373], since this polymer is relatively stable *in vivo* and possesses lower degradation rate compared to PGS [374,375]. Therefore, PCL/PGS fibrous blend scaffolds appear to be particularly interesting for TE, since PCL can ensure structural support at the site of implantation, while faster degrading PGS can provide essential space for the new ECM deposition. Indeed, elastic blended PCL/PGS electrospun fiber mats with various constituent ratios have been already successfully tested as materials for the heart valve regeneration [368,376,377]. Advanced electrospun PCL/PGS fiber mats with patterned topographical features as well as PCL/PGS scaffolds functionalized with vascular endothelial growth factors for cardiac patch application, were then developed [358,378]. Moreover, Kalakonda and co-workers studied the antibacterial properties of PGS/PCL fibrous scaffolds coated with silver [379].

During the fabrication step of PCL/PGS electrospun scaffolds, harsh solvents, such as a mixture of anhydrous chloroform, dichloromethane or dimethyl carbonate with ethanol or methanol, are mainly used. It should be noted that an appropriate solvent selection plays a pivotal role for the obtainment of smooth, bead-free fibers. Recently, the substitution of the toxic solvents mentioned above with more environmental friendly benign solvents was attempted [380,381]. Acetic acid (AA), according to guideline established on the International Conference on Harmonization of Technical Requirements for Registration of Pharmaceuticals for Human use (ICH), falls within the class 3 of solvents which are considered less toxic and harmful for humans [382]. Vogt et al. firstly reported on the possibility to obtain PCL/PGS (1:1) fibrous mats using AA for cardiac patch applications [357].

Recently, the scientific community has focused its attention on the use of bioactive glasses (BG) for soft tissue engineering applications [316,383]. Indeed, as already mentioned in Chapter 3, researches conducted so far have been mainly oriented on the investigation of osteogenic properties of bioactive glasses, thus addressed to bone regeneration. After demonstrating the ability of bioactive glasses to promote angiogenesis, as a consequence of the dissolution products arising from the contact between BG and body fluids, more attention was dedicated to all the applications related to healing of soft tissue wounds [384,385].

9.2 Aim

In this framework, the aim of the present research work is to fabricate electrospun PCL/PGS composite fibrous structures, where silicate 13-93 and borosilicate 13-93BS bioactive glass particles are introduced as inorganic part, and acetic acid is utilized as a solvent. The biocompatibility of seven different compositions is examined, including cell metabolic activity, attachment and proliferation. The influence of fibers composition on the mechanical properties and degradation characteristics is also assessed.

9.3 Materials and method

9.3.1 Solution preparation

Electrospun fiber mats with 7 different compositions, as reported in Table 9.1, were fabricated starting from PCL (80 kDa, Sigma Aldrich®, Munich, Germany) solutions. Glacial acetic acid (AA, VWR, Darmstadt, Germany) was utilized as a solvent.

Synthesis of the PGS polymer ($(C_{13}H_{22}O_5)_n$) was performed according to the protocol of Wang et al. [353]. Briefly, in order to obtain PGS prepolymer (PGS_p), 0.1 M sebacic acid (99%, SigmaAldrich®, Munich, Germany) and 0.1 M polyol glycerol (BioXtra, 99%, SigmaAldrich®, Munich, Germany) were mixed and subsequently heated at 120°C under inert nitrogen atmosphere for 24h. A mildly cross-linked PGS polymer (PGS_{mxl}) was further synthesized from PGS_p precursor by the additional treatment at 120°C in an oven under vacuum ($1.3–2.5\times10^{-2}$ mTorr) for 24 h, as previously reported by Vogt et al. [357].

Silicate and borosilicate glasses (13-93 and 13-93BS, respectively) were synthesized by melt-quenching according to the procedure described by Schuhladen et al. [386]. Briefly, the starting reagents (all from Sigma-Aldrich®, Munich, Germany), namely, H_3BO_3, $(CaHPO_4)(2(H_2O))$, $CaCO_3$, K_2CO_3, Na_2CO_3, MgO, and Belgian quartz sand, were melted in a platinum crucible under the following conditions: 1100 °C for 3 h (13-93BS) and 1360 °C for 3 h (13–93). Further, all compositions were cast and annealed at 520°C. To ensure homogeneity, melting was performed twice. The glass product was then crushed using a Jaw Crusher (Retsch, Germany) and grounded to fine powder with average particle size of 5–20 μm, using a zirconia planetary ball mill (Retsch, Germany). The composition of both glasses is reported in Table 9.2. The solution preparation was performed according to the following procedure: firstly,

Sample name	Solution concentration [% *w/v*] / polymer-BG ratio PCL:PGS:BG	Voltage [kV]	Distance tip-target [cm]	Needle diameter	Flow rate [mL/ h]	Temperature [^{o}C]	Relative humidity [%]
(S1) PCL/PGS_{p}	20/1:0.5:0	15	11	21G	0.4	24±0.8	34±12
(S2) PCL/PGS_{mxl}	20/1:0.5:0	15	11	21G	0.4	24±0.8	34±12
(S3) PCL/PGS_{mxl}/ 13-93	20/1:0.5:0.3	15	11	18G	0.4	24±0.8	34±12
(S4) PCL/PGS_{mxl}/ 13-93BS	20/1:0.5:0.3	15	11	18G	0.4	24±0.8	34±12
(S5) PCL	20/1:0:0	15	11	21G	0.4	24±0.8	34±12
(S6) PCL/13-93	20/1:0:0.3	15	11	18G	0.4	24±0.8	34±12
(S7) PCL/13-93BS	20/1:0.5:0.3	15	11	18G	0.4	24±0.8	34±12

Table 9.1: Composition of PCL and PCL/PGS polymeric solutions and operating parameters for electrospinning of PCL and PCL/PGS fiber mats.

20% *w/v* solution of PCL in acetic acid was prepared, stirred overnight at room temperature and sonicated for 30 min prior to addition of PGS. PGS_p or PGS_{mxl} (Table 9.1) were further added to the solution, stirred and sonicated for additional 30 min. The bioactive glass powders, 13-93 or 13-93BS, were homogeneously dispersed (Table 9.1) in the polymeric solution and stirred for 5 min. Electrospinning was performed immediately after in order to avoid possible alterations of bioactive glass particles in acetic acid.

Bioactive glass denomination	SiO_2	B_2O_3	CaO	K_2O	Na_2O	MgO	P_2O_5
13-93	56.6	-	18.5	11.1	5.5	4.6	3.7
13-93BS	20	36.6	18.5	11.1	5.5	4.6	3.7

Table 9.2: Composition (wt.%) of the synthesized bioactive glasses used for the preparation of the composite fibers.

9.3.2 Electrospinning process

Electrospun fiber mats were obtained using a commercially available setup (Starter Kit 40KV Web, Linari Engineering srl, Valpiana (GR), Italy). The utilized parameters for the electrospinning process, as well as temperature and relative humidity, are summarized in Table 9.1.

9.3.3 Characterisation

9.3.3.1 Microstructure and composition

SEM analysis (FE-SEM-EDS, Auriga 0750, Carl-Zeiss, Jena, Germany) was conducted for examining the microstructure and morphology of the series of electrospun mats. Prior to this analysis, the samples were sputtered with gold using a sputter coater (Q150T, Quorum Technologies Ltd., Germany). Magnification was varied in a range of 1000 to 45,000x. The average fiber diameter was calculated using

a Fiji 1.51s analysis software (NIH, Bethesda, MD, USA). The measurement of the diameter of 30 randomly chosen fibers was performed for each sample [387].

FTIR analysis of the sample's composition was carried out in attenuated total reflectance mode (ATR), using a FTIR spectrometer (IRAffinity-1S, Shimadzu, Japan). For the analysis, 40 spectral scans in absorbance mode were averaged across the wavenumber range of 4000 to 400 cm^{-1} with a resolution of 4 cm^{-1}.

9.3.3.2 Mechanical characterisation

Mechanical properties of a set of fiber mats were investigated by uniaxial tensile strength tests (3366 Dual Column Tabletop Testing System, Instron®, Darmstadt, Germany). Measurements were performed at a crosshead speed of 10 mm/min using 50 N load cell. To avoid any undesired stretching of fiber mats before the tensile test, specimens were cut into rectangular shape (3 mm x 20 mm) and arranged into paper frames (20 mm x 20 mm). Average values and standard deviations of Young's modulus (E), ultimate tensile strength (UTS) and strain to failure (FS), were determined based on the five measurements for each composition.

9.3.3.3 Wettability

The measurements of static water contact angle of the fibrous specimens were conducted by the sessile drop method (DSA30, Krüss GmbH, Hamburg, Germany) in air. To this aim, drops of 3 μL deionized water were placed onto the fiber mats. At least five measurements at room temperature were performed for each blend. The data were collected and analysed using the DSA software (DSA4 2.0, Krüss GmbH, Hamburg, Germany).

9.3.3.4 *In vitro* degradation

The *in vitro* degradation study of the as-spun samples was carried out in phosphate buffered saline (PBS) (VWR Life Science AMRESCO®, USA).

For each composition, sample triplicates were immersed in 16 ml of PBS solution at 37°C. Experiments were performed in a standard incubator (KS 4000 i Control, IKA®-Werke GmbH & Co. KG, Germany) with mild shaking (82 rpm). During the incubation period, pH was monitored and recorded at the following time points: 1h; 2h; 4h; 1 day; 4 and 7 days. After 1 and 7 days, the samples were removed from the solution, rinsed with ultra-pure water, dried and examined by SEM and ATR-FTIR analysis, to evidance changes in morphology and chemical composition. A falcon tube containing solutions of PBS without any samples was also incubated for the entire period of the experiment, to ensure and control overtime solution stability.

9.3.3.5 Cell culture

The biological assay was performed using the bone marrow-derived stromal cells, ST-2, (Deutsche Sammlung von Mikroorganismen und Zellkulturen GmbH, Braunschweig, Germany). Before the seeding step, ST-2 cells were cultured in RPMI 1640 medium (Thermo Fisher Scientific), supplemented with 10% fetal bovine serum (Lonza) as well as 1% penicillin/streptomycin (Lonza), and incubated at 37°C with 5% CO_2. Cell viability, proliferation and morphology after 1 and 7 days were evaluated according to the protocol developed by Liverani et al. [388]. Briefly, prior to the cell test, all the samples were cut and fixed on a holder for 24 well plates (Scaffdex, Sigma). To disinfect the specimens, treatment under UV light was carried out for 1 h. ST-2 cells were drop seeded onto fixed fiber samples with a density of $2.5 \cdot 10^5$ cells/mL in a droplet of 100 µl of RPMI media per sample and incubated for 15 min. Then, 1mL of RPMI medium was added to each well.

After 1 and 7 days, cell proliferation and cytotoxicity were assessed using colorimetric Cell Counting Kit-8 (CCK-8) assay based on tetrazolium salt WST-8 (2-(2-methoxy-4-nitrophenyl)-3-(4-nitrophenyl)-5-(2,4-disulfophenyl)-2H-tetrazolium, monosodium salt). The reduction of WST-8 by cellular dehydrogenases to an orange formazan product was measured in absorbance mode at 450 nm by the plate reader

(PHOmo microplate reader, Autobio Labtec Instruments Co. Ltd., Zhengzhou City, China).

Cell morphology was investigated after 1 and 7 days upon seeding. To this aim, samples were exposed to fluorescence microscopy (Axio Scope A1, Zeiss). Prior to analysis, seeded samples were stained with rhodamine phalloidin and DAPI (Thermo Fisher Scientific, Massachusetts, USA), according to the protocol reported previously by Liverani et al. [389]. Briefly, sample's fixation was carried out using a solution containing 1,4-piperazinediethanesulfonic acid buffer, ethylene glycol tetraacetic acid, polyethylene glycol, paraformaldehyde, PBS, and sodium hydroxide (Sigma Aldrich®, Munich, Germany). Then, the specimens were rinsed three times with PBS and immersed in a permeabilization buffer containing Triton X-100, sucrose and PBS (Sigma Aldrich®, Munich, Germany). Prior to characterization, fixed samples were stained using Rhodamine phalloidin solution (8 µL/mL) and DAPI solution (1 µL/mL).

9.3.3.6 Statistics

All experimental data are presented as average values ± standard deviation. One-way analysis of variance (ANOVA, Origin) was used to analyze the differences between groups with a probability defined as *(* $p < 0.05$).

9.4 Results and discussion

9.4.1 Fiber morphology

SEM micrographs of the seven series of as-spun porous samples are reported in Figs. 9.1(a)-(g). In the present work, the selection of the key parameters for the electrospinning process, namely, the solution concentration and applied voltage, was adapted from Liverani et al. [390]. Indeed, it was shown that homogeneous, bead-free neat PCL fiber mats can be obtained using *20 w/v%* solution of PCL in acetic acid and 15kV applied voltage. These parameters, as well as distance tip-target and flow

rate (Table 9.1), were maintained constant in order to better clarify the influence of the composition, i.e. presence of PGS polymer and bioactive glass particles (BG), on the mechanical and biological performances of fiber mats.

The average fiber diameter of the different series of blend electrospun mats is reported in Table 9.3. It can be seen that, the addition of PGS polymer leads to an increase of the average fiber diameter. This phenomenon can be ascribed to the increasing total amount of polymer content in the solution. The value (0.9±0.4 μm) of the average fiber diameter for the neat PCL mats falls within the range of 0.11-3.85 μm reported in literature [389–391]. Moreover, the estimated values of average diameter for PCL/PGSp (1.5±0.5 μm) and PCL/PGS_{mxl} (1.5±0.6 μm) are also in accordance with the literature, where the fiber diameter of PCL/PGS blends were reported to vary in a range between 0.55 and 4.7 μm [368,377,392,393]. These features are important as they demonstrate that the use of benign solvents did not affect the morphology of the electrospun composite fibers, since the average fiber diameter is comparable with the fibers obtained with standard solvents for ES.

The amount of bioactive glass added in the present work, to fabricate composite fiber mats, was fixed at 30 wt% and maintained constant for all composite blends, in particular for PCL/13-93, PCL/13-93BS, PCL/PGS_{mxl}/13-93, and PCL/PGS_{mxl}/13-93BS. The incorporation of glass microparticles into fiber scaffolds can be observed in Fig. 9.1 (d)-(g). The presence of BG particles inside the as-spun mats was also confirmed by the SEM/EDX analysis (Fig. 9.2). As reported in Table 9.3, the addition of glass did not alter significantly the average fiber diameter. However, the standard deviation in samples with the glass, i.e. PCL/13-93, PCL/13-93BS, PCL/PGS_{mxl}/13-93, and PCL/PGS_{mxl}/13-93BS, was found to increase. Correspondingly, the distributions of fibers diameter reported in Fig. 9.1 (l)-(p) show that maximum and minimum vary more noticeably. This effect can be caused by the increasing conductivity of the polymeric solution in presence of bioactive glass particles.

a

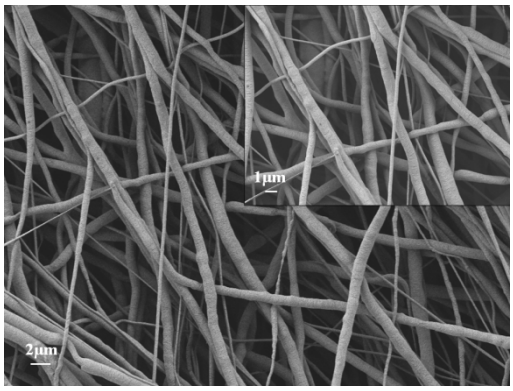
1μm
2μm

h

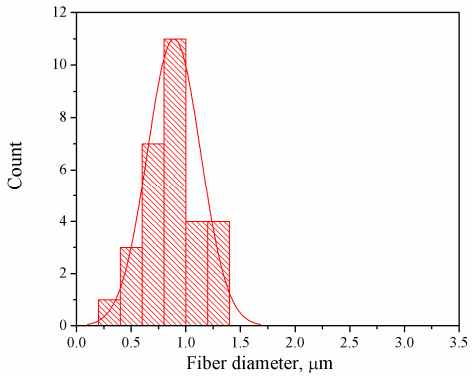
Count
Fiber diameter, μm

b

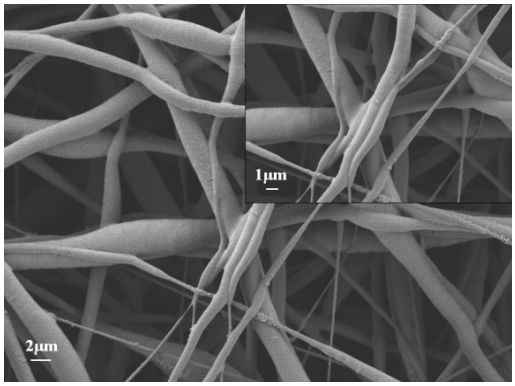
1μm
2μm

i

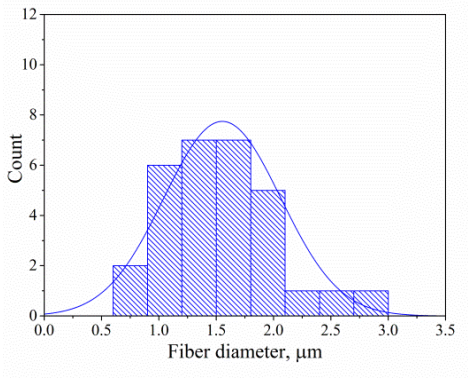
Count
Fiber diameter, μm

c

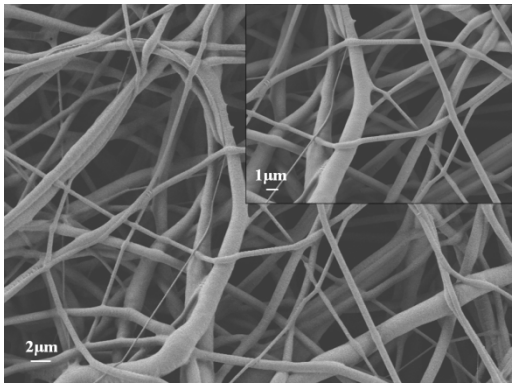
1μm
2μm

k

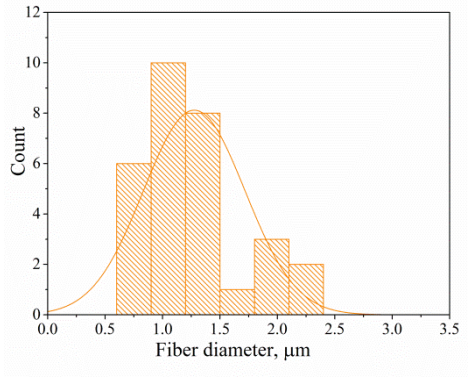
Count
Fiber diameter, μm

d

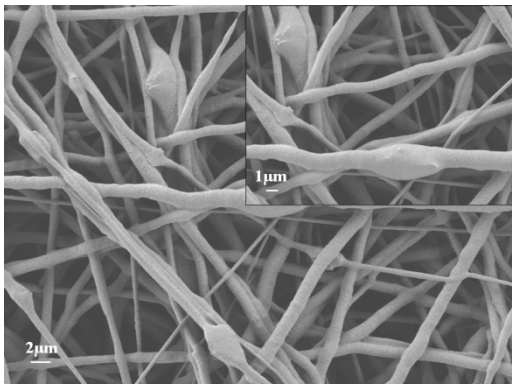
1μm
2μm

l

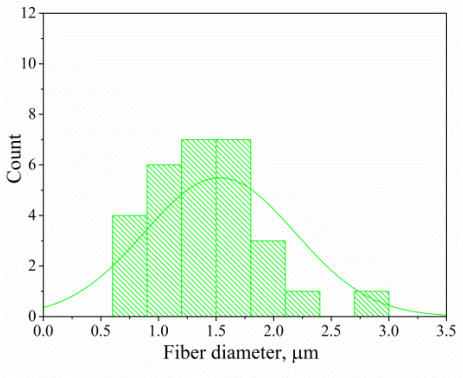
Count
Fiber diameter, μm

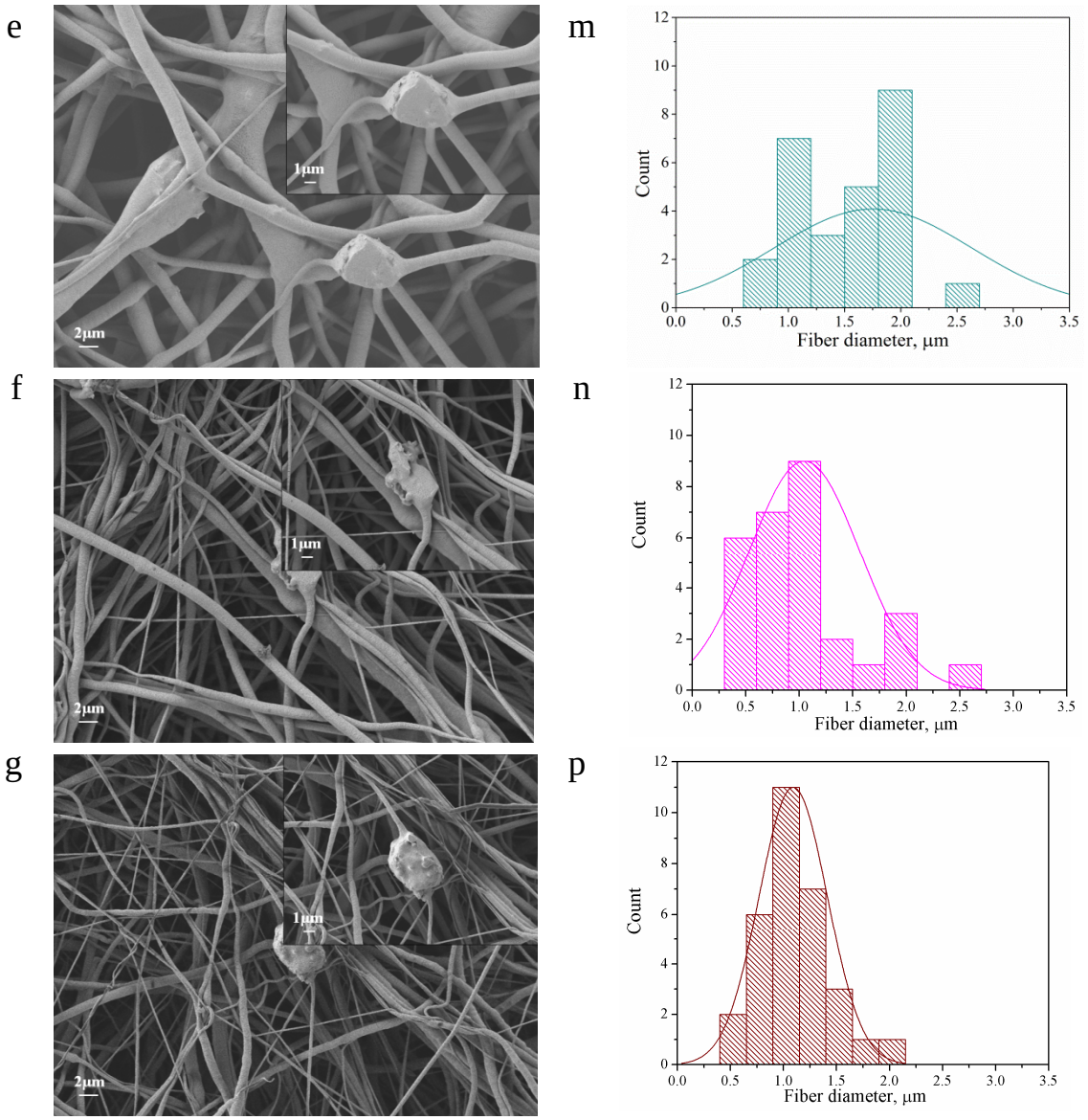

Figure 9.1: SEM images of electrospun fiber mats and corresponding fiber diameter distribution: (a), (h) neat PCL; (b), (i) PCL/PGS_p; (c), (k) PCL/PGS_{mxl}; (d), (l) PCL/PGS_{mxl}/13-93; (e), (m) PCL/PGS_{mxl}/13-93BS; (f), (n) PCL/13-93 and (g),(p) PCL/13-93BS, respectively.

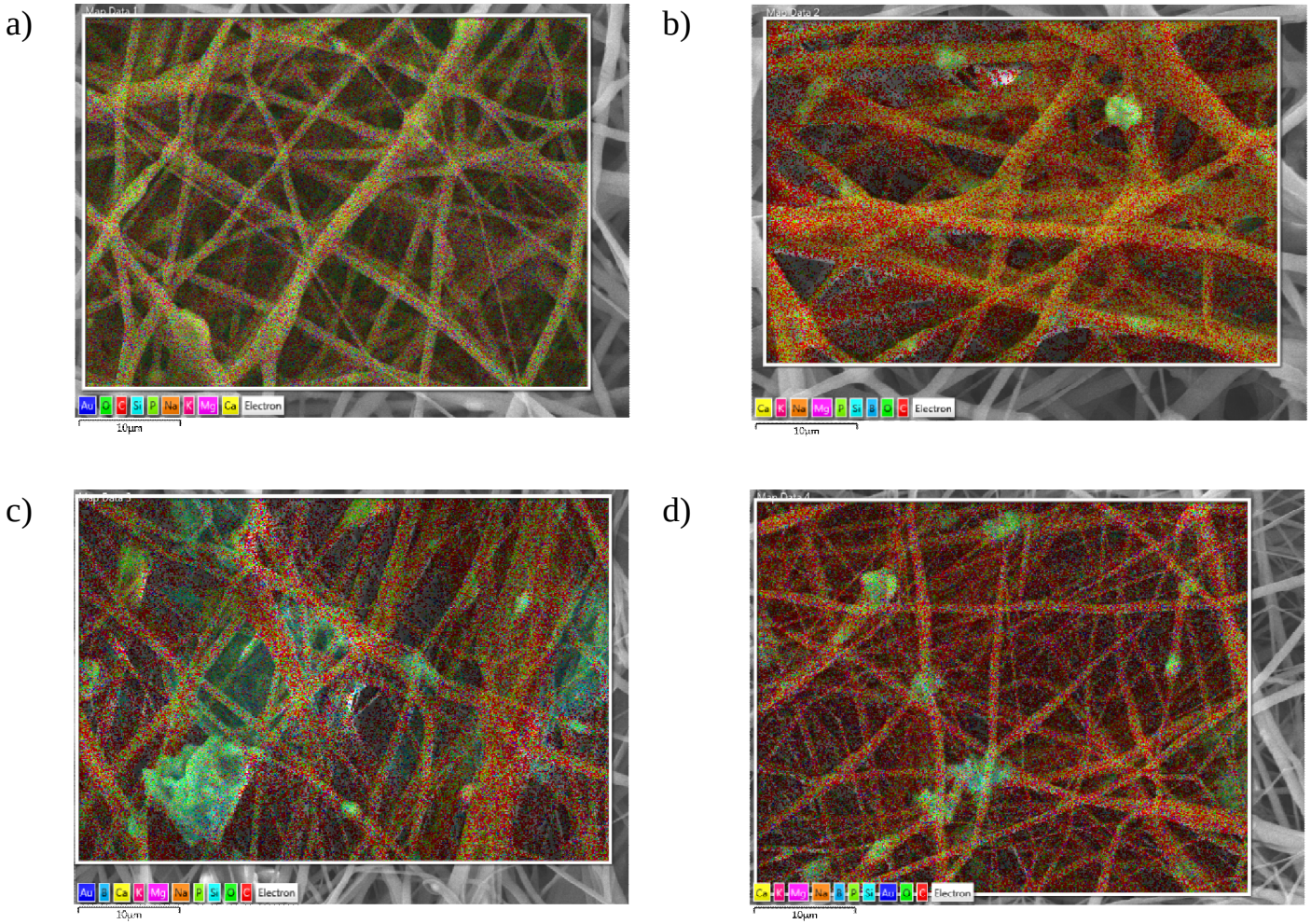

Figure 9.2: SEM/EDX images, confirming the presence of BG particles in (a) PCL/PGSmxl/13-93, (b) PCL/PGSmxl/13-93BS, (c) PCL/13-93, (b) PCL/13-93BS, samples.

Sample name	Average fiber diameter [μm]	Young's Modulus [MPa]	Ultimate tensile strength [MPa]	Failure strain [%]
PCL	0.9±0.4	2.4±0.5	1.3±0.2	447±226
PCL/PGS_p	1.5±0.5	3.8±0.8	1.0±0.2	219±112
PCL/PGS_{mxl}	1.5±0.6	4.4±0.3	1.2±0.2	200±103
PCL/PGS_{mxl}/13-93	1.6±0.7	4.5±0.3	1.0±0.1	117±62
PCL/PGS_{mxl}/13-93BS	1.7±0.9	1.2±0.4	0.6±0.1	185±106
PCL/13-93	1.1±0.7	2.2±0.4	1.1±0.2	228±139
PCL/13-93BS	1.1±0.7	0.5±0.3	0.9±0.2	115±57

Table 9.3: Average fiber diameter and mechanical properties of electrospun fiber mats.

9.4.2 Chemical characterization of as-spun mats

FTIR analysis was performed to examine the chemical composition of prepared fiber mats. Fig. 9.3 illustrates the obtained spectra of neat PCL, PCL/PGS_p, PCL/PGS_{mxl} and polymer/BG fiber composites. No typical absorption bands of acetic acid were detected, confirming that this solvent totally evaporated during the electrospinning process.

All spectra exhibit the characteristic PCL bands already reported in the literature [357,392,393]: 2942 cm^{-1}, 2865 cm^{-1} and 1366 cm^{-1}, relative to stretching of alkyl group (CH_2); 1240 cm^{-1} and 1165 cm^{-1} peaks, attributed to symmetric and asymmetric C─O─C stretching, respectively; the peak centered around 1722 cm^{-1} of carbonyl stretching (C═O); finally, the additional peak around 1294 cm^{-1} is due to the backbone C─O and C─C stretching.

PGS vibration bands, namely, 2929 cm^{-1}, 2851 cm^{-1} and 1384 cm^{-1}, are attributed to alkyl groups, the peak around 1734 cm^{-1} is associated to carbonyl stretching (C═O); and C─O band stretching vibration at 1165 cm^{-1} [392], are overlapping with PCL absorption bands. Moreover, the broad band between 3300 cm^{-1} and 2500 cm^{-1}, corresponding to the stretch vibration of hydroxyl bond, cannot also be distinguished, since a relatively small amount of PGS was used to fabricate PCL/PGS mats (50wt% with respect to PCL). Only a slight shift to lower wavenumbers, typical for PGS, can be noticed when spectra of PCL/PGS blends were analyzed.

A similar situation can be observed in samples containing BG particles (PCL/13-93, PCL/13-93BS, PCL/PGS_{mxl}/13-93, PCL/PGS_{mxl}/13-93BS). Characteristic absorption bands of silicate glass 13-93 [386], namely, Si─O─Si and Si─O stretching modes, which are located in the range between 900 and 1100 cm^{-1}, along with that one of Si─O─Si bending mode at 470 cm^{-1}, are relatively weak and cannot be detected. Peaks of borosilicate glass 13-93BS exhibit the same vibrations as silicate 13-93 glass and the additional peaks are attributed to the B─O stretching mode of

tetrahedral BO_4 groups located around 700 cm^{-1} and in the range between 900 and1100 cm^{-1}; finally, B─O stretching bands of BO_3 group are situated in 1150-1300 cm^{-1} and 1200-1500 cm^{-1} ranges.

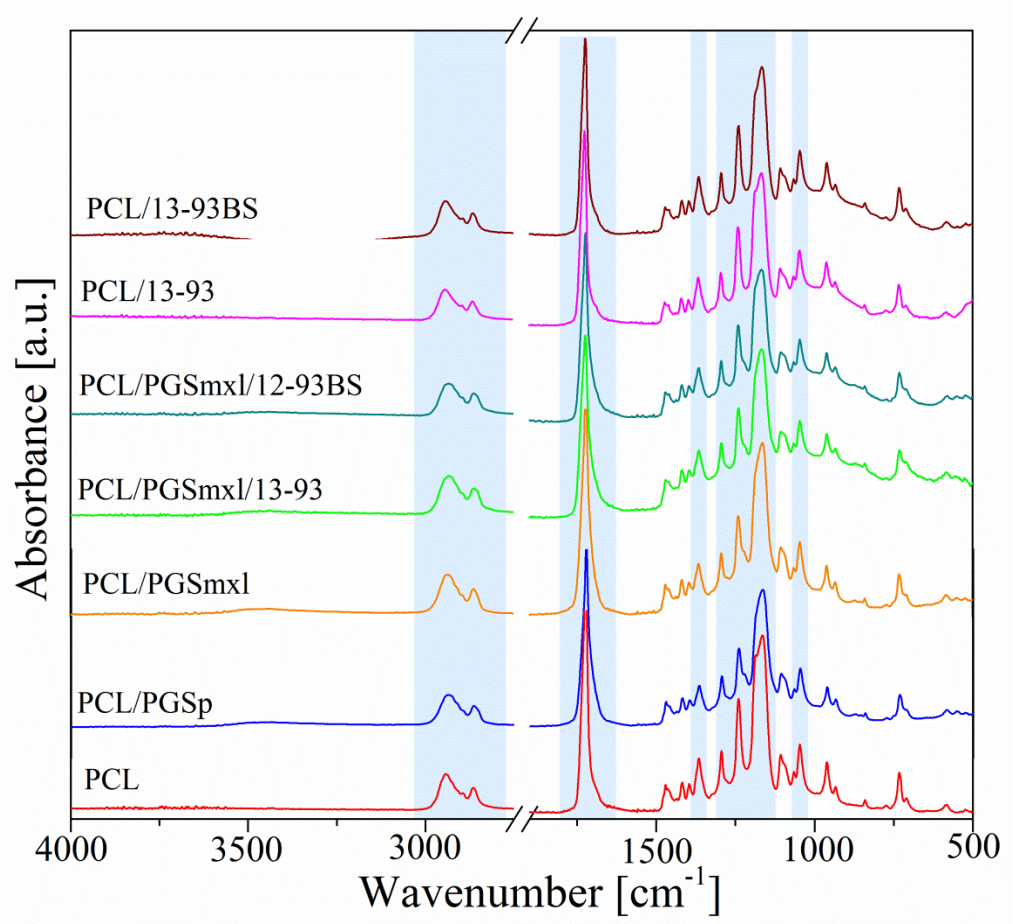

Figure 9.3: ATR-FTIR spectra of as-spun fiber mats.

9.4.3 Wettability

Surface wettability or hydrophilicity represents one of the key parameters for a biomaterial, which affect cell behavior via protein adsorption, platelet adhesion/activation, blood coagulation and cell bacterial adhesion [394,395]. It was found that either strongly hydrophobic or hydrophilic surfaces are not favorable for cell attachment. Indeed, the optimal water contact angle range, which allows effective cell adhesion should lay in the range between 40° and 70° [394,396].

As mentioned in section 9.3.2.3, in the present study, the wettabilty of as-spun fiber mats was evaluated by contact angle measurements. Fiber mats containing only PCL polymer, i.e. PCL, PCL/13-93, PCL/13-93BS, were found to exhibit an hydrophobic behavior, with contact angles of 100 ± 5^{o}, 100 ± 4^{o} and 101 ± 4^{o}, respectively. Therefore, the estimated values lay in the range between 98^{o} and 133^{o} previously reported in the literature for PCL electrospun mats [357,368,392]. Such outcome confirms that the presence of BG particles and the related roughness of the composite mats do not affect the wettability.

On the contrary, blended fibers containing PGS polymer, namely, PCL/PGSp, PCL/PGS$_{mxl}$, PCL/PGS$_{mxl}$/13-93, and PCL/PGS$_{mxl}$/13-93BS showed a highly hydrophilic behaviour. Indeed, the contact angle was not even detectable, since the water drop deposited on their surface rapidly penetrated and spread through all the tested compositions. Thus, being strongly hydrophilic, due to the hydroxyl groups attached to its backbone, PGS is found to markedly affect the wettability of PCL/PGS blend mats [368,392].

9.4.4 Degradation

It is known that when biomaterials exposed to biological environments undergo degradation, their initial physicochemical properties change. In particular, in case of polymers, degradation leads to the polymer chain scissions.

PCL and PGS belong to aliphatic polyesters and are subjected to hydrolytic degradation through the cleavage of ester linkages, but with different rates. Total resorption of PGS *in vivo* was observed within few weeks after implantation [375,397]. On the other hand, PCL, being semi-crystalline at room temperature, is relatively stable *in vivo* and possesses low resorption rate [374,398]. It was found that crystallinity and molecular weight of PCL strongly affect its degradation rate [374,399]. In this perspective, it is particularly interesting to study PGS/PCL blends, in order to obtain hybrid materials that exhibit modulated degradation.

To investigate degradation features, neat PCL, PCL/PGS and PCL/PGS/BG blends were subjected to *in vitro* immersion tests in PBS solution. Over the course of the tests, the change of pH was monitored. Measurements were performed after 1h, 2h, 4h, 24h, 96h and 168h of incubation. The curves of pH change during immersion (up to 5 and 168h) are shown in Fig. 9.4 (a) and (b), respectively.

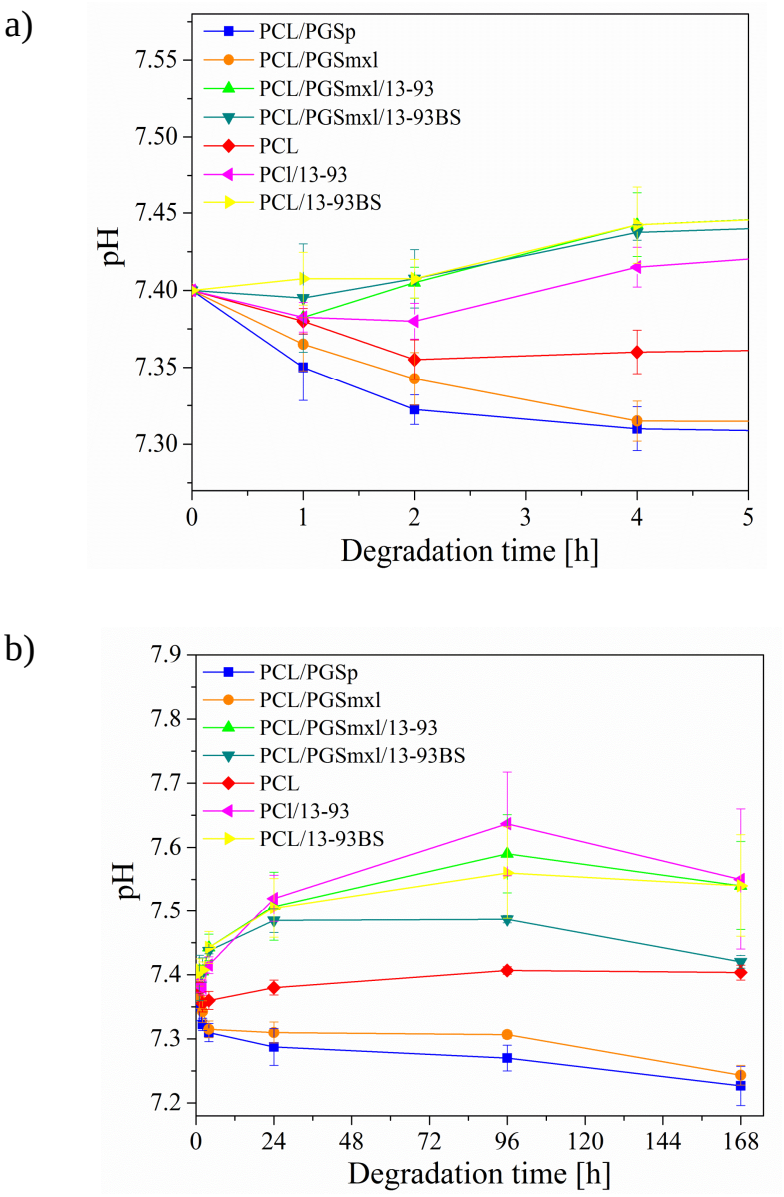

Figure 9.4: Change of pH during immersion of as-spun samples: (a) after 5h; (b) after 168h.

It can be observed, that during the first 4 hours, pH values in PBS solutions in contact with PCL/PGS_p and PCL/PGS_{mxl} mats drop more significantly, indicating the acidification of the media; on the contrary, neat PCL samples determine only modest changes. In addition, after 168h of immersion, pH of the solutions containing PCL/PGS_p and PCL/PGS_{mxl} were found to be 7.22±0.3 and 7.24±0.15, respectively. Such acidification effect of PGS, which is ascribed to the leaching of non-reacted monomers, was already reported in literature [400,401]. In order to remove residual monomers and oligomers, which potentially can be harmful for cells, authors utilized either sample's washing in a mixture of ethanol and water or pre-conditioning of PGS containing mats in the culture medium.

Some representative SEM micrographs of PCL/PGS_p and PCL/PGS_{mxl} after 1 and 7 days of immersion in PBS, are reported in Fig. 9.5 (b), (i) and (c), (k), respectively. They clearly indicate the fiber s degradation takes place already after 1 day of immersion. According to the literature, PGS degradation occurs via surface erosion [375,402]. The occurrence of this phenomenon, which is evidenced through the formation of porous structure and polymer leaching, can be observed in Fig. 9.5 (b), (c).

A different situation was encountered with samples containing neat PCL (Fig. 9(a), (h)), which did not exhibit, even after 7 days of immersion, significant evidence of degradation, thus confirming the results arising from pH measurements.

On the other hand, Fig. 9.4 shows that blends containing both PGS polymer and bioactive glass particles, i.e. PCL/PGS_{mxl}/13-93 and PCL/PGS_{mxl}/13-93BS, in contact with PBS did not promote media acidification. In contrast, the value of pH increased after 4 hours of immersion, reached a maximum value after 96 hours and slightly dropped after 168 hours. This effect could be ascribed to the ion release from the glass, which took place and compensated the acidification effect of PGS polymer.

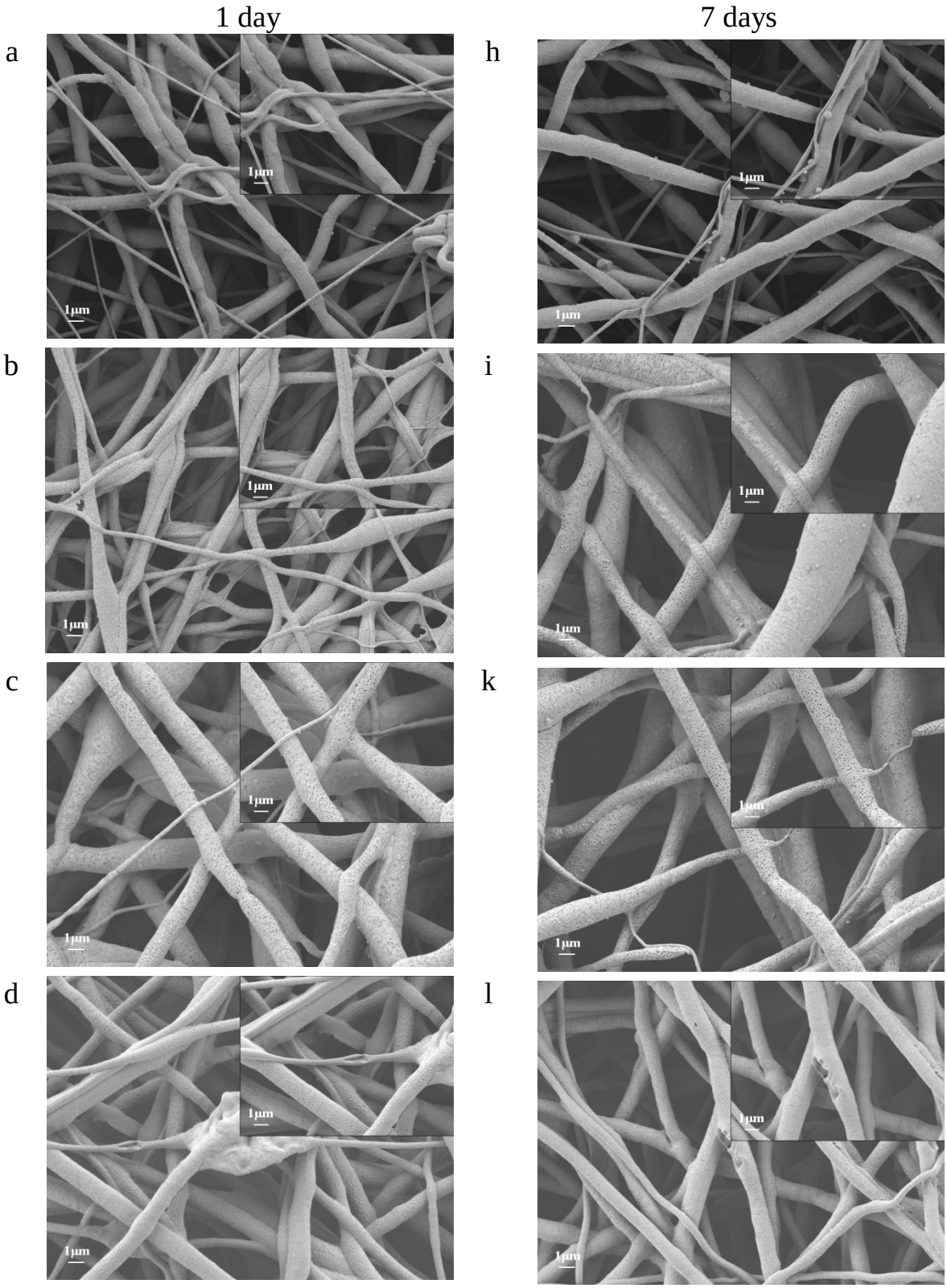
1 day
7 days
a
h
b
i
c
k
d
l
1μm

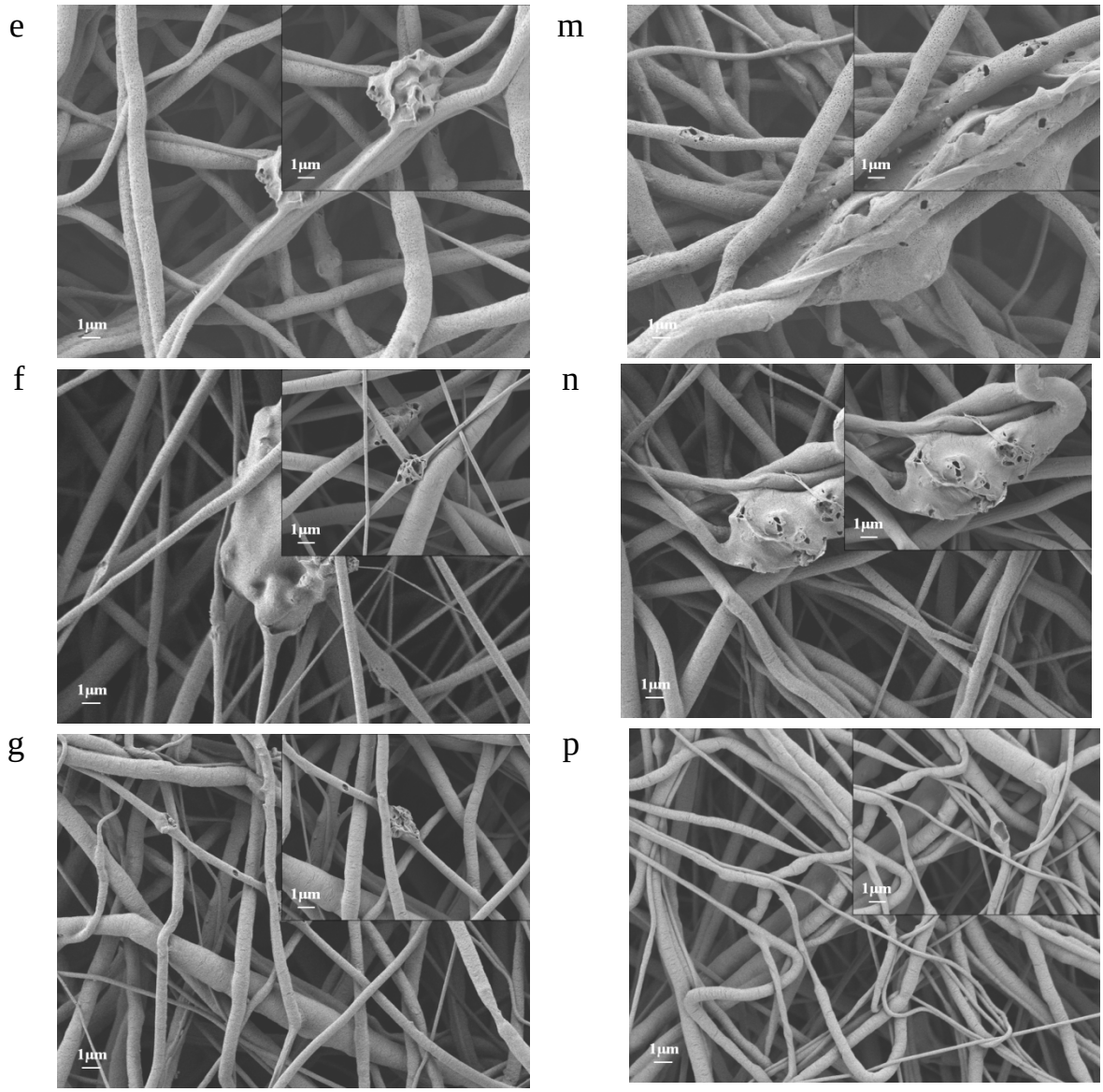

Figure 9.5: SEM images of electrospun fiber mats after immersion in PBS solution: (a), (h) neat PCL; (b), (i) PCL/PGS_p; (c), (k) PCL/PGS_{mxl}; (d), (l) PCL/PGS_{mxl}/13-93; (e), (m) PCL/PGS_{mxl}/13-93BS; (f), (n) PCL/13-93 and (g),(p) PCL/13-93BS, respectively.

This holds also true in samples containing only PCL and bioactive glass, i.e. PCL/13-93 and PCL/13-93BS, where pH increased due glass dissolution and ions release. Correspondingly, the SEM micrographs of PCL/PGS_{mxl}/13-93, PCL/PGS_{mxl}/13-93BS, PCL/13-93, and PCL/13-93BS, evidenced huge empty pores, as a consequence of the dissolution of bioactive glass particles (Fig. 9.5 (f), (n), (g), (p)).

9.4.5 Mechanical properties

It is known that, to ensure structural integrity and provide a support to the cells, the mechanical properties of biodegradable fiber scaffolds should match those of the regenerating tissues. In the present study, uniaxial tensile testing was carried out to evaluate the mechanical properties of the as-spun fiber mats under external stress. Resulting stress-strain curves as well as the averaged values of Young's modulus, ultimate tensile strength and failure strain are reported in Fig. 9.6 (a), (b) and Table 9.3, respectively. The stress-strain profiles of all tested fiber mats are consistent with the profiles typical of elastomeric materials.

The obtained values of the Young's modulus for PCL specimens (2.4±0.5 MPa) were found to be lower with respect to the previously published data [357,390]. On the other hand, values of E for PCL/PGS blends (3.8±0.8 MPa and 4.4±0.5 MPa for PCL/PGS_p and PCL/PGS_{mxl}, respectively) were close to those ones reported in the literature [377,393]. Therefore, Young's modulus of PCL/PGS_p and PCL/PGS_{mxl} blends increased in comparison to neat PCL tested samples, thus indicating the improvement achieved in scaffold's stiffness with PGS introduction (Fig. 9.6 (b)). However, as reported in Table 9.3, UTS values of PGS/PCL samples were found to be comparable, while failure strain decreased when PCL/PGS blends were considered.

It should be noted that the mechanical properties of fiber scaffolds depend particularly on the microstructural parameters such as the fiber diameter and the average fiber diameter distribution. As seen in Fig. 9.6 (a), the mechanical properties of the samples containing BG particles were found, as expected, to be lower, due to the increased inhomogeneity in the distribution of the average fiber. As reported previously by Liverani et al. [390], the presence of the interface between organic-inorganic phases likely contributes to the decreased mechanical properties.

a) b)

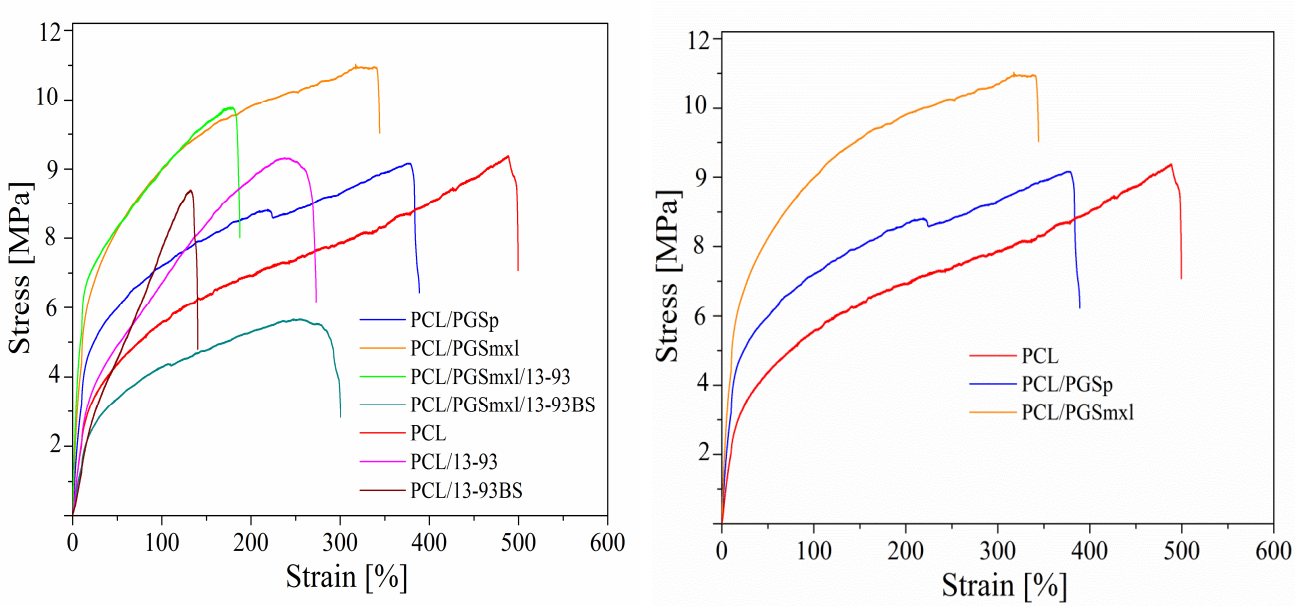

Figure 9.6: Mechanical properties of as spun samples: (a) all compositions; (b) compositions containing only polymers.

9.4.6 Cell study

Cellular tests using the stromal cell line ST-2 were performed to access cell viability, proliferation and adhesion in presence of as-spun mats. The results of the WST-8 assay after 1 and 7 days of incubation are presented in Fig. 9.7. It can be noticed that cell viability is significantly lower in all samples containing the PGS polymer, i.e. PCL/PGS_p, PCL/PGS_{mxl} and PCL/PGS_{mxl}/13-93, and PCL/PGS_{mxl}/13-93BS, as compared to neat PCL control. However, different authors reported an improved cell adhesion and proliferation when PCL/PGS fiber mats were considered. In this regard, it is worth to mention that, according to the literature, an immersion in aqueous ethanol solution followed by UV light treatment is usually utilized for the sample's disinfection before cellular tests. This two steps procedure aimed not only to disinfect the samples, but also to remove all unreacted monomers and oligomers from the PGS structure. The presence of residual monomers can strongly affect the pH of culture medium and be harmful for cells. In this regard, Vogt and co-workers [357] studied

possible effects of the disinfection procedure (using of 70% v/v aqueous ethanol versus UV light treatment) on the chemical composition and morphology of as-spun PCL/PGS mats. Results arising from their study indicate that immersion in ethanol even for 1h leads to the complete removal of PGS from the blend. Authors also pointed that leaching of PGS is accompanied by the formation of pores on the fiber's surface. In the present study, UV light was used for 1h to disinfect the samples. Then, samples pre-conditioning in culture medium was performed just for 1 min before cell seeding.

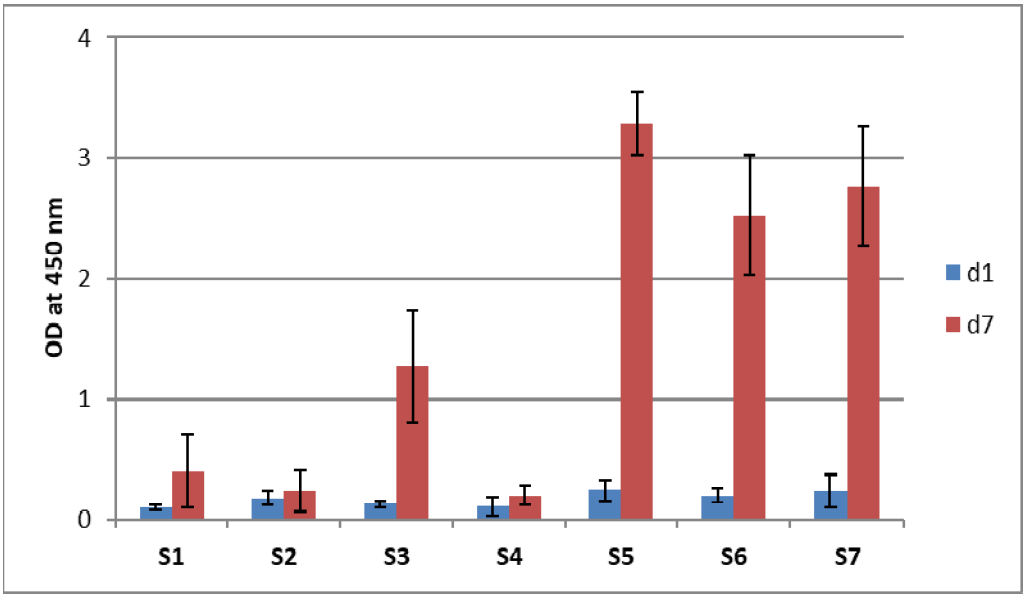

Figure 9.7: WST-8 analysis: optical density at 450 nm for all samples 1 and 7 days after seeding.

Results of the WST-8 assay for the blended and composite fiber mats presented in Fig. 9.7 show no statistically significant differences in cell viability with respect to neat PCL after 1 day from the seeding. The results are different after 7 days, since it is possible to evidence an increase of the measured optical density (OD) values for all samples.

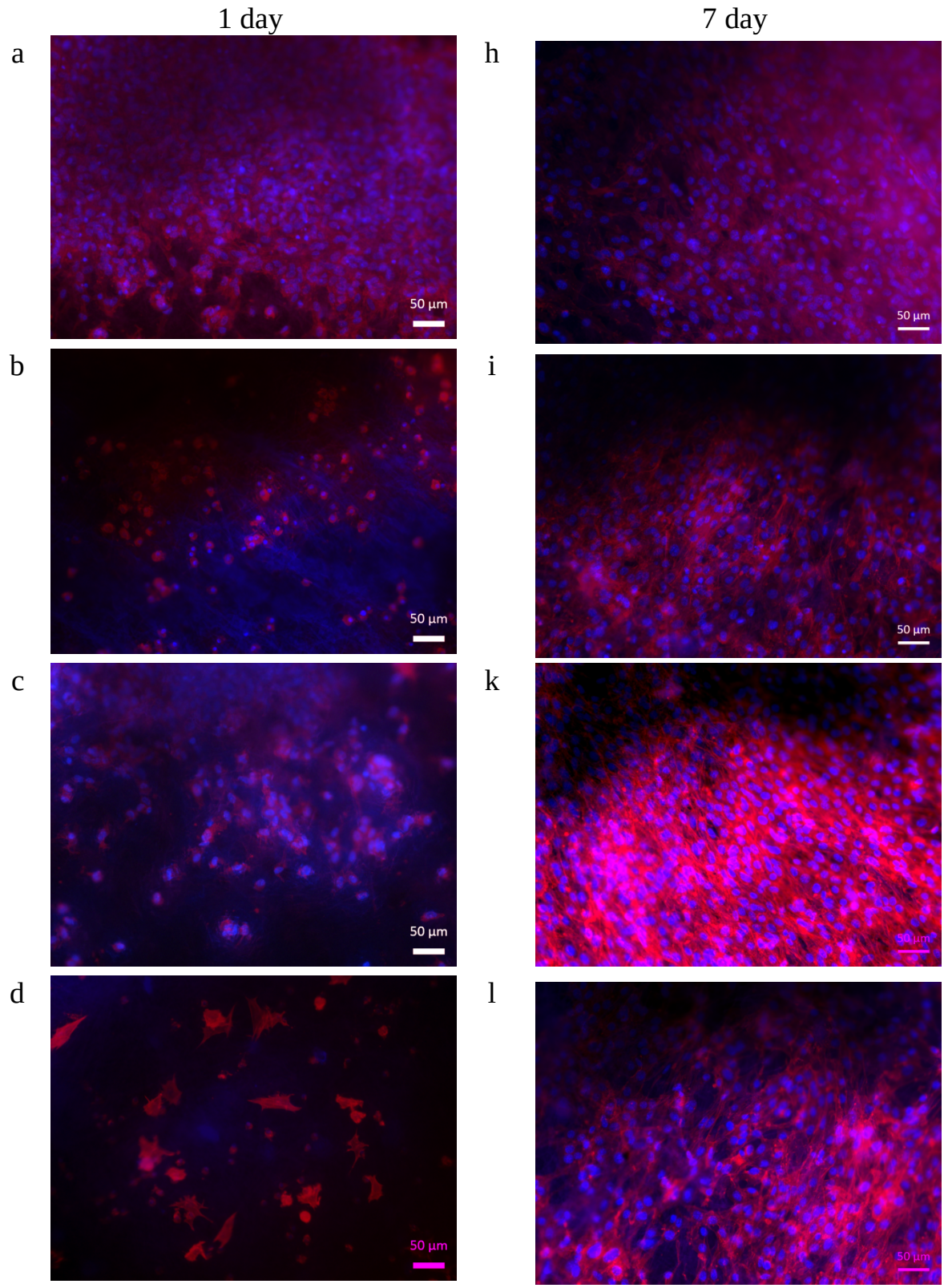
1 day
7 day
a
h
b
i
c
k
d
l
50 µm

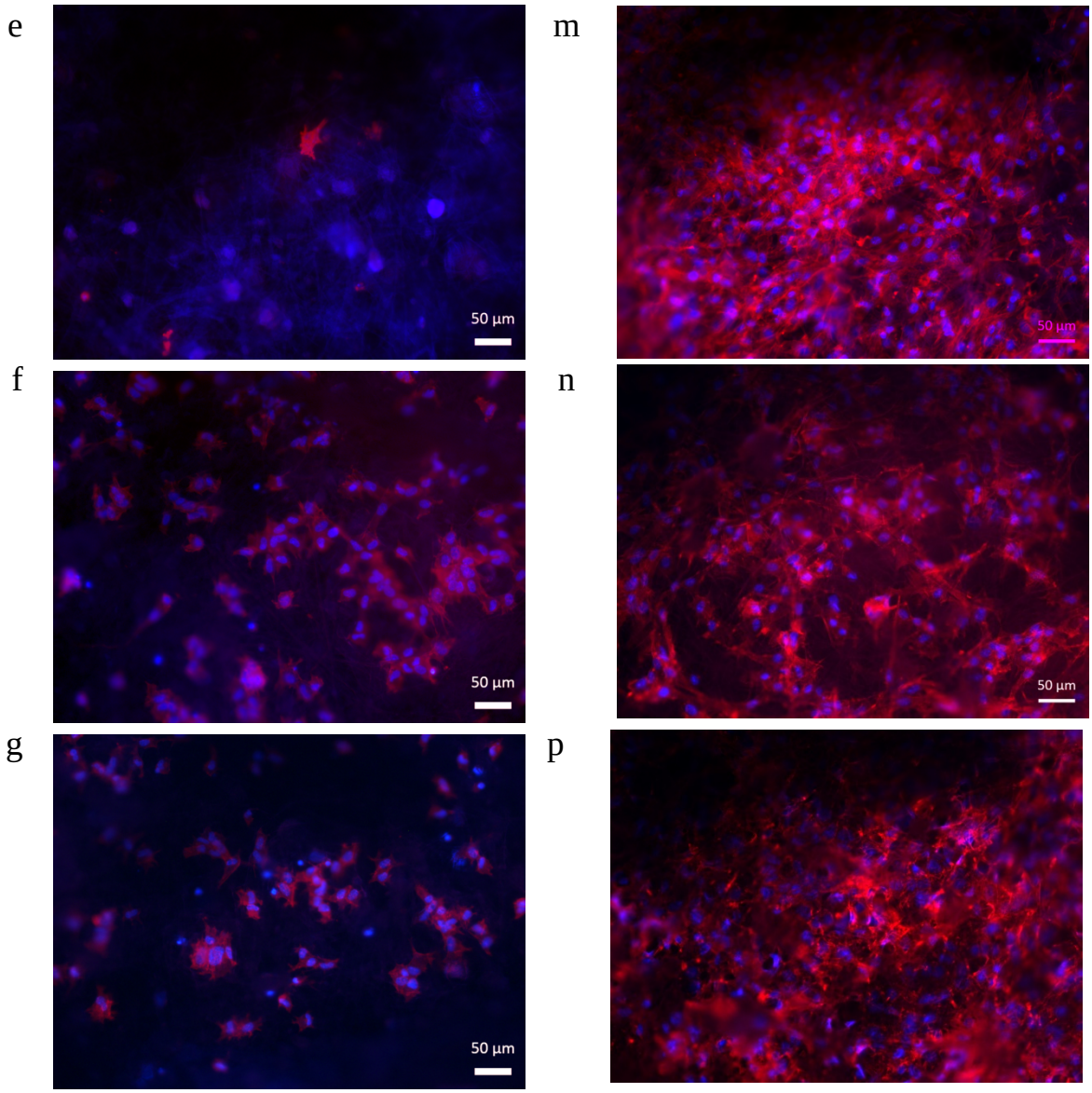

Figure 9.8: Fluorescence images of ST-2 cells on as-spun mats after 1 and 7 days of incubation: (a), (h) neat PCL; (b), (i) PCL/PGS_p; (c), (k) PCL/PGS_{mxl}; (d), (l) PCL/PGS_{mxl}/13-93; (e), (m) PCL/PGS_{mxl}/13-93BS; (f), (n) PCL/13-93 and (g),(p) PCL/13-93BS, respectively.

The normalized ratio values, expressed as (d7-d1)/d1, are reported in Table 9.4. It is clear that the presence of PGS and its related fast degradation rate affect not only cells adhesion but also their proliferation. This aspect appears to be mitigated by the presence of bioactive glass particles 13-93, while the same effect is not detectable in the sample containing 13-93-BS. These differences, related to the bioactive glass composition, are not noticeable in the neat PCL composite samples. In fact, the

presence of bioactive glass particles seems not to be pivotal in the proliferation rate of samples which are not containing PGS. The fluorescence images of tested samples, presented in Fig. 9.8 confirmed findings arised from the WST-8 assay. Indeed, well spread cells can be detected at 7 day after seeding in samples without PGS polymer.

Sample denomination	S1	S2	S3	S4	S5	S6	S7
Ratio ODd7/ODd1	4	1	10	2	14	13	12

Table 9.4: WST-8 assay: measured OD values (at 450nm) expressed as ratio between the measured OD at 7 days after seeding respect to the OD value at 1 day.

9.5 Conclusions

Homogeneous bead-free fiber mats with different compositions were prepared using degradable polymers such as PCL, PGS_p and PGS_{mxl}. Bioglass particles of two different compositions, namely 13-93 and 13-93BS, were successfully incorporated within the structures of electrospun polymeric mats. A benign solvent (acetic acid) for electrospinning was utilized to fabricate blended and composite mats.

Biocompatibility of the obtained mats was examined including cell metabolic activity, attachment and proliferation. Results indicated that the presence of PGS polymer can negatively influence the cell viability. Indeed, the acidification of the media observed in samples containing PGS is thought to be linked to the polymer fast degradation. In the present study, samples disinfection was performed using UV light. In this regard, the release of residual monomers, which can be removed only after immersion in ethanol solution, was found to have a negative effect on cells proliferation. However, such treatment could possibly alter the composition of fiber mats. The effect of fibers composition on the mechanical properties and degradation characteristics was also assessed. In particular, samples containing the PGS polymer showed an improved scaffold's stiffness. On the other hand, the incorporation of bioactive glass particles led to the overall decrease of mechanical properties, due to

the increased fibers inhomogeneity. Finally, the degradation study in PBS solution revealed that PGS polymer tends to dissolve the already after 1 day. Correspondingly, leaching accompanied be the pores formation on the surface of the fibers was observed.

On the basis of the obtained results two crucial aspects have to be solved:

- The identification of an alternative method for samples disinfection, since the presence of undesired residual monomers after UV treatment (with no ethanol) has negative consequences on cell proliferation.
- Improvement of fibers homogeneity after the incorporation of BG particles: the use of smaller sized powders is expected to provide a beneficial effect in this regard.

Remarks

This part of PhD was carried out thanks to the collaboration between the Institute of Biomaterials (Friedrich–Alexander University Erlangen–Nürnberg, Germany) and the University of Cagliari. During my internship, I worked on the samples fabrication via electrospinning technique, as well as physico-chemical, mechanical and biological characterization. Study was guided by Dr. Liliana Liverani and Prof. Dr.-Ing. habil. Aldo R. Boccaccini.

Article to be submitted in a European Polymer Journal:

Electrospun PCL/PGS composite fibers incorporating bioactive glass particles for soft tissue engineering applications

Chapter 10. Concluding remarks

Since in the present thesis are described and discussed the results of different research projects conducted during my PhD program, the conclusions, reported in the follows, are divided according the chapters order.

The effects produced by devitrification phenomena which takes place during the consolidation of amorphous powder on the biological behavior of the resulting material was considered in **Chapter 5**. Such effects remain highly controversial still nowadays, and, in general, thought to negatively affect biological properties of bioceramics. However, more recent studies highlighted that this aspect depends also on the type of bioglass, crystallization degree achieved, the specific crystalline phases formed as well as the size of their crystallites. In turn, these features are specifically related to the sintering technique adopted.

In the present study, the biological response during *in vitro* tests in SBF of three groups of dense samples, produced by SPS from a recently developed glass with high CaO content, was investigated in detail.

The main findings can summarized as following:

- The mildest sintering conditions adopted (730°C – holding temperature, 2min dwell time) provided a completely dense and amorphous material, with superior capability to generate in shorter times (less than 3 days) amounts of the apatite phase (up to 27 wt.%) on the glass surface.
- The 79 wt.% crystallized specimens obtained by SPS at 850°C and 2min, mainly consisting α-$CaSiO_3$ crystallites with smaller amounts of β-$CaSiO_3$ and other minor phases, exhibited only a slightly reduced ability in generating the HCA layer.

- In contrast, the apatite formation process significantly slowed down when the SBF solution was interfaced with the third group of glass-ceramic samples produced at 1000°C and 20 min and mainly consisting of β-$CaSiO_3$.

Thus, the presence of the latter phase in CaMix derived products seems to play the major role, rather than the relatively modest increase of the crystallization degree (from 79 to 88 wt.%), to determine the observed reduction in the generation of the apatite layer. This feature is readily associated to the correspondingly lower weight loss, pH increase and ions released, to indicate a scarce interaction of these materials with the physiological fluid.

In **Chapter 6,** the biocompatibility of different HA/BG composites, as well as pure bioactive CaO-rich glass and HA samples, all sintered using the SPS technique, was systematically evaluated using murine long bone osteocytes, by means of both direct (NR uptake) and indirect test (XTT and BrdU). The obtained results were compared to previous findings arised from the SBF test.

The main findings are described below:

- Even though none of the samples considered in the present study was found to be cytotoxic, the outcomes of cellular test did not confirm the ones arising from the SBF assay. In particular, the direct test results did not show an enhanced “biological performance” in samples with increasing glass content. This fact may be ascribed to the high release of ions and particulate from the glassy phase, which could negatively influence the cell viability; in this regard, it should be noted that, as reported in the literature the presence of particulate in the culture medium may affect the accuracy of the absorbance readings employed in the colorimetric assay.
- The performance of the CaMix alone is, in general, better during the indirect test. In particular, the samples with the higher glass content (CaMix, 80BG_20HA and 50BG_50HA) slightly stimulate the cell proliferation.

Regardless the specific glass-ceramic composition, it was confirmed in this study that SPS is a promising technique to produce sintered bioglasses and bioglass-based composites without negatively affecting the biocompatibility of the final system.

Most importantly, the present work demonstrated once more that the results obtained using SBF assays should be interpreted with great care, and need to be confirmed with suitable cellular tests.

Preliminary results obtained during the fabrication of Functionally Graded samples based on HA/CaO-rich bioactive glass using the SPS technique were described in **Chapter 7**. The main goal of this study was to identify the optimal SPS parameters which could allow to obtain crack-free stepwise FGM specimens, with the more reactive CaO-rich glass surface on the one side of the device and more stable HA phase on the another side. The optimized operating conditions for the two different systems studied were determined (FGM-S1 and FGM-S2, compositions are reported in Table 7.1), including the design of a modified die configuration able to provide the required temperature gradient across the sample.

Mechanical and biological characterizations are still in progress.

Chapter 8 was dedicated to the development of novel highly bioresorbable ceramics for bone tissue regeneration. In particular, carbonated and magnesium co-doped amorphous calcium phosphate (ACP) powders with different compositions were synthesized by a precipitation method and then consolidated by Spark Plasma Sintering at low temperature, according to cold sintering approach.

The main findings of this investigation are listed in what follows:

- ACP powders with high carbonate content (about 18.3 wt.%) were prepared.
- Cold-sintering at 150^{o}C by SPS was found to be effective to consolidate all types of powders.

- The influence of the introduction of carbonate and magnesium ions in ACP on the consolidation process was also investigated. After SPS, undoped ACP, carbonated ACP (cACP) and 5/15 wt.% Mg-doped cACP transformed into low crystallinity apatites. However, a high carbonation degree (mostly B-type) was preserved even after SPS; high resorption rates when operating *in vivo* and the concomitant fast release of bioactive ions are then expected. In conclusion, the highly carbonated low crystalline apatite-based ceramics obtained in this work will most likely exhibit enhanced biological behavior in terms of reactivity and resorbability.

The most important finding of the present investigation is the identification of the experimental conditions allowing, for the first time, to retain the amorphous nature of ACP materials even after SPS. The suitable sintering conditions, associated to adequate Mg and CO_3^{2-} substitutions, were determined. These findings open the way to the development of consolidated ACP-based bioceramics with high (bio)reactivity.

Finally, in **Chapter 9**, electrospun PCL/PGS composite fibers incorporating bioactive glass particles were fabricated and characterized for possible soft tissue engineering applications. Indeed, only recently, the ability of bioactive glasses to promote angiogenesis, due to dissolution phenomena arising from the contact between BG and body fluids, was proved. In this light, the incorporation of bioactive glass particles within the structure of the polymeric mats was attempted. Homogeneous bead-free fiber mats with different compositions were prepared using degradable polymers such as PCL, PGS_p and PGS_{mxl}. Bioglass particles of two different compositions, namely 13-93 and 13-93BS, were successfully introduced within the structures of electrospun polymeric mats. A benign solvent (acetic acid) for electrospinning was utilized to fabricate blended and composite mats. Biocompatibility of obtained samples was evaluated through cell metabolic activity, attachment and proliferation. It was found that the presence of PGS polymer can negatively influence cell viability. Indeed, the acidification of the media observed in the samples containing PGS is thought to be

linked to the polymer fast degradation. The release of residual monomers, which can be removed only by the immersion in ethanol solution, represents a crucial problem since it can have negative effects on cell proliferation. However, the treatment with ethanol could alter the composition of fiber mats. Therefore, future research work should be focused on the identification of the suitable disinfection methods, with respect to those adopted so far in the literature.

Regarding the mechanical properties, samples containing PGS polymer showed the improvement of scaffold's stiffness. On the other hand, incorporation of bioactive glass particle led to the overall decrease of mechanical properties due to the increased inhomogeneity of fibers. The use of finer BG particles is expected to provide beneficial effects in this regard.

As a general conclusion, it is possible to state that the results obtained in the framework of the present PhD thesis will provide a useful contribution to the scientific community involved in the identification of more suitable bioactive/bioresorbable materials with respect to the state of the art. Indeed, although, as mentioned above, several crucial aspects are still unsolved, some of the obtained findings are very promising in view of the development of novel advanced biomaterials with improved performances for tissue applications.

Appendix. Characterization techniques, software and equipment exploited in this thesis.

Chapter	Characterization technique/equipment/software	Aim
5	X-ray diffraction analysis (**XRD**) (Philips PW 1830, Netherlands) using a Ni filtered Cu Kα radiation (λ =1.5405Å).	Phase identification of the glass-ceramic samples before and after their immersion in the SBF solution.
	High resolution scanning electron microscopy (**HRSEM**) (mod. S4000, Hitachi, Tokyo, Japan) equipped with a UltraDry Energy-dispersive X-ray Detector (**EDS**) (Thermo Fisher Scientific, Waltham, MA, USA)	Microstructural and compositional characterization of samples before and after their immersion in the SBF solution.
	Inductively Coupled Plasma Optical Emission Spectroscopy (**ICP**) (ICP-OES CCD Simultaneous, Vista – MPX Varian, Mulgrave, Australia).	Assessment of compositional changes induced in the SBF solution during immersion of the three classes of glass-ceramics.
	Rietveld technique (MAUD program)	Determination of the relative content of the different phases and the corresponding average crystallite size.
6	X-ray diffraction analysis (**XRD**) (Philips PW 1830, Netherlands) using a Ni filtered Cu Kα radiation	Phase identification in bulk bioactive glass, hydroxyapatite, and composite samples produced by SPS.
	Optical microscopy (**OM**) (Nikon TMF, Japan)	Observation of cells morphology after direct/indirect contact with the glass/ceramic samples.
	Spectrophotometry (Multiscan RC by Thermolab system, Finland)	Evaluation of cell viability after exposure to the samples' eluates.
7	X-ray diffraction analysis (**XRD**) (Philips PW 1830, Netherlands) using a Ni filtered Cu Kα radiation	Compositional/structural character-rization of the initial powders and the surfaces of bulk FGM samples.
8	X-ray diffraction analysis (**XRD**) (BRUKER D8 Advanced diffractometer with a Cu Kα)	Phase identification of initial powders and bulk samples obtained after SPS.
	Fourier transform infrared vibrational spectrometry (**FTIR**) using KBr method (Nicolet 5700 spectrometer)	Evaluation of the composition of crystalline and amorphous samples, to assess, in particular, the incorporation of the carbonate ion group.

	OMNIC software (Thermo Fisher Scientific).	Analysis of FTIR spectra.
9	Scanning electron microscopy (**SEM**) (FE-SEM-EDS, Auriga 0750, Carl-Zeiss, Jena, Germany)	Observation of the microstructure and morphology of the different series of electrospun mats.
	Fiji 1.51s analysis software (NIH, Bethesda, MD, USA)	Evaluation of the average fiber diameter
	FTIR in attenuated total reflectance mode (**FTIR-ATR**) (IRAffinity-1S, Shimadzu, Japan)	Analysis of the polymeric electrospun mat composition (before and after immersion in SBF and PBS solutions).
	Uniaxial tensile strength (3366 Dual Column Tabletop Testing System, Instron®, Darmstadt, Germany).	Evaluation of Young's modulus, UTS, and failure strain of a set of fiber mats.
	Sessile drop method (DSA30, Krüss GmbH, Hamburg, Germany)	Measurement of wettability properties of the fibrous specimens.
	Fuorescence microscopy (**FLUO**) (Axio Scope A1, Zeiss)	Observation of cell morphology upon seeding.

References

[1] S. Weiner, H. Lowenstam, Organization of extracellularly mineralized tissues: A comparative study of biological crystal growt, Crit. Rev. Biochem. Mol. Biol. (1986). doi:10.3109/10409238609081998.

[2] H.C. Margolis, S.Y. Kwak, H. Yamazaki, Role of mineralization inhibitors in the regulation of hard tissue biomineralization: Relevance to initial enamel formation and maturation, Front. Physiol. (2014). doi:10.3389/fphys.2014.00339.

[3] C. Slater, "Atlas of Anatomy" - A M Gilroy, B R MacPherson, L M Ross (ISBN: 978-1-60406-745-3), South African Med. J. (2016). doi:10.7196/samj.6350.

[4] S.W. Jacob, Sobotta Atlas of Human Anatomy, JAMA J. Am. Med. Assoc. (2003). doi:10.1001/jama.282.19.1880.

[5] S. Marksjr, P. Odgren, Structure and Development of the Skeleton, in: Princ. Bone Biol., 2007. doi:10.1016/b978-012098652-1/50103-7.

[6] B. Clarke, Normal bone anatomy and physiology., Clin. J. Am. Soc. Nephrol. (2008). doi:10.2215/CJN.04151206.

[7] J. Sarko, Bone and mineral metabolism, Emerg. Med. Clin. North Am. (2005). doi:10.1016/j.emc.2005.03.017.

[8] H. Segawa, A. Hanazaki, K. ichi Miyamoto, Intracellular and extracellular functions of phosphorus compound in the body, Clin. Calcium. (2016).

[9] D.B. Burr, The anatomy and biology of the human skeleton, J. Hum. Evol. (2006). doi:10.1016/0047-2484(89)90056-0.

[10] F.F. Safadi, M.F. Barbe, S.M. Abdelmagid, M.C. Rico, R.A. Aswad, J. Litvin, S.N. Popoff, Bone structure, development and bone biology, in: Bone Pathol., 2009. doi:10.1007/978-1-59745-347-9_1.

[11] S.M. Ott, Cortical or Trabecular Bone: What's the Difference?, Am. J. Nephrol. (2018). doi:10.1159/000489672.

[12] P.A. Downey, M.I. Siegel, Bone biology and the clinical implications for osteoporosis, Phys. Ther. (2006). doi:10.1093/ptj/86.1.77.

[13] L.L. Hench, Bioceramics: From Concept to Clinic, J. Am. Ceram. Soc. (1991). doi:10.1111/j.1151-2916.1991.tb07132.x.

[14] D.T. Reilly, A.H. Burstein, V.H. Frankel, The elastic modulus for bone, J. Biomech. (1974). doi:10.1016/0021-9290(74)90018-9.

[15] S. Yang, K.-F. Leong, Z. Du, C.-K. Chua, The Design of Scaffolds for Use in

Tissue Engineering. Part I. Traditional Factors, Tissue Eng. (2002). doi:10.1089/107632701753337645.

[16] V.I. Sikavitsas, J.S. Temenoff, A.G. Mikos, Biomaterials and bone mechanotransduction, Biomaterials. (2001). doi:10.1016/S0142-9612(01)00002-3.

[17] S.C. Cowin, The mechanical properties of bone, Stud. Appl. Mech. (1981). doi:10.1016/B978-0-444-41979-8.50017-2.

[18] No Title, (n.d.). https://training.seer.cancer.gov/anatomy/skeletal/tissue.html.

[19] J.A. Buckwalter, M.J. Glimcher, R.R. Cooper, R. Recker, Bone biology. Part I: Structure, blood supply, cells, matrix, and mineralization, J. Bone Jt. Surg. - Ser. A. (1995). doi:10.2106/00004623-199508000-00019.

[20] A.G. Robling, A.B. Castillo, C.H. Turner, Biomedical and molecular regulation of bone remodeling, Annu. Rev. Biomed. Eng. (2006). doi:10.1146/annurev.bioeng.8.061505.095721.

[21] R. Florencio-Silva, G.R.D.S. Sasso, E. Sasso-Cerri, M.J. Simões, P.S. Cerri, Biology of Bone Tissue: Structure, Function, and Factors That Influence Bone Cells, Biomed Res. Int. (2015). doi:10.1155/2015/421746.

[22] M. Capulli, R. Paone, N. Rucci, Osteoblast and osteocyte: Games without frontiers, Arch. Biochem. Biophys. (2014). doi:10.1016/j.abb.2014.05.003.

[23] V. Everts, J.M. Delaissié, W. Korper, D.C. Jansen, W. Tigchelaar-Gutter, P. Saftig, W. Beertsen, The bone lining cell: Its role in cleaning Howship's lacunae and initiating bone formation, J. Bone Miner. Res. (2002). doi:10.1359/jbmr.2002.17.1.77.

[24] S.C. Miller, L. de Saint-Georges, B.M. Bowman, W.S. Jee, Bone lining cells: structure and function., Scanning Microsc. (1989).

[25] T.A. Franz-Odendaal, B.K. Hall, P.E. Witten, Buried alive: How osteoblasts become osteocytes, Dev. Dyn. (2006). doi:10.1002/dvdy.20603.

[26] G.Y. Rochefort, S. Pallu, C.L. Benhamou, Osteocyte: The unrecognized side of bone tissue, Osteoporos. Int. (2010). doi:10.1007/s00198-010-1194-5.

[27] X. Feng, J.M. McDonald, Disorders of Bone Remodeling, Annu. Rev. Pathol. Mech. Dis. (2011). doi:10.1146/annurev-pathol-011110-130203.

[28] J.F. Charles, A.O. Aliprantis, Osteoclasts: More than "bone eaters," Trends Mol. Med. (2014). doi:10.1016/j.molmed.2014.06.001.

[29] M.S. Rahman, N. Akhtar, H.M. Jamil, R.S. Banik, S.M. Asaduzzaman, TGF-β/BMP signaling and other molecular events: Regulation of osteoblastogenesis and bone formation, Bone Res. (2015). doi:10.1038/boneres.2015.5.

[30] S.L. Teitelbaum, Bone resorption by osteoclasts, Science (80-.). (2000).

doi:10.1126/science.289.5484.1504.

[31] K. Tanaka-Kamioka, H. Kamioka, H. Ris, S.S. Lim, Osteocyte shape is dependent on actin filaments and osteocyte processes are unique actin-rich projections, J. Bone Miner. Res. (1998). doi:10.1359/jbmr.1998.13.10.1555.

[32] A.L. Boskey, Bone composition: relationship to bone fragility and anti-osteoporotic drug effects, Bonekey Rep. (2015). doi:10.1038/bonekey.2015.79.

[33] M. Centrella, T.L. McCarthy, M.C. Horowitz, J.M. Wozney, Transforming growth factor-β gene family members and bone, Endocr. Rev. (1994). doi:10.1210/edrv-15-1-27.

[34] J.I. Jones, D.R. Clemmons, Insulin-like growth factors and their binding proteins: Biological actions, Endocr. Rev. (1995). doi:10.1210/edrv-16-1-3.

[35] B. Bragdon, O. Moseychuk, S. Saldanha, D. King, J. Julian, A. Nohe, Bone Morphogenetic Proteins: A critical review, Cell. Signal. (2011). doi:10.1016/j.cellsig.2010.10.003.

[36] A. Aszódi, R. Fässler, J. F. Bateman, R. Boot-Handford, E. Gustafsson, Mammalian Skeletogenesis and Extracellular Matrix. What can We Learn from Knockout Mice?, Cell Struct. Funct. (2002). doi:10.1247/csf.25.73.

[37] M.J. Glimcher, Mechanism of calcification: Role of collagen fibrils and collagen phosphoprotein complexes in vitro and in vivo, Anat. Rec. (1989). doi:10.1002/ar.1092240205.

[38] F. Nudelman, K. Pieterse, A. George, P.H.H. Bomans, H. Friedrich, L.J. Brylka, P.A.J. Hilbers, G. De With, N.A.J.M. Sommerdijk, The role of collagen in bone apatite formation in the presence of hydroxyapatite nucleation inhibitors, Nat. Mater. (2010). doi:10.1038/nmat2875.

[39] F.H. Silver, W.J. Landis, Deposition of apatite in mineralizing vertebrate extracellular matrices: A model of possible nucleation sites on type I collagen, Connect. Tissue Res. (2011). doi:10.3109/03008207.2010.551567.

[40] Y. Wang, T. Azaïs, M. Robin, A. Vallée, C. Catania, P. Legriel, G. Pehau-Arnaudet, F. Babonneau, M.M. Giraud-Guille, N. Nassif, The predominant role of collagen in the nucleation, growth, structure and orientation of bone apatite, Nat. Mater. (2012). doi:10.1038/nmat3362.

[41] E. Canalis, Growth factor control of bone mass, J. Cell. Biochem. (2009). doi:10.1002/jcb.22322.

[42] P. Ducy, C. Desbois, B. Boyce, G. Pinero, B. Story, C. Dunstan, E. Smith, J. Bonadio, S. Goldstein, C. Gundberg, A. Bradley, G. Karsenty, Increased bone formation in osteocalcin-deficient mice, Nature. (1996). doi:10.1038/382448a0.

[43] A. Gericke, C. Qin, L. Spevak, Y. Fujimoto, W.T. Butler, E.S. Sørensen, A.L. Boskey, Importance of phosphorylation for osteopontin regulation of

biomineralization, Calcif. Tissue Int. (2005). doi:10.1007/s00223-004-1288-1.

[44] C. Qin, O. Baba, W.T. Butler, Post-translational modifications of SIBLING proteins and their roles in osteogenesis and dentinogenesis, Crit. Rev. Oral Biol. Med. (2004). doi:10.1177/154411130401500302.

[45] W. De Jong, Le substance minerale dans le os, Recl. Trav. Chim. Pays-Bas. (1926).

[46] R.A. Robinson, M.L. Watson, Collagen-crystal relationships in bone as seen in the electron microscope., Anat. Rec. (1952). doi:10.1002/ar.1091140302.

[47] S.J. Eppell, W. Tong, J. Lawrence Katz, L. Kuhn, M.J. Glimcher, Shape and size of isolated bone mineralites measured using atomic force microscopy, J. Orthop. Res. (2001). doi:10.1016/S0736-0266(01)00034-1.

[48] W. Tong, M.J. Glimcher, J.L. Katz, L. Kuhn, S.J. Eppell, Size and shape of mineralites in young bovine bone measured by atomic force microscopy, in: Calcif. Tissue Int., 2003. doi:10.1007/s00223-002-1077-7.

[49] R. Legros, N. Balmain, G. Bonel, Age-related changes in mineral of rat and bovine cortical bone, Calcif. Tissue Int. 41 (1987) 137–144. doi:10.1007/BF02563793.

[50] Y. Wu, L.T. Kuhn, M.J. Glimcher, C. Rey, C.-K. Loong, C. Combes, S.-H. Chen, Evidence of hydroxyl-ion deficiency in bone apatites: an inelastic neutron-scattering study, Bone. (2002). doi:10.1016/s8756-3282(00)00273-8.

[51] C. Rey, J.L. Miquel, L. Facchini, A.P. Legrand, M.J. Glimcher, Hydroxyl groups in bone mineral, Bone. (1995). doi:10.1016/8756-3282(95)00101-I.

[52] J.D. Pasteris, B. Wopenka, J.J. Freeman, K. Rogers, E. Valsami-Jones, J.A.M. Van Der Houwen, M.J. Silva, Lack of OH in nanocrystalline apatite as a function of degree of atomic order: Implications for bone and biomaterials, Biomaterials. (2004). doi:10.1016/S0142-9612(03)00487-3.

[53] R.M. Biltz, E.D. Pellegrino, The Nature of Bone Carbonate, Clin. Orthop. Relat. Res. (2006). doi:10.1097/00003086-197711000-00040.

[54] R.Z. LeGeros, Biological and synthetic apatites, in: B.C. Paul W. Brown (Ed.), Hydroxyapatite Relat. Mater., 1st edn, Taylor & Francis Group, Boca Raton, 2017: pp. 3–28. doi:10.1201/9780203751367.

[55] J.C. Elliott, D.W. Holcomb, R.A. Young, Infrared determination of the degree of substitution of hydroxyl by carbonate ions in human dental enamel, Calcif. Tissue Int. 37 (1985) 372–375. doi:10.1007/BF02553704.

[56] M. Vallet-Regí, J.M. González-Calbet, Calcium phosphates as substitution of bone tissues, Prog. Solid State Chem. 32 (2004) 1–31. doi:10.1016/j.progsolidstchem.2004.07.001.

[57] C. Rey, B. Collins, T. Goehl, I.R. Dickson, M.J. Glimcher, The carbonate environment in bone mineral: A resolution-enhanced fourier transform infrared spectroscopy study, Calcif. Tissue Int. (1989). doi:10.1007/BF02556059.

[58] C. Rey, V. Renugopalakrishman, B. Collins, M.J. Glimcher, Fourier transform infrared spectroscopic study of the carbonate ions in bone mineral during aging, Calcif. Tissue Int. 49 (1991) 251–258. doi:10.1007/BF02556214.

[59] J.C. Heughebaert, G. Montel, Conversion of amorphous tricalcium phosphate into apatitic tricalcium phosphate, Calcif. Tissue Int. (1982).

[60] M. Mathew, W.E. Brown, L.W. Schroeder, B. Dickens, Crystal structure of octacalcium bis(hydrogenphosphate) tetrakis(phosphate)pentahydrate, Ca8(HP04)2(PO4)4·5H2O, J. Crystallogr. Spectrosc. Res. (1988). doi:10.1007/BF01194315.

[61] L.D. Mkukuma, J.M.S. Skakle, I.R. Gibson, C.T. Imrie, R.M. Aspden, D.W.L. Hukins, Effect of the proportion of organic material in bone on thermal decomposition of bone mineral: An investigation of a variety of bones from different species using thermogravimetric analysis coupled to mass spectrometry, high-temperature X-ray diffraction, Calcif. Tissue Int. (2004). doi:10.1007/s00223-004-0199-5.

[62] S. V Dorozhkin, Calcium Orthophosphates: Occurrence, Properties and Major Applications, Bioceram. Dev. Appl. 4 (2016) 1–20. doi:10.4172/2090-5025.1000081.

[63] W.F. Neuman, M.W. Neuman, The nature of the mineral phase of bone, Chem. Rev. (1953). doi:10.1021/cr60164a001.

[64] M.W. Neuman, W.F. Neuman, On the measurement of water compartments, pH, and gradients in calvaria, Calcif. Tissue Int. (1980). doi:10.1007/BF02407174.

[65] W.F. Neuman, B.J. Bareham, Further studies on the nature of fluid compartmentalization in chick calvaria, Calcif. Tissue Res. (1975). doi:10.1007/BF02546688.

[66] S. Wallach, Availability of body magnesium during magnesium deficiency., Magnesium. (1987).

[67] R.K. Rude, Chapter 24 - Magnesium Homeostasis, in: Princ. Bone Biol., 2008. doi:http://dx.doi.org/10.1016/B978-0-12-373884-4.00043-4.

[68] Y. Wu, M.J. Glimcher, C. Rey, J.L. Ackerman, A unique protonated phosphate group in bone mineral not present in synthetic calcium phosphates. Identification by phosphorus-31 solid state NMR spectroscopy, J. Mol. Biol. (1994). doi:10.1006/jmbi.1994.1740.

[69] C. Rey, M. Shimizu, B. Collins, M.J. Glimcher, Resolution-enhanced fourier

transform infrared spectroscopy study of the environment of phosphate ion in the early deposits of a solid phase of calcium phosphate in bone and enamel and their evolution with age: 2. Investigations in the v3 PO4 domain, Calcif. Tissue Int. (1991). doi:10.1007/BF02555847.

[70] D. Eichert, M. Salomé, M. Banu, J. Susini, C. Rey, Preliminary characterization of calcium chemical environment in apatitic and non-apatitic calcium phosphates of biological interest by X-ray absorption spectroscopy, Spectrochim. Acta - Part B At. Spectrosc. (2005). doi:10.1016/j.sab.2005.05.012.

[71] Y. Wu, M.J. Glimcher, H.-M. Kim, C. Rey, J.L. Ackerman, A. Barroug, Nuclear Magnetic Resonance Spin-Spin Relaxation of the Crystals of Bone, Dental Enamel, and Synthetic Hydroxyapatites, J. Bone Miner. Res. (2006). doi:10.1359/jbmr.2002.17.3.472.

[72] S. Cazalbou, C. Combes, D. Eichert, C. Rey, M.J. Glimcher, Poorly crystalline apatites: Evolution and maturation in vitro and in vivo, J. Bone Miner. Metab. (2004). doi:10.1007/s00774-004-0488-0.

[73] C. Rey, C. Combes, Physical Chemistry of Biological Apatites, in: M.P.G. Conrado Aparicio (Ed.), Biominer. Biomater. Fundam. Appl., 1st edn, Woodhead Publishing, Sawston, Cambridge, 2015: pp. 95–128. doi:10.1016/B978-1-78242-338-6.00004-1.

[74] C. Jäger, T. Welzel, W. Meyer-Zaika, M. Epple, A solid-state NMR investigation of the structure of nanocrystalline hydroxyapatite, Magn. Reson. Chem. (2006). doi:10.1002/mrc.1774.

[75] Y. Wang, S. Von Euw, F.M. Fernandes, S. Cassaignon, M. Selmane, G. Laurent, G. Pehau-Arnaudet, C. Coelho, L. Bonhomme-Coury, M.M. Giraud-Guille, F. Babonneau, T. Azaïs, N. Nassif, Water-mediated structuring of bone apatite, Nat. Mater. 12 (2013) 1144–1153. doi:10.1038/nmat3787.

[76] S.J. Huang, Y.L. Tsai, Y.L. Lee, C.P. Lin, J.C.C. Chan, Structural model of rat dentin revisited, Chem. Mater. (2009). doi:10.1021/cm9006537.

[77] Y.H. Tseng, Y.L. Tsai, T.W.T. Tim, C.P. Lin, S.H. Huang, C.Y. Mou, J.C.C. Chan, Double-quantum filtered heteronuclear correlation spectroscopy under magic angle spinning, Solid State Nucl. Magn. Reson. (2007). doi:10.1016/j.ssnmr.2007.01.001.

[78] Y.H. Tseng, Y.L. Tsai, T.W.T. Tsai, J.C.H. Chao, C.P. Lin, S.H. Huang, C.Y. Mou, J.C.C. Chan, Characterization of the phosphate units in rat dentin by solid-state NMR spectroscopy, Chem. Mater. (2007). doi:10.1021/cm070531n.

[79] M.R. Allen, D.B. Burr, Bone Modeling and Remodeling, in: Basic Appl. Bone Biol., 2013. doi:10.1016/B978-0-12-416015-6.00004-6.

[80] D.J. Hadjidakis, I.I. Androulakis, Bone remodelinHadjidakis DJ, Androulakis II (2006) Bone remodeling. Annals of the New York Academy of Sciences 1092:385–396 Available at: http://www.ncbi.nlm.nih.gov/pubmed/17308163 [Accessed November 4, 2012].g., Ann. N. Y. Acad. Sci. (2006). doi:10.1196/annals.1365.035.

[81] Y. Tanaka, S. Nakayamada, Y. Okada, Osteoblasts and Osteoclasts in Bone Remodeling and Inflammation, Curr. Drug Target -Inflammation Allergy. (2005). doi:10.2174/1568010054022015.

[82] L.J. Raggatt, N.C. Partridge, Cellular and molecular mechanisms of bone remodeling, J. Biol. Chem. (2010). doi:10.1074/jbc.R109.041087.

[83] J.A. Siddiqui, N.C. Partridge, Physiological Bone Remodeling: Systemic Regulation and Growth Factor Involvement, Physiology. (2016). doi:10.1152/physiol.00061.2014.

[84] M. Peacock, Calcium metabolism in health and disease, Clin. J. Am. Soc. Nephrol. (2010). doi:10.2215/CJN.05910809.

[85] M.J. Glimcher, Bone: Nature of the Calcium Phosphate Crystals and Cellular, Structural, and Physical Chemical Mechanisms in Their Formation, Rev. Mineral. Geochemistry. (2006). doi:10.2138/rmg.2006.64.8.

[86] No Title, (n.d.) https://www.britannica.com/science/bone-remodeling.

[87] A. Schindeler, M.M. McDonald, P. Bokko, D.G. Little, Bone remodeling during fracture repair: The cellular picture, Semin. Cell Dev. Biol. (2008). doi:10.1016/j.semcdb.2008.07.004.

[88] No Title, (n.d.) http://msgallagherlhs.weebly.com/fracture--repair.

[89] E.H. Schemitsch, Size Matters: Defining Critical in Bone Defect Size!, J. Orthop. Trauma. (2017). doi:10.1097/BOT.0000000000000978.

[90] E. Roddy, M.R. DeBaun, A. Daoud-Gray, Y.P. Yang, M.J. Gardner, Treatment of critical-sized bone defects: clinical and tissue engineering perspectives, Eur. J. Orthop. Surg. Traumatol. (2018). doi:10.1007/s00590-017-2063-0.

[91] C. Bosch, B. Melsen, K. Vargervik, Importance of the critical-size bone defect in testing bone-regenerating materials, J. Craniofac. Surg. (1998). doi:10.1097/00001665-199807000-00004.

[92] Y. Li, S.K. Chen, L. Li, L. Qin, X.L. Wang, Y.X. Lai, Bone defect animal models for testing efficacy of bone substitute biomaterials, J. Orthop. Transl. (2015). doi:10.1016/j.jot.2015.05.002.

[93] F. Loi, L.A. Córdova, J. Pajarinen, T. hua Lin, Z. Yao, S.B. Goodman, Inflammation, fracture and bone repair, Bone. (2016). doi:10.1016/j.bone.2016.02.020.

[94] A. Wiese, H.C. Pape, Bone Defects Caused by High-energy Injuries, Bone Loss, Infected Nonunions, and Nonunions, Orthop. Clin. North Am. (2010). doi:10.1016/j.ocl.2009.07.003.

[95] B. a. Allo, D.O. Costa, S.J. Dixon, K. Mequanint, A.S. Rizkalla, Bioactive and Biodegradable Nanocomposites and Hybrid Biomaterials for Bone Regeneration, J. Funct. Biomater. (2012). doi:10.3390/jfb3020432.

[96] J.A. Planell, S.M. Best, D. Lacroix, A. Merolli, Bone repair biomaterials, 2009. doi:10.1533/9781845696610.

[97] V. Campana, G. Milano, E. Pagano, M. Barba, C. Cicione, G. Salonna, W. Lattanzi, G. Logroscino, Bone substitutes in orthopaedic surgery: from basic science to clinical practice, J. Mater. Sci. Mater. Med. (2014). doi:10.1007/s10856-014-5240-2.

[98] R. Langer, J.P. Vacanti, - 1. ARTICLES Tissue Engineering, Science (80-.). (1993). doi:10.1126/science.8493529.

[99] W.G. De Long, T.A. Einhorn, K. Koval, M. McKee, W. Smith, R. Sanders, T. Watson, Bone grafts and bone graft substitutes in orthopaedic trauma surgery: A critical analysis, J. Bone Jt. Surg. - Ser. A. (2007). doi:10.2106/00004623-200703000-00026.

[100] A.S. Brydone, D. Meek, S. MacLaine, Bone grafting, orthopaedic biomaterials, and the clinical need for bone engineering, in: Proc. Inst. Mech. Eng. Part H J. Eng. Med., 2010. doi:10.1243/09544119JEIM770.

[101] H.C. Pape, A. Evans, P. Kobbe, Autologous bone graft: Properties and techniques, J. Orthop. Trauma. (2010). doi:10.1097/BOT.0b013e3181cec4a1.

[102] G. Kumar, B. Narayan, Morbidity at bone graft donor sites, in: Class. Pap. Orthop., 2014. doi:10.1007/978-1-4471-5451-8_132.

[103] J. Baumhauer, M.S. Pinzur, R. Donahue, W. Beasley, C. Digiovanni, Site selection and pain outcome after autologous bone graft harvest, Foot Ankle Int. (2014). doi:10.1177/1071100713511434.

[104] G.F. Rogers, A.K. Greene, Autogenous bone graft: Basic science and clinical implications, J. Craniofac. Surg. (2012). doi:10.1097/SCS.0b013e318241dcba.

[105] E. Chiarello, M. Cadossi, G. Tedesco, P. Capra, C. Calamelli, A. Shehu, S. Giannini, Autograft, allograft and bone substitutes in reconstructive orthopedic surgery, in: Aging Clin. Exp. Res., 2013. doi:10.1007/s40520-013-0088-8.

[106] F.G. Lakkis, R.I. Lechler, Origin and biology of the allogeneic response, Cold Spring Harb. Perspect. Med. (2013). doi:10.1101/cshperspect.a014993.

[107] A.S. Herford, E. Stoffella, C.M. Stanford, Bone Grafts and Bone Substitute Materials, in: Princ. Pract. Single Implant Restorations, 2013. doi:10.1016/b978-1-4557-4476-3.00005-6.

[108] D.F. Williams, On the mechanisms of biocompatibility, Biomaterials. (2008). doi:10.1016/j.biomaterials.2008.04.023.

[109] I. Kulinets, Biomaterials and their applications in medicine, in: Regul. Aff. Biomater. Med. Devices, 2014. doi:10.1533/9780857099204.1.

[110] A.A. Kulkarni, P.S. Rao, Synthesis of polymeric nanomaterials for biomedical applications, in: Nanomater. Tissue Eng. Fabr. Appl., 2013. doi:10.1533/9780857097231.1.27.

[111] A.M.C. Barradas, H. Yuan, C.A. van Blitterswijk, P. Habibovic, Osteoinductive biomaterials: current knowledge of properties, experimental models and biological mechanisms., Eur. Cell. Mater. (2011). doi:10.22203/eCM.v021a31.

[112] M. Łączka, K. Cholewa-Kowalska, A.M. Osyczka, Bioactivity and osteoinductivity of glasses and glassceramics and their material determinants, Ceram. Int. (2016). doi:10.1016/j.ceramint.2016.06.077.

[113] T. Albrektsson, C. Johansson, Osteoinduction, osteoconduction and osseointegration, Eur. Spine J. (2001). doi:10.1007/s005860100282.

[114] A.J. Wagoner Johnson, B.A. Herschler, A review of the mechanical behavior of CaP and CaP/polymer composites for applications in bone replacement and repair, Acta Biomater. (2011). doi:10.1016/j.actbio.2010.07.012.

[115] G. Hannink, J.J.C. Arts, Bioresorbability, porosity and mechanical strength of bone substitutes: What is optimal for bone regeneration?, Injury. (2011). doi:10.1016/j.injury.2011.06.008.

[116] V. Karageorgiou, D. Kaplan, Porosity of 3D biomaterial scaffolds and osteogenesis, Biomaterials. (2005). doi:10.1016/j.biomaterials.2005.02.002.

[117] E. Tsuruga, H. Takita, H. Itoh, Y. Wakisaka, Y. Kuboki, Pore size of porous hydroxyapatite as the cell-substratum controls BMP-induced osteogenesis, J. Biochem. (1997). doi:10.1093/oxfordjournals.jbchem.a021589.

[118] I.A. I., Y.H. O., E. Clifford, K.K. H., A.H. T., Pore diameter of more than 100 μm is not requisite for bone ingrowth in rabbits, J. Biomed. Mater. Res. (2002). doi:10.1002/jbm.1069.

[119] S. Mitragotri, J. Lahann, Physical approaches to biomaterial design, Nat. Mater. (2009). doi:10.1038/nmat2344.

[120] K. Anselme, A. Ponche, M. Bigerelle, Relative influence of surface topography and surface chemistry on cell response to bone implant materials. Part 2: Biological aspects, in: Proc. Inst. Mech. Eng. Part H J. Eng. Med., 2010. doi:10.1243/09544119JEIM901.

[121] Z.Y. Qiu, C. Chen, X.M. Wang, I.S. Lee, Advances in the surface modification techniques of bone-related implants for last 10 years, Regen. Biomater. (2014). doi:10.1093/rb/rbu007.

[122] B. Thavornyutikarn, N. Chantarapanich, K. Sitthiseripratip, G.A. Thouas, Q. Chen, Bone tissue engineering scaffolding: computer-aided scaffolding techniques, 2014. doi:10.1007/s40204-014-0026-7.

[123] Nanostructured Materials and Coatings for Biomedical and Sensor Applications, 2011. doi:10.1007/978-94-010-0157-1.

[124] S. V. Dorozhkin, Calcium orthophosphate bioceramics, Ceram. Int. (2015). doi:10.1016/j.ceramint.2015.08.004.

[125] S. Ramakrishna, M. Ramalingam, T. Kumar, W. Soboyejo, Overview of Biomaterials, in: Biomaterials, 2013. doi:10.1201/b15739-2.

[126] D.R. Haynes, S.D. Rogers, S. Hay, M.J. Pearcy, D.W. Howie, The differences in toxicity and release of bone-resorbing mediators induced by titanium and cobalt-chromium-alloy wear particles, J. Bone Jt. Surg. - Ser. A. (1993). doi:10.2106/00004623-199306000-00004.

[127] C.M.J.M. Pypen, K. Dessein, J.A. Helsen, M. Gomes, H. Leenders, J.D. De Bruijn, Comparison of the cytotoxicity of molybdenum as powder and as alloying element in a niobium-molybdenum alloy, J. Mater. Sci. Mater. Med. (1998). doi:10.1023/A:1008919422520.

[128] S. Bose, M. Roy, A. Bandyopadhyay, Recent advances in bone tissue engineering scaffolds, Trends Biotechnol. (2012). doi:10.1016/j.tibtech.2012.07.005.

[129] W. He, R. Benson, Polymeric Biomaterials, in: Appl. Plast. Eng. Handb. Process. Mater. Appl. Second Ed., 2016. doi:10.1016/B978-0-323-39040-8.00008-0.

[130] R. Narayan, Biomedical materials, 2009. doi:10.1007/978-0-387-84872-3.

[131] M. Vallet-Regí, Evolution of bioceramics within the field of biomaterials, Comptes Rendus Chim. (2010). doi:10.1016/j.crci.2009.03.004.

[132] M. Vallet-Regí, Bioceramics: Where Do We Come from and which are the Future Expectations, Key Eng. Mater. (2009). doi:10.4028/www.scientific.net/kem.377.1.

[133] J. Park, Bioceramics: Properties, characterizations, and applications, 2009. doi:10.1007/978-0-387-09545-5.

[134] S.M. Best, A.E. Porter, E.S. Thian, J. Huang, Bioceramics: Past, present and for the future, J. Eur. Ceram. Soc. (2008). doi:10.1016/j.jeurceramsoc.2007.12.001.

[135] C. Piconi, A.A. Porporati, Bioinert ceramics: Zirconia and alumina, in: Handb. Bioceram. Biocomposites, 2016. doi:10.1007/978-3-319-12460-5_4.

[136] C. Piconi, S.G. Condo, T. Kosmač, Alumina- and Zirconia-based Ceramics for Load-bearing Applications, in: Adv. Ceram. Dent., 2014. doi:10.1016/B978-0-

12-394619-5.00011-0.

[137] D.F. Williams, On the nature of biomaterials, Biomaterials. (2009). doi:10.1016/j.biomaterials.2009.07.027.

[138] W. Cao, L.L. Hench, Bioactive materials, Ceram. Int. (1996). doi:10.1016/0272-8842(95)00126-3.

[139] S. V. Dorozhkin, Calcium orthophosphates as bioceramics: State of the art, J. Funct. Biomater. (2010). doi:10.3390/jfb1010022.

[140] S. V. Dorozhkin, Calcium orthophosphate-based bioceramics, Materials (Basel). (2013). doi:10.3390/ma6093840.

[141] S. Samavedi, A.R. Whittington, A.S. Goldstein, Calcium phosphate ceramics in bone tissue engineering: A review of properties and their influence on cell behavior, Acta Biomater. 9 (2013) 8037–8045. doi:10.1016/j.actbio.2013.06.014.

[142] S. Pokhrel, Hydroxyapatite: Preparation, Properties and Its Biomedical Applications, Adv. Chem. Eng. Sci. (2018). doi:10.4236/aces.2018.84016.

[143] A. Sobczak-Kupiec, D. Malina, R. Kijkowska, Z. Wzorek, Comparative study of hydroxyapatite prepared by the authors with selected commercially available ceramics, Dig. J. Nanomater. Biostructures. (2012).

[144] T.J. White, D. ZhiLi, Structural derivation and crystal chemistry of apatites, Acta Crystallogr. Sect. B Struct. Sci. (2003). doi:10.1107/S0108768102019894.

[145] P. Rulis, L. Ouyang, W.Y. Ching, Electronic structure and bonding in calcium apatite crystals: Hydroxyapatite, fluorapatite, chlorapatite, and bromapatite, Phys. Rev. B - Condens. Matter Mater. Phys. (2004). doi:10.1103/PhysRevB.70.155104.

[146] R. Snyders, D. Music, D. Sigumonrong, B. Schelnberger, J. Jensen, J.M. Schneider, Experimental and ab initio study of the mechanical properties of hydroxyapatite, Appl. Phys. Lett. (2007). doi:10.1063/1.2738386.

[147] Y. Cai, R. Tang, Calcium phosphate nanoparticles in biomineralization and biomaterials, J. Mater. Chem. (2008). doi:10.1039/b805407j.

[148] K. Lin, J. Chang, Structure and properties of hydroxyapatite for biomedical applications, in: Hydroxyapatite Biomed. Appl., 2015. doi:10.1016/B9781782420330000001-8.

[149] A.L. Giraldo-Betancur, D.G. Espinosa-Arbelaez, A. Del Real-López, B.M. Millan-Malo, E.M. Rivera-Muñoz, E. Gutierrez-Cortez, P. Pineda-Gomez, S. Jimenez-Sandoval, M.E. Rodriguez-García, Comparison of physicochemical properties of bio and commercial hydroxyapatite, Curr. Appl. Phys. (2013). doi:10.1016/j.cap.2013.04.019.

[150] M. Bohner, J. Lemaitre, Can bioactivity be tested in vitro with SBF solution?, Biomaterials. (2009). doi:10.1016/j.biomaterials.2009.01.008.

[151] S. Bertazzo, W.F. Zambuzzi, D.D.P. Campos, T.L. Ogeda, C. V. Ferreira, C.A. Bertran, Hydroxyapatite surface solubility and effect on cell adhesion, Colloids Surfaces B Biointerfaces. (2010). doi:10.1016/j.colsurfb.2010.02.027.

[152] S.J. Kalita, A. Bhardwaj, H.A. Bhatt, Nanocrystalline calcium phosphate ceramics in biomedical engineering, Mater. Sci. Eng. C. (2007). doi:10.1016/j.msec.2006.05.018.

[153] H. Zhu, D. Guo, L. Sun, H. Li, D.A.H. Hanaor, F. Schmidt, K. Xu, Nanostructural insights into the dissolution behavior of Sr-doped hydroxyapatite, J. Eur. Ceram. Soc. (2018). doi:10.1016/j.jeurceramsoc.2018.07.056.

[154] K. Lin, L. Chen, J. Chang, Fabrication of dense hydroxyapatite nanobioceramics with enhanced mechanical properties via two-step sintering process, Int. J. Appl. Ceram. Technol. (2012). doi:10.1111/j.1744-7402.2011.02654.x.

[155] W. Suchanek, M. Yoshimura, Processing and properties of hydroxyapatite-based biomaterials for use as hard tissue replacement implants, J. Mater. Res. (1998). doi:10.1557/JMR.1998.0015.

[156] S. V. Dorozhkin, Calcium orthophosphates in dentistry, J. Mater. Sci. Mater. Med. (2013). doi:10.1007/s10856-013-4898-1.

[157] L. Sun, C.C. Berndt, K.A. Gross, A. Kucuk, Material fundamentals and clinical performance of plasma-sprayed hydroxyapatite coatings: A review, J. Biomed. Mater. Res. (2001). doi:10.1002/jbm.1056.

[158] S. V. Dorozhkin, Calcium orthophosphate deposits: Preparation, properties and biomedical applications, Mater. Sci. Eng. C. (2015). doi:10.1016/j.msec.2015.05.033.

[159] Y.D. Park, S.H. Jeong, S.O. Jang, K.N. Kim, B.I. Kim, H.K. Kwon, Tooth Whitening Effect of Toothpastes Containing Nano-Hydroxyapatite, Key Eng. Mater. (2009). doi:10.4028/www.scientific.net/kem.309-311.541.

[160] M. Markovic, B.O. Fowler, M.S. Tung, Preparation and comprehensive characterization of a calcium hydroxyapatite reference material, J. Res. Natl. Inst. Stand. Technol. (2012). doi:10.6028/jres.109.042.

[161] A. Szcześ, L. Hołysz, E. Chibowski, Synthesis of hydroxyapatite for biomedical applications, Adv. Colloid Interface Sci. (2017). doi:10.1016/j.cis.2017.04.007.

[162] C. Rey, C. Combes, C. Drouet, M.J. Glimcher, Bone mineral: update on chemical composition and structure., Osteoporos. Int. 20 (2009) 1013–1021. doi:10.1007/s00198-009-0860-y.

[163] C. Drouet, F. Bosc, M. Banu, C. Largeot, C. Combes, G. Dechambre, C. Estournès, G. Raimbeaux, C. Rey, Nanocrystalline apatites: From powders to biomaterials, Powder Technol. 190 (2009) 118–122. doi:10.1016/j.powtec.2008.04.041.

[164] S. V. Dorozhkin, Calcium Orthophosphate-Based Bioceramics and Biocomposites, 2016. doi:10.1002/9783527699315.

[165] R.Z. LeGeros, Biodegradation and bioresorption of calcium phosphate ceramics, Clin. Mater. (1993). doi:10.1016/0267-6605(93)90049-D.

[166] D. Eichert, C. Drouet, H. Sfihi, C. Rey, C. Combes, Nanocrystalline apatite-based biomaterials : Synthesis , processing and characterization, in: Jason B. Kendall (Ed.), Biomater. Res. Adv., Nova Science Publishers, New York, 2007: pp. 93–143.

[167] C. Rey, A. Hina, A. Tofighi, M. Glimcher, Maturation of poorly crystalline apatites: Chemical and structural aspects in vivo and in vitro, CELLS Mater. (1995).

[168] M. Iafisco, J.M. Delgado-López, C. Drouet, Nanocrystalline Apatites: Synthesis, Physical-Chemical and Thermodynamic Characterization, Apatite Synth. Stuctural Charact. Biomed. Appl. (2014).

[169] N. Vandecandelaere, C. Rey, C. Drouet, Biomimetic apatite-based biomaterials: On the critical impact of synthesis and post-synthesis parameters, J. Mater. Sci. Mater. Med. (2012). doi:10.1007/s10856-012-4719-y.

[170] B. Bourgeois, O. Laboux, L. Obadia, O. Gauthier, E. Betti, E. Aguado, G. Daculsi, J.M. Bouler, Calcium-deficient apatite: A first in vivo study concerning bone ingrowth, J. Biomed. Mater. Res. - Part A. (2003). doi:10.1002/jbm.a.10518.

[171] E.D. Eanes, Amorphous Calcium Phosphate: Thermodynamic and Kinetic Considerations, in: Calcium Phosphates Biol. Ind. Syst., 2011. doi:10.1007/978-1-4615-5517-9_2.

[172] F. Betts, A.S. Posner, An X-ray radial distribution study of amorphous calcium phosphate, Mater. Res. Bull. 9 (1974) 353–360. doi:10.1016/0025-5408(74)90087-7.

[173] N.J. Crane, V. Popescu, M.D. Morris, P. Steenhuis, M.A. Ignelzi, Raman spectroscopic evidence for octacalcium phosphate and other transient mineral species deposited during intramembranous mineralization, Bone. (2006). doi:10.1016/j.bone.2006.02.059.

[174] E. Beniash, R.A. Metzler, R.S.K. Lam, P.U.P.A. Gilbert, Transient amorphous calcium phosphate in forming enamel, J. Struct. Biol. (2009). doi:10.1016/j.jsb.2009.02.001.

[175] J. Mahamid, A. Sharir, L. Addadi, S. Weiner, Amorphous calcium phosphate is a major component of the forming fin bones of zebrafish: Indications for an amorphous precursor phase, Proc. Natl. Acad. Sci. (2008). doi:10.1073/pnas.0803354105.

[176] C. Combes, C. Rey, Amorphous calcium phosphates: Synthesis, properties and uses in biomaterials, Acta Biomater. (2010). doi:10.1016/j.actbio.2010.02.017.

[177] J.C. Heughebaert, Contribution à l'étude de l'évolution des orthophosphates de calcium précipités amorphes en orthophosphates apatitiques, Institut National Polytechnique de Toulouse, 1977.

[178] B.D. Ratner, A.S. Hoffman, F.J. Schoen, J.E. Lemons, Biomaterials Science: An Introduction to Materials: Third Edition, 2013. doi:10.1016/B978-0-08-087780-8.00148-0.

[179] J.R. Jones, Review of bioactive glass and glass: From Hench to hybrids, Acta Biomater. (2012). doi:10.1016/j.actbio.2012.08.023.

[180] L.L. Hench, The story of Bioglass®, in: J. Mater. Sci. Mater. Med., 2006. doi:10.1007/s10856-006-0432-z.

[181] L.L. Hench, Opening paper 2015- some comments on bioglass: Four eras of discovery and development, Biomed. Glas. (2015). doi:10.1515/bglass-2015-0001.

[182] L.L. Hench, J.R. Jones, Bioactive Glasses: Frontiers and Challenges, Front. Bioeng. Biotechnol. (2015). doi:10.3389/fbioe.2015.00194.

[183] A. Hoppe, V. Mouriño, A.R. Boccaccini, Therapeutic inorganic ions in bioactive glasses to enhance bone formation and beyond, Biomater. Sci. (2013). doi:10.1039/c2bm00116k.

[184] V. Krishnan, T. Lakshmi, Bioglass: A novel biocompatible innovation, J. Adv. Pharm. Technol. Res. (2014). doi:10.4103/2231-4040.111523.

[185] M. Brink, The influence of alkali and alkaline earths on the working range for bioactive glasses, J. Biomed. Mater. Res. (1997). doi:10.1002/(SICI)1097-4636(199707)36:1<109::AID-JBM13>3.0.CO;2-D.

[186] W. Huang, M.N. Rahaman, D.E. Day, Y. Li, Mechanisms for converting bioactive silicate, borate, and borosilicate glasses to hydroxyapatite in dilute phosphate solution, Phys. Chem. Glas. Eur. J. Glas. Sci. Technol. Part B. (2006).

[187] E.A. Abou Neel, D.M. Pickup, S.P. Valappil, R.J. Newport, J.C. Knowles, Bioactive functional materials: A perspective on phosphate-based glasses, J. Mater. Chem. (2009). doi:10.1039/b810675d.

[188] J.R. Jones, A.G. Clare, Bio-Glasses: An Introduction, 2012. doi:10.1002/9781118346457.

[189] R. Li, A.E. Clark, L.L. Hench, An investigation of bioactive glass powders by sol-gel processing., J. Appl. Biomater. (1991). doi:10.1002/jab.770020403.

[190] C.Z. Chen, X.G. Meng, H.J. Yu, H. Yang, T. He, D.G. Wang, S.G. Zhao, Preparation and Development of Bioglass by Sol-Gel Method, Key Eng. Mater. (2013). doi:10.4028/www.scientific.net/kem.591.34.

[191] Z. Hong, A. Liu, L. Chen, X. Chen, X. Jing, Preparation of bioactive glass ceramic nanoparticles by combination of sol-gel and coprecipitation method, J. Non. Cryst. Solids. (2009). doi:10.1016/j.jnoncrysol.2008.12.003.

[192] H. Oonishi, L.L. Hench, J. Wilson, F. Sugihara, E. Tsuji, M. Matsuura, S. Kin, T. Yamamoto, S. Mizokawa, Quantitative comparison of bone growth behavior in granules of Bioglass®, A-W glass-ceramic, and hydroxyapatite, J. Biomed. Mater. Res. (2000). doi:10.1002/(SICI)1097-4636(200007)51:1<37::AID-JBM6>3.0.CO;2-T.

[193] L. Gendreau, A.P.S. Barlow, S.C. Mason, Overview of the clinical evidence for the use of NovaMin in providing relief from the pain of dentin hypersensitivity, J. Clin. Dent. (2011).

[194] L.L. Hench, Chronology of Bioactive Glass Development and Clinical Applications, New J. Glas. Ceram. (2013). doi:10.4236/njgc.2013.32011.

[195] L. Lefebvre, L. Gremillard, J. Chevalier, R. Zenati, D. Bernache-Assolant, Sintering behaviour of 45S5 bioactive glass, Acta Biomater. (2008). doi:10.1016/j.actbio.2008.05.019.

[196] O.P. Filho, G.P. Latorre, L.L. Hench, Effect of crystallization on apatite-layer formation of bioactive glass 45S5, J. Biomed. Mater. Res. (1996). doi:10.1002/(SICI)1097-4636(199604)30:4<509::AID-JBM9>3.0.CO;2-T.

[197] A.R. Boccaccini, Q. Chen, L. Lefebvre, L. Gremillard, J. Chevalier, Sintering, crystallisation and biodegradation behaviour of Bioglass®-derived glass-ceramics, Faraday Discuss. (2007). doi:10.1039/b616539g.

[198] S. Montinaro, L. Desogus, R. Orrù, S. Garroni, F. Delogu, P.C. Ricci, G. Cao, A comprehensive study on compositional and structural changes in 45S5 bioglass products exposed to simulated body fluid, J. Am. Ceram. Soc. (2018). doi:10.1111/jace.15199.

[199] X. Chatzistavrou, P. Newby, A.R. Boccaccini, Bioactive glass and glass-ceramic scaffolds for bone tissue engineering, in: Bioact. Glas. Mater. Prop. Appl., 2011. doi:10.1016/B978-1-84569-768-6.50005-3.

[200] J. Will, L.-C. Gerhardt, A.R. Boccaccini, Bioactive Glass-Based Scaffolds for Bone Tissue Engineering, in: 2011. doi:10.1007/10_2011_106.

[201] T. Kokubo, Surface chemistry of bioactive glass-ceramics, J. Non. Cryst. Solids. (1990). doi:10.1016/0022-3093(90)90199-V.

[202] P. Valerio, M.M. Pereira, A.M. Goes, M.F. Leite, The effect of ionic products from bioactive glass dissolution on osteoblast proliferation and collagen production, Biomaterials. (2004). doi:10.1016/j.biomaterials.2003.09.086.

[203] H. Sun, C. Wu, K. Dai, J. Chang, T. Tang, Proliferation and osteoblastic differentiation of human bone marrow-derived stromal cells on akermanite-bioactive ceramics, Biomaterials. (2006). doi:10.1016/j.biomaterials.2006.07.027.

[204] T. Kokubo, H. Takadama, How useful is SBF in predicting in vivo bone bioactivity?, Biomaterials. (2006). doi:10.1016/j.biomaterials.2006.01.017.

[205] A.R.B. Gerhardt L. C., Bioactive glass and glass-ceramic scaffolds for bone tissue engineering, Materials (Basel). 3 (2010) 3867–3910. doi:10.1016/B978-1-84569-768-6.50005-3.

[206] C. Wu, Y. Xiao, Evaluation of the In Vitro Bioactivity of Bioceramics, Bone Tissue Regen. Insights. (2009). doi:10.4137/btri.s3188.

[207] C. Wu, Y. Ramaswamy, P. Boughton, H. Zreiqat, Improvement of mechanical and biological properties of porous CaSiO3 scaffolds by poly(d,l-lactic acid) modification, Acta Biomater. (2008). doi:10.1016/j.actbio.2007.08.010.

[208] S. Xu, K. Lin, Z. Wang, J. Chang, L. Wang, J. Lu, C. Ning, Reconstruction of calvarial defect of rabbits using porous calcium silicate bioactive ceramics, Biomaterials. (2008). doi:10.1016/j.biomaterials.2008.03.013.

[209] R.M. German, Sintering theory and practice, Theory Pract. (1996).

[210] S. V. Dorozhkin, Bioceramics of calcium orthophosphates, Biomaterials. 31 (2010) 1465–1485. doi:10.1016/j.biomaterials.2009.11.050.

[211] http://www.ltu.se/cms_fs/1.5838!/fafc1546.pdf, (n.d.).

[212] E. Champion, Sintering of calcium phosphate bioceramics, Acta Biomater. (2013). doi:10.1016/j.actbio.2012.11.029.

[213] O. Bretcanu, X. Chatzistavrou, K. Paraskevopoulos, R. Conradt, I. Thompson, A.R. Boccaccini, Sintering and crystallisation of 45S5 Bioglass® powder, J. Eur. Ceram. Soc. (2009). doi:10.1016/j.jeurceramsoc.2009.06.035.

[214] http://home.anadolu.edu.tr/~esuvaci/egitim/Sintering%20of%20Ceramics-Overview.pdf, (n.d.).

[215] G. Muralithran, S. Ramesh, The Effects of sintering temperature on the properties of hydroxyapatite, Ceram. Int. (2000). doi:10.1016/S0272-8842(99)00046-2.

[216] H. Palmour, Rate Controlled Sintering for Ceramics and Selected Powder Metals, in: Sci. Sinter., 2013. doi:10.1007/978-1-4899-0933-6_29.

[217] K. Maca, Microstructure evolution during pressureless sintering of bulk oxide

ceramics, Process. Appl. Ceram. (2013). doi:10.2298/pac0902013m.

[218] R. German, Sintering: From Empirical Observations to Scientific Principles, 2014. doi:10.1016/C2012-0-00717-X.

[219] S. Hashmi, Comprehensive Materials Processing, 2014. doi:10.1016/C2009-1-63473-0.

[220] N.L. Loh, K.Y. Sia, An overview of hot isostatic pressing, J. Mater. Process. Tech. (1992). doi:10.1016/0924-0136(92)90038-T.

[221] H. V. Atkinson, S. Davies, Fundamental aspects of hot isostatic pressing: An overview, Metall. Mater. Trans. A Phys. Metall. Mater. Sci. (2000). doi:10.1007/s11661-000-0078-2.

[222] L.F. Francis, Powder Processes, in: Mater. Process., 2016. doi:10.1016/B978-0-12-385132-1.00005-7.

[223] http://www.azom.com/article.aspx?ArticleID=5769, (n.d.).

[224] J. Guo, J. Li, H. Kou, Chemical preparation of advanced ceramic materials, in: Mod. Inorg. Synth. Chem., 2011. doi:10.1016/B978-0-444-53599-3.10019-8.

[225] R. Orrù, R. Licheri, A.M. Locci, A. Cincotti, G. Cao, Consolidation/synthesis of materials by electric current activated/assisted sintering, Mater. Sci. Eng. R Reports. 63 (2009) 127–287. doi:10.1016/j.mser.2008.09.003.

[226] J.L. Huang, P.K. Nayak, Strengthening alumina ceramic matrix nanocomposites using spark plasma sintering, in: Adv. Ceram. Matrix Compos. Second Ed., 2018. doi:10.1016/B978-0-08-102166-8.00010-4.

[227] Z.A. Munir, U. Anselmi-Tamburini, M. Ohyanagi, The effect of electric field and pressure on the synthesis and consolidation of materials: A review of the spark plasma sintering method, J. Mater. Sci. (2006). doi:10.1007/s10853-006-6555-2.

[228] A. Cuccu, S. Montinaro, R. Orrù, G. Cao, D. Bellucci, A. Sola, V. Cannillo, Consolidation of different hydroxyapatite powders by SPS: Optimization of the sintering conditions and characterization of the obtained bulk products, Ceram. Int. (2015). doi:10.1016/j.ceramint.2014.08.131.

[229] E. Jajarmi, L. Desogus, R. Orrù, S.A. Sajjadi, G. Cao, On the fabrication of functional graded 3Y-PSZ/316L materials by SPS: Process optimization and characterization of the obtained products, Ceram. Int. (2016). doi:10.1016/j.ceramint.2016.02.050.

[230] M. Radwan, M. Nygren, K. Flodström, S. Esmaelzadeh, Fabrication of crack-free SUS316L/Al2O3 functionally graded materials by spark plasma sintering, J. Mater. Sci. (2011). doi:10.1007/s10853-011-5536-2.

[231] G. Udupa, S.S. Rao, K.V. Gangadharan, Functionally Graded Composite

Materials: An Overview, Procedia Mater. Sci. (2014). doi:10.1016/j.mspro.2014.07.442.

[232] B. Kieback, A. Neubrand, H. Riedel, Processing techniques for functionally graded materials, Mater. Sci. Eng. A. (2003). doi:10.1016/S0921-5093(03)00578-1.

[233] N. Zhang, T. Khan, H. Guo, S. Shi, W. Zhong, W. Zhang, Functionally Graded Materials: An Overview of Stability, Buckling, and Free Vibration Analysis, Adv. Mater. Sci. Eng. (2019). doi:10.1155/2019/1354150.

[234] R.M. Mahamood, E.T.A. Member, M. Shukla, S. Pityana, Functionally Graded Material : An Overview, in: Proc. World Congr. Eng., 2012.

[235] F. Watari, M. Omori, T. Hirai, A. Yokoyama, H. Matsuno, M. Uo, R. Miyako, Y. Tamura, T. Kawasaki, Fabrication and Properties of FGM for Biomedical Application., J. Japan Soc. Powder Powder Metall. (2011). doi:10.2497/jjspm.47.1226.

[236] D. Lin, Q. Li, W. Li, M. Swain, Bone remodeling induced by dental implants of functionally graded materials, J. Biomed. Mater. Res. - Part B Appl. Biomater. (2010). doi:10.1002/jbm.b.31531.

[237] F. Watari, H. Kondo, S. Matsuo, R. Miyao, A. Yokoyama, M. Omori, T. Hirai, Y. Tamura, M. Uo, N. Ohara, T. Kawasaki, Development of Functionally Graded Implant and Dental Post for Bio-Medical Application, Mater. Sci. Forum. (2009). doi:10.4028/www.scientific.net/msf.423-425.321.

[238] A. Sola, D. Bellucci, V. Cannillo, Functionally graded materials for orthopedic applications – an update on design and manufacturing, Biotechnol. Adv. (2016). doi:10.1016/j.biotechadv.2015.12.013.

[239] F. Watari, A. Yokoyama, H. Matsuno, F. Saso, M. Uo, T. Kawasaki, Biocompatibility of Titanium/Hydroxyapatite and Titanium/Cobalt Functionally Graded Implants, Mater. Sci. Forum. (2009). doi:10.4028/www.scientific.net/msf.308-311.356.

[240] F. Watari, A. Yokoyama, F. Saso, M. Uo, T. Kawasaki, Fabrication and properties of functionally graded dental implant, Compos. Part B Eng. (2002). doi:10.1016/s1359-8368(96)00021-2.

[241] W. Pompe, H. Worch, M. Epple, W. Friess, M. Gelinsky, P. Greil, U. Hempel, D. Scharnweber, K. Schulte, Functionally graded materials for biomedical applications, Mater. Sci. Eng. A. (2003). doi:10.1016/S0921-5093(03)00580-X.

[242] H. Mishina, Y. Inumaru, K. Kaitoku, Fabrication of ZrO2/AISI316L functionally graded materials for joint prostheses, Mater. Sci. Eng. A. (2008). doi:10.1016/j.msea.2007.05.004.

[243] J. Li, K. Zhao, Y.F. Tang, D.Y. Li, Flexural strength of zirconia/stainless steel

functionally graded materials, J. Cent. South Univ. Technol. (English Ed. (2009). doi:10.1007/s11771-009-0148-6.

[244] M. Thieme, K.P. Wieters, F. Bergner, D. Scharnweber, H. Worch, J. Ndop, T.J. Kim, W. Grill, Titanium powder sintering for preparation of a porous functionally graded material destined for orthopaedic implants, J. Mater. Sci. Mater. Med. (2001). doi:10.1023/A:1008958914818.

[245] M.J. Suk, S. Il Choi, J.S. Kim, Y. Do Kim, Y.S. Kwon, Fabrication of a Porous Material with a Porosity Gradient by a Pulsed Electric Current Sintering Process, Met. Mater. Int. (2003). doi:10.1007/BF03027261.

[246] A. Tampieri, G. Celotti, S. Sprio, A. Delcogliano, S. Franzese, Porosity-graded hydroxyapatite ceramics to replace natural bone, Biomaterials. (2001). doi:10.1016/S0142-9612(00)00290-8.

[247] L.M. Rodríguez-Lorenzo, J.M.F. Ferreira, Development of porous ceramic bodies for applications in tissue engineering and drug delivery systems, Mater. Res. Bull. (2004). doi:10.1016/j.materresbull.2003.09.014.

[248] S. Grasso, R.K. Chinnam, H. Porwal, A.R. Boccaccini, M.J. Reece, Low temperature spark plasma sintering of 45S5 Bioglass®, J. Non. Cryst. Solids. (2013). doi:10.1016/j.jnoncrysol.2012.11.009.

[249] L. Desogus, A. Cuccu, S. Montinaro, R. Orrù, G. Cao, D. Bellucci, A. Sola, V. Cannillo, Classical Bioglass® and innovative CaO-rich bioglass powders processed by Spark Plasma Sintering: A comparative study, J. Eur. Ceram. Soc. (2015). doi:10.1016/j.jeurceramsoc.2015.07.023.

[250] D.C. Clupper, L.L. Hench, Crystallization kinetics of tape cast bioactive glass 45S5, J. Non. Cryst. Solids. (2003). doi:10.1016/S0022-3093(02)01857-4.

[251] D. Bellucci, V. Cannillo, A. Sola, An overview of the effects of thermal processing on bioactive glasses, Sci. Sinter. (2010). doi:10.2298/SOS1003307B.

[252] M. Plewinski, K. Schickle, M. Lindner, A. Kirsten, M. Weber, H. Fischer, The effect of crystallization of bioactive bioglass 45S5 on apatite formation and degradation, Dent. Mater. (2013). doi:10.1016/j.dental.2013.09.016.

[253] D. Bellucci, A. Anesi, R. Salvatori, L. Chiarini, V. Cannillo, A comparative in vivo evaluation of bioactive glasses and bioactive glass-based composites for bone tissue repair, Mater. Sci. Eng. C. (2017). doi:10.1016/j.msec.2017.05.062.

[254] D. Bellucci, V. Cannillo, A. Sola, Calcium and potassium addition to facilitate the sintering of bioactive glasses, Mater. Lett. (2011). doi:10.1016/j.matlet.2011.03.060.

[255] D. Bellucci, V. Cannillo, A. Sola, A new highly bioactive composite for scaffold applications: A feasibility study, Materials (Basel). (2011).

doi:10.3390/ma4020339.

[256] D. Bellucci, A. Sola, V. Cannillo, Low temperature sintering of innovative bioactive glasses, J. Am. Ceram. Soc. (2012). doi:10.1111/j.1551-2916.2012.05100.x.

[257] D. Bellucci, A. Sola, A. Anesi, R. Salvatori, L. Chiarini, V. Cannillo, Bioactive glass/hydroxyapatite composites: Mechanical properties and biological evaluation, Mater. Sci. Eng. C. (2015). doi:10.1016/j.msec.2015.02.041.

[258] D. Bellucci, R. Salvatori, M. Cannio, M. Luginina, R. Orru, S. Montinaro, A. Anesi, L. Chiarini, G. Cao, V. Cannillo, Bioglass and bioceramic composites processed by Spark Plasma Sintering (SPS): Biological evaluation Versus SBF test, Biomed. Glas. (2018). doi:10.1515/bglass-2018-0003.

[259] A. Le Bail, Modelling the silica glass structure by the Rietveld method, J. Non. Cryst. Solids. (1995). doi:10.1016/0022-3093(94)00664-4.

[260] L. Lutterotti, R. Ceccato, R. Dal Maschio, E. Pagani, Quantitative Analysis of Silicate Glass in Ceramic Materials by the Rietveld Method, Mater. Sci. Forum. (2009). doi:10.4028/www.scientific.net/msf.278-281.87.

[261] T.A. Baser, M. Baricco, S. Enzo, G. Vaughan, A.R. Yavari, Analysis of crystallization behavior of Fe48Cr15 Mo14Y2 C15B6 bulk metallic glass by synchrotron radiation, J. Mater. Res. (2008). doi:10.1557/jmr.2008.0264.

[262] C.V. Brovarone, E. Verné, P. Appendino, Macroporous bioactive glass-ceramic scaffolds for tissue engineering, in: J. Mater. Sci. Mater. Med., 2006. doi:10.1007/s10856-006-0533-8.

[263] H. Liu, H. Yazici, C. Ergun, T.J. Webster, H. Bermek, An in vitro evaluation of the Ca/P ratio for the cytocompatibility of nano-to-micron particulate calcium phosphates for bone regeneration, Acta Biomater. (2008). doi:10.1016/j.actbio.2008.02.025.

[264] X. Liu, C. Ding, Z. Wang, Apatite formed on the surface of plasma-sprayed wollastonite coating immersed in simulated body fluid, Biomaterials. (2001). doi:10.1016/S0142-9612(00)00386-0.

[265] P. Siriphannon, Y. Kameshima, A. Yasumori, K. Okada, S. Hayashi, Formation of hydroxyapatite on CaSiO3 powders in simulated body fluid, J. Eur. Ceram. Soc. (2002). doi:10.1016/S0955-2219(01)00301-6.

[266] A. Sola, D. Bellucci, V. Cannillo, Enamelled coatings produced with low-alkaline bioactive glasses, Surf. Coatings Technol. (2014). doi:10.1016/j.surfcoat.2014.03.025.

[267] M. Miola, E. Verné, F.E. Ciraldo, L. Cordero-Arias, A.R. Boccaccini, Electrophoretic Deposition of Chitosan/45S5 Bioactive Glass Composite Coatings Doped with Zn and Sr, Front. Bioeng. Biotechnol. (2015).

doi:10.3389/fbioe.2015.00159.

[268] M. Araújo, M. Miola, G. Baldi, J. Perez, E. Verné, Bioactive glasses with low Ca/P ratio and enhanced bioactivity, Materials (Basel). (2016). doi:10.3390/ma9040226.

[269] A.B.Y. Hazar, Preparation and in vitro bioactivity of CaSiO3 powders, Ceram. Int. (2007). doi:10.1016/j.ceramint.2006.12.013.

[270] X. Liu, M. Morra, A. Carpi, B. Li, Bioactive calcium silicate ceramics and coatings, Biomed. Pharmacother. (2008). doi:10.1016/j.biopha.2008.07.051.

[271] R. Abd Rashid, R. Shamsudin, M.A. Abdul Hamid, A. Jalar, In-vitro bioactivity of wollastonite materials derived from limestone and silica sand, Ceram. Int. (2014). doi:10.1016/j.ceramint.2013.12.004.

[272] F. Zhang, K. Lin, J. Chang, J. Lu, C. Ning, Spark plasma sintering of macroporous calcium phosphate scaffolds from nanocrystalline powders, J. Eur. Ceram. Soc. (2008). doi:10.1016/j.jeurceramsoc.2007.07.012.

[273] K. Do Woo, S.M. Kwak, T. Lee, S.T. Oh, J.N. Woo, Microstructure and biocompatibility of porous BCP(HA/β-TCP) biomaterials consolidated by SPS using space holder, Korean J. Mater. Res. (2016). doi:10.3740/MRSK.2016.26.8.449.

[274] M. Rizwan, M. Hamdi, W.J. Basirun, K. Kondoh, J. Umeda, Low pressure spark plasma sintered hydroxyapatite and Bioglass® composite scaffolds for bone tissue repair, Ceram. Int. (2018). doi:10.1016/j.ceramint.2018.09.108.

[275] U. Ripamonti, L.C. Roden, L.F. Renton, Osteoinductive hydroxyapatite-coated titanium implants, Biomaterials. (2012). doi:10.1016/j.biomaterials.2012.01.050.

[276] L. Lin, K.L. Chow, Y. Leng, Study of hydroxyapatite osteoinductivity with an osteogenic differentiation of mesenchymal stem cells, J. Biomed. Mater. Res. - Part A. (2009). doi:10.1002/jbm.a.31994.

[277] M.J. Yaszemski, R.G. Payne, W.C. Hayes, R. Langer, A.G. Mikos, Evolution of bone transplantation: Molecular, cellular and tissue strategies to engineer human bone, Biomaterials. 17 (1996) 175–185. doi:10.1016/0142-9612(96)85762-0.

[278] J.M. Spivak, A. Hasharoni, Use of hydroxyapatite in spine surgery, Eur. Spine J. 10 (2001) S197–S204. doi:10.1007/s005860100286.

[279] A. Tampieri, G. Celotti, F. Szontagh, E. Landi, Sintering and characterization of HA and TCP bioceramics with control of their strength and phase purity, J. Mater. Sci. Mater. Med. (1997). doi:10.1023/A:1018538212328.

[280] D. Bellucci, A. Sola, V. Cannillo, Hydroxyapatite and tricalcium phosphate composites with bioactive glass as second phase: State of the art and current

applications, J. Biomed. Mater. Res. - Part A. (2016). doi:10.1002/jbm.a.35619.

[281] M. Karadjian, C. Essers, S. Tsitlakidis, B. Reible, A. Moghaddam, A.R. Boccaccini, F. Westhauser, Biological properties of calcium phosphate bioactive glass composite bone substitutes: Current experimental evidence, Int. J. Mol. Sci. (2019). doi:10.3390/ijms20020305.

[282] A.A. Gorustovich, J.A. Roether, A.R. Boccaccini, Effect of Bioactive Glasses on Angiogenesis: A Review of In Vitro and In Vivo Evidences , Tissue Eng. Part B Rev. (2009). doi:10.1089/ten.teb.2009.0416.

[283] I. Allan, H. Newman, M. Wilson, Antibacterial activity of particulate Bioglass® against supra- and subgingival bacteria, Biomaterials. (2001). doi:10.1016/S0142-9612(00)00330-6.

[284] A. Hoppe, N.S. Güldal, A.R. Boccaccini, A review of the biological response to ionic dissolution products from bioactive glasses and glass-ceramics., Biomaterials. (2011). doi:10.1016/j.biomaterials.2011.01.004.

[285] D. Bellucci, F. Chiellini, G. Ciardelli, M. Gazzarri, P. Gentile, A. Sola, V. Cannillo, Processing and characterization of innovative scaffolds for bone tissue engineering, J. Mater. Sci. Mater. Med. (2012). doi:10.1007/s10856-012-4622-6.

[286] Q.Z. Chen, I.D. Thompson, A.R. Boccaccini, 45S5 Bioglass®-derived glass-ceramic scaffolds for bone tissue engineering, Biomaterials. (2006). doi:10.1016/j.biomaterials.2005.11.025.

[287] D. Bellucci, L. Desogus, S. Montinaro, R. Orrù, G. Cao, V. Cannillo, Innovative hydroxyapatite/bioactive glass composites processed by spark plasma sintering for bone tissue repair, J. Eur. Ceram. Soc. (2017). doi:10.1016/j.jeurceramsoc.2016.11.012.

[288] A. Cattini, D. Bellucci, A. Sola, L. Pawłowski, V. Cannillo, Suspension plasma spraying of optimised functionally graded coatings of bioactive glass/hydroxyapatite, Surf. Coatings Technol. (2013). doi:10.1016/j.surfcoat.2013.09.037.

[289] D. Bellucci, V. Cannillo, G. Ciardelli, P. Gentile, A. Sola, Potassium based bioactive glass for bone tissue engineering, Ceram. Int. (2010). doi:10.1016/j.ceramint.2010.07.009.

[290] F. Matthews, R. Rawlings, Composite Materials: Engineering and Science., Chapman&Hall, 1994.

[291] International Standard 10993-5, Biological Evaluation of Medical Devices - Part 5: Tests for Cytotoxicity: In Vitro Methods, (2009).

[292] International Standard 10993-12, Biological Evaluation of Medical Devices - Part 12: Sample Preparation and Reference Materials, (2007).

[293] N.W. Roehm, G.H. Rodgers, S.M. Hatfield, A.L. Glasebrook, An improved colorimetric assay for cell proliferation and viability utilizing the tetrazolium salt XTT, J. Immunol. Methods. (1991). doi:10.1016/0022-1759(91)90114-U.

[294] M. V. Berridge, P.M. Herst, A.S. Tan, Tetrazolium dyes as tools in cell biology: New insights into their cellular reduction, Biotechnol. Annu. Rev. (2005). doi:10.1016/S1387-2656(05)11004-7.

[295] D. Bellucci, A. Sola, R. Salvatori, A. Anesi, L. Chiarini, V. Cannillo, Sol-gel derived bioactive glasses with low tendency to crystallize: Synthesis, post-sintering bioactivity and possible application for the production of porous scaffolds, Mater. Sci. Eng. C. (2014). doi:10.1016/j.msec.2014.07.037.

[296] S. Kotani, Y. Fujita, T. Kitsugi, T. Nakamura, T. Yamamuro, C. Ohtsuki, T. Kokubo, Bone bonding mechanism of β-tricalcium phosphate, J. Biomed. Mater. Res. (1991). doi:10.1002/jbm.820251010.

[297] W.R. Walsh, P. Morberg, Y. Yu, J.L. Yang, W. Haggard, P.C. Sheath, M. Svehla, W.J.M. Bruce, Response of a calcium sulfate bone graft substitute in a confined cancellous defect, Clin. Orthop. Relat. Res. (2003). doi:10.1097/00003086-200301000-00033.

[298] F. Theiss, D. Apelt, B. Brand, A. Kutter, K. Zlinszky, M. Bohner, S. Matter, C. Frei, J.A. Auer, B. Von Rechenberg, Biocompatibility and resorption of a brushite calcium phosphate cement, Biomaterials. (2005). doi:10.1016/j.biomaterials.2004.11.056.

[299] Y. Kato, J.J. Windle, B.A. Koop, G.R. Mundy, L.F. Bonewald, Establishment of an Osteocyte-like Cell Line, MLO-Y4, J. Bone Miner. Res. (2006). doi:10.1359/jbmr.1997.12.12.2014.

[300] L.F. Bonewald, Establishment and characterization of an osteocyte-like cell line, MLO- Y4, in: J. Bone Miner. Metab., 1999. doi:10.1007/s007740050066.

[301] G. Fotakis, J.A. Timbrell, In vitro cytotoxicity assays: Comparison of LDH, neutral red, MTT and protein assay in hepatoma cell lines following exposure to cadmium chloride, Toxicol. Lett. (2006). doi:10.1016/j.toxlet.2005.07.001.

[302] R. Fautz, B. Husein, C. Hechenberger, Application of the neutral red assay (NR assay) to monolayer cultures of primary hepatocytes: rapid colorimetric viability determination for the unscheduled DNA synthesis test (UDS), Mutat. Res. Mutagen. Relat. Subj. (1991). doi:10.1016/0165-1161(91)90130-Z.

[303] E. Borenfreund, J.A. Puerner, A simple quantitative procedure using monolayer cultures for cytotoxicity assays (HTD/NR-90), J. Tissue Cult. Methods. (1985). doi:10.1007/BF01666038.

[304] G. Ciapetti, D. Granchi, E. Verri, L. Savarino, D. Cavedagna, A. Pizzoferrato, Application of a combination of neutral red and amido black staining for rapid,

reliable cytotoxicity testing of biomaterials, Biomaterials. (1996). doi:10.1016/0142-9612(96)88670-4.

[305] J. Weyermann, D. Lochmann, A. Zimmer, A practical note on the use of cytotoxicity assays, Int. J. Pharm. (2005). doi:10.1016/j.ijpharm.2004.09.018.

[306] A. Kroll, M.H. Pillukat, D. Hahn, J. Schnekenburger, Current in vitro methods in nanoparticle risk assessment: Limitations and challenges, Eur. J. Pharm. Biopharm. (2009). doi:10.1016/j.ejpb.2008.08.009.

[307] C.J. Goodwin, S.J. Holt, S. Downes, N.J. Marshall, Microculture tetrazolium assays: a comparison between two new tetrazolium salts, XTT and MTS, J. Immunol. Methods. (1995). doi:10.1016/0022-1759(94)00277-4.

[308] A.M. Crane, S.K. Bhattacharya, The use of bromodeoxyuridine incorporation assays to assess corneal stem cell proliferation, Methods Mol. Biol. (2013). doi:10.1007/978-1-62703-432-6-4.

[309] I.D. Xynos, M.V.J. Hukkanen, J.J. Batten, L.D. Buttery, L.L. Hench, J.M. Polak, Bioglass ®45S5 stimulates osteoblast turnover and enhances bone formation in vitro: Implications and applications for bone tissue engineering, Calcif. Tissue Int. (2000). doi:10.1007/s002230001134.

[310] P. Habibovic, F. Barrère, C.A. Blitterswijk, K. Groot, P. Layrolle, Biomimetic Hydroxyapatite Coating on Metal Implants, J. Am. Ceram. Soc. (2010). doi:10.1111/j.1151-2916.2002.tb00126.x.

[311] C.Y. Zhao, H.S. Fan, X.D. Zhang, Advances in Biomimetic Apatite Coating on Metal Implants, in: Adv. Biomimetics, 2012. doi:10.5772/14938.

[312] R. Shu, R. McMullen, M.J. Baumann, L.R. McCabe, Hydroxyapatite accelerates differentiation and suppresses growth of MC3T3-E1 osteoblasts, J. Biomed. Mater. Res. - Part A. (2003). doi:10.1002/jbm.a.20021.

[313] P. Balasubramanian, L. Hupa, B. Jokic, R. Detsch, A. Grünewald, A.R. Boccaccini, Angiogenic potential of boron-containing bioactive glasses: in vitro study, J. Mater. Sci. (2017). doi:10.1007/s10853-016-0563-7.

[314] M. Ojansivu, S. Vanhatupa, L. Björkvik, H. Häkkänen, M. Kellomäki, R. Autio, J.A. Ihalainen, L. Hupa, S. Miettinen, Bioactive glass ions as strong enhancers of osteogenic differentiation in human adipose stem cells, Acta Biomater. (2015). doi:10.1016/j.actbio.2015.04.017.

[315] S. Begum, W.E. Johnson, T. Worthington, R.A. Martin, The influence of pH and fluid dynamics on the antibacterial efficacy of 45S5 Bioglass, Biomed. Mater. (2016). doi:10.1088/1748-6041/11/1/015006.

[316] M.N. Rahaman, D.E. Day, B. Sonny Bal, Q. Fu, S.B. Jung, L.F. Bonewald, A.P. Tomsia, Bioactive glass in tissue engineering, Acta Biomater. (2011). doi:10.1016/j.actbio.2011.03.016.

[317] T.R. Arnett, Extracellular pH regulates bone cell function., J. Nutr. (2008). doi:10.1093/jn/138.2.415S.

[318] R.Z. LeGeros, Calcium phosphates in oral biology and medicine., Monogr. Oral Sci. 15 (1991) 1–201.

[319] N. Eliaz, N. Metoki, Calcium phosphate bioceramics: A review of their history, structure, properties, coating technologies and biomedical applications, Materials (Basel). 10 (2017) 1–104. doi:10.3390/ma10040334.

[320] C. Combes, S. Cazalbou, C. Rey, Apatite biominerals, Minerals. 6 (2016) 1–25. doi:10.3390/min6020034.

[321] S. Von Euw, Y. Wang, G. Laurent, C. Drouet, F. Babonneau, N. Nassif, T. Azaïs, Bone mineral: new insights into its chemical composition, Sci. Rep. 9 (2019) 1–11. doi:10.1038/s41598-019-44620-6.

[322] J.P. Lafon, E. Champion, D. Bernache-Assollant, Processing of AB-type carbonated hydroxyapatite Ca10-x(PO4)6-x(CO3)x(OH)2-x-2y(CO3)y ceramics with controlled composition, J. Eur. Ceram. Soc. 28 (2008) 139–147. doi:10.1016/j.jeurceramsoc.2007.06.009.

[323] C. Rey, C. Combes, C. Drouet, S. Cazalbou, D. Grossin, F. Brouillet, S. Sarda, Surface properties of biomimetic nanocrystalline apatites; Applications in biomaterials, Prog. Cryst. Growth Charact. Mater. 60 (2014) 63–73. doi:10.1016/j.pcrysgrow.2014.09.005.

[324] C. Drouet, A. Al-kattan, M. Choimet, A. Tourrette Diallo, V. Santran, J. Dexpert-Ghys, B. Pipy, F. Brouillet, M. Tourbin, Biomimetic Apatite-Based Functional Nanoparticles as Promising Newcomers in Nanomedicine: Overview of 10 Years of Initiatory Research, Intern. Med. Prim. Healthc. 1 (2015) 1–9. doi:10.24966/imph-2493/100001.

[325] A.A. Campbell, M. LoRe, G.H. Nancollas, The influence of carbonate and magnesium ions on the growth of hydroxyapatite, carbonated apatite and human powdered enamel, Colloids and Surfaces. 54 (1991) 25–31. doi:10.1016/0166-6622(91)80046-Q.

[326] H.A. Lowenstam, S. Weiner, Transformation of amorphous calcium phosphate to crystalline dahllite in the radular teeth of chitons, Science (80-.). 227 (1985) 51–53. doi:10.1126/science.227.4682.51.

[327] J. Mahamid, B. Aichmayer, E. Shimoni, R. Ziblat, C. Li, S. Siegel, O. Paris, P. Fratzl, S. Weiner, L. Addadi, Mapping amorphous calcium phosphate transformation into crystalline mineral from the cell to the bone in zebrafish fin rays, Proc. Natl. Acad. Sci. U. S. A. 107 (2010) 6316–6321. doi:10.1073/pnas.0914218107.

[328] J. Mahamid, A. Sharir, D. Gur, E. Zelzer, L. Addadi, S. Weiner, Bone

mineralization proceeds through intracellular calcium phosphate loaded vesicles: A cryo-electron microscopy study, J. Struct. Biol. 174 (2011) 527–535. doi:10.1016/j.jsb.2011.03.014.

[329] F.C.M. Dricssens, J.A. Flanell, M.G. Boltong, I. Khairoun, M.P. Ginebra, Osteotransductive bone cements, Proc. Inst. Mech. Eng. Part H J. Eng. Med. 212 (1998) 427–435.

[330] A. Tofighi, S. Mounic, P. Chakravarthy, C. Rey, D. Lee, Setting reactions involved in injectable cements based on amorphous calcium phosphate, Key Eng. Mater. 192–195 (2001) 769–772.

[331] S. Somrani, M. Banu, M. Jemal, C. Rey, Physico-chemical and thermochemical studies of the hydrolytic conversion of amorphous tricalcium phosphate into apatite, J. Solid State Chem. 178 (2005) 1337–1348. doi:10.1016/j.jssc.2004.11.029.

[332] T. Yu, J. Ye, Y. Wang, Synthesis and property of a novel calcium phosphate cement, J. Biomed. Mater. Res. - Part B Appl. Biomater. 90B (2009) 745–751. doi:10.1002/jbm.b.31343.

[333] C. Drouet, C. Largeot, G. Raimbeaux, C. Estournès, G. Dechambre, C. Combes, C. Rey, Bioceramics: Spark Plasma Sintering (SPS) of Calcium Phosphates, Adv. Sci. Technol. 49 (2006) 45–50. doi:10.4028/www.scientific.net/ast.49.45.

[334] D. Grossin, S. Rollin-Martinet, C. Estournès, F. Rossignol, E. Champion, C. Combes, C. Rey, C. Geoffroy, C. Drouet, Biomimetic apatite sintered at very low temperature by spark plasma sintering: Physico-chemistry and microstructure aspects, Acta Biomater. 6 (2010) 577–585. doi:10.1016/j.actbio.2009.08.021.

[335] F. Brouillet, D. Laurencin, D. Grossin, C. Drouet, C. Estournes, G. Chevallier, C. Rey, Biomimetic apatite-based composite materials obtained by spark plasma sintering (SPS): physicochemical and mechanical characterizations, J. Mater. Sci. Mater. Med. 26 (2015) 1–11. doi:10.1007/s10856-015-5553-9.

[336] C. Ortali, I. Julien, M. Vandenhende, C. Drouet, E. Champion, Consolidation of bone-like apatite bioceramics by spark plasma sintering of amorphous carbonated calcium phosphate at very low temperature, J. Eur. Ceram. Soc. 38 (2018) 2098–2109. doi:10.1016/j.jeurceramsoc.2017.11.051.

[337] D. Eichert, Etude de la reactivite de surface d'apatites de synthese nanocrystallines, Institut National Polytechnique de Toulouse, 2001.

[338] C. Holt, M.J.J.M. Van Kemenade, L.S. Nelson, D.W.L. Hukins, R.T. Bailey, J.E. Harries, S.S. Hasnain, P.L. De Bruyn, Amorphous calcium phosphates prepared at pH 6.5 and 6.0, Mater. Res. Bull. 24 (1989) 55–62. doi:10.1016/0025-5408(89)90008-1.

[339] A.S. Posner, F. Betts, N.C. Blumenthal, Formation and structure of synthetic and bone hydroxyapatites, Prog. Cryst. Growth Charact. 3 (1980) 49–64. doi:10.1016/0146-3535(80)90011-8.

[340] L. Berzina-Cimdina, N. Borodajenko, Research of Calcium Phosphates Using Fourier Transform Infrared Spectroscopy, in: T. Theophanides (Ed.), Infrared Spectrosc. - Mater. Sci. Eng. Technol., InTech, Rijeka, 2012: pp. 124–148. doi:10.5772/36942.

[341] C. Drouet, Apatite formation: Why it may not work as planned, and how to conclusively identify apatite compounds, Biomed Res. Int. 2013 (2013) 1–12. doi:10.1155/2013/490946.

[342] C. Rey, C. Combes, C. Drouet, D. Grossin, Bioactive Ceramics: Physical Chemistry, in: P. Ducheyne, W.D. Ducheyne, W.D. Grainger, C.J. Kirkpatrick (Eds.), Compr. Biomater., 1st edn, Elsevier Science, Amsterdam, 2011: pp. 187–221. doi:10.1016/B978-0-08-055294-1.00178-1.

[343] A. Grunenwald, C. Keyser, A.M. Sautereau, E. Crubézy, B. Ludes, C. Drouet, Revisiting carbonate quantification in apatite (bio)minerals: A validated FTIR methodology, J. Archaeol. Sci. 49 (2014) 134–141. doi:10.1016/j.jas.2014.05.004.

[344] M. Vignoles, G. Bonel, D.W. Holcomb, R.A. Young, Influence of preparation conditions on the composition of type B carbonated hydroxyapatite and on the localization of the carbonate ions, Calcif. Tissue Int. 43 (1988) 33–40. doi:10.1007/BF02555165.

[345] A. Grunenwald, C. Keyser, A.M. Sautereau, E. Crubézy, B. Ludes, C. Drouet, Novel contribution on the diagenetic physicochemical features of bone and teeth minerals, as substrates for ancient DNA typing, Anal. Bioanal. Chem. 406 (2014) 4691–4704. doi:10.1007/s00216-014-7863-z.

[346] S. Shimoda, T. Aoba, E.C. Moreno, Y. Miake, Effect of Solution Composition on Morphological and Structural Features of Carbonated Calcium Apatites, J. Dent. Res. 69 (1990) 1731–1740. doi:10.1177/00220345900690110501.

[347] Y. Doi, T. Shibutani, Y. Moriwaki, T. Kajimoto, Y. Iwayama, Sintered carbonate apatites as bioresorbable bone substitutes, J. Biomed. Mater. Res. 7 (1998) 111–122. doi:10.1002/(SICI)1097-4636(19980315)39:4<603::AID-JBM15>3.0.CO;2-7.

[348] B. Subia, J. Kundu, S. C., Biomaterial Scaffold Fabrication Techniques for Potential Tissue Engineering Applications, in: Tissue Eng., 2010. doi:10.5772/8581.

[349] N. Bhardwaj, S.C. Kundu, Electrospinning: A fascinating fiber fabrication technique, Biotechnol. Adv. (2010). doi:10.1016/j.biotechadv.2010.01.004.

[350] J.D. Schiffman, C.L. Schauer, A review: Electrospinning of biopolymer nanofibers and their applications, Polym. Rev. (2008). doi:10.1080/15583720802022182.

[351] V. Pillay, C. Dott, Y.E. Choonara, C. Tyagi, L. Tomar, P. Kumar, L.C. Du Toit, V.M.K. Ndesendo, A review of the effect of processing variables on the fabrication of electrospun nanofibers for drug delivery applications, J. Nanomater. (2013). doi:10.1155/2013/789289.

[352] A. Haider, S. Haider, I.K. Kang, A comprehensive review summarizing the effect of electrospinning parameters and potential applications of nanofibers in biomedical and biotechnology, Arab. J. Chem. (2018). doi:10.1016/j.arabjc.2015.11.015.

[353] Y. Wang, G.A. Ameer, B.J. Sheppard, R. Langer, A tough biodegradable elastomer, Nat. Biotechnol. (2002). doi:10.1038/nbt0602-602.

[354] R. Rai, M. Tallawi, A. Grigore, A.R. Boccaccini, Synthesis, properties and biomedical applications of poly(glycerol sebacate) (PGS): A review, Prog. Polym. Sci. (2012). doi:10.1016/j.progpolymsci.2012.02.001.

[355] Q.Z. Chen, A. Bismarck, U. Hansen, S. Junaid, M.Q. Tran, S.E. Harding, N.N. Ali, A.R. Boccaccini, Characterisation of a soft elastomer poly(glycerol sebacate) designed to match the mechanical properties of myocardial tissue, Biomaterials. (2008). doi:10.1016/j.biomaterials.2007.09.010.

[356] R. Rai, M. Tallawi, N. Barbani, C. Frati, D. Madeddu, S. Cavalli, G. Graiani, F. Quaini, J.A. Roether, D.W. Schubert, E. Rosellini, A.R. Boccaccini, Biomimetic poly(glycerol sebacate) (PGS) membranes for cardiac patch application, Mater. Sci. Eng. C. (2013). doi:10.1016/j.msec.2013.04.058.

[357] L. Vogt, L.R. Rivera, L. Liverani, A. Piegat, M. El Fray, A.R. Boccaccini, Poly(ε-caprolactone)/poly(glycerol sebacate) electrospun scaffolds for cardiac tissue engineering using benign solvents, Mater. Sci. Eng. C. (2019). doi:10.1016/j.msec.2019.04.091.

[358] R. Ranjana, T. Marwa, F. Caterina, F. Angela, G. Andrea, Q. Federico, R.J. A., H. Tobias, S.D. W., S. Lothar, B. Niccoletta, L. Luigi, R. Elisabetta, B.A. R., Bioactive Electrospun Fibers of Poly(glycerol sebacate) and Poly(ε-caprolactone) for Cardiac Patch Application, Adv. Healthc. Mater. (2015). doi:10.1002/adhm.201500154.

[359] N. Masoumi, K.L. Johnson, M.C. Howell, G.C. Engelmayr, Valvular interstitial cell seeded poly(glycerol sebacate) scaffolds: Toward a biomimetic in vitro model for heart valve tissue engineering, Acta Biomater. (2013). doi:10.1016/j.actbio.2013.01.001.

[360] J.M. Kemppainen, S.J. Hollister, Tailoring the mechanical properties of 3D-designed poly(glycerol sebacate) scaffolds for cartilage applications, J. Biomed.

Mater. Res. - Part A. (2010). doi:10.1002/jbm.a.32653.

[361] Y. Liu, K. Tian, J. Hao, T. Yang, X. Geng, W. Zhang, Biomimetic poly(glycerol sebacate)/polycaprolactone blend scaffolds for cartilage tissue engineering, J. Mater. Sci. Mater. Med. (2019). doi:10.1007/s10856-019-6257-3.

[362] C.A. Sundback, J.Y. Shyu, A.J. Wu, T.P. Sheahan, Y. Wang, W.C. Faquin, R.S. Langer, J.P. Vacanti, T.A. Hadlock, In vitro and in vivo biocompatibility analysis of poly (glycerol sebacate) as a potential nerve guide material, in: Mater. Res. Soc. Symp. Proc., 2004.

[363] A. Saudi, M. Rafienia, A. Zargar Kharazi, H. Salehi, A. Zarrabi, M. Karevan, Design and fabrication of poly (glycerol sebacate)-based fibers for neural tissue engineering: Synthesis, electrospinning, and characterization, Polym. Adv. Technol. (2019). doi:10.1002/pat.4575.

[364] C.D. Pritchard, K.M. Arnér, R.A. Neal, W.L. Neeley, P. Bojo, E. Bachelder, J. Holz, N. Watson, E.A. Botchwey, R.S. Langer, F.K. Ghosh, The use of surface modified poly(glycerol-co-sebacic acid) in retinal transplantation, Biomaterials. (2010). doi:10.1016/j.biomaterials.2009.11.074.

[365] F. Ghosh, W.L. Neeley, K. Arnér, R. Langer, Selective removal of photoreceptor cells in vivo using the biodegradable elastomer poly(glycerol sebacate), Tissue Eng. - Part A. (2011). doi:10.1089/ten.tea.2008.0450.

[366] A.M. Wieland, C.A. Sundback, A. Hart, K. Kulig, P.T. Masiakos, C.J. Hartnick, Poly(glycerol sebacate)-engineered plugs to repair chronic tympanic membrane perforations in a chinchilla model, Otolaryngol. - Head Neck Surg. (2010). doi:10.1016/j.otohns.2010.01.025.

[367] C.A. Sundback, J. McFadden, A. Hart, K.M. Kulig, A.M. Wieland, M.J.N. Pereira, I. Pomerantseva, C.J. Hartnick, P.T. Masiakos, Behavior of poly(glycerol sebacate) plugs in chronic tympanic membrane perforations, J. Biomed. Mater. Res. - Part B Appl. Biomater. (2012). doi:10.1002/jbm.b.32761.

[368] S. Sant, C.M. Hwang, S.H. Lee, A. Khademhosseini, Hybrid PGS-PCL microfibrous scaffolds with improved mechanical and biological properties, J. Tissue Eng. Regen. Med. (2011). doi:10.1002/term.313.

[369] L. Vogt, L. Liverani, J.A. Roether, A.R. Boccaccini, Electrospun zein fibers incorporating poly(glycerol sebacate) for soft tissue engineering, Nanomaterials. (2018). doi:10.3390/nano8030150.

[370] M. Abedalwafa, F. Wang, L. Wang, C. Li, Biodegradable poly-epsilon-caprolactone (PCL) for tissue engineering applications: A review, Rev. Adv. Mater. Sci. (2013).

[371] E. Malikmammadov, T.E. Tanir, A. Kiziltay, V. Hasirci, N. Hasirci, PCL and PCL-based materials in biomedical applications, J. Biomater. Sci. Polym. Ed. (2018). doi:10.1080/09205063.2017.1394711.

[372] A.G.A. Coombes, S.C. Rizzi, M. Williamson, J.E. Barralet, S. Downes, W.A. Wallace, Precipitation casting of polycaprolactone for applications in tissue engineering and drug delivery, Biomaterials. (2004). doi:10.1016/S0142-9612(03)00535-0.

[373] H. Chim, D.W. Hutmacher, A.M. Chou, A.L. Oliveira, R.L. Reis, T.C. Lim, J.T. Schantz, A comparative analysis of scaffold material modifications for load-bearing applications in bone tissue engineering, Int. J. Oral Maxillofac. Surg. (2006). doi:10.1016/j.ijom.2006.03.024.

[374] H. Sun, L. Mei, C. Song, X. Cui, P. Wang, The in vivo degradation, absorption and excretion of PCL-based implant, Biomaterials. (2006). doi:10.1016/j.biomaterials.2005.09.019.

[375] Y. Wang, Y.M. Kim, R. Langer, In vivo degradation characteristics of poly(glycerol sebacate), J. Biomed. Mater. Res. - Part A. (2003). doi:10.1002/jbm.a.10534.

[376] S. Sant, D. Iyer, A.K. Gaharwar, A. Patel, A. Khademhosseini, Effect of biodegradation and de novo matrix synthesis on the mechanical properties of valvular interstitial cell-seeded polyglycerol sebacate-polycaprolactone scaffolds, Acta Biomater. (2013). doi:10.1016/j.actbio.2012.11.014.

[377] N. Masoumi, B.L. Larson, N. Annabi, M. Kharaziha, B. Zamanian, K.S. Shapero, A.T. Cubberley, G. Camci-Unal, K.B. Manning, J.E. Mayer, A. Khademhosseini, Electrospun PGS: PCL Microfibers Align Human Valvular Interstitial Cells and Provide Tunable Scaffold Anisotropy, Adv. Healthc. Mater. (2014). doi:10.1002/adhm.201300505.

[378] M. Tallawi, D. Dippold, R. Rai, D. D'Atri, J.A. Roether, D.W. Schubert, E. Rosellini, F.B. Engel, A.R. Boccaccini, Novel PGS/PCL electrospun fiber mats with patterned topographical features for cardiac patch applications, Mater. Sci. Eng. C. (2016). doi:10.1016/j.msec.2016.06.083.

[379] P. Kalakonda, M.A. Aldhahri, M.S. Abdel-Wahab, A. Tamayol, K.M. Moghaddam, F. Ben Rached, A. Pain, A. Khademhosseini, A. Memic, S. Chaieb, Microfibrous silver-coated polymeric scaffolds with tunable mechanical properties, RSC Adv. (2017). doi:10.1039/c6ra25151j.

[380] L. Liverani, L. Vester, A.R. Boccaccini, Biomaterials Produced via Green Electrospinning, in: Electrospun Biomater. Relat. Technol., 2017. doi:10.1007/978-3-319-70049-6_5.

[381] M.J. Mochane, T.S. Motsoeneng, E.R. Sadiku, T.C. Mokhena, J.S. Sefadi, Morphology and properties of electrospun PCL and its composites for medical

applications: A mini review, Appl. Sci. (2019). doi:10.3390/app9112205.

[382] ICH, Impurities: Guideline for Residual Solvents Q3C (R5), Int. Conf. Harmon. Tech. Requir. Regist. Pharm. Hum. Use. (2011).

[383] V. Miguez-Pacheco, L.L. Hench, A.R. Boccaccini, Bioactive glasses beyond bone and teeth: Emerging applications in contact with soft tissues, Acta Biomater. (2015). doi:10.1016/j.actbio.2014.11.004.

[384] A.A. Gorustovich, J.A. Roether, A.R. Boccaccini, Effect of bioactive glasses on angiogenesis: a review of in vitro and in vivo evidences., Tissue Eng. Part B. Rev. (2010). doi:10.1089/ten.teb.2009.0416.

[385] S. Kargozar, F. Baino, S. Hamzehlou, R.G. Hill, M. Mozafari, Bioactive Glasses: Sprouting Angiogenesis in Tissue Engineering, Trends Biotechnol. (2018). doi:10.1016/j.tibtech.2017.12.003.

[386] K. Schuhladen, X. Wang, L. Hupa, A.R. Boccaccini, Dissolution of borate and borosilicate bioactive glasses and the influence of ion (Zn, Cu) doping in different solutions, J. Non. Cryst. Solids. (2018). doi:10.1016/j.jnoncrysol.2018.08.037.

[387] J. Schindelin, I. Arganda-Carreras, E. Frise, V. Kaynig, M. Longair, T. Pietzsch, S. Preibisch, C. Rueden, S. Saalfeld, B. Schmid, J.-Y. Tinevez, D.J. White, V. Hartenstein, K. Eliceiri, P. Tomancak, A. Cardona, Fiji: an open-source platform for biological-image analysis., Nat. Methods. (2012). doi:10.1038/nmeth.2019.

[388] L. Liverani, E. Boccardi, A.M. Beltran, A.R. Boccaccini, Incorporation of calcium containing mesoporous (MCM-41-type) particles in electrospun PCL fibers by using benign solvents, Polymers (Basel). (2017). doi:10.3390/polym9100487.

[389] L. Liverani, M.S. Killian, A.R. Boccaccini, Fibronectin Functionalized Electrospun Fibers by Using Benign Solvents: Best Way to Achieve Effective Functionalization, Front. Bioeng. Biotechnol. (2019). doi:10.3389/fbioe.2019.00068.

[390] L. Liverani, A. Boccaccini, Versatile Production of Poly(Epsilon-Caprolactone) Fibers by Electrospinning Using Benign Solvents, Nanomaterials. (2016). doi:10.3390/nano6040075.

[391] H.H. Kim, M.J. Kim, S.J. Ryu, C.S. Ki, Y.H. Park, Effect of fiber diameter on surface morphology, mechanical property, and cell behavior of electrospun poly(ε-caprolactone) mat, Fibers Polym. (2016). doi:10.1007/s12221-016-6350-x.

[392] S. Salehi, M. Fathi, S.H. Javanmard, T. Bahners, J.S. Gutmann, S. Ergün, K.P. Steuhl, T.A. Fuchsluger, Generation of PGS/PCL blend nanofibrous scaffolds

mimicking corneal stroma structure, Macromol. Mater. Eng. (2014). doi:10.1002/mame.201300187.

[393] A.K. Gaharwar, M. Nikkhah, S. Sant, A. Khademhosseini, Anisotropic poly (glycerol sebacate)-poly (-caprolactone) electrospun fibers promote endothelial cell guidance, Biofabrication. (2015). doi:10.1088/1758-5090/7/1/015001.

[394] L.C. Xu, C.A. Siedlecki, Effects of surface wettability and contact time on protein adhesion to biomaterial surfaces, Biomaterials. (2007). doi:10.1016/j.biomaterials.2007.03.032.

[395] K. Anselme, Osteoblast adhesion on biomaterials., Biomaterials. (2000).

[396] Y. Arima, H. Iwata, Effect of wettability and surface functional groups on protein adsorption and cell adhesion using well-defined mixed self-assembled monolayers, Biomaterials. (2007). doi:10.1016/j.biomaterials.2007.03.013.

[397] C.A. Sundback, J.Y. Shyu, Y. Wang, W.C. Faquin, R.S. Langer, J.P. Vacanti, T.A. Hadlock, Biocompatibility analysis of poly(glycerol sebacate) as a nerve guide material, Biomaterials. (2005). doi:10.1016/j.biomaterials.2005.02.004.

[398] N. Bölgen, Y.Z. Menceloğlu, K. Acatay, I. Vargel, E. Pişkin, In vitro and in vivo degradation of non-woven materials made of poly(ε-caprolactone) nanofibers prepared by electrospinning under different conditions, J. Biomater. Sci. Polym. Ed. (2005). doi:10.1163/156856205774576655.

[399] C.X.F. Lam, M.M. Savalani, S.H. Teoh, D.W. Hutmacher, Dynamics of in vitro polymer degradation of polycaprolactone-based scaffolds: Accelerated versus simulated physiological conditions, Biomed. Mater. (2008). doi:10.1088/1748-6041/3/3/034108.

[400] Q.Z. Chen, H. Ishii, G.A. Thouas, A.R. Lyon, J.S. Wright, J.J. Blaker, W. Chrzanowski, A.R. Boccaccini, N.N. Ali, J.C. Knowles, S.E. Harding, An elastomeric patch derived from poly(glycerol sebacate) for delivery of embryonic stem cells to the heart, Biomaterials. (2010). doi:10.1016/j.biomaterials.2010.01.108.

[401] E.M. Jeffries, R.A. Allen, J. Gao, M. Pesce, Y. Wang, Highly elastic and suturable electrospun poly(glycerol sebacate) fibrous scaffolds, Acta Biomater. (2015). doi:10.1016/j.actbio.2015.02.005.

[402] I. Pomerantseva, N. Krebs, A. Hart, C.M. Neville, A.Y. Huang, C.A. Sundback, Degradation behavior of poly(glycerol sebacate), J. Biomed. Mater. Res. - Part A. (2009). doi:10.1002/jbm.a.32327.